

# A Detailed Treatment of the Measurement of Transport Coefficients in Transient Grating Experiments

Von der Universität Bayreuth  
zur Erlangung des Grades eines  
Doktors der Naturwissenschaften (Dr. rer. nat.)  
genehmigte Abhandlung

von

Marianne Hartung

geboren am 22.08.1978 in Würzburg

1. Gutachter: Prof. Dr. W. Köhler
2. Gutachter: Prof. Dr. A. Seilmeier
3. Gutachter: Prof. Dr. J. K. G. Dhont

Tag der Einreichung: 19. Juli 2007

Tag des Kolloquiums: 27. November 2007



# Contents

<b>Composition Variables and Partial Specific Quantities</b>	<b>1</b>
<b>1 Introduction</b>	<b>3</b>
<b>2 Thermodynamic–Phenomenological Theory</b>	<b>9</b>
2.1 Entropy Production and Phenomenological Equations . . . . .	9
2.1.1 First Law and Definition of Heat . . . . .	9
2.1.2 Entropy Production . . . . .	11
2.1.3 Phenomenological Equations and Onsager Coefficients . . . . .	23
2.2 Reference Velocities . . . . .	31
2.2.1 Reference Velocities and Diffusion Currents . . . . .	31
2.2.2 Prigogine’s Theorem . . . . .	34
2.2.3 Definition of Diffusion Coefficients . . . . .	38
2.2.4 Evolution Equations . . . . .	41
2.2.5 Thermodynamic Driving Forces . . . . .	53
2.2.6 Equations for the Analysis of Transient Grating Experiments . . . . .	61
<b>3 Boundary Effects in Holographic Grating Experiments</b>	<b>62</b>
3.1 Heat and Mass Diffusion Analysis . . . . .	62
3.1.1 One-dimensional Model . . . . .	63
3.1.2 Two-dimensional Model . . . . .	64
3.1.3 Stationary Solutions . . . . .	67
3.1.4 Time Dependent Solutions . . . . .	71
3.2 Experimental Technique and Sample Preparation . . . . .	80
3.3 Results and Discussion . . . . .	81
3.3.1 Measurements on Pure Toluene . . . . .	81
3.3.2 Measurements on Binary Systems . . . . .	84
3.4 Conclusion . . . . .	88
<b>4 Optical Diffusion Cell with Periodic Resistive Heating</b>	<b>89</b>
4.1 Experimental Setup and Principles of Measurement . . . . .	89
4.1.1 Setup . . . . .	89
4.1.2 Fabrication of Multilayer Structures . . . . .	91
4.1.3 Heterodyne Detection . . . . .	95

---

4.1.4	Sample Preparation . . . . .	99
4.2	Heat and Mass Diffusion Analysis . . . . .	99
4.2.1	Evolution Equations . . . . .	101
4.2.2	Refractive Index Grating and Heterodyne Diffraction Efficiency . . . . .	102
4.2.3	Stationary Solutions . . . . .	103
4.2.4	Time Dependent Solutions . . . . .	110
4.2.5	Sample Heating . . . . .	115
4.3	Validation of the Method . . . . .	116
4.3.1	Measurement of Heat Diffusion . . . . .	116
4.3.2	Thermal Stability of the Heterodyne Signal . . . . .	120
4.3.3	Measurement of Mass and Thermal Diffusion . . . . .	123
4.4	Conclusion . . . . .	126
<b>5</b>	<b>Summary</b>	<b>128</b>
	<b>Deutsche Zusammenfassung</b>	<b>130</b>
	<b>Bibliography</b>	<b>I</b>
	<b>Danksagung</b>	<b>IX</b>

## Composition Variables and Partial Specific Quantities

Almost the same nomenclature as in the book by de Groot and Mazur [16] is used. Composition variables and partial specific quantities will be abbreviated as follows:

$K$	number of components in the mixture
$m_k$	total mass of component $k$ <sup>1</sup>
$m = \sum m_k$	total mass
$N_k$	total number of particle of component $k$
$N = \sum N_k$	total number of particles
$V_k$	volume occupied by species $k$
$V = \sum V_k$	volume
$\rho = m/V = \sum \rho_k$	total mass density
$\rho_k = m_k/V$	mass density of component $k$ <sup>2</sup>
$n = N/V = \sum n_k$	total number density
$n_k = N_k/V$	number density of component $k$
$M_k = m_k/N_k = \rho_k/n_k$	molecular mass of component $k$ <sup>1</sup>
$c_k = m_k/m = \rho_k/\rho$	weight fraction of component $k$
$x_k = N_k/N = n_k/n$	mole fraction of component $k$
$\phi_k = V_k/V = v_k\rho_k$	volume fraction of component $k$
$U$	internal energy
$u = U/m$	specific internal energy
$u_k = \left(\frac{\partial U}{\partial m_k}\right)_{p,T,m_1,\dots,m_{k-1},m_{k+1},\dots,m_K}$	partial specific internal energy of component $k$

---

<sup>1</sup>Note that in the book by de Groot and Mazur [16]  $m_k$  and  $M_k$  are defined reversely.

<sup>2</sup>Only  $(K - 1)$  mass densities  $\rho_k$  are independent, since, for given temperature  $T$  and pressure  $p$  an equation of state  $\rho_K = f(p, T, \rho_1, \dots, \rho_{K-1})$  holds in (local) thermodynamic equilibrium.

---

$S$	entropy
$s = S/m$	specific entropy
$s_k = \left(\frac{\partial S}{\partial m_k}\right)_{p,T,m_1,\dots,m_{k-1},m_{k+1},\dots,m_K}$	partial specific entropy of component $k$
$H = U + pV$	enthalpy
$h = H/m$	specific enthalpy
$h_k = \left(\frac{\partial H}{\partial m_k}\right)_{p,T,m_1,\dots,m_{k-1},m_{k+1},\dots,m_K}$	partial specific enthalpy of component $k$
$G = U - TS + pV$	Gibbs free energy
$g = G/m$	specific Gibbs free energy
$\mu_k = \left(\frac{\partial G}{\partial m_k}\right)_{p,T,m_1,\dots,m_{k-1},m_{k+1},\dots,m_K}$	chemical potential of component $k$
$\mu'_k = \left(\frac{\partial G}{\partial N_k}\right)_{p,T,N_1,\dots,N_{k-1},N_{k+1},\dots,N_K} = M_k \mu_k$	chemical potential of component $k$ per particle
$v = V/m = 1/\rho$	specific volume
$v_k = \left(\frac{\partial V}{\partial m_k}\right)_{p,T,m_1,\dots,m_{k-1},m_{k+1},\dots,m_K}$	partial specific volume of component $k$

# Chapter 1

## Introduction

The interest in transport coefficients of multicomponent liquid mixtures is rooted both in their relevance for technical applications and in their fundamental importance for a better theoretical understanding of fluids. During the last decade especially the number of publications on the Soret effect [60, 93], also known as the Ludwig-Soret effect, thermal diffusion, or thermodiffusion, has constantly been growing. This off-diagonal effect accounts for the occurrence of mass diffusion that is not driven by a concentration but rather by a temperature gradient. Even though the phenomenon was discovered by Ludwig already in 1856, it is still poorly understood at the microscopic level. There exists, however, a successful thermodynamic phenomenological theory [16], which relates the mass diffusion flux  $\vec{J}$  in a binary mixture to the gradients of temperature and concentration by

$$\vec{J} = -\rho D \vec{\nabla} c - \rho D_T c(1 - c) \vec{\nabla} T. \quad (1.1)$$

$c$  is the concentration of component 1 in weight fractions,  $\rho$  the density, and  $T$  the temperature. Of course, the magnitude of the mass diffusion coefficient  $D$  and the thermal diffusion coefficient  $D_T$  can only be determined from a microscopic theory. Nevertheless a deep understanding of the thermodynamic phenomenological theory is indispensable, since all microscopic theories have to be in agreement with thermodynamics. There are comprehensive textbooks on irreversible thermodynamics by de Groot and Mazur [16] and by Haase [40], which treat all classes of irreversible phenomena in a very general way. However, as the underlying concepts are sometimes rather complex, it is difficult and time consuming for a reader who is mainly interested in the Soret effect, to find the relevant information. Furthermore, since thermal diffusion is only one irreversible phenomenon among many others, these books do not treat it to the last detail. We will therefore give a brief overview of the aspects of the thermodynamic phenomenological theory being important for the description of diffusion and thermal diffusion. Our considerations are based on the above mentioned books, but go beyond them in some cases. To mention only two examples, the differences between irreversible and reversible mass transfer between the two homogenous phases of a heterogenous system or the invariance of transport coefficients against shifts of entropy or enthalpy zero and its consequences have not been considered in Refs. [16, 40] and will be treated in detail. Moreover, we will briefly discuss recent literature work, where thermodynamic principles

have not been correctly incorporated.

The rest of the thesis deals with the measurement of heat, mass, and thermal diffusion. Eq. (1.1) is not suitable for the interpretation of time-resolved experiments. Usually, the heat equation for the temperature  $T$ ,

$$\rho c_p \partial_t T = \vec{\nabla} \cdot [\kappa \vec{\nabla} T] + \dot{Q}, \quad (1.2)$$

and the extended diffusion equation for the concentration  $c$ ,

$$\partial_t c = \vec{\nabla} \cdot [D \vec{\nabla} c + c(1 - c) D_T \vec{\nabla} T], \quad (1.3)$$

are used for the description of coupled heat and mass transport in binary liquids. Here  $c_p$  is the specific heat at constant pressure,  $\kappa$  the thermal conductivity, and  $\dot{Q}$  a source term. The derivation of Eqs. (1.2, 1.3) is not as trivial as it might appear at first glance. Strictly speaking, they only hold if the center of mass velocity  $\vec{v}$  vanishes. It will be shown, that Eqs. (1.2, 1.3) can also be used in case of non-zero  $\vec{v}$ , if all gradients are small and second order terms may be neglected. For that purpose we will generalize the considerations of Ref. [16] to non-isothermal systems.

Although the concept expressed by Eqs. (1.2, 1.3) appears rather simple, experiments that are not hampered by artifacts are not easily conducted. Especially unwanted convection caused by the unavoidable temperature gradients is a major obstacle, and microgravity experiments have been conducted [101] to overcome this problem. Over the years a certain body of experimental data for the Soret coefficient had been accumulated but hardly any values had been cross-checked by another group, and if so, agreement was not guaranteed [51]. In 2003 the results of a measurement campaign with five participating laboratories utilizing different experimental techniques were published and reliable Soret coefficients could be established for three equimolar reference systems [75].

Challenged by the experimental difficulties a number of methods have been developed, which all have certain strengths and weaknesses. A popular classical method is based on the determination of the degree of separation of the fluid components that can be obtained in a thermogravitational experiment. This method has a long history and a large amount of the thermal diffusion data accumulated in the literature has been obtained with this technique [18, 58, 63, 26, 27, 28]. A comprehensive description can be found in the book by Tyrell [98]. Nowadays mainly annular thermogravitational columns are used [9] and in some experiments the space between the two cylinders is filled with a porous medium [14]. Another recent development in this field are thermogravitational columns with laser Doppler velocimetry as optical detection [25, 76]. As all thermogravitational methods are based on the interplay of thermodiffusion and convection, the interpretation of the measurements is necessarily complex. The amount of material needed is substantial and can be a problem



---

in case of expensive isotopic or biological samples. Additional complications arise in case of negative separation ratios.

Another method where flow and thermal diffusion are combined is thermal field flow fractionation (TFFF), which mainly aims at the separation of polymers and colloids in dilute solution [87]. It is neither suitable for higher concentrations nor, because of their rapid diffusion, for small molecules.

Methods that allow for minute sample volumes and small temperature gradients are typically based on optical techniques, either for detection or both for detection and generation of the temperature gradients.

In an optical beam deflection experiment a diffusion cell is heated from above and cooled from below. The concentration gradient induced by the temperature gradient is detected by deflection of a laser beam which passes through the cell in a direction parallel to the top and bottom plates. The time dependence of the deflection angle contains a fast contribution stemming from the temperature and a slow contribution from the concentration gradient. Beam deflection is caused by changes of the refractive index of the liquid associated with the nonuniform temperature and concentration. Optical beam deflection was already used by Meyerhoff and Nachtigall, who employed a Schlieren technique [67, 66], and later by Giglio and Vendramini [36, 37], by Kolodner et al. [54], Zhang et al. [116, 117], and Piazza et al. [74]. Since the diffusion length, the distance between the two plates, is of the order of a few millimeters to one centimeter, establishment of equilibrium is rather slow, especially for systems with small diffusion coefficients such as polymers and systems close to the critical point.

In holographic grating experiments (thermal diffusion forced Rayleigh scattering, TDFRS) light is used not only for detection but also for heating of the fluid. A holographic interference grating is written into the sample. An added dye absorbs and thermalizes the energy of the light field and a temperature grating builds up. The temperature gradients of the temperature grating give rise to thermal diffusion, and a secondary concentration grating is generated. Both the temperature grating and the concentration grating are accompanied by a refractive index grating, which can be read by Bragg diffraction of a readout laser beam. Thyagarajan and Lallemand were the first who observed the Soret effect with forced Rayleigh scattering in the binary liquid mixture CS<sub>2</sub>/ethanol [97]. Later, Pohl studied a critical mixture of 2,6-lutidine/water with the same technique [77]. By using heterodyne detection schemes [52] high sensitivity is achieved and TDFRS has successfully been applied to a broad class of systems ranging from small molecules [17, 111, 70] to polymer solutions of arbitrary concentration [84, 45, 83, 108, 15, 50], colloidal suspensions [94, 69], and critical polymer blends [34, 33].

Another all-optical technique for heating and detection is the thermal-lens method, where the signal is derived from the defocusing of a laser beam transmitted through a slightly absorbing sample. The suitability of the method has been demonstrated in recent experiments [2, 3, 86],

but convection problems are not easily avoided with this technique.

For some special systems, where fluorescent labels can be attached to large molecules such as DNA, Duhr and Braun have demonstrated a further optical method for the study of thermal diffusion [22, 24]. By local heating with an infrared laser and fluorescence detection of the concentration distribution, Soret coefficients of aqueous colloidal solutions could be determined within microfluidic devices.

When comparing all these techniques, TDFRS has a number of indisputable advantages. The micrometer diffusion length within the grating reduces the diffusion time to the millisecond range, which is easily accessible and about six orders of magnitude faster than in case of macroscopic diffusion cells. In particular for systems with small diffusion coefficients of the order of  $10^{-10}$  cm<sup>2</sup>/s, such as binary glass formers [84] or critical polymer blends [34], diffusion times can still be kept within the range of seconds. In a thermal diffusion cell they would already exceed a week, which is hardly feasible. Another major advantage is that only a single Fourier component, the one of the grating vector  $q$ , contributes to the signal, which makes its interpretation particularly simple and even allows for a deconvolution into multiple decay functions for e.g. determination of the molar mass distribution in polymer analysis [53]. Due to the short diffusion lengths, the thin samples and the orientation of the fringes of the grating parallel to the direction of gravity, convection problems can easily be avoided. Being all-optical, the method is non-invasive and ideally suited for remote sensing without direct contact to the sample. The sample volume can be below 1  $\mu$ L. Furthermore it should be mentioned that this technique is not restricted to the determination of mass and thermal diffusion but also allows for the measurement of heat conduction in liquids and solids. In fact, the first holographic grating experiments by Eichler et al. [30] and Pohl et al. [78] in 1973 aimed at the measurement of heat conduction. Whereas Eichler et al. determined the thermal diffusivity of methanol, glycerin and ruby crystals, Pohl et al. studied heat transport in inorganic crystals at low temperatures. Later the method has been used to determine the anisotropic thermal conductivity in liquid crystals [46, 95] and sheared polymer melts [102], to mention only two examples.

There remain, however, unresolved questions and experimental problems of the holographic grating technique. Two of them will be treated in this thesis.

The first one is related to the correct analysis of the detected diffraction efficiency. When treating the problem in one dimension, an analytical expression for the time dependent diffraction efficiency is easily found [8]. The thermal diffusivity  $D_{th} = \kappa/(\rho c_p)$ , the mass diffusion coefficient  $D$ , and the thermal diffusion coefficient  $D_T$  are obtained from a fit of the model to the measured diffraction efficiency. Most holographic grating experiments are interpreted in terms of this one-dimensional description and heat flow into the cell walls and a nonuniform temperature distribution along the optical axis are usually neglected. This is, however, only permissible, if the grating period  $d$  is much smaller than the sample thickness  $l_s$ .

---

If this assumption is not fulfilled, the influence of the heat conducting walls must be taken into account. A few attempts have been undertaken to incorporate the effect of heat conducting walls on the measurement of the thermal diffusivity. The influence of three-dimensional temperature profiles on the determination of mass diffusion and of the Soret effect, however, which requires normalization of the amplitude of the concentration grating to the one of the temperature grating, has not yet been considered. Nagasaka et al. [68] used Green's functions to determine the systematic errors of the measured thermal diffusivities evaluated according to the one-dimensional model. Different aspects of the experiment, like heat conducting walls or a finite beam diameter, were treated independently and the resulting errors were added up. Wang et al. [105, 106] developed a complex three-dimensional model which depends on a large number of parameters and also takes the spatial profile of the heating laser beam into account. We will develop a reasonably simple, practically applicable, two-dimensional model to account for heat conducting walls in transient grating experiments for the measurement of both heat and mass transport. The model will be verified by experiments over a wide range of grating periods  $d$  and sample thicknesses  $l_s$ .

Having solved the problem of heat diffusion into the windows, we are still facing fundamental experimental difficulties. A significant drawback of the holographic technique is related to the generation of the temperature grating within the sample. For optical heating of the usually transparent samples with a laser, a small amount of dye has to be added. This has to be inert and should not give rise to additional signal contributions. While this requirement can usually be fulfilled for organic liquids, it imposes a severe problem to the study of aqueous systems, where suitable dyes are rare. In this respect, contact heating techniques, like optical beam deflection in a diffusion cell, have clear advantages. Additionally, they do not require an expensive laser source.

Ideally, one would combine the short diffusion length and the single  $q$  value of the TDFRS technique with the advantages of a diffusion cell. A direct down-scaling approach is, however, not viable, since the deflected laser cannot be focused down to the required diameter over a distance sufficient to accumulate an appreciable deflection angle. Putnam and Cahill [81] have designed a handy, miniaturized micron-scale beam deflection apparatus that no longer relies on two parallel plates but rather employs two heated metal strips sputtered onto a glass substrate. While this approach leads to significantly shorter equilibration times than the conventional parallel plate diffusion cell, some drawbacks like the multiple Fourier components contributing to the signal, remain.

We will present a new transient grating technique that avoids many of above disadvantages. Its key component is a regular array of strips of indium tin oxide (ITO) with  $10\ \mu\text{m}$  width and  $10\ \mu\text{m}$  spacing on one inner window of the cuvette. It can be heated electrically in order to create a periodic temperature modulation which acts, in the same way as in holographic grating experiments, as a source term for the build-up of a superimposed concentration grating. With such a setup most advantages of TDFRS, like the small sample volume, the insensi-

tivity to convection, short equilibration times, one single Fourier component contributing to the signal, and optical readout by Bragg-diffraction, are retained. They are combined with the major advantages of the beam deflection cell, namely the avoidance of a dye and an expensive writing laser. Similar to holographic grating experiments with very thin sample cells, heat conduction into the walls plays a major role and will be treated in detail.

## Chapter 2

# Thermodynamic–Phenomenological Theory

At first we will give a brief overview of the thermodynamic–phenomenological theory of diffusion and thermodiffusion based on the books by Haase [40] and by de Groot and Mazur [16]. The two fundamental laws of thermodynamics are the first law or law of conservation of energy, and the second law or entropy law. Since the description of non–equilibrium processes must also be built upon these two laws, these laws will first be formulated in an appropriate way. Then the phenomenological equations can be derived from the entropy law or, more specifically, from the entropy production. Also some own results and comments on recent literature work will be included.

Furthermore we will discuss the issue of different reference velocities. Existing models will be modified and extended to become suitable for the description of non–isothermal, multi–component mixtures. We will show, under which conditions simple evolution equations for temperature and composition variables can be obtained. These evolution equations are necessary for the interpretation of our heat, mass and thermal diffusion experiments of Chaps. 3 and 4.

Contrary to Haase and de Groot and Mazur, who present more general treatments of non–equilibrium thermodynamics, we will in particular focus on the precise formulation of all aspects directly related to the Soret effect.

## 2.1 Entropy Production and Phenomenological Equations

### 2.1.1 First Law and Definition of Heat

For a closed system, which may exchange heat but not matter with its surroundings, the first law of thermodynamics reads

$$dE = dQ + dW. \quad (\text{closed system}) \quad (2.1)$$

$dE$  is the change of the total energy  $E$ , which is the sum of internal energy  $U$ , potential energy  $E_{\text{pot}}$  and kinetic energy  $E_{\text{kin}}$ ,

$$E = U + E_{\text{pot}} + E_{\text{kin}}, \quad (2.2)$$

in an infinitesimal state change.  $dQ$  is the heat supplied to the system and

$$dW = dW_l + dW_{\text{diss}} + dW_a = - \sum_i L_i dl_i + dW_{\text{diss}} + dW_a \quad (2.3)$$

is the work done on the system during the same infinitesimal state change. Here, the  $L_i$  and  $l_i$  denote the work coefficients and work coordinates, respectively.  $dW_l$  contains the reversible deformation work ( $-pdV$  with pressure  $p$  and volume  $V$ ) as well as reversible electrification and magnetization work done on the entire system. In the following electrification and magnetization work will be excluded and

$$dW_l = -pdV \quad (2.4)$$

will be used throughout.  $dW_{\text{diss}}$  or  $dW_a$  is the work related to dissipative effects (friction, turbulence or plastic flow during deformation, hysteresis phenomena during electrification or magnetization, electric conduction due to external sources of current, etc.) or to forces, respectively, which accelerate the entire system. For internal state changes ( $dE = dU$ ,  $dW_a = 0$ ) in closed systems it follows from Eqs. (2.1, 2.2, 2.3)

$$dU = dQ + dW_l + dW_{\text{diss}}. \quad (\text{closed system}) \quad (2.5)$$

In open systems the terms work and heat are ambiguous, as has been demonstrated by means of simple examples [39]. To overcome this difficulty we follow Haase [40], who uses Eq. (2.3) also for open systems. This means that the work in an open system is that work which would be done on the system if it was closed. Furthermore we define the heat absorbed by an open phase from the surroundings during an infinitesimal state change as follows

$$dQ = dE - dW - \sum_{k=1}^K h_k d_e m_k. \quad (2.6)$$

$h_k$  is the partial specific enthalpy of species  $k$  in the  $K$ -nary mixture.  $d_e m_k$  is the infinitesimal increase of the total mass  $m_k$  of substance  $k$  due to external causes, i.e. not by chemical reactions inside the phase but by exchange of matter with the outside world. For zero transfer of matter Eq. (2.6) reduces to the first law of thermodynamics in closed systems (Eq. (2.1)).

For internal state changes ( $dE = dU, dW_a = 0$ ) the first law in open systems is thus given by

$$dU = dQ + dW_l + dW_{\text{diss}} + \sum_{k=1}^K h_k d_e m_k. \quad (2.7)$$

If no dissipative, electrification and magnetization effects are present, Eq. (2.7) further reduces to

$$dU = dQ - pdV + \sum_{k=1}^K h_k d_e m_k. \quad (2.8)$$

On the basis of the last equation we can see that the definition of heat for open systems according to Eq. (2.6) is physically meaningful. We consider a homogenous fluid mixture of constant temperature and under constant pressure to which is added more liquid of the same temperature, the same pressure, and the same composition. From Eq. (2.8) follows

$$dQ = dU + pdV - \sum_{k=1}^K h_k d_e m_k = dH - \sum_{k=1}^K h_k d_e m_k = 0, \quad (2.9)$$

where  $H = U + pV$  is the enthalpy of the system. This result is felt to be reasonable. It would not have been obtained for another definition of heat.

### 2.1.2 Entropy Production

Irreversible processes are usually characterized by the entropy balance equation

$$\frac{dS}{dt} = \frac{dS_e}{dt} + \frac{dS_i}{dt}, \quad (2.10)$$

and the relation

$$\frac{dS_i}{dt} \geq 0, \quad (2.11)$$

where the equality sign is valid for the reversible limiting case.  $(dS_e/dt)$  denotes the rate of increase of the entropy of the system by exchange of heat and matter with the surroundings and is called entropy flow. The entropy production  $(dS_i/dt)$  is the rate of increase of entropy of the system due to processes which occur inside the system.

The total rate of increase of the entropy of the system  $(dS/dt)$  and the entropy flow  $(dS_e/dt)$  can be positive, negative, or zero, according to the direction and quantity of the heat and mass fluxes through which the system is connected to the surroundings. The entropy production  $(dS_i/dt)$  on the other hand is never negative and disappears only in the reversible limiting case. For stationary non-equilibrium states there results  $(dS_i/dt) = -(dS_e/dt) > 0$  and  $(dS/dt) = 0$ .

Following Haase [40], the entropy flow and the entropy production will be derived for homogenous, heterogenous (discontinuous), and continuous systems. In all three cases the entropy

balance equation is calculated with the help of the Gibbs relation on considering mass and energy balances.

Strictly speaking, the Gibbs relation

$$TdS = dU + pdV - \sum_{k=1}^K \mu_k dm_k, \quad (2.12)$$

with  $T$  and  $\mu_k$  being the temperature and the chemical potential of component  $k$ , only holds for thermodynamic equilibrium, where the entropy is a state function

$$S = S(U, V, m_1, \dots, m_K) \quad (\text{thermodynamic equilibrium}) \quad (2.13)$$

and can be calculated from the values of the state parameters  $U$ ,  $V$ ,  $m_1$ ,  $\dots$ ,  $m_K$ . The important assumption of non–equilibrium thermodynamics is that each volume element of the system is in a state of local equilibrium with

$$\frac{S}{V} = \frac{S}{V} \left( \frac{U}{V}, \frac{m_1}{V}, \dots, \frac{m_K}{V} \right) \quad (\text{local equilibrium}), \quad (2.14)$$

although the macroscopic state is a non-equilibrium state. Then the Gibbs relation

$$Td \left( \frac{S}{V} \right) = d \left( \frac{U}{V} \right) - \sum_{k=1}^K \mu_k d \left( \frac{m_k}{V} \right) \quad (2.15)$$

holds for each volume element of the system.

### 2.1.2.1 Entropy Production in Homogenous Systems

In a homogenous open system the mass balance of each of the  $K$  components of the mixture is given by

$$dm_k = d_e m_k + d_i m_k = d_e m_k + \sum_{j=1}^r \nu_{kj} d\zeta_j \quad k = 1 \dots K. \quad (2.16)$$

The increase of the total mass  $m_k$  of component  $k$  may be due to mass exchange with the surroundings ( $d_e m_k$ ) or due to internal causes ( $d_i m_k$ ). The internal causes are  $r$  chemical reactions inside the system with  $\nu_{kj}/M_k$  and  $\zeta_j$  the stoichiometric number and the extent of the  $j$ -th chemical reaction, and thus  $\nu_{kj} d\zeta_j$  the production of species  $k$  in the reaction  $j$ .  $M_k$  is the molecular mass of component  $k$ .<sup>1</sup> Since mass is conserved in each separate chemical reaction we have

$$\sum_{k=1}^K \nu_{kj} = 0 \quad j = 1 \dots r. \quad (2.17)$$

<sup>1</sup>If only one ( $r = 1$ ) chemical reaction ( $2 \text{ H}_2 + \text{O}_2 \rightarrow 2 \text{ H}_2\text{O}$ ) takes place in the ternary mixture of hydrogen ( $k = 1$ ), oxygen ( $k = 2$ ), and water ( $k = 3$ ), the stoichiometric numbers are as follows:  $\nu_{11}/M_1 = -2$  (hydrogen),  $\nu_{21}/M_2 = -1$  (oxygen),  $\nu_{31}/M_3 = 2$  (water).



The energy balance is given by Eq. (2.8) which, strictly speaking, represents a definition of heat  $dQ$  for an infinitesimal state change in an open phase without electrification and magnetization and without dissipative effects.

$$dU = dQ - pdV + \sum_{k=1}^K h_k d_e m_k$$

In order to calculate the entropy flow and the entropy production, mass and energy balance Eqs. (2.16, 2.8) have to be inserted into the Gibbs relation (2.12)

$$TdS = dU + pdV - \sum_{k=1}^K \mu_k dm_k$$

Using

$$Ts_k = h_k - \mu_k, \quad (2.18)$$

and defining the affinity of reaction  $j$  by<sup>2</sup>

$$A_j = - \sum_{k=1}^K \nu_{kj} \mu_k \quad (2.19)$$

one obtains

$$TdS = dQ + T \sum_{k=1}^K s_k d_e m_k + \sum_{j=1}^r A_j d\zeta_j, \quad (2.20)$$

where  $s_k$  is the partial specific entropy of component  $k$ . If Eq. (2.20) is compared to the general form of the entropy balance equation Eq. (2.10)

$$\frac{dS}{dt} = \frac{d_e S}{dt} + \frac{d_i S}{dt}$$

one can identify the entropy flow

$$\frac{d_e S}{dt} = \frac{1}{T} \frac{dQ}{dt} + \sum_{k=1}^K s_k \frac{d_e m_k}{dt} \quad (2.21)$$

and the entropy production

$$\frac{d_i S}{dt} = \frac{1}{T} \sum_{j=1}^r A_j \frac{d\zeta_j}{dt} \geq 0. \quad (2.22)$$

The inequality in Eq. (2.22) is valid for an actual (irreversible) path of the reaction, the equality for the reversible limiting case. The entropy flow Eq. (2.21) includes the “heat flow” ( $dQ/dt$ ) and the “flows of matter” ( $d_e m_k/dt$ ), which pass from the surroundings into the homogenous system under consideration. In closed systems, the terms with the mass flows

<sup>2</sup>Note that in the book by de Groot and Mazur [16] the affinity is defined with the opposite sign.

phase'		phase''	
temperature $T'$	pressure $p'$	temperature $T''$	pressure $p''$
volume $V'$	masses $m'_k$	volume $V''$	masses $m''_k$
internal energy $U'$	entropy $S'$	internal energy $U''$	entropy $S''$
chemical potential $\mu'_k$	partial specific enthalpy $h'_k$	chemical potential $\mu''_k$	partial specific enthalpy $h''_k$
...		...	

**Figure 2.1:** Heterogenous (discontinuous) system which consists of two homogenous subsystems (phase' and phase'')

drop out, and one obtains the well known relation  $dS \geq dQ/T$ , where the equality holds for reversible processes.

### 2.1.2.2 Entropy Production in Heterogenous (Discontinuous) Systems

The heterogenous system is shown in Fig. 2.1. It consists of two homogenous subsystems – phase' (temperature  $T'$ , pressure  $p'$ , volume  $V'$ , masses  $m'_k$ , internal energy  $U'$ , entropy  $S'$ , chemical potentials  $\mu'_k$ , partial specific enthalpies  $h'_k$ , partial specific entropies  $s'_k$ ) and phase'' ( $T''$ ,  $p''$ ,  $V''$ ,  $m''_k$ ,  $U''$ ,  $S''$ ,  $\mu''_k$ ,  $h''_k$ ,  $s''_k$ ) – that can exchange mass and heat. The total system shall be closed, so that mass exchange only takes place between the two subsystems. For simplicity chemical reactions are excluded. Then the mass balance of the  $k$ -th component of the  $K$ -nary mixture reads:

$$dm'_k = -dm''_k \quad k = 1 \dots K \quad (2.23)$$

$dm'_k$  ( $dm''_k$ ) is the increase of the mass  $m'_k$  ( $m''_k$ ) of component  $k$  in phase' (phase'').

The energy balance of phase' is given by Eq. (2.8)

$$dU' = d_e Q' + d_i Q' - p' dV' + \sum_{k=1}^K h'_k dm'_k, \quad (2.24)$$

if no electrification, magnetization, dissipative effects or interfacial phenomena are present.  $d_e Q'$  is the heat supplied to phase' from the surroundings of the total system.  $d_i Q'$  is the heat that flows from phase'' to phase'. Accordingly one finds for phase'':

$$dU'' = d_e Q'' + d_i Q'' - p'' dV'' + \sum_{k=1}^K h''_k dm''_k, \quad (2.25)$$

The energy balance of the total system is given by

$$dU = dQ + dW \quad (2.26)$$

with

$$dQ = d_e Q' + d_e Q'' \quad (2.27)$$

$$dW = -p' dV' - p'' dV''. \quad (2.28)$$

On the other hand one has

$$dU = dU' + dU'', \quad (2.29)$$

from which follows with Eqs. (2.24) – (2.28)

$$d_i Q' + \sum_{k=1}^K h'_k dm'_k + d_i Q'' + \sum_{k=1}^K h''_k dm''_k = 0. \quad (2.30)$$

The Gibbs relations of phase' and phase'' are

$$T' dS' = dU' + p' dV' - \sum_{k=1}^K \mu'_k dm'_k \quad (2.31)$$

$$T'' dS'' = dU'' + p'' dV'' - \sum_{k=1}^K \mu''_k dm''_k. \quad (2.32)$$

The change of entropy of the total system  $dS$  can be calculated by inserting the mass balance (2.23) and the energy balances (2.24, 2.25) in the Gibbs relations

$$\begin{aligned} dS = dS' + dS'' &= \frac{d_e Q'}{T'} + \frac{d_e Q''}{T''} + \left( \frac{1}{T'} - \frac{1}{T''} \right) \left( d_i Q' + \sum_{k=1}^K h'_k dm'_k \right) \\ &\quad - \sum_{k=1}^K \left( \frac{\mu'_k}{T'} - \frac{\mu''_k}{T''} \right) dm'_k. \end{aligned} \quad (2.33)$$

Here the relation (2.30) has been used. From comparison of Eq. (2.33) to the general form of the entropy balance equation Eq. (2.10)

$$\frac{dS}{dt} = \frac{d_e S}{dt} + \frac{d_i S}{dt}$$

one obtains the entropy flow

$$\frac{d_e S}{dt} = \frac{1}{T'} \frac{dQ'_e}{dt} + \frac{1}{T''} \frac{dQ''_e}{dt} \quad (2.34)$$

and the entropy production

$$\frac{d_i S}{dt} = \left( J_Q + \sum_{k=1}^K h'_k J_k \right) \left( \frac{1}{T'} - \frac{1}{T''} \right) - \sum_{k=1}^K J_k \left( \frac{\mu'_k}{T'} - \frac{\mu''_k}{T''} \right) \geq 0, \quad (2.35)$$

where  $J_Q = (d_i Q'/dt)$  is the heat flux from phase'' to phase' and  $J_k = (dm'_k/dt)$  the mass flux from phase'' to phase'. The inequality sign in Eq. (2.35) is true for actual (irreversible) processes in the system, the equality sign for reversible limiting cases. Apart from the trivial case in which the phase boundary is impermeable to matter and heat ( $J_k = J_Q = 0$ ) the entropy production only disappears for  $T' = T''$  and  $\mu'_k = \mu''_k$ . From the inequality sign in Eq. (2.35) follows that for  $\mu'_k = \mu''_k$  heat flows from the box with higher temperature to the box with lower temperature. For  $T' = T''$  matter flows from the box with higher chemical potential to the box with lower chemical potential.

**Comments on recent literature work** We will now deal with a special case of the discontinuous system displayed in Fig. 2.1. Mass and heat are exchanged between the two subsystems, but their pressures  $p'$  and  $p''$  and their temperatures  $T'$  and  $T''$  shall be kept constant. According to Eq. (2.28) the work done on the total system is given by

$$dW = -p'dV' - p''dV'' = -\sum_{k=1}^K (p'v'_k - p''v''_k)dm'_k \quad (2.36)$$

with  $v'_k$  and  $v''_k$  the partial specific volumes of component  $k$  in phase' and phase''. As pressure and temperature are kept constant, the entropy change of phase' is

$$dS' = \sum_{k=1}^K s'_k dm'_k. \quad (2.37)$$

From comparison to Eq. (2.21) it follows

$$d_i Q' + d_e Q' = 0 \quad (2.38)$$

In the same way one obtains for phase''

$$d_e Q'' + d_i Q'' = 0. \quad (2.39)$$

With the help of Eq. (2.30) the relation

$$d_e Q' + d_e Q'' = -(d_i Q' + d_i Q'') = \sum_{k=1}^K (h'_k - h''_k)dm'_k. \quad (2.40)$$

is found. Replacing  $d_i Q'$  in Eq. (2.35) according to Eqs. (2.38, 2.40) and using  $h''_k = \mu''_k + T''s''_k$  yields

$$T'd_i S = -\left[\frac{d_e Q''}{T''} + \sum_{k=1}^K s''_k dm'_k\right](T' - T'') - \sum_{k=1}^K (\mu'_k - \mu''_k)dm'_k \geq 0. \quad (2.41)$$

$T'd_iS$  is the dissipation function. It can also be interpreted in terms of dissipated work. As will be shown below (page 17), the heterogenous systems performs the work

$$dW_{\text{rev}} = dW - T'd_iS, \quad (2.42)$$

if the masses are exchanged reversibly between the two subsystems. Here  $dW$  is given by Eq. (2.36).

Although Dhont [19, 20, 21] considers exactly the same discontinuous system with  $K = 2$ , he obtains a different result. His expression for the reversible work reads

$$dW_{\text{rev}} \stackrel{?}{=} (\mu'_1 - \mu''_1)dm'_1 + (\mu'_2 - \mu''_2)dm'_2 = \sum_{k=1}^2 (\mu'_k - \mu''_k)dm'_k. \quad (2.43)$$

Obviously both,  $dW$  and the first term of the dissipation function Eq. (2.41) are missing in the description of Dhont. The first term of the dissipation function, however, is quite important and should not be neglected. It vanishes only in the absence of temperature gradients ( $T' = T''$ ) and expresses the often forgotten fact that heat flows all the time through the system thus permanently producing entropy. Dhont uses a relation  $dF \stackrel{?}{=} dW_{\text{rev}} - SdT$ , which he derives by relating the reversibly exchanged heat to the reversibly exchanged entropy by  $dQ^{\text{rev}} \stackrel{?}{=} TdS$ . This is, however, only true for closed homogenous systems, where no particles are exchanged with the surroundings (see Eq. (2.21)). At this point it should also be stated that all interpretations of thermodynamic potentials in terms of maximum work ( $(\Delta F)_T$ ), maximum non expansion work ( $(\Delta G)_{p,T}$ ), exchanged heat ( $(\Delta H)_p$ ) are not necessarily true for open systems, where the first law is no longer given by  $dU = dQ + dW$ .

**Work for reversible mass exchange** In the literature reversible heat and mass exchange is hardly ever treated. To our knowledge, reversible mass exchange between two subsystems at different temperatures has only been considered by Dhont [19, 20, 21], who obtained Eq. (2.43) by relating the change in free energy to the reversible work. Since this procedure is not necessarily correct for open systems, we will now explicitly calculate the work performed, if heat and mass are reversibly exchanged between the two subsystems of Fig. 2.1 [44]. Again  $p'$ ,  $p''$ ,  $T'$  and  $T''$  shall be kept constant. We will assume  $T' < T''$ . The heat  $d_eQ''$  is supplied to the heterogenous system from the hot thermal bath and the mass  $dm'_1$  is reversibly transferred from phase'' to phase'.

1. First phase'' is brought in contact with a particle reservoir of pure substance 1 with temperature  $T''$ , chemical potential  $\mu''_1$ , and pressure  $p'' - \pi''$  with  $\pi''$  being the osmotic pressure of components 2,  $\dots$ ,  $K$  in phase''. This particle reservoir will be called system  $A$  with volume  $V_A$ , entropy  $S_A$ , total mass  $m_A$ , specific entropy  $s_A = S_A/m_A$ , specific enthalpy  $h_A$ , and specific volume  $v_A = V_A/m_A$ . The mass  $dm'_1$  can be moved from

phase” to the particle reservoir without any dissipative effects.

2. After separating system  $A$  from phase”, it is first isothermally expanded or compressed and then adiabatically expanded to be converted into system  $B$ , which has temperature  $T' < T''$ , chemical potential  $\mu'_1$ , and pressure  $p' - \pi'$ .  $\pi'$  is the osmotic pressure of species 2,  $\dots$ ,  $K$  in phase’. Further state parameters of system  $B$  are  $V_B$ ,  $m_B = m_A$ ,  $S_B$ ,  $s_B$ ,  $h_B$ ,  $v_B$ .
3. In the next step system  $B$  is brought in contact with phase’.  $dm'_1$  can be reversibly transferred from system  $B$  to phase’.
4. The total heat supplied to the heterogenous system from the hot thermal bath at  $T''$  is  $d_e Q''$ . Part of this heat has already been used in steps 1 and 2. The remaining heat  $dQ''_4$  can now be used to drive a reversible heat engine between the hot thermal bath ( $T''$ ) and the cold thermal bath ( $T'$ ). The performed work is given by [5]

$$dW_4 = -dQ''_4 \left(1 - \frac{T'}{T''}\right). \quad (2.44)$$

The corresponding works and heats are:

- (a) heat and mass exchange between phase”/phase’ and particle reservoir (steps 1 and 3):  
Phase” and system  $A$  as well as phase’ and system  $B$  are heterogenous systems where pressures and temperatures are kept constant within the subsystems. Therefore they may be described by Eqs. (2.36)– (2.40). For step 1 it is found

$$dW''_1 = p'' v''_1 dm'_1 \quad (2.45)$$

$$dW_1^A = -(p'' - \pi'') v_A dm'_1 \quad (2.46)$$

$$d_e Q_1^A + d_e Q_1'' = (h_A - h''_1) dm'_1, \quad (2.47)$$

and accordingly for step 3

$$dW'_3 = -p' v'_1 dm'_1 \quad (2.48)$$

$$dW_3^B = (p' - \pi') v_B dm'_1 \quad (2.49)$$

$$d_e Q'_3 + d_e Q_3^B = (h'_1 - h_B) dm'_1. \quad (2.50)$$

- (b) isothermal expansion/compression and adiabatic expansion of particle reservoir (step 2):

The particle reservoir is first isothermally ( $T''$ ) expanded or compressed until its entropy is equal to  $S_B$ . In a second step it is adiabatically expanded until its temperature equals

$T'$ . During these two processes it exchanges the heat

$$\Delta Q_2 = T''(S_B - S_A). \quad (2.51)$$

with the thermal bath of temperature  $T''$  and it performs the work

$$\begin{aligned} \Delta W_2 &= \Delta U_2 - \Delta Q_2 \\ &= (\mu'_1 - \mu''_1)m_A - (p' - \pi')V_B + (p'' - \pi'')V_A + T'S_B - T''S_A - \Delta Q_2 \\ &= (\mu'_1 - \mu''_1)m_A - (p' - \pi')V_B + (p'' - \pi'')V_A + S_B(T' - T''). \end{aligned} \quad (2.52)$$

Here the first law for closed systems and  $U = \mu m - pV + TS$  have been used. The contributions of the mass  $dm'_1$  to  $\Delta Q_2$  and  $\Delta W_2$  are

$$dW_2 = [(\mu'_1 - \mu''_1) - (p' - \pi')v_B + (p'' - \pi'')v_A + s_B(T' - T'')]dm'_1 \quad (2.53)$$

$$dQ_2 = T''(s_B - s_A)dm'_1. \quad (2.54)$$

(c) reversible heat engine between thermal bathes at  $T''$  and  $T' < T''$  (step 4):

Already in step 1 and step 2 heat has been extracted from the hot thermal bath ( $T''$ ).

There remains

$$dQ''_4 = d_e Q'' - d_e Q''_1^A - d_e Q''_1 - dQ_2. \quad (2.55)$$

By inserting Eqs. (2.47, 2.54) into Eq. (2.55) and by using

$$\mu''_1 = h_A - T'' s_A = h''_1 - T'' s''_1 \quad (2.56)$$

one obtains

$$dQ''_4 = d_e Q'' + T''(s''_1 - s_B)dm'_1. \quad (2.57)$$

Hence, according to Eq. (2.44) the heat engine performs the work

$$dW_4 = -\frac{d_e Q''}{T''}(T'' - T') - (s''_1 - s_B)(T'' - T')dm'_1 \quad (2.58)$$

and supplies the heat

$$dQ'_4 = -dW_4 - dQ''_4 = -d_e Q'' \frac{T'}{T''} - T'(s''_1 - s_B)dm'_1 \quad (2.59)$$

to the cold thermal bath ( $T'$ ).

Now we have to sum over steps 1–4. The total work performed can be obtained from Eqs. (2.45, 2.46, 2.48, 2.49, 2.53, 2.58)

$$\begin{aligned} dW^{\text{rev}} &= dW_1'' + dW_1^A + dW_2 + dW_3' + dW_3^B + dW_4 \\ &= -(p'v_1' - p''v_1'')dm_1' + \left[ \frac{d_e Q''}{T''} + s_1'' dm_1' \right] (T' - T'') + (\mu_1' - \mu_1'') dm_1' \end{aligned} \quad (2.60)$$

in perfect agreement with Eqs. (2.36, 2.41, 2.42).

The heats exchanged with the hot ( $T''$ ) and cold ( $T'$ ) thermal baths are given by

$$dQ^{\text{rev, hot}} = d_e Q_1^A + d_e Q_1'' + dQ_2 + dQ_4'' = d_e Q'' \quad (2.61)$$

$$dQ^{\text{rev, cold}} = dQ_4' + d_e Q_3' + d_e Q_3^B = d_e Q' - (dW^{\text{rev}} - dW) \quad (2.62)$$

as can be shown with the help of Eqs. (2.55, 2.50, 2.59, 2.40, 2.38, 2.60, 2.36, 2.56) and by using  $\mu_1' = h_B - T's_B$ .  $d_e Q'$  is the heat exchanged between the heterogenous system and the cold thermal bath in the irreversible process. From Eq. (2.42) and from the positive sign of the dissipation function it follows that

$$-dQ^{\text{rev, cold}} = -d_e Q' + (dW^{\text{rev}} - dW) = -d_e Q' - T'd_i S \leq -d_e Q'. \quad (2.63)$$

If the two subsystems reversibly exchange heat and mass, less heat is supplied to the cold thermal bath ( $T'$ ) than for irreversible heat and mass transfer. This heat difference is converted into work in the reversible case. The change in internal energy is independent of the path of the process, since it is merely determined by the initial and the final state.

### 2.1.2.3 Entropy Production in Continuous Systems

In a continuous system, intensive quantities such as density, pressure, temperature, concentration, etc., depend on the space–coordinates in a continuous manner. The mass balance of each of the  $K$  components of the mixture is thus given by a continuity equation

$$\frac{\partial \rho_k}{\partial t} = -\vec{\nabla} \cdot (\rho_k \vec{v}_k) + \sum_{j=1}^r \nu_{kj} J_j \quad k = 1 \dots K, \quad (2.64)$$

where  $\rho_k = m_k/V$  is the mass density of component  $k$ ,  $\vec{v}_k$  is the velocity of component  $k$ ,  $\nu_{kj}/M_k$  is the stoichiometric number and  $\nu_{kj} J_j$  the production of  $k$  per unit volume in the  $j$ -th chemical reaction. Summing Eq. (2.64) over all substances  $k$  and using Eq. (2.17) one obtains the law of conservation of mass

$$\frac{\partial \rho}{\partial t} = -\vec{\nabla} \cdot (\rho \vec{v}) \quad (2.65)$$



with the total density

$$\rho = \sum_{k=1}^K \rho_k = \sum_{k=1}^K \frac{m_k}{V} = \frac{m}{V} \quad (2.66)$$

and the center of mass velocity

$$\vec{v} = \sum_{k=1}^K \frac{\rho_k}{\rho} \vec{v}_k = c_k \vec{v}_k, \quad (2.67)$$

where the total mass  $m = \sum m_k$  and the weight fractions  $c_k = m_k/m$  have been introduced.

The energy balance for a volume element of a continuous system arises from the concept of heat, since such a space element represents an open region. We have seen in Sec. 2.1.1 that it was meaningful and useful to define the heat  $dQ$  supplied to a single open phase for an infinitesimal state change using Eq. (2.6). Then the corresponding change of internal energy is given by

$$dU = dE - dE_{\text{kin}} - dE_{\text{pot}} = dQ + \sum_{k=1}^K h_k d_e m_k + dW - dE_{\text{kin}} - dE_{\text{pot}}. \quad (2.68)$$

The conversion of Eq. (2.68) to continuous systems reads

$$\underbrace{\frac{\partial(\rho u)}{\partial t} + \vec{\nabla} \cdot (\rho u \vec{v})}_{\Rightarrow dU} = -\underbrace{\vec{\nabla} \cdot (\vec{J}_Q + \sum_{k=1}^K h_k \vec{J}_k)}_{\Rightarrow dQ + \sum_{k=1}^K h_k d_e m_k} + \underbrace{\sum_{k=1}^K \vec{J}_k \cdot \vec{F}_k - p \vec{\nabla} \cdot \vec{v}}_{\Rightarrow dW - dE_{\text{kin}} - dE_{\text{pot}}} - \underbrace{\sum_{i,j=1}^3 \Pi_{ij} \frac{\partial v_i}{\partial x_j}}_{\Rightarrow \text{viscous flow}}, \quad (2.69)$$

where  $u = U/m$  is the specific internal energy and  $\vec{J}_Q$  is the heat flow<sup>3</sup>, which is defined by this equation. Furthermore

$$\vec{J}_k = \rho_k (\vec{v}_k - \vec{v}) \quad (2.70)$$

is the mass flow of component  $k$ ,  $\vec{F}_k$  the force per unit mass exerted on component  $k$ ,  $\Pi_{ij}$  the viscous pressures,  $v_i$  the three components of  $\vec{v}$  in a rectangular coordinate system, and  $x_j$  the three cartesian space coordinates. The brackets and arrows show which terms in Eq. (2.69) correspond to which terms in Eq. (2.68). This is not immediately obvious for the expressions containing work, kinetic energy and potential energy. For a derivation see Ref. [40].

From the Gibbs relation (2.15) we obtain for the local rate of increase of the entropy density in the volume element

$$\frac{\partial(\rho s)}{\partial t} = \frac{1}{T} \frac{\partial(\rho u)}{\partial t} - \frac{1}{T} \sum_{k=1}^K \mu_k \frac{\partial \rho_k}{\partial t}, \quad (2.71)$$

where  $s = S/m$  is the specific entropy.

<sup>3</sup>In the book by de Groot and Mazur [16]  $\vec{J}_Q$  is called reduced heat flow ( $\vec{J}_q$ ).

Just in the same way as for homogenous systems (Sec. 2.1.2.1) and heterogenous systems (Sec. 2.1.2.2) the entropy balance equation is derived by inserting mass balance (2.64) and energy balance (2.69) in the Gibbs relation (2.71). If the following relations are used

$$\vec{\nabla}\left(\frac{\mu_k}{T}\right) = h_k \vec{\nabla}\left(\frac{1}{T}\right) + \frac{1}{T}(\vec{\nabla}\mu_k)_T \quad (2.72)$$

$$\vec{\nabla}p = \sum_{k=1}^K \rho_k (\vec{\nabla}\mu_k)_T \quad (\text{Gibbs Duhem relation}) \quad (2.73)$$

$$Ts_k = h_k - \mu_k \quad (2.74)$$

$$T\rho s = \sum_{k=1}^K \rho_k (h_k - \mu_k) = \rho u + p - \sum_{k=1}^K \rho_k \mu_k, \quad (2.75)$$

one obtains

$$\frac{\partial(\rho s)}{\partial t} + \vec{\nabla} \cdot (\rho s \vec{v}) = -\vec{\nabla} \cdot \vec{J}_S + \sigma \quad (2.76)$$

with the entropy flow

$$\vec{J}_S = \frac{\vec{J}_Q}{T} + \sum_{k=1}^K s_k \vec{J}_k \quad (2.77)$$

and the local entropy production

$$\begin{aligned} \sigma = & \left[ \vec{J}_Q + \sum_{k=1}^K h_k \vec{J}_k \right] \cdot \vec{\nabla}\left(\frac{1}{T}\right) - \frac{1}{T} \sum_{k=1}^K \vec{J}_k \cdot \left[ T \vec{\nabla}\left(\frac{\mu_k}{T}\right) - \vec{F}_k \right] \\ & + \frac{1}{T} \sum_{j=1}^r A_j J_j - \frac{1}{T} \sum_{i,j=1}^3 \Pi_{ij} \frac{\partial v_i}{\partial x_j} \geq 0, \end{aligned} \quad (2.78)$$

where the affinity  $A_j$  has been defined by Eq. (2.19). The entropy flow has its analog in Eq. (2.21) for the entropy flow in homogenous systems. Three of the terms in Eq. (2.78) have already been encountered in homogenous (Sec. 2.1.2.1) and heterogenous (Sec. 2.1.2.2) systems. The first part of Eq. (2.78) including heat ( $\vec{J}_Q$ ) and mass ( $\vec{J}_k$ ) fluxes is analogous to the entropy production in a discontinuous system (Eq. (2.35)), where chemical reactions are excluded. Entropy production because of chemical reactions ( $\sum A_j J_j / T$ ) also appears in homogenous systems (Eq. (2.22)). Only the terms concerning external forces ( $\vec{F}_k$ ) and viscous flow ( $\Pi_{ij}$ ) have not been considered before. The inequality sign in Eq. (2.78) is valid for the actual irreversible course of the processes inside the volume element. The equality sign holds for the reversible limiting case, i.e. if the thermodynamic equilibrium conditions are satisfied within the system.

Alternative expressions for the local entropy production are

$$\sigma = \vec{J}_Q \cdot \vec{\nabla} \left( \frac{1}{T} \right) - \frac{1}{T} \sum_{k=1}^K \vec{J}_k \cdot \left[ (\vec{\nabla} \mu_k)_T - \vec{F}_k \right] + \frac{1}{T} \sum_{j=1}^r A_j J_j - \frac{1}{T} \sum_{i,j=1}^3 \Pi_{ij} \frac{\partial v_i}{\partial x_j} \quad (2.79)$$

$$\sigma = T \vec{J}_S \cdot \vec{\nabla} \left( \frac{1}{T} \right) - \frac{1}{T} \sum_{k=1}^K \vec{J}_k \cdot \left[ (\vec{\nabla} \mu_k) - \vec{F}_k \right] + \frac{1}{T} \sum_{j=1}^r A_j J_j - \frac{1}{T} \sum_{i,j=1}^3 \Pi_{ij} \frac{\partial v_i}{\partial x_j} \quad (2.80)$$

which follow from Eq. (2.78) with Eq. (2.72) or with Eqs. (2.74, 2.77), respectively.

### 2.1.3 Phenomenological Equations and Onsager Coefficients

It is known empirically that for a large class of irreversible phenomena and under a wide range of experimental conditions the irreversible flows are linear functions of the thermodynamic forces [16]

$$J_i = \sum_j L_{ij} X_j, \quad (2.81)$$

where  $J_i$  and  $X_i$  are any of the cartesian components of the independent fluxes and thermodynamic forces appearing in the expression for the entropy production, which is of the form

$$\sigma = \sum_i J_i X_i. \quad (2.82)$$

The quantities  $L_{ij}$  are called phenomenological coefficients or Onsager coefficients and the relations (2.81) will be referred to as the phenomenological equations, Onsager equations or linear laws. From the requirement  $\sigma \geq 0$  follows that all diagonal elements are positive  $L_{ii} \geq 0$ , whereas the off-diagonal elements must satisfy conditions of the form  $L_{ii} L_{kk} \geq \frac{1}{4} (L_{ik} + L_{ki})^2$ . Furthermore the Onsager Reciprocal Relations imply  $L_{ik} = L_{ki}$ .

In the following the phenomenological equations (2.81) will be given in explicit form for continuous systems without chemical reactions and viscous flow phenomena. Relations between the Onsager coefficients and the experimentally accessible diffusion coefficients and heat conductivities will be deduced for binary liquids. The dependence of Onsager coefficients on the choice of enthalpy or entropy zero will be discussed. Finally, an expression for the Soret coefficient in dilute solutions will be derived, which will be compared to the result of Duhr and Braun [24].

### 2.1.3.1 Phenomenological Equations

If we exclude chemical reactions and viscous flow phenomena and if we replace the  $K$ -th diffusion current  $\vec{J}_K$  in the entropy production (2.79) by

$$\vec{J}_K = - \sum_{k=1}^{K-1} \vec{J}_k \quad (2.83)$$

we obtain

$$\sigma = -\frac{1}{T^2} \vec{J}_Q \cdot \vec{\nabla} T - \frac{1}{T} \sum_{k=1}^{K-1} \vec{J}_k \cdot [\{\vec{\nabla}(\mu_k - \mu_K)\}_T - \vec{F}_k + \vec{F}_K], \quad (2.84)$$

which contains only independent fluxes and forces. Hence the phenomenological equations read

$$\vec{J}_Q = -L_{qq} \frac{\vec{\nabla} T}{T^2} - \sum_{k=1}^{K-1} L_{qk} \frac{\{\vec{\nabla}(\mu_k - \mu_K)\}_T - \vec{F}_k + \vec{F}_K}{T} \quad (2.85)$$

$$\vec{J}_i = -L_{iq} \frac{\vec{\nabla} T}{T^2} - \sum_{k=1}^{K-1} L_{ik} \frac{\{\vec{\nabla}(\mu_k - \mu_K)\}_T - \vec{F}_k + \vec{F}_K}{T} \quad i = 1 \dots K-1 \quad (2.86)$$

with Onsager reciprocal relations  $L_{qi} = L_{iq}$  and  $L_{ik} = L_{ki}$ . An important special case of Eqs. (2.85, 2.86) is a binary mixture ( $K = 2$ ) in the absence of external forces ( $\vec{F}_1 = \vec{F}_2 = 0$ )

$$\vec{J}_Q = -L_{qq} \frac{\vec{\nabla} T}{T^2} - L_{q1} \frac{\{\vec{\nabla}(\mu_1 - \mu_2)\}_T}{T} \quad (2.87)$$

$$\vec{J}_1 = -L_{1q} \frac{\vec{\nabla} T}{T^2} - L_{11} \frac{\{\vec{\nabla}(\mu_1 - \mu_2)\}_T}{T}, \quad (2.88)$$

where  $L_{11} \geq 0$ ,  $L_{qq} \geq 0$ ,  $L_{1q} = L_{q1}$ , and  $L_{11}L_{qq} - L_{1q}^2 \geq 0$ .<sup>4</sup> In mechanical equilibrium

$$\vec{\nabla} p = \sum_{k=1}^K \rho_k \vec{F}_k \quad (2.89)$$

pressure gradients vanish in the absence of external forces and from the Gibbs Duhem relation (2.73) follows

$$\{\vec{\nabla}(\mu_1 - \mu_2)\}_{p,T} = \frac{1}{c_2} (\vec{\nabla} \mu_1)_{p,T}. \quad (2.90)$$

---

<sup>4</sup> $L_{11}$ ,  $L_{1q}$ ,  $L_{q1}$  and  $L_{qq}$  are the phenomenological coefficients used by de Groot and Mazur [16] (see also footnote 3).

Therefore instead of Eqs. (2.87, 2.88) one may write

$$\vec{J}_Q = -L_{qq} \frac{\vec{\nabla}T}{T^2} - L_{q1} \frac{(\vec{\nabla}\mu_1)_{p,T}}{c_2 T} \quad (2.91)$$

$$\vec{J}_1 = -L_{1q} \frac{\vec{\nabla}T}{T^2} - L_{11} \frac{(\vec{\nabla}\mu_1)_{p,T}}{c_2 T}. \quad (2.92)$$

Eqs. (2.87, 2.88) are based on the expression (2.79) for the entropy production  $\sigma$ . Alternatively  $\sigma$  from Eq. (2.78) or from Eq. (2.80) may be used as a starting point. Using Eq. (2.78) the phenomenological equations for a binary liquid in the absence of external forces read

$$\vec{J}_Q + (h_1 - h_2)\vec{J}_1 = -l_{qq} \frac{\vec{\nabla}T}{T^2} - l_{q1} \vec{\nabla} \left( \frac{\mu_1 - \mu_2}{T} \right) \quad (2.93)$$

$$\vec{J}_1 = -l_{1q} \frac{\vec{\nabla}T}{T^2} - l_{11} \vec{\nabla} \left( \frac{\mu_1 - \mu_2}{T} \right) \quad (2.94)$$

with  $l_{11} \geq 0$ ,  $l_{qq} \geq 0$ ,  $l_{1q} = l_{q1}$ , and  $l_{11}l_{qq} - l_{1q}^2 \geq 0$ . Starting from Eq. (2.80) one obtains

$$T\vec{J}_S = \vec{J}_Q + T(s_1 - s_2)\vec{J}_1 = -\gamma T^2 \frac{\vec{\nabla}T}{T^2} - \delta T \frac{\vec{\nabla}(\mu_1 - \mu_2)}{T} \quad (2.95)$$

$$\vec{J}_1 = -\beta T^2 \frac{\vec{\nabla}T}{T^2} - \alpha T \frac{\vec{\nabla}(\mu_1 - \mu_2)}{T} \quad (2.96)$$

with  $\alpha \geq 0$ ,  $\gamma \geq 0$ ,  $\delta = \beta T$ , and  $\alpha\gamma - \beta^2 T \geq 0$ .<sup>5</sup>

Of course all descriptions Eqs. (2.87, 2.88), Eqs. (2.93, 2.94), and Eqs. (2.95, 2.96) are equally valid and any of the sets of Onsager coefficients may be used. It will turn out, however, that  $L_{1q}$  and  $L_{qq}$  are invariant against shifts of entropy or energy zero. In contrast,  $l_{1q}$  and  $l_{qq}$  depend on choice of enthalpy zero and  $\beta$  and  $\gamma$  depend on choice of entropy zero.

### 2.1.3.2 Relation between Onsager Coefficients, Diffusion Coefficients and Heat Conductivities

The experimentally accessible coefficients are the heat conductivity in the uniform state  $\kappa_0$  ( $\vec{\nabla}c_1 = 0$ ), the heat conductivity in the stationary state  $\kappa_\infty$  ( $\vec{J}_1 = 0$ ),<sup>6</sup> the Dufour coefficient  $D''$ , the heat of transport  $Q_1^*$ , the thermal diffusion coefficient  $D_T$ , and the diffusion coefficient

<sup>5</sup> $\alpha$ ,  $\beta$ ,  $\gamma$ , and  $\delta$  are the phenomenological coefficients as introduced by Landau [57]. Landau uses the abbreviation  $\mu = \mu_1 - \mu_2$ . Landau's heat flow  $\vec{q}$  is related to  $\vec{J}_Q$  by  $\vec{q} = \vec{J}_Q + (h_1 - h_2)\vec{J}_1$ .

<sup>6</sup>The heat conductivity  $\lambda$  of de Groot and Mazur [16] corresponds to  $\kappa_0$ , whereas Landau's  $\kappa$  [57] is identical to  $\kappa_\infty$ .

D. They are defined by

$$\begin{aligned}\vec{J}_Q &= -\kappa_0 \vec{\nabla} T - \rho_1 \left( \frac{\partial \mu_1}{\partial c_1} \right)_{p,T} T D'' \vec{\nabla} c_1 \\ &= -\kappa_\infty \vec{\nabla} T + Q_1^* \vec{J}_1\end{aligned}\quad (2.97)$$

$$\vec{J}_1 = -\rho D \vec{\nabla} c_1 - \rho c_1 c_2 D_T \vec{\nabla} T. \quad (2.98)$$

By comparing Eqs. (2.87, 2.88), Eqs. (2.93, 2.94), and Eqs. (2.95, 2.96) to Eqs. (2.97, 2.98) one obtains the following relations between phenomenological coefficients, diffusion coefficients and heat conductivities

$$\kappa_\infty = \frac{1}{T^2} \left( L_{qq} - \frac{L_{1q}^2}{L_{11}} \right) = \frac{1}{T^2} \left( l_{qq} - \frac{l_{1q}^2}{l_{11}} \right) = \gamma - \beta^2 \frac{T}{\alpha} \geq 0 \quad (2.99)$$

$$D = \frac{L_{11}}{\rho c_2 T} \left( \frac{\partial \mu_1}{\partial c_1} \right)_{p,T} = \frac{l_{11}}{\rho c_2 T} \left( \frac{\partial \mu_1}{\partial c_1} \right)_{p,T} = \frac{\alpha}{\rho c_2} \left( \frac{\partial \mu_1}{\partial c_1} \right)_{p,T} \geq 0 \quad (2.100)$$

$$c_1 c_2 D_T = \frac{L_{1q}}{\rho T^2} = \frac{l_{1q} - l_{11}(h_1 - h_2)}{\rho T^2} = \frac{\alpha}{\rho} \left[ \frac{\partial(\mu_1 - \mu_2)}{\partial T} \right]_{p,c_1} + \frac{\beta}{\rho} \quad (2.101)$$

$$D'' = D_T \quad (2.102)$$

$$Q_1^* = c_1 \left( \frac{\partial \mu_1}{\partial c_1} \right)_{p,T} T \frac{D_T}{D} \quad (2.103)$$

$$\kappa_0 = \kappa_\infty + \rho c_1 c_2 Q_1^* D_T \geq \kappa_\infty. \quad (2.104)$$

Here Eq. (2.72), Eq. (2.90)<sup>7</sup> and

$$\vec{\nabla} \mu_i = (\vec{\nabla} \mu_i)_T + \left( \frac{\partial \mu_i}{\partial T} \right)_{c_1,p} \vec{\nabla} T = \left( \frac{\partial \mu_i}{\partial c_1} \right)_{p,T} \vec{\nabla} c_1 + \left( \frac{\partial \mu_i}{\partial T} \right)_{c_1,p} \vec{\nabla} T \quad (2.105)$$

have been used. The inequalities  $L_{ii} \geq 0$  and  $L_{ii} L_{kk} - L_{ik}^2 \geq 0$  imply  $\kappa_\infty > 0$ ,  $\kappa_0 > 0$  and  $D > 0$ . From the reciprocal relation  $L_{ik} = L_{ki}$  follows  $D'' = D_T$ . The thermal conductivity for the uniform state  $\kappa_0$  is larger than the thermal conductivity for the stationary state  $\kappa_\infty$ .

### 2.1.3.3 Invariance against Shifts of Enthalpy or Entropy Zero

It has already been noted, that not all Onsager coefficients are invariant against shifts of enthalpy or entropy zero. Most authors, however, seem to be unaware of this fact, and only in Ref. [62] there is one sentence mentioning the problem. Therefore we will now explain in detail the reasons and consequences. Firstly, one has to calculate the derivations of the chemical potentials and the partial specific enthalpies appearing in Eqs. (2.100, 2.101) from

<sup>7</sup>Landau's result [57] for  $D$  is recovered by replacing  $c_2^{-1} [\partial \mu_1 / \partial c_1]_{p,T}$  by  $[\partial \mu / \partial c_1]_{p,T}$  in Eq. (2.100).

the Gibbs free energy of mixing

$$\begin{aligned}\Delta G_{\text{mix}} &= G(p, T, m_1, m_2) - G_1^0(p, T, m_1) - G_2^0(p, T, m_2) \\ &= m \left( c_1 [\mu_1(p, T, c_1) - \mu_1^0(p, T)] + c_2 [\mu_2(p, T, c_1) - \mu_2^0(p, T)] \right).\end{aligned}\quad (2.106)$$

$G$  is the Gibbs free energy of the mixture,  $G_i^0$  the Gibbs free energy of pure component  $i$ ,  $m_i$  the total mass of component  $i$  in the mixture,  $\mu_i$  the chemical potential of component  $i$  in the mixture,  $\mu_i^0$  the chemical potential of pure component  $i$ , and  $m = m_1 + m_2$  the total mass.  $\Delta G_{\text{mix}}$  can be obtained from an equation of state and is invariant against shifts of enthalpy or entropy zero.

With  $c_2 = 1 - c_1$  and Eq. (2.90) follows

$$\mu_1(p, T, c_1) - \mu_2(p, T, c_1) = \left[ \frac{\partial(\Delta G_{\text{mix}}/m)}{\partial c_1} \right]_{p, T} + \mu_1^0(p, T) - \mu_2^0(p, T) \quad (2.107)$$

and thus

$$\frac{1}{c_2} \left( \frac{\partial \mu_1}{\partial c_1} \right)_{p, T} = \left[ \frac{\partial(\mu_1 - \mu_2)}{\partial c_1} \right]_{p, T} = \left[ \frac{\partial^2(\Delta G_{\text{mix}}/m)}{\partial c_1^2} \right]_{p, T} \quad (2.108)$$

$$\left[ \frac{\partial(\mu_1 - \mu_2)}{\partial T} \right]_{p, c_1} = -(s_1 - s_2) = \left[ \frac{\partial^2(\Delta G_{\text{mix}}/m)}{\partial c_1 \partial T} \right]_p - (s_1^0 - s_2^0) \quad (2.109)$$

$$h_1 - h_2 = \left[ \frac{\partial(\Delta G_{\text{mix}}/m)}{\partial c_1} \right]_{p, T} - T \left[ \frac{\partial^2(\Delta G_{\text{mix}}/m)}{\partial c_1 \partial T} \right]_p + (h_1^0 - h_2^0) \quad (2.110)$$

Here  $s_i$  and  $h_i$  are the partial specific entropy and enthalpy of component  $i$  in the mixture, and  $s_i^0$  and  $h_i^0$  are the specific entropy and enthalpy of the pure substance  $i$ .  $s_i^0$  and  $h_i^0$  depend on choice of entropy or enthalpy zero and therefore  $[\partial(\mu_1 - \mu_2)/\partial T]_{p, c_1}$  and  $(h_1 - h_2)$  also do. Note that component 1 and 2 generally have different zero points of entropy and enthalpy. The measurable coefficients  $\kappa_\infty$ ,  $D$ , and  $D_T$ , in contrast, have to be invariant under shifts of enthalpy or entropy zero. This has the following consequences for the Onsager coefficients (cf. Eqs. (2.99-2.101)):  $L_{11} = l_{11} = \alpha T$ ,  $L_{1q}$  and  $L_{qq}$  do not depend on the choice of enthalpy or entropy zero.  $l_{1q}$  and  $l_{qq}$  depend on the choice of enthalpy zero.  $\beta$  and  $\gamma$  depend on the choice of entropy zero. In particular, by inserting Eq. (2.109) into Eq. (2.101)  $\beta$  is found to be of the form

$$\beta = \alpha(s_1^0 - s_2^0) + \Delta\beta, \quad (2.111)$$

where  $\Delta\beta$  does not depend on entropy zeros.

It is instructive to consider the experiments that correspond to the terms appearing in Eq. (2.109):

$$-s_1 + s_2 \quad \text{and} \quad \left[ \frac{\partial^2(\Delta G_{\text{mix}}/m)}{\partial c_1 \partial T} \right]_p = -s_1 + s_2 + s_1^0 - s_2^0 \quad (2.112)$$

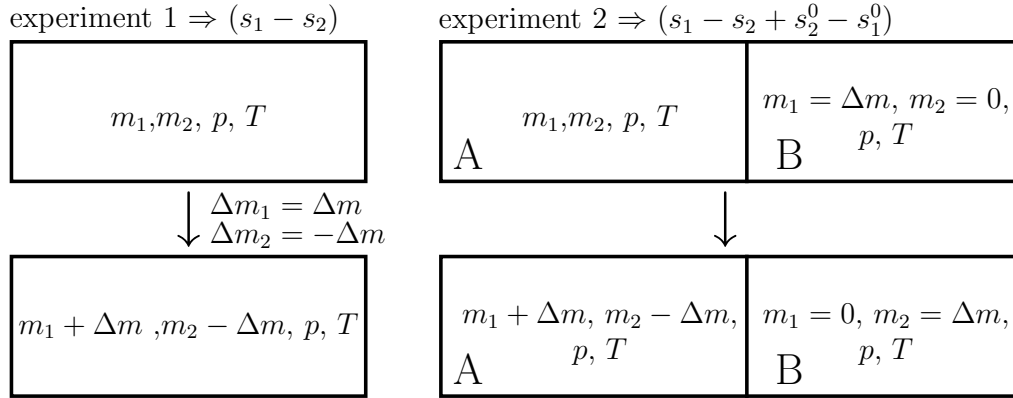


**Figure 2.2:** Experiments corresponding to the two terms of (2.112).

The first term of (2.112) is related to an experiment in an open system, to which an amount  $\Delta m$  of substance 1 is added and from which an amount of  $\Delta m$  of substance 2 is removed (see Fig. 2.2, experiment 1). The entropy change of the system is given by

$$\Delta S^{\text{open}} = (s_1 - s_2)\Delta m. \quad (2.113)$$

According to Eq. (2.21) the entropy change of the open system cannot be directly related to the heat exchanged with the surroundings. Therefore  $\Delta S^{\text{open}}$  is not a measurable quantity. Accordingly the term  $-(s_1 - s_2)$  depends on the choice of the zero point of entropy.

The second term in (2.112) corresponds to an experiment in a closed system consisting of two subsystems. At the beginning subsystem A contains the masses  $m_1^A = m_1$ ,  $m_2^A = m_2$  and subsystem B contains the masses  $m_1^B = \Delta m$ ,  $m_2^B = 0$ . At the end of the experiment A has  $m_1^A = m_1 + \Delta m$ ,  $m_2^A = m_2 - \Delta m$  and B has  $m_1^B = 0$ ,  $m_2^B = \Delta m$  (see Fig. 2.2, experiment 2). The entropy change of the total system is made up from the entropy changes of the two subsystems

$$\Delta S^{\text{closed}} = \Delta S^A + \Delta S^B = (s_1 - s_2)\Delta m + (s_2^0 - s_1^0)\Delta m. \quad (2.114)$$

If the experiment is performed reversibly, the entropy change  $\Delta S^{\text{closed}}$  can be measured by measuring the heat exchanged with the surroundings. This is in agreement with the invariance of  $(-s_1 + s_2 + s_1^0 - s_2^0)$  against shifts of entropy zero.



### 2.1.3.4 Expression for the Soret Coefficient of a Dilute Solution

The Soret coefficient  $S_T$  is the ratio of the thermal diffusion coefficient  $D_T$  and the diffusion coefficient  $D$ . From Eqs. (2.100, 2.101) follows

$$S_T := \frac{D_T}{D} = \left\{ \left[ \frac{\partial(\mu_1 - \mu_2)}{\partial T} \right]_{p, c_1} + \frac{\beta}{\alpha} \right\} \left\{ c_1 \left( \frac{\partial \mu_1}{\partial c_1} \right)_{p, T} \right\}^{-1}. \quad (2.115)$$

For ideal mixtures or dilute solutions with  $c_1 \rightarrow 0$  one has [57]

$$\left( \frac{\partial \mu_1}{\partial c_1} \right)_{p, T} c_1 = \frac{kT}{M_1}, \quad (2.116)$$

where  $M_1$  is the mass of one particle of component 1. With the definition

$$\Delta S^* = (s_1 - s_2 + s_2^0 - s_1^0) M_1 \quad (2.117)$$

Eq. (2.115) becomes

$$S_T = -\frac{\Delta S^*}{kT} + \frac{M_1 \left( \frac{\beta}{\alpha} + s_2^0 - s_1^0 \right)}{kT} = -\frac{\Delta S^*}{kT} + \frac{M_1}{kT} \frac{\Delta \beta}{\alpha}. \quad (2.118)$$

$\Delta S^*$  is the change of entropy for the experiment 2 sketched in Fig. 2.2, where one particle of substance 1 is added to subsystem  $A$  and  $M_1/M_2$  particles of substance 2 are withdrawn from subsystem  $A$ .  $\Delta \beta$  has been introduced in Eq. (2.111). Both  $\Delta S^*$  and  $\Delta \beta/\alpha$  are invariant against shifts of entropy zero.

Duhr and Braun [23, 24] derived for a solute–solvent system

$$S_T = -\frac{\Delta S}{kT}, \quad (2.119)$$

where  $\Delta S$  is the solvation entropy. Here the solute (component 1) is assumed to be highly diluted in the solvent (component 2). If we identify  $\Delta S$  with  $\Delta S^*$  from Eq. (2.117), it follows from comparison to Eq. (2.118)

$$\beta \stackrel{?}{=} \alpha(s_1^0 - s_2^0), \quad \Delta \beta \stackrel{?}{=} 0 \quad (2.120)$$

in the model of Duhr and Braun. This implies

$$\vec{J}_1 \stackrel{?}{=} \alpha [\vec{\nabla}(\mu_1 - \mu_2) + (s_1^0 - s_2^0) \vec{\nabla} T] = \alpha \vec{\nabla}(\mu_1 - \mu_2 - \mu_1^0 + \mu_2^0). \quad (2.121)$$

In thermodynamic equilibrium one has  $\vec{\nabla} T = \vec{\nabla} \mu = 0$ . In the description of Duhr and Braun, both the non–equilibrium and the equilibrium stationary states are characterized by the same condition  $\vec{\nabla}(\mu_1 - \mu_2 - \mu_1^0 + \mu_2^0) = 0$ , regardless whether temperature gradients are present or not. This might be questionable.

According to Ref. [24] the solvation entropy is given by

$$\Delta S = \Delta S^{(\text{hydr})} + \Delta S^{(\text{ionic})} = A \left( \Delta s_{\text{hydr}} - \frac{\tilde{\beta} \sigma_{\text{eff}}^2}{4\epsilon \epsilon_0 T} \times \lambda_{\text{DH}} \right), \quad (2.122)$$

where  $S^{(\text{hydr})}$  and  $S^{(\text{ionic})}$  are the entropy of water hydration and the entropy of ionic shielding,  $A$  is the surface of one particle of component 1,  $\Delta s_{\text{hydr}} = \Delta S^{(\text{hydr})}/A$  is the particle area specific hydration entropy,  $\epsilon_0$  is the vacuum permittivity,  $\epsilon$  is the dielectric constant,  $\tilde{\beta} = 1 + \frac{T}{\epsilon} \frac{\partial \epsilon}{\partial T} = 2.3$ ,  $\sigma_{\text{eff}}$  is the effective surface charge density, and  $\lambda_{\text{DH}}$  is the Debye length. Duhr and Braun measured the Soret coefficients of single DNA and polystyrene beads in aqueous solutions and analyzed the dependence on salt concentration, i.e. on  $\lambda_{\text{DH}}$ , on temperature  $T$ , and on molecule size  $A$ . They found a good agreement between experimental data and their model Eqs. (2.119, 2.122). However, it might be possible to explain their data just as well by Eq. (2.118) with  $\Delta S^* = \Delta S$  from Eq. (2.122), if appropriate assumptions about  $\Delta\beta/\alpha$  are made. For example one could conclude from Fig. 3(a) in Ref. [24], that  $\Delta\beta/\alpha$  does not depend on the Debye length  $\lambda_{\text{DH}}$ . We are not sure, whether  $\Delta\beta = 0$  and thus  $\beta = \alpha(s_1^0 - s_2^0)$  necessarily follows from the data presented in Ref. [24].

To summarize, the following questions come up from the model of Duhr and Braun: Does  $\beta = \alpha(s_1^0 - s_2^0)$  hold? Or equivalently: Are non–equilibrium stationary states characterized by the condition  $\vec{\nabla}(\mu_1 - \mu_2 - \mu_1^0 + \mu_2^0) = 0$ ? Answers can be given, if Onsager coefficients are calculated from diffusion and thermal diffusion data by Eqs. (2.100, 2.101). For that purpose the derivations of the chemical potentials have to be calculated from an equation of state according to Eqs. (2.108, 2.109). The answer to above questions is “No” in case of polymer blends, as was recently shown by Voit [104]. He obtained Onsager coefficients for poly(dimethyl-siloxane)/poly(ethyl-methyl-siloxane) over a wide concentration range from diffusion and thermal diffusion data by using the Flory Huggins theory. The expression  $\Delta\beta/\alpha = (\beta/\alpha + s_2^0 - s_1^0)$  was found to depend on concentration and to be of same order of magnitude as  $\Delta S^*/M_1$  in Eq. (2.118). In a next step Onsager coefficients of simple mixtures and polymer solutions should be evaluated, as for these systems there exist both, reliable diffusion and thermal diffusion data (simple mixtures: e.g. Ref. [110]; polymer solutions: e.g. Ref. [82]), as well as successful equations of state (simple mixtures: Peng–Robinson equation of state [79], Soave Redlich Kong equation of state [79]; polymer solutions: cubic equation of state [59], perturbed hard sphere chain equation of state [38]).

In case of polymer solutions, another important argument should be mentioned in this context. It can be shown theoretically and experimentally, that the Onsager coefficient  $L_{11} = \alpha T$  depends on hydrodynamic interaction, whereas the thermal diffusion coefficient  $D_T$  as well as the Onsager coefficient  $L_{1q}$  do not (see Ref. [11, 87, 117, 85] and Sec. 2.2.5). According to Eq. (2.101) and with the help of Eq. (2.109),  $\beta$  can be expressed in terms of  $L_{1q}$  as follows

$$\beta = \alpha(s_1 - s_2) + \frac{L_{1q}}{T^2}. \quad (2.123)$$

$L_{1q}$  does neither depend on entropy zeros nor on hydrodynamic interaction. If  $\beta = \alpha(s_1^0 - s_2^0)$  was valid,  $L_{1q} \propto \alpha$  would follow, which contradicts both, experimental and theoretical findings.

## 2.2 Reference Velocities

### 2.2.1 Reference Velocities and Diffusion Currents

In chapter 2.1 the diffusion flow was always given by

$$\vec{J}_k = \rho_k(\vec{v}_k - \vec{v}) \quad k = 1 \dots K, \quad (2.124)$$

where  $\vec{v}$  was the center of mass velocity. Because of

$$\sum_{k=1}^K \vec{J}_k = 0 \quad (2.125)$$

only  $K - 1$  diffusion flows are independent. Sometimes it is more convenient to use a diffusion flow [40]

$$\vec{J}_k^a = \rho_k(\vec{v}_k - \vec{v}^a) \quad k = 1 \dots K \quad (2.126)$$

with an arbitrary reference velocity

$$\vec{v}^a = \sum_{k=1}^K a_k \vec{v}_k \quad (2.127)$$

and

$$\sum_{k=1}^K a_k = 1. \quad (2.128)$$

From Eqs. (2.126, 2.127, 2.128) one obtains the following relation between the fluxes:

$$\sum_{k=1}^K \frac{a_k}{c_k} \vec{J}_k^a = 0 \quad (2.129)$$

For  $a_k = c_k$  one has  $\vec{v}^a = \vec{v}$  and  $\vec{J}_k^a = \vec{J}_k$ . The three other important reference velocities are:

1. the mean volume velocity

$$\vec{v}^{\text{vol}} = \sum_{k=1}^K \rho_k v_k \vec{v}_k = \sum_{k=1}^K \phi_k \vec{v}_k \quad (2.130)$$

with weights  $a_k = \rho_k v_k = \phi_k$ .  $v_k$  and  $\phi_k$  are the partial specific volume and the volume

fraction of component  $k$  in the mixture. The corresponding diffusion flows

$$\vec{J}_k^{\text{vol}} = \rho_k(\vec{v}_k - \vec{v}^{\text{vol}}) \quad k = 1 \dots K \quad (2.131)$$

are related to each other by

$$\sum_{k=1}^K v_k \vec{J}_k^{\text{vol}} = 0. \quad (2.132)$$

2. the velocity  $\vec{v}_K$  of species  $K$  with weights  $a_k = \delta_{kK}$ . Hence

$$\vec{J}_k^{\text{rel}} = \rho_k(\vec{v}_k - \vec{v}_K) \quad k = 1 \dots K - 1 \quad (2.133)$$

are independent and

$$\vec{J}_K^{\text{rel}} = 0. \quad (2.134)$$

3. the mean molar velocity

$$\vec{v}^{\text{mol}} = \sum_{k=1}^K x_k \vec{v}_k \quad (2.135)$$

with weights  $a_k = x_k = N_k/N$  (mole fraction of species  $k$ ). The fluxes

$$\vec{J}_k^{\text{mol}} = \rho_k(\vec{v}_k - \vec{v}^{\text{mol}}) \quad k = 1 \dots K \quad (2.136)$$

fulfill the relation

$$\sum_{k=1}^K \frac{\vec{J}_k^{\text{mol}}}{M_k} = 0, \quad (2.137)$$

where  $M_k$  is the molecular mass of component  $k$ .

Conversion from a reference velocity  $\vec{v}^a$  to a second velocity  $\vec{v}^b$  is often necessary. The transition from the diffusion current

$$\vec{J}_j^a = \rho_j(\vec{v}_j - \vec{v}^a) \quad (2.138)$$

to the second diffusion current

$$\vec{J}_k^b = \rho_k(\vec{v}_k - \vec{v}^b) \quad (2.139)$$

is realized by [16]

$$\vec{J}_j^a = \sum_{k=1}^{K-1} \left[ \delta_{jk} + \left( a_K \frac{b_k}{b_K} - a_k \right) \frac{c_j}{c_k} \right] \vec{J}_k^b =: \sum_{k=1}^{K-1} B_{jk}^{ab} \vec{J}_k^b \quad j = 1 \dots K - 1, \quad (2.140)$$

where  $a_k$  ( $b_k$ ) are the weights corresponding to  $\vec{v}^a$  ( $\vec{v}^b$ ) according to Eq. (2.127). The proof of Eq. (2.140) is found by expressing both  $\vec{J}_j^a$  and  $\vec{J}_k^b$  in terms of the set of independent velocities  $\vec{v}_1, \vec{v}_2, \dots, \vec{v}_K$  (this is done with the help of Eqs. (2.126, 2.127)) and by identifying

the coefficients of these velocities. Three special cases of Eq. (2.140) shall be considered.

1. binary mixture ( $K = 2$ ): Using  $a_1 + a_2 = b_1 + b_2 = 1$ , Eq. (2.140) reduces to

$$\vec{J}_1^a = \left[ 1 + \left( a_2 \frac{1 - b_2}{b_2} - (1 - a_2) \right) \frac{c_1}{c_1} \right] \vec{J}_1^b = \frac{a_2}{b_2} \vec{J}_1^b. \quad (2.141)$$

Important examples are

$$\vec{J}_1^{\text{vol}} = \rho_2 v_2 \vec{J}_1^{\text{rel}} = \phi_2 \vec{J}_1^{\text{rel}} \quad (2.142)$$

and

$$\vec{J}_1 = \frac{c_2}{\rho_2 v_2} \vec{J}_1^{\text{vol}} = \frac{1}{\rho v_2} \vec{J}_1^{\text{vol}} = \frac{c_2}{\phi_2} \vec{J}_1^{\text{vol}} = c_2 \vec{J}_1^{\text{rel}}. \quad (2.143)$$

2. transformation from center of mass velocity to mean molar velocity: Taking into account

$$x_j = \frac{N_j}{\sum_{i=1}^K N_i} = \frac{c_j/M_j}{\sum_{i=1}^K c_i/M_i} \quad (2.144)$$

one obtains from Eq. (2.140)

$$\vec{J}_j^{\text{mol}} = \sum_{k=1}^{K-1} \left[ \delta_{jk} + c_j \left( \frac{x_K}{c_K} - \frac{x_k}{c_k} \right) \right] \vec{J}_k = \sum_{k=1}^{K-1} \frac{c_j}{x_j} \left( \frac{\partial x_j}{\partial c_k} \right) \vec{J}_k \quad j = 1 \dots K - 1, \quad (2.145)$$

where the abbreviation

$$(\partial/\partial c_k) \equiv (\partial/\partial c_k)_{p,T,c_1,\dots,c_{k-1},c_{k+1},\dots,c_{K-1}}. \quad (2.146)$$

has been introduced. Accordingly the inverse transformation is given by

$$\vec{J}_j = \sum_{k=1}^{K-1} \frac{x_k}{c_k} \left( \frac{\partial c_j}{\partial x_k} \right) \vec{J}_k^{\text{mol}} \quad j = 1 \dots K - 1 \quad (2.147)$$

with

$$(\partial/\partial x_k) \equiv (\partial/\partial x_k)_{p,T,x_1,\dots,x_{k-1},x_{k+1},\dots,x_{K-1}}. \quad (2.148)$$

3. transformation from center of mass velocity to mean volume velocity: With  $\rho_k = c_k \rho$  it follows from Eq. (2.140)

$$\begin{aligned} \vec{J}_j^{\text{vol}} &= \sum_{k=1}^{K-1} \left[ \delta_{jk} + (\rho_K v_K \frac{c_k}{c_K} - \rho_k v_k) \frac{c_j}{c_k} \right] \vec{J}_k \\ &= \sum_{k=1}^{K-1} \left[ \delta_{jk} + \rho_j (v_K - v_k) \right] \vec{J}_k \quad j = 1 \dots K - 1. \end{aligned} \quad (2.149)$$

With the help of

$$\frac{\partial \rho}{\partial c_k} = -\rho^2 \left( \frac{\partial V}{\partial m_k} \right)_{p,T,m_1,\dots,m_{k-1},m_{k+1},\dots,m_{K-1},m} = -\rho^2 (v_k - v_K) \quad (2.150)$$

and

$$\frac{\partial \rho_j}{\partial c_k} = \frac{\partial(\rho c_j)}{\partial c_k} = \rho \delta_{jk} + c_j \frac{\partial \rho}{\partial c_k} \stackrel{(2.150)}{=} \rho \left[ \delta_{jk} + \rho_j (v_K - v_k) \right] \quad j, k = 1 \dots K-1 \quad (2.151)$$

the conversion relation (2.149) takes the simple form

$$\vec{J}_j^{\text{vol}} = \sum_{k=1}^{K-1} \frac{1}{\rho} \frac{\partial \rho_j}{\partial c_k} \vec{J}_k \quad j = 1 \dots K-1. \quad (2.152)$$

Then the inverse transformation is given by

$$\vec{J}_j = \sum_{k=1}^{K-1} \rho \frac{\partial c_j}{\partial \rho_k} \vec{J}_k^{\text{vol}} \quad j = 1 \dots K-1, \quad (2.153)$$

with

$$(\partial/\partial \rho_k) \equiv (\partial/\partial \rho_k)_{p,T,\rho_1,\dots,\rho_{k-1},\rho_{k+1},\dots,\rho_{K-1}} \quad (2.154)$$

and

$$(\partial c_j / \partial \rho_k) = \frac{1}{\rho} \left[ \delta_{jk} + c_j \left( \frac{v_k}{v_K} - 1 \right) \right]. \quad (2.155)$$

Up to now we have discussed different reference velocities, which are not necessarily equal to zero. All descriptions are equally valid, and any of the reference velocities can be chosen. The transformation from one reference velocity to a second reference velocity according to Eq. (2.140) does not involve any problems. The situation is more complicated, if the vanishing of a reference velocity is considered. In general it is not possible to conclude from the vanishing of one reference velocity that also all other reference velocities are equal to zero. Remember that the reference velocities are generally complicated functions of space and time

$$\vec{v}^a = \vec{v}^a(\vec{r}, t). \quad (2.156)$$

### 2.2.2 Prigogine's Theorem

According to Eq. (2.79) the local entropy production without chemical reactions and viscous flow phenomena is given by

$$\sigma = \vec{J}_Q \cdot \vec{\nabla} \left( \frac{1}{T} \right) - \frac{1}{T} \sum_{k=1}^K \rho_k (\vec{v}_k - \vec{v}) \cdot \left[ (\vec{\nabla} \mu_k)_T - \vec{F}_k \right], \quad (2.157)$$

where  $\vec{J}_k = \rho_k(\vec{v}_k - \vec{v})$  has been used. Thus  $\sigma$  depends on the center of mass velocity  $\vec{v}$ . For mechanical equilibrium Prigogine [80] has shown that the center of mass velocity  $\vec{v}$  in Eq. (2.157) can be replaced by any other velocity  $\vec{v}_0$ .

$$\sigma = \vec{J}_Q \cdot \vec{\nabla} \left( \frac{1}{T} \right) - \frac{1}{T} \sum_{k=1}^K \rho_k (\vec{v}_k - \vec{v}_0) \cdot [(\vec{\nabla} \mu_k)_T - \vec{F}_k] \quad (2.158)$$

The proof of this theorem follows from the equality

$$\sum_{k=1}^K \rho_k [(\vec{\nabla} \mu_k)_T - \vec{F}_k] = 0, \quad (2.159)$$

which can be derived by combining the mechanical equilibrium condition (2.89) with the Gibbs Duhem relation (2.73).

It should be noted that  $\vec{v}_0$  can take any value. For example by choosing  $\vec{v}_0 = 0$  one obtains

$$\sigma = \vec{J}_Q \cdot \vec{\nabla} \left( \frac{1}{T} \right) - \frac{1}{T} \sum_{k=1}^K \vec{J}_k^{\text{lab}} \cdot [(\vec{\nabla} \mu_k)_T - \vec{F}_k], \quad (2.160)$$

where

$$\vec{J}_k^{\text{lab}} = \rho_k \vec{v}_k \quad k = 1 \dots K \quad (2.161)$$

is the mass flow in the laboratory reference frame. It is, however, not possible to derive phenomenological equations from Eq. (2.160). This can only be done, if  $\sigma = \sum J_i X_i$  contains independent fluxes  $J_i$  and forces  $X_i$ . The fluxes  $\vec{J}_k^{\text{lab}}$  in Eq. (2.160) do not fulfill this requirement since they are related by

$$\sum_{k=1}^K \vec{J}_k^{\text{lab}} = \rho \vec{v}. \quad (2.162)$$

Eliminating the  $K$ -th mass flow  $\vec{J}_K^{\text{lab}}$  from Eq. (2.160) does not solve the problem, because then the resulting entropy production is no longer of the form  $\sigma = \sum J_i X_i$ .

Phenomenological equations can only be written down for  $\vec{v}_0 = \vec{v}^a$ , where  $\vec{v}^a$  is a reference velocity as given by Eqs. (2.127, 2.128). Then the linear homogenous relation (2.129) between the diffusion fluxes  $\vec{J}_k^a = \rho_k(\vec{v}_k - \vec{v}^a)$  allows to express the entropy production in the required form. More specifically, eliminating the  $K$ -th diffusion flow  $\rho_K(\vec{v}_K - \vec{v}^a)$  from Eq. (2.158) and using the abbreviation

$$\vec{X}_k^a = [(\vec{\nabla} \mu_k)_T - \vec{F}_k] - \frac{a_k c_K}{a_K c_k} [(\vec{\nabla} \mu_K)_T - \vec{F}_K] \quad (2.163)$$

$$\stackrel{(2.159)}{=} \sum_{i=1}^{K-1} \left( \delta_{ik} + \frac{a_k c_i}{a_K c_k} \right) [(\vec{\nabla} \mu_i)_T - \vec{F}_i], \quad (2.164)$$

one finds

$$\sigma = \vec{J}_Q \cdot \vec{\nabla} \left( \frac{1}{T} \right) - \frac{1}{T} \sum_{k=1}^{K-1} \vec{J}_k^a \cdot \vec{X}_k^a, \quad (2.165)$$

which contains only independent fluxes and forces. Hence the phenomenological equations read

$$\vec{J}_Q = -L_{qq}^a \frac{\vec{\nabla} T}{T^2} - \sum_{k=1}^{K-1} L_{qk}^a \frac{\vec{X}_k^a}{T} \quad (2.166)$$

$$\vec{J}_i^a = -L_{iq}^a \frac{\vec{\nabla} T}{T^2} - \sum_{k=1}^{K-1} L_{ik}^a \frac{\vec{X}_k^a}{T} \quad i = 1 \dots K-1 \quad (2.167)$$

where  $L_{qq}^a$ ,  $L_{iq}^a$ , and  $L_{ik}^a$  are the Onsager coefficients corresponding to the reference velocity  $\vec{v}^a$ . Onsager's reciprocity law states  $L_{ik}^a = L_{ki}^a$  and  $L_{iq}^a = L_{qi}^a$ . For  $a_k = c_k$  one has  $\vec{v}^a = \vec{v}$ ,  $L_{qq}^a = L_{qq}$ ,  $L_{iq}^a = L_{iq}$ ,  $L_{ik}^a = L_{ik}$  and the phenomenological equations (2.85, 2.86) from Sec. 2.1.3.1 are recovered.

The Onsager coefficients corresponding to  $\vec{v}^a$  ( $L_{qq}^a$ ,  $L_{iq}^a$ ,  $L_{ik}^a$ ) are related to the Onsager coefficients corresponding to  $\vec{v}^b$  ( $L_{qq}^b$ ,  $L_{iq}^b$ ,  $L_{ik}^b$ ) by

$$L_{qq}^a = L_{qq}^b \quad (2.168)$$

$$L_{iq}^a = L_{qi}^a = \sum_{j=1}^{K-1} B_{ij}^{ab} L_{jq}^b = \sum_{j=1}^{K-1} B_{ij}^{ab} L_{qj}^b \quad (2.169)$$

$$L_{ik}^a = \sum_{j,l=1}^{K-1} B_{ij}^{ab} L_{jl}^b B_{kl}^{ab}, \quad (2.170)$$

where  $B_{ij}^{ab}$  has been defined in Eq. (2.140). Eqs. (2.168)–(2.170) are easily derived from Eq. (2.140) and

$$\vec{X}_l^b = \sum_{k=1}^{K-1} B_{kl}^{ab} \vec{X}_k^a \quad l = 1 \dots K-1, \quad (2.171)$$

where  $\vec{X}_k^a$  and  $\vec{X}_l^b$  are given by Eq. (2.164) and by the corresponding formulae with  $b$  instead of  $a$ . Note that Eq. (2.164) and Eq. (2.171) are only true for mechanical equilibrium (Eq. (2.89)).

An important special case of Eqs. (2.170)–(2.171) is a binary mixture with

$$L_{11}^a = \frac{a_2^2}{b_2^2} L_{11}^b, \quad B_{11} = \frac{a_2}{b_2}, \quad \vec{J}_1^a = \frac{a_2}{b_2} \vec{J}_1^b, \quad \vec{X}_1^a = \frac{1}{a_2} [(\vec{\nabla} \mu_1)_T - \vec{F}_1] = \frac{b_2}{a_2} \vec{X}_1^b. \quad (2.172)$$

The concluding remarks of Sec. 2.2.1 can be similarly repeated here: In mechanical equilibrium symmetric Onsager coefficients can be introduced for any reference velocity and the corresponding phenomenological equations are all equally valid. The transformation from



one set of Onsager coefficients ( $L_{qq}^a, L_{iq}^a, L_{ik}^a$ , reference velocity  $\vec{v}^a$ ) to a second set of Onsager coefficients ( $L_{qq}^b, L_{iq}^b, L_{ik}^b$ , reference velocity  $\vec{v}^b$ ) is easily performed with the help of Eqs. (2.168)–(2.170). Only the fluxes in the laboratory reference frame  $\vec{J}_k^{\text{lab}} = \rho_k \vec{v}_k$  are problematic. Even though the entropy production might be expressed in terms of  $\vec{J}_k^{\text{lab}}$ , phenomenological equations cannot be written down for these fluxes.

**Frictional formalism** At the very end of this section we would like to mention the frictional formalism of non-equilibrium thermodynamics and the relation between friction coefficients and Onsager coefficients. According to Ref. [103],<sup>8</sup> in the absence of external forces and temperature gradients, multicomponent diffusion can be described by the general friction equations

$$\sum_{j=1}^K f_{ij} \rho_j (\vec{v}_i - \vec{v}_j) = -(\vec{\nabla} \mu_i)_{p,T} \quad i = 1 \dots K \quad (2.173)$$

and the entropy production

$$\sigma = \frac{1}{2T} \sum_{i,j=1}^K f_{ij} \rho_i \rho_j (\vec{v}_i - \vec{v}_j)^2. \quad (2.174)$$

The symmetric friction coefficients  $f_{ij}$  can be related to the Onsager coefficients  $L_{ik}^{\text{rel}}$  as follows

$$f_{ik}^{-1} = -\frac{L_{ik}^{\text{rel}}}{T} \quad i, k = 1 \dots K-1 \quad (2.175)$$

$$f_{Ki} = f_{iK} = -\frac{1}{\rho_K} \sum_{k=1}^{K-1} f_{ki} \rho_k \quad i = 1 \dots K-1. \quad (2.176)$$

Eqs. (2.173)–(2.176) follow from the Gibbs Duhem relation (2.73) and Eqs. (2.165, 2.167) with  $\vec{J}_i^{\text{rel}} = \rho_i (\vec{v}_i - \vec{v}_K)$  and  $\vec{X}_i^{\text{rel}} = (\vec{\nabla} \mu_i)_{p,T}$ , if the symmetry  $f_{ik} = f_{ki}$  is taken into account.

For a binary liquid ( $K = 2$ ) it is found from Eqs. (2.174, 2.176)

$$f_{12} = \frac{\rho_1}{\rho_2} \frac{T}{L_{11}^{\text{rel}}} = \frac{c_1}{c_2} \frac{T}{L_{11}^{\text{rel}}} \quad (2.177)$$

$$T\sigma = \vec{J}_1^{\text{rel}} \vec{X}_1^{\text{rel}} = (\vec{J}_1^{\text{rel}})^2 / L_{11}^{\text{rel}} = f_{12} \rho_1 \rho_2 (\vec{v}_1 - \vec{v}_2)^2 \quad (2.178)$$

with  $\vec{J}_1^{\text{rel}} = \rho_1 (\vec{v}_1 - \vec{v}_2)$ .

<sup>8</sup>Vink [103] uses the number density  $n_k = N_k/V$  instead of the mass density  $\rho_k = m_k/V$  and accordingly the chemical potential per particle  $\mu'_k = M_k \mu_k$ .

### 2.2.3 Definition of Diffusion Coefficients

Most generally, thermal diffusion coefficients  $D_{i,T}^{a,y}$ , barodiffusion coefficients  $D_{i,p}^{a,y}$  and mutual diffusion coefficients  $D_{ik}^{a,y}$  may be defined by

$$\vec{J}_i^a = -D_{i,T}^{a,y} \vec{\nabla}T - D_{i,p}^{a,y} \vec{\nabla}p - \sum_{k=1}^{K-1} D_{ik}^{a,y} \vec{\nabla}y_k \quad i = 1 \dots K-1, \quad (2.179)$$

where  $\vec{J}_i^a = \rho_i(\vec{v}_i - \vec{v}^a)$  is the mass flux with an arbitrary reference velocity ( $a = \text{mass, vol, rel, mol, } \dots$ ; see Sec. 2.2.1) and  $y_k$  is a composition variable ( $y_k = \rho_k, c_k, x_k, \dots$ ). This is the generalization of Eq. (XI.51) from Ref. [16] to non–isothermal, non–isobaric systems. It is, of course, possible to relate these diffusion coefficients to the Onsager coefficients  $L_{qq}^a, L_{iq}^a, L_{ik}^a$ , which have been introduced in the last section by Eqs. (2.166, 2.167). From the Onsager reciprocal relations one thus obtains symmetry relations between the diffusion coefficients. However, we will not discuss this subject here, but will concentrate on transformations between reference velocities and composition variables.

The transition from one composition variable  $y_k$  to a second composition variable  $z_l$  in the presence of temperature and pressure gradients is realized by

$$\vec{\nabla}z_l = \left(\frac{\partial z_l}{\partial T}\right)_{p,\{y_i\}} \vec{\nabla}T + \left(\frac{\partial z_l}{\partial p}\right)_{T,\{y_i\}} \vec{\nabla}p + \sum_{k=1}^{K-1} \left(\frac{\partial z_l}{\partial y_k}\right)_{p,T,y_1,\dots,y_{k-1},y_{k+1},\dots,y_{K-1}} \vec{\nabla}y_k. \quad (2.180)$$

For example,  $\vec{\nabla}\rho_l$  (gradients in mass density) can be evaluated from  $\vec{\nabla}c_k$  (gradients in weight fraction) by

$$\vec{\nabla}\rho_l = -\rho_l\alpha\vec{\nabla}T + \rho_l\kappa\vec{\nabla}p + \sum_{k=1}^{K-1} \frac{\partial\rho_l}{\partial c_k} \vec{\nabla}c_k \quad l = 1 \dots K-1, \quad (2.181)$$

with the thermal expansion coefficient  $\alpha = V^{-1}(\partial V/\partial T)_{p,m_1,\dots,m_K}$ , the isothermal compressibility  $\kappa = -V^{-1}(\partial V/\partial p)_{T,m_1,\dots,m_K}$ , and  $(\partial/\partial c_k)$  from Eq. (2.146).<sup>9</sup>

The diffusion coefficients  $D_{i,T}^{b,z}$ ,  $D_{i,p}^{b,z}$  and  $D_{ik}^{b,z}$ , which are defined by

$$\vec{J}_j^b = -D_{j,T}^{b,z} \vec{\nabla}T - D_{j,p}^{b,z} \vec{\nabla}p - \sum_{l=1}^{K-1} D_{jl}^{b,z} \vec{\nabla}z_l, \quad (2.182)$$

can be related to the diffusion coefficients  $D_{i,T}^{a,y}$ ,  $D_{i,p}^{a,y}$  and  $D_{ik}^{a,y}$  from Eq. (2.179) with the

<sup>9</sup>In [61]  $\vec{\nabla}\rho_l = \sum(\partial\rho_l/\partial c_i)\vec{\nabla}c_i$  is used, although thermal diffusion phenomena are studied. The obtained results are only true for mixtures with negligible thermal expansion.

help of Eq. (2.140) and Eq. (2.180):

$$D_{i,T}^{a,y} = \sum_{j=1}^{K-1} B_{ij}^{ab} \left[ D_{j,T}^{b,z} + \sum_{l=1}^{K-1} D_{jl}^{b,z} \left( \frac{\partial z_l}{\partial T} \right)_{p,\{y_i\}} \right] \quad (2.183)$$

$$D_{i,p}^{a,y} = \sum_{j=1}^{K-1} B_{ij}^{ab} \left[ D_{j,p}^{b,z} + \sum_{l=1}^{K-1} D_{jl}^{b,z} \left( \frac{\partial z_l}{\partial p} \right)_{T,\{y_i\}} \right] \quad (2.184)$$

$$D_{ik}^{a,y} = \sum_{j,l=1}^{K-1} B_{ij}^{ab} D_{jl}^{b,z} \left( \frac{\partial z_l}{\partial y_k} \right)_{p,T,y_1,\dots,y_{k-1},y_{k+1},\dots,y_{K-1}} \quad (2.185)$$

Conventional choices of reference velocities  $\vec{v}^a$  and composition variables  $y_k$  are: the center of mass velocity  $\vec{v}$  combined with weight fractions  $c_k$ , the mean volume velocity  $\vec{v}^{\text{mol}}$  together with mass densities  $\rho_k$ , and the mean molar velocity in combination with mole fractions  $x_k$ . In the absence of pressure gradients it is practical to introduce diffusion coefficients  $\mathcal{D}_{i,T}$ ,  $\mathcal{D}_{ik}$ ,  $D_{i,T}^*$ ,  $D_{ik}^*$ ,  $D_{i,T}$ ,  $D_{ik}$  as follows:

$$\vec{J}_i = -\rho c_i c_K \mathcal{D}_{i,T} \vec{\nabla} T - \rho \sum_{k=1}^{K-1} \mathcal{D}_{ik} \vec{\nabla} c_k \quad i = 1 \dots K-1, \quad (2.186)$$

$$\frac{\vec{J}_i^{\text{mol}}}{M_i} = -n x_i x_K D_{i,T}^* \vec{\nabla} T - n \sum_{k=1}^{K-1} D_{ik}^* \vec{\nabla} x_k \quad i = 1 \dots K-1, \quad (2.187)$$

$$\vec{J}_i^{\text{vol}} = -\rho_i \phi_K D_{i,T} \vec{\nabla} T - \sum_{k=1}^{K-1} D_{ik} \vec{\nabla} \rho_k \quad i = 1 \dots K-1, \quad (2.188)$$

Here  $\vec{J}_i^{\text{mol}}/M_i$  is a particle diffusion flux and  $n = N/V$  the total number density. The prefactor of the thermal diffusion coefficients  $n x_i x_K$  in Eq. (2.187) has been chosen in agreement with the result of Ghorayeb and Firoozabadi [35]. They have shown that the expression  $n x_i (1 - x_i) D_{i,T}^*$ , which is used in Refs. [48, 100], is only correct for binary systems.

With the help of Eq. (2.145) and Eqs. (2.183, 2.185) the relation between the diffusion coefficients  $D_{i,T}^*$ ,  $D_{ik}^*$  and  $\mathcal{D}_{i,T}$ ,  $\mathcal{D}_{ik}$  is easily found.

$$D_{ik}^* = \sum_{j,l=1}^{K-1} \left( \frac{\partial x_i}{\partial c_j} \right) \mathcal{D}_{jl} \left( \frac{\partial c_l}{\partial x_k} \right) \quad (2.189)$$

$$D_{i,T}^* x_i x_K = \sum_{j=1}^{K-1} \left( \frac{\partial x_i}{\partial c_j} \right) \mathcal{D}_{j,T} c_j c_K, \quad (2.190)$$

where  $(\partial/\partial c_k)$  and  $(\partial/\partial x_k)$  have been defined by Eqs. (2.146) and (2.148).

The transition from diffusion coefficients  $\mathcal{D}_{i,T}$ ,  $\mathcal{D}_{ik}$  to  $D_{i,T}$ ,  $D_{ik}$  is more complicated, because in the presence of temperature gradients the mass density can change alone due to the thermal expansion of the medium. From Eq. (2.152) and the general conversion formulae

Eqs. (2.183, 2.185) one obtains

$$D_{ik} = \sum_{j,l=1}^{K-1} \left( \frac{\partial \rho_i}{\partial c_j} \right) \mathcal{D}_{jl} \left( \frac{\partial c_l}{\partial \rho_k} \right) \quad (2.191)$$

$$D_{i,T\rho_i\phi_K} = \sum_{j=1}^{K-1} \left( \frac{\partial \rho_i}{\partial c_j} \right) \left[ \mathcal{D}_{j,T} c_j c_K + \alpha \sum_{k,l=1}^{K-1} \mathcal{D}_{jl} \left( \frac{\partial c_l}{\partial \rho_k} \right) \rho_k \right]. \quad (2.192)$$

Here the abbreviation  $(\partial/\partial\rho_k)$  from Eq. (2.154) has been used and

$$\left( \frac{\partial c_l}{\partial T} \right)_{p,\{\rho_i\}} = - \sum_{k=1}^{K-1} \frac{\partial c_l}{\partial \rho_k} \left( \frac{\partial \rho_k}{\partial T} \right)_{p,\{c_i\}} = - \sum_{k=1}^{K-1} \frac{\partial c_l}{\partial \rho_k} (-\alpha \rho_k) \quad (2.193)$$

has been taken into account. The thermal expansion coefficient  $\alpha$  has been introduced before.<sup>10</sup>

For binary mixtures ( $K = 2$ ) all diffusion coefficients can be expressed in terms of the general binary diffusion coefficients  $D$  and  $D_T$  from Sec. 2.1.3.2. Using  $(\partial x_1/\partial c_1) = x_1 x_2/(c_1 c_2)$  and  $(\partial \rho_1/\partial c_1) = \rho^2 v_2 = \rho_1 \phi_2/(c_1 c_2)$  it follows from Eqs. (2.189)–(2.192)

$$D_{11}^* = \left( \frac{\partial x_1}{\partial c_1} \right) \mathcal{D}_{11} \left( \frac{\partial c_1}{\partial x_1} \right) = \mathcal{D}_{11} = D \quad (2.194)$$

$$D_{1,T}^* = \left( \frac{\partial x_1}{\partial c_1} \right) \frac{c_1 c_2}{x_1 x_2} \mathcal{D}_{1,T} = \mathcal{D}_{1,T} = D_T \quad (2.195)$$

$$D_{11} = \left( \frac{\partial \rho_1}{\partial c_1} \right) \mathcal{D}_{11} \left( \frac{\partial c_1}{\partial \rho_1} \right) = \mathcal{D}_{11} = D \quad (2.196)$$

$$D_{1,T} = \frac{1}{\rho_1 \phi_2} \left( \frac{\partial \rho_1}{\partial c_1} \right) \left[ \mathcal{D}_{1,T} c_1 c_2 + \alpha \mathcal{D}_{11} \left( \frac{\partial c_1}{\partial \rho_1} \right) \rho_1 \right] = D_T + \frac{\alpha}{\phi_2} D. \quad (2.197)$$

Hence the three fluxes from Eqs. (2.186)–(2.188) are given by

$$\vec{J}_1 = -\rho c_1 c_2 D_T \vec{\nabla} T - \rho D \vec{\nabla} c_1 \quad (2.198)$$

$$\frac{\vec{J}_1^{\text{mol}}}{M_1} = -n x_1 x_2 D_T \vec{\nabla} T - n D \vec{\nabla} x_1 \quad (2.199)$$

$$\vec{J}_1^{\text{vol}} = -\rho_1 \phi_2 D_T \vec{\nabla} T - \rho_1 \alpha D \vec{\nabla} T - D \vec{\nabla} \rho_1. \quad (2.200)$$

The term  $\rho_1 \alpha D \vec{\nabla} T$  in Eq. (2.200) must not be neglected for small Soret coefficients  $S_T := D_T/D$ . For example in mixtures of organic liquids one typically has  $S_T \approx \pm(1 \dots 10) \times 10^{-3}/\text{K}$  [51, 112] and  $\alpha \approx 1 \times 10^{-3}/\text{K}$  [64]. Hence  $\phi_2 D_T$  and  $\alpha D$  are of same order of magnitude. Some authors define the Soret coefficient of dilute solutions in a different way

$$\vec{J}_1^{\text{vol}} = -D[\vec{\nabla} \rho_1 + \rho_1 S_T^* \vec{\nabla} T] \quad (c_1 \ll 1, \phi_2 \simeq 1). \quad (2.201)$$

<sup>10</sup>The second term on the right hand side of Eq. (2.192) is missing in Eq. (64) in Ref. [61].

$S_T = D_T/D$  and  $S_T^*$  are related by

$$S_T^* = S_T + \alpha. \quad (2.202)$$

In ideal gases  $\alpha$  is simply given by  $1/T$  and  $S_T^* - S_T = 1/T$  is sometimes called the ideal gas contribution [24, 113] to the Soret coefficient. This is, however, rather misleading, since it originates from thermal expansion and has nothing to do with thermal diffusion. Actually,  $\rho_1$  is not the most appropriate composition variable in the presence of temperature gradients.  $x_1$  or  $c_1$ , which are not affected by thermal expansion, are preferable.

According to Eqs. (2.198, 2.199) the diffusion coefficients in a binary mixture do not change, if the mass flux  $\vec{J}_1$ , the total mass density  $\rho$  and the weight fractions  $c_i$  are replaced by the particle diffusion flux  $\vec{J}_1^{\text{mol}}/M_1$ , the total number density  $n$  and the mole fractions  $x_i$  [72]. The corresponding reference velocities, however, are generally not identical ( $\vec{v} \neq \vec{v}^{\text{mol}}$ ).

Again we repeat, that any reference velocity  $\vec{v}^a$  or composition variable  $y_k$  may be used for the description of the problem and transition to another reference velocity  $\vec{v}^b$  or composition variable  $z_k$  is always possible. The transformation of the corresponding diffusion coefficients is especially simple in case of binary mixtures, but of course also possible for multicomponent mixtures.

### 2.2.4 Evolution Equations

Up to now we have derived equations, which relate a flux (mass or heat flux) to the gradients of the composition variables  $\vec{\nabla}y_1, \dots, \vec{\nabla}y_{K-1}$  and the temperature gradient  $\vec{\nabla}T$ . (The pressure is assumed to be constant.) These equations do not allow for determination of the space- and time-dependent composition and temperature fields  $y_1(\vec{r}, t), \dots, y_{K-1}(\vec{r}, t), T(\vec{r}, t)$ . For this one needs evolution equations

$$\frac{\partial y_i}{\partial t} = f(y_1, \dots, y_{K-1}, \vec{\nabla}y_1, \dots, \vec{\nabla}y_{K-1}, \Delta y_1, \dots, \Delta y_{K-1}, T, \vec{\nabla}T, \Delta T, \vec{v}^a, \vec{v}) \quad (2.203)$$

$$\frac{\partial T}{\partial t} = f(y_1, \dots, y_{K-1}, \vec{\nabla}y_1, \dots, \vec{\nabla}y_{K-1}, \Delta y_1, \dots, \Delta y_{K-1}, T, \vec{\nabla}T, \Delta T, \vec{v}^a, \vec{v}), \quad (2.204)$$

where the reference velocity  $\vec{v}^a$  and the center of mass velocity  $\vec{v}$  have to be determined separately. Under certain conditions the evolution equations (2.203, 2.204) take a very simple form

$$\frac{\partial y_i}{\partial t} = D_{i,T}^{a,y} \Delta T + \sum_{k=1}^{K-1} D_{ik}^{ay} \Delta y_k \quad (2.205)$$

$$\frac{\partial T}{\partial t} = D_{th} \Delta T. \quad (2.206)$$

Eq. (2.205) and Eq. (2.206) are often called extended diffusion equation and heat equation. In this section we will derive the general evolution equations (2.203, 2.204) and will discuss under which conditions they simplify to Eqs. (2.205, 2.206).

### 2.2.4.1 General Evolution Equations for Composition Variables

According to Eq. (2.64) the time derivative of the mass density of component  $k$  is given by

$$\frac{\partial \rho_k}{\partial t} = -\vec{\nabla} \cdot (\rho_k \vec{v}_k) = -\vec{\nabla} \cdot \vec{J}_k^{\text{lab}} \quad k = 1 \dots K, \quad (2.207)$$

if chemical reactions are excluded. Onsager equations cannot be derived for the fluxes in the laboratory reference frame (cf. Sec. 2.2.2). Therefore  $\vec{J}_k^{\text{lab}}$  in Eq. (2.207) has to be replaced by  $\vec{J}_k^a = \rho_k(\vec{v}_k - \vec{v}^a)$

$$\frac{\partial \rho_k}{\partial t} = -\vec{\nabla} \cdot \vec{J}_k^a - \vec{\nabla} \cdot (\rho_k \vec{v}^a) \quad k = 1 \dots K. \quad (2.208)$$

If  $\vec{J}_k^a$  is expressed in terms of  $\vec{\nabla} \rho_1, \dots, \vec{\nabla} \rho_{K-1}$  (Eq. (2.179) with  $y_k = \rho_k$  and  $\vec{\nabla} p = 0$ ), the general evolution equation for the mass density  $\rho_k$  is obtained:

$$\frac{\partial \rho_k}{\partial t} = \vec{\nabla} \cdot \left[ D_{k,T}^{a,\rho} \vec{\nabla} T + \sum_{j=1}^{K-1} D_{kj}^{a,\rho} \vec{\nabla} \rho_j \right] - \vec{\nabla} \cdot (\rho_k \vec{v}^a) \quad k = 1 \dots K - 1. \quad (2.209)$$

From Eq. (2.208) and

$$\frac{\partial \rho}{\partial t} = -\vec{\nabla} \cdot (\rho \vec{v}) \quad (2.210)$$

follows

$$\begin{aligned} \frac{\partial c_k}{\partial t} &= \frac{\partial}{\partial t} \left( \frac{\rho_k}{\rho} \right) = \frac{1}{\rho} \frac{\partial \rho_k}{\partial t} - \frac{\rho_k}{\rho^2} \frac{\partial \rho}{\partial t} \\ &= -\frac{1}{\rho} \left[ \vec{\nabla} \cdot \vec{J}_k^a + \vec{\nabla} \cdot (\rho_k \vec{v}^a) - c_k \vec{\nabla} \cdot (\rho \vec{v}) \right] \quad k = 1 \dots K - 1. \end{aligned} \quad (2.211)$$

The general evolution equation for the weight fractions is thus given by

$$\frac{\partial c_k}{\partial t} = \frac{1}{\rho} \vec{\nabla} \cdot \left[ D_{k,T}^{a,c} \vec{\nabla} T + \sum_{j=1}^{K-1} D_{kj}^{a,c} \vec{\nabla} c_j \right] - \frac{1}{\rho} \left[ \vec{\nabla} \cdot (c_k \rho \vec{v}^a) - c_k \vec{\nabla} \cdot (\rho \vec{v}) \right], \quad (2.212)$$

where Eq. (2.179) with  $y_k = c_k$  and  $\vec{\nabla} p = 0$  has been used.

The general evolution equation for the mole fractions is found from Eq. (2.208) and

$$\frac{\partial n}{\partial t} = -\vec{\nabla} \cdot (n \vec{v}^{\text{mol}}). \quad (2.213)$$

One obtains

$$\begin{aligned}\frac{\partial x_k}{\partial t} &= \frac{\partial}{\partial t} \left( \frac{n_k}{n} \right) = \frac{1}{M_k n} \frac{\partial \rho_k}{\partial t} - \frac{n_k}{n^2} \frac{\partial n}{\partial t} \\ &= -\frac{1}{n} \left[ \vec{\nabla} \cdot \frac{\vec{J}_k^a}{M_k} + \vec{\nabla} \cdot (n_k \vec{v}^a) - x_k \vec{\nabla} \cdot (n \vec{v}^{\text{mol}}) \right] \quad k = 1 \dots K-1.\end{aligned}\quad (2.214)$$

$n_k = N_k/V$  is the number density of particles of component  $k$ . Replacing  $\vec{J}_k^a$  according to Eq. (2.179) with  $y_k = x_k$  and  $\vec{\nabla} p = 0$  yields

$$\frac{\partial x_k}{\partial t} = \frac{1}{n M_k} \vec{\nabla} \cdot \left[ D_{k,T}^{a,x} \vec{\nabla} T + \sum_{j=1}^{K-1} D_{kj}^{a,x} \vec{\nabla} x_j \right] - \frac{1}{n} \left[ \vec{\nabla} \cdot (n_k \vec{v}^a) - x_k \vec{\nabla} \cdot (n \vec{v}^{\text{mol}}) \right]. \quad (2.215)$$

### 2.2.4.2 Extended Diffusion Equations for Composition Variables ...

**... in case of vanishing reference velocities** It can sometimes be argued that a certain reference velocity  $\vec{v}^a$  vanishes (see Sec. 2.2.4.3 below). Then the composition variables solve the so called extended diffusion equations.

In case of vanishing mean volume velocity  $\vec{v}^{\text{vol}} = 0$  it follows from Eq. (2.208) and Eq. (2.188)

$$\frac{\partial \rho_i}{\partial t} = -\vec{\nabla} \cdot \vec{J}_i^{\text{vol}} = \vec{\nabla} \cdot \left[ \rho_i \phi_K D_{i,T} \vec{\nabla} T + \sum_{k=1}^{K-1} D_{ik} \vec{\nabla} \rho_k \right] \quad i = 1 \dots K-1. \quad (2.216)$$

For small gradients  $\rho_i \approx \rho_{i,0}$ ,  $\phi_K \approx \phi_{K,0}$ ,  $D_{i,T}$ , and  $D_{ik}$  can be taken as constant. Here  $y_{k,0}$  denotes the equilibrium value of the composition variable  $y_k$ . Hence the extended diffusion equation for the mass density  $\rho_i$  reads

$$\frac{\partial \rho_i}{\partial t} = \rho_{i,0} \phi_{K,0} D_{i,T} \Delta T + \sum_{k=1}^{K-1} D_{ik} \Delta \rho_k \quad i = 1 \dots K-1. \quad (2.217)$$

If the center of mass velocity  $\vec{v}$  vanishes it is found from Eq. (2.211) and Eq. (2.186)

$$\frac{\partial c_i}{\partial t} = -\frac{1}{\rho} \vec{\nabla} \cdot \vec{J}_i = \frac{1}{\rho} \vec{\nabla} \cdot \left[ \rho c_i c_K \mathcal{D}_{i,T} \vec{\nabla} T + \rho \sum_{k=1}^{K-1} \mathcal{D}_{ik} \vec{\nabla} c_k \right] \quad i = 1 \dots K-1. \quad (2.218)$$

In isothermal, isobaric systems it follows from vanishing center of mass velocity that  $\vec{\nabla} \rho = 0$  (cf. Eq. (2.253) below) and one obtains

$$\frac{\partial c_i}{\partial t} = -\frac{1}{\rho} \vec{\nabla} \cdot \vec{J}_i = -\vec{\nabla} \cdot \left( \frac{\vec{J}_i}{\rho} \right) = \vec{\nabla} \cdot \left[ \sum_{k=1}^{K-1} \mathcal{D}_{ik} \vec{\nabla} c_k \right] \quad i = 1 \dots K-1. \quad (2.219)$$

For small gradients ( $\rho \approx \rho_0$ ,  $c_k \approx c_{k,0}$ ) Eq. (2.218) simplifies to the extended diffusion

equation for the weight fractions  $c_i$

$$\frac{\partial c_i}{\partial t} = c_{i,0} c_{K,0} \mathcal{D}_{i,T} \Delta T + \sum_{k=1}^{K-1} \mathcal{D}_{ik} \Delta c_k \quad i = 1 \dots K - 1. \quad (2.220)$$

For vanishing mean molar velocity Eq. (2.214) and Eq. (2.187) can be combined to

$$\frac{\partial x_i}{\partial t} = -\frac{1}{n} \vec{\nabla} \cdot \left( \frac{\vec{J}_i^{\text{mol}}}{M_i} \right) = \frac{1}{n} \vec{\nabla} \cdot \left[ n x_i x_K D_{i,T}^* \vec{\nabla} T + n \sum_{k=1}^{K-1} D_{ik}^* \vec{\nabla} x_k \right] \quad i = 1 \dots K - 1. \quad (2.221)$$

In the absence of temperature and pressure gradients the number density is uniform as a consequence of vanishing mean molar velocity and one has

$$\frac{\partial x_i}{\partial t} = -\frac{1}{n} \vec{\nabla} \cdot \left( \frac{\vec{J}_i^{\text{mol}}}{M_i} \right) = -\vec{\nabla} \cdot \left( \frac{\vec{J}_i^{\text{mol}}}{M_i n} \right) = \vec{\nabla} \cdot \left[ \sum_{k=1}^{K-1} D_{ik}^* \vec{\nabla} x_k \right] \quad i = 1 \dots K - 1. \quad (2.222)$$

In case of small gradients  $n \approx n_0$ ,  $x_i \approx x_{i,0}$ ,  $x_K \approx x_{K,0}$ ,  $D_{i,T}^*$ , and  $D_{ik}^*$  are approximately constant and the extended diffusion equation for the mole fractions  $x_i$  is obtained

$$\frac{\partial x_i}{\partial t} = x_{i,0} x_{K,0} D_{i,T}^* \Delta T + \sum_{k=1}^{K-1} D_{ik}^* \Delta x_k \quad i = 1 \dots K - 1. \quad (2.223)$$

**... in case of small perturbations** In case of non-zero reference velocities, it is still possible to derive simple evolution equations, if temperature and concentration gradients are kept small and appropriate composition variables and fluxes are chosen.

For small deviations from equilibrium, the temperature gradient  $\vec{\nabla} T$  and the gradients of the composition variables  $\vec{\nabla} y_k$  are small. Taking into account the phenomenological equations also the fluxes  $\vec{J}_k^a$  and the particle velocities  $\vec{v}_k$  are found to be small. One may then introduce an  $\varepsilon \ll 1$  by

$$\vec{\nabla} T \sim \varepsilon, \quad \vec{\nabla} y_k \sim \varepsilon, \quad \vec{J}_k^a \sim \varepsilon, \quad \vec{v}_k \sim \varepsilon, \quad \vec{v}^a = \sum a_k \vec{v}_k \sim \varepsilon \quad (2.224)$$

and neglect all terms of the order  $\varepsilon^2$ .

Setting  $\vec{J}_k^a = \vec{J}_k$  and  $\vec{v}^a = \vec{v}$  in Eq. (2.211) yields

$$\begin{aligned} \frac{\partial c_k}{\partial t} &= -\frac{1}{\rho} \left[ \vec{\nabla} \cdot \vec{J}_k + \vec{\nabla} \cdot (\rho_k \vec{v}) - c_k \vec{\nabla} \cdot (\rho \vec{v}) \right] \\ &= -\vec{\nabla} \cdot \left( \frac{\vec{J}_k}{\rho} \right) - \frac{1}{\rho^2} \vec{J}_k \vec{\nabla} \rho - \vec{v} \vec{\nabla} c_k \quad k = 1 \dots K - 1. \end{aligned} \quad (2.225)$$

For small gradients the second order terms  $\vec{J}_k \vec{\nabla} \rho$  and  $\vec{v} \vec{\nabla} c_k$  can be neglected and the weight



fractions solve

$$\begin{aligned} \frac{\partial c_k}{\partial t} &\approx -\vec{\nabla} \cdot \left( \frac{\vec{J}_k}{\rho} \right) = \vec{\nabla} \cdot \left[ c_k c_K \mathcal{D}_{k,T} \vec{\nabla} T + \sum_{i=1}^{K-1} \mathcal{D}_{ki} \vec{\nabla} c_i \right] \\ &\approx c_{k,0} c_{K,0} \mathcal{D}_{k,T} \Delta T + \sum_{i=1}^{K-1} \mathcal{D}_{ki} \Delta c_i \quad k = 1 \dots K-1, \end{aligned} \quad (2.226)$$

where Eq. (2.186) has been used.

Similarly one obtains for the mole fractions from Eq. (2.214) with  $\vec{J}_k^a = \vec{J}_k^{\text{mol}}$  and  $\vec{v}^a = \vec{v}^{\text{mol}}$ :

$$\begin{aligned} \frac{\partial x_k}{\partial t} &= -\frac{1}{n} \left[ \vec{\nabla} \cdot \left( \frac{\vec{J}_k^{\text{mol}}}{M_k} \right) + \vec{\nabla} \cdot (n_k \vec{v}^{\text{mol}}) - x_k \vec{\nabla} \cdot (n \vec{v}^{\text{mol}}) \right] \\ &= -\vec{\nabla} \cdot \left( \frac{\vec{J}_k^{\text{mol}}}{n M_k} \right) - \frac{1}{n^2} \frac{\vec{J}_k^{\text{mol}}}{M_k} \vec{\nabla} n - \vec{v}^{\text{mol}} \vec{\nabla} x_k \quad k = 1 \dots K-1 \end{aligned} \quad (2.227)$$

Again for small gradients the terms  $\vec{J}_k^{\text{mol}} \vec{\nabla} n$  and  $\vec{v}^{\text{mol}} \vec{\nabla} x_k$  are of order  $\varepsilon^2$  and therefore negligible. With Eq. (2.187) there results

$$\begin{aligned} \frac{\partial x_k}{\partial t} &\approx -\vec{\nabla} \cdot \left( \frac{\vec{J}_k^{\text{mol}}}{n M_k} \right) = \vec{\nabla} \cdot \left[ x_k x_K D_{k,T}^* \vec{\nabla} T + \sum_{i=1}^{K-1} D_{ki}^* \vec{\nabla} x_i \right] \\ &\approx x_{k,0} x_{K,0} D_{k,T}^* \Delta T + \sum_{i=1}^{K-1} D_{ki}^* \Delta x_i \quad k = 1 \dots K-1. \end{aligned} \quad (2.228)$$

By replacing  $\vec{J}_k^a$  and  $\vec{v}^a$  in Eq. (2.208) by  $\vec{J}_k^{\text{vol}}$  and  $\vec{v}^{\text{vol}}$  an evolution equation for the mass density is obtained

$$\frac{\partial \rho_k}{\partial t} = -\vec{\nabla} \cdot \vec{J}_k^{\text{vol}} - \vec{\nabla} \cdot (\rho_k \vec{v}^{\text{vol}}) \quad k = 1 \dots K-1. \quad (2.229)$$

Here the situation is more complicated than for the weight fractions Eq. (2.225) and for the mole fractions Eq. (2.227). According to Eq. (2.224) the terms  $\vec{\nabla} \cdot (\rho_k \vec{v}^{\text{vol}})$  and  $\vec{\nabla} \cdot \vec{J}_k^{\text{vol}}$  are of same order of magnitude. In Sec. 2.2.4.3 we will derive (Eq. (2.248) below)

$$\vec{\nabla} \cdot (\rho_k \vec{v}^{\text{vol}}) = \rho_k \alpha \frac{\partial T}{\partial t} + \text{second order terms}, \quad (2.230)$$

where  $\alpha$  is the thermal expansion coefficient. Hence, if all gradients are small and second order terms can be neglected, the evolution equation for the mass density is given by

$$\frac{\partial \rho_k}{\partial t} \approx -\vec{\nabla} \cdot \vec{J}_k^{\text{vol}} - \rho_k \alpha \frac{\partial T}{\partial t} \quad k = 1 \dots K-1. \quad (2.231)$$

Only in case of steady temperature the second term on the right hand side of Eq. (2.231)

can be dropped. Then a simple diffusion equation is obtained with the help of Eq. (2.188)

$$\begin{aligned} \frac{\partial \rho_k}{\partial t} &\approx -\vec{\nabla} \cdot \vec{J}_k^{\text{vol}} = \vec{\nabla} \cdot \left[ \rho_k \phi_K D_{k,T} \vec{\nabla} T + \sum_{i=1}^{K-1} D_{ki} \vec{\nabla} \rho_i \right] \\ &\approx \rho_{k,0} \phi_{K,0} D_{k,T} \Delta T + \sum_{i=1}^{K-1} D_{ki} \Delta \rho_i \quad k = 1 \dots K-1. \end{aligned} \quad (2.232)$$

To resume, it could be shown that

$$\frac{\partial c_k}{\partial t} \approx -\vec{\nabla} \cdot \left( \frac{\vec{J}_k}{\rho} \right) \quad (\text{Eq. (2.226)})$$

$$\frac{\partial x_k}{\partial t} \approx -\vec{\nabla} \cdot \left( \frac{\vec{J}_k^{\text{mol}}}{nM_k} \right) \quad (\text{Eq. (2.228)})$$

$$\frac{\partial \rho_k}{\partial t} \approx -\vec{\nabla} \cdot \vec{J}_k^{\text{vol}} - \rho_k \alpha \frac{\partial T}{\partial t} \quad (\text{Eq. (2.231)})$$

are simultaneously valid, if second order terms may be neglected. No additional assumptions about the reference velocities  $\vec{v}$ ,  $\vec{v}^{\text{mol}}$ , and  $\vec{v}^{\text{vol}}$  are necessary. This means, for small gradients, Eq. (2.226), Eq. (2.228), and Eq. (2.231) also hold in case of non zero reference velocities.

Note that Eq. (2.228) immediately follows from Eq. (2.226) because of

$$\frac{\vec{J}_k^{\text{mol}}}{nM_k} = \sum_{i=1}^{K-1} \left( \frac{\partial x_k}{\partial c_i} \right) \frac{\vec{J}_i}{\rho} \quad (\text{Eq. (2.145)}) \quad \text{and} \quad \frac{\partial x_k}{\partial t} = \sum_{i=1}^{K-1} \left( \frac{\partial x_k}{\partial c_i} \right) \frac{\partial c_i}{\partial t} \quad (2.233)$$

with the abbreviation  $(\partial/\partial c_i)$  from Eq. (2.146). Similarly, with the help of

$$\vec{J}_k^{\text{vol}} = \sum_{i=1}^{K-1} \left( \frac{\partial \rho_k}{\partial c_i} \right) \frac{\vec{J}_i}{\rho} \quad (\text{Eq. (2.152)}) \quad \text{and} \quad \frac{\partial \rho_k}{\partial t} = \sum_{i=1}^{K-1} \left( \frac{\partial \rho_k}{\partial c_i} \right) \frac{\partial c_i}{\partial t} - \alpha \rho_k \frac{\partial T}{\partial t} \quad (2.234)$$

Eq. (2.231) can be directly obtained from Eq. (2.226).<sup>11</sup>

### 2.2.4.3 Conditions for Vanishing of a Reference Velocity

The normal components of all velocities vanish at the boundary of the vessel. Therefore the reference velocity  $\vec{v}^a$  vanishes everywhere, if  $\vec{\nabla} \times \vec{v}^a = 0$  and  $\vec{\nabla} \cdot \vec{v}^a = 0$ . Many diffusion experiments are performed in the absence of convection with  $\vec{\nabla} \times \vec{v}_k = 0$  for  $k = 1 \dots K$  and hence  $\vec{\nabla} \times \vec{v}^a = 0$ . We will consider in the following only convection–free situations, where it follows  $\vec{v}^a = 0$  from  $\vec{\nabla} \cdot \vec{v}^a = 0$ .

<sup>11</sup>In Ref. [61] all effects due to thermal expansion have been neglected ( $\alpha = 0$ ).  $\rho_k(x, t)$  is obtained by solving  $(\partial \rho_k / \partial t) = -\vec{\nabla} \cdot \vec{J}_k^{\text{vol}}$ . From  $\rho_k(x, t)$  the weight fractions are calculated according to  $c_k(x, t) = c_{k,0} + \sum (\partial c_k / \partial \rho_i) [\rho_i(x, t) - \rho_{i,0}]$ . It is stated that another solution  $c'_k(x, t)$  would have been obtained from solving  $(\partial c_k / \partial t) = -\vec{\nabla} \cdot (\vec{J}_k / \rho)$ . This is not correct and can be easily disproved by means of Eq. (2.153).

By combining arguments of Agar [1] and Kirkwood et al. [49], we will derive a general expression for  $\vec{\nabla} \cdot \vec{v}^a$ . Note that de Groot and Mazur [16] also treated the problem of vanishing reference velocities. They derived the following equations

$$\vec{\nabla} \cdot \vec{v}^{\text{vol}} = \sum_{k=1}^K \left( \rho_k \frac{\partial v_k}{\partial t} + \rho_k \vec{v}_k \vec{\nabla} v_k \right) \quad (2.235)$$

$$\vec{\nabla} \cdot \vec{v} = -\frac{1}{\rho} \left( \frac{\partial \rho}{\partial t} + \vec{v} \vec{\nabla} \rho \right) \quad (2.236)$$

$$\vec{\nabla} \cdot \vec{v}^{\text{mol}} = -\frac{1}{n} \left( \frac{\partial n}{\partial t} + \vec{v}^{\text{mol}} \vec{\nabla} n \right) \quad (2.237)$$

and followed that  $\vec{v}^{\text{vol}}$  ( $\vec{v}$  or  $\vec{v}^{\text{mol}}$ ) vanishes, if the partial specific volumes (the mass or particle density) are (is) uniform and constant in time. They considered, however, only isothermal systems. In the presence of temperature gradients, partial specific volumes and densities are space-dependent merely due to thermal expansion. Nevertheless reference velocities can also vanish in non-isothermal systems.

From Eq. (2.208) it follows that

$$\rho_k \vec{\nabla} \cdot \vec{v}^a = -\frac{\partial \rho_k}{\partial t} - \vec{v}^a \vec{\nabla} \rho_k - \vec{\nabla} \cdot \vec{J}_k^a \quad k = 1 \dots K. \quad (2.238)$$

Eq. (2.238) may be simplified with the help of

$$-\sum_{k=1}^K v_k (d\rho_k)_p = \sum_{k=1}^K \rho_k (dv_k)_p = \alpha dT, \quad (2.239)$$

which is found from

$$\sum_{k=1}^K \phi_k = \sum_{k=1}^K \rho_k v_k = 1 \quad (2.240)$$

and

$$(dV)_p = V \alpha dT + \sum_{k=1}^K v_k dm_k = \left[ d \left( \sum_{k=1}^K v_k m_k \right) \right]_p = \sum_{k=1}^K m_k (dv_k)_p + \sum_{k=1}^K v_k dm_k. \quad (2.241)$$

By multiplying Eq. (2.238) by  $v_k$ , summing over all components, and using the relations (2.239, 2.240) one obtains the general expression

$$\vec{\nabla} \cdot \vec{v}^a = \alpha \frac{\partial T}{\partial t} + \alpha \vec{v}^a \vec{\nabla} T + \Sigma^a \quad (2.242)$$

with

$$\Sigma^a = -\sum_{k=1}^K v_k \vec{\nabla} \cdot \vec{J}_k^a = -\vec{\nabla} \cdot \left[ \sum_{k=1}^K v_k \vec{J}_k^a \right] + \sum_{k=1}^K \vec{J}_k^a \vec{\nabla} v_k. \quad (2.243)$$

Before we discuss Eqs. (2.242, 2.243) for the reference velocities  $\vec{v}^{\text{vol}}$ ,  $\vec{v}$ , and  $\vec{v}^{\text{mol}}$ , we can draw a few general conclusions which hold for an arbitrary reference velocity:

- For time–dependent temperature the reference velocities do not vanish.  $(\partial T/\partial t)$  as well as  $\vec{v}^a$  are then of first order  $\sim \varepsilon$ , where  $\varepsilon$  has been introduced in Eq. (2.224).
- For steady temperature the reference velocity vanishes (is of first/second order), if  $\Sigma^a$  vanishes (is of first/second order).
- The term  $\alpha \vec{v}^a \vec{\nabla} T$  is not important. For steady temperature and vanishing  $\Sigma^a$  one has

$$\vec{\nabla} \cdot \vec{v}^a = \alpha \vec{v}^a \vec{\nabla} T. \quad (2.244)$$

with the solution  $\vec{v}^a \equiv 0$  due to the boundary conditions. Otherwise, if  $\vec{v}^a$  is of order  $n$ , then  $\vec{v}^a \vec{\nabla} T$  is of order  $n + 1$  and can be neglected for small gradients.

- If all diffusion currents  $\vec{J}_k^a = J_k^a \vec{e}_x$  of the individual species lie in one spatial direction and if the system is isothermal,  $\vec{v}^a = v^a \vec{e}_x$  can be calculated from Eq. (2.242) by

$$\vec{v}^a = \int_{-L}^x \Sigma^a dx, \quad (2.245)$$

where  $x = -L$  is the bottom of the cell.

**Mean volume velocity** Eq. (2.243) can be simplified by using Eq. (2.132)

$$\Sigma^{\text{vol}} = \sum_{k=1}^K \vec{J}_k^{\text{vol}} \vec{\nabla} v_k. \quad (2.246)$$

$\Sigma^{\text{vol}}$  and, in case of steady temperature, also  $\vec{v}^{\text{vol}}$  vanishes, if

- the partial specific volumes are uniform with  $\vec{\nabla} v_k = 0$ . This occurs in isothermal diffusion experiments where the partial specific volumes do not depend on concentration. Examples of such systems are liquid mixtures where volume changes of mixing can be neglected.
- the partial specific volumes are independent of concentration and have all the same temperature dependence with  $\alpha_k = v_k^{-1} (\partial v_k / \partial T)_{p, \{c_i\}} = \alpha$ . Then  $\Sigma^{\text{vol}}$  vanishes according to Eq. (2.132), if

$$\vec{\nabla} v_k = \frac{dv_k}{dT} \vec{\nabla} T = \alpha v_k \vec{\nabla} T \quad (2.247)$$

is taken into account.

- (c) all diffusing species have identical partial specific volumes ( $v_i = v = \rho^{-1}$  for  $i = 1 \dots K$ ). This is because of Eq. (2.150) a special case of (b). In this case also the center of mass velocity vanishes (cf. page 49).
- (d) all diffusing species have identical partial molar volumes, which is again a special case of (b). Then also the mean molar velocity vanishes (cf. page 50).

Otherwise  $\Sigma^{\text{vol}}$  is a second order term  $\sim \varepsilon^2$  with  $\varepsilon$  from Eq. (2.224). Hence, for stationary temperature distributions, also  $\vec{v}^{\text{vol}}$  is of second order  $\sim \varepsilon^2$  and may be neglected if compared to  $\vec{v}_k \sim \varepsilon$ .

For time dependent temperature one obtains

$$\vec{\nabla} \cdot \vec{v}^{\text{vol}} = \alpha \frac{\partial T}{\partial t} + \text{second order terms.} \quad (2.248)$$

In isothermal, one-dimensional systems  $\vec{v}^{\text{vol}} = v^{\text{vol}} \vec{e}_x$  may be evaluated with the help of Eq. (2.245) [49]. Especially simple results are obtained for a binary mixture with

$$\Sigma^{\text{vol}} = J_1^{\text{vol}} \frac{\partial v_1}{\partial x} + J_2^{\text{vol}} \frac{\partial v_2}{\partial x} = \left(1 + \frac{v_1 \rho_1}{v_2 \rho_2}\right) J_1^{\text{vol}} \frac{\partial v_1}{\partial x} = \frac{J_1^{\text{vol}}}{\rho_2 v_2} \frac{\partial v_1}{\partial x} = -\frac{D}{\rho_2 v_2} \frac{\partial \rho_1}{\partial x} \frac{\partial v_1}{\partial x}, \quad (2.249)$$

Here Eqs. (2.132, 2.239, 2.240, 2.200) have been used. Then the mean volume velocity and the flux in the laboratory reference frame are given by

$$v^{\text{vol}} = -\int_{-L}^x \frac{D}{\rho_2 v_2} \frac{\partial \rho_1}{\partial x} \frac{\partial v_1}{\partial x} dx. \quad (2.250)$$

$$J_1^{\text{lab}} = J_1^{\text{vol}} + \rho_1 v^{\text{vol}} = -D \frac{\partial \rho_1}{\partial x} - \rho_1 \int_{-L}^x \frac{D}{\rho_2 v_2} \frac{\partial \rho_1}{\partial x} \frac{\partial v_1}{\partial x} dx. \quad (2.251)$$

**Center of mass velocity** With  $\vec{J}_k^a = \vec{J}_k$  Eq. (2.243) becomes

$$\Sigma = -\sum_{k=1}^K v_k \vec{\nabla} \cdot \vec{J}_k. \quad (2.252)$$

$\Sigma$  and, in case of steady temperature, also  $\vec{v}$  vanishes, if

- all species have the same partial specific volume ( $v_i = v$  for  $i = 1 \dots K$ ). Then  $\Sigma$  is equal to zero because of Eq. (2.125). Examples for such systems are isomer mixtures or isotopic mixtures with not too different molecular masses.

Otherwise  $\Sigma$  as well as  $\vec{v}$  are first order terms which may not be neglected.

In case of vanishing center of mass velocity it follows from Eq. (2.150) and Eq. (2.210)

$$\vec{\nabla} \rho = -\alpha \rho \vec{\nabla} T, \quad \frac{\partial \rho}{\partial t} = 0 \quad (\vec{v} = 0), \quad (2.253)$$

i.e. only in isothermal (and isobaric) experiments the density is uniform.

With the help of Eq. (2.149) the mean volume velocity can be related to the center of mass velocity

$$\rho_k(\vec{v} - \vec{v}^{\text{vol}}) = \vec{J}_k^{\text{vol}} - \vec{J}_k = \sum_{i=1}^{K-1} \rho_k(v_K - v_i)\vec{J}_i. \quad (2.254)$$

Obviously it follows from  $\vec{v} = 0$  (which is equivalent to  $v_K - v_i = 0$ ) that also  $\vec{v}^{\text{vol}} = 0$ . The converse is, however, not true: In general one may not conclude  $\vec{v} = 0$  from  $\vec{v}^{\text{vol}} = 0$ .

**Mean molar velocity** Setting  $\vec{J}_k^a = \vec{J}_k^{\text{mol}}$  in Eq. (2.243) yields

$$\Sigma^{\text{mol}} = - \sum_{i=1}^K v_i M_i \vec{\nabla} \cdot \frac{\vec{J}_i^{\text{mol}}}{M_i}. \quad (2.255)$$

$\Sigma^{\text{mol}}$  and, in case of steady temperature, also  $\vec{v}^{\text{mol}}$  vanishes, if

- all components of the mixture have the same partial molar volume ( $v_i M_i = v_K M_K$  for  $i = 1 \dots K - 1$ ). This is fulfilled in diffusion experiments in perfect gases. In this case  $\Sigma^{\text{mol}}$  vanishes according to Eq. (2.137).

Otherwise  $\Sigma^{\text{mol}}$  as well as  $\vec{v}^{\text{mol}}$  are first order terms, which may not be neglected.

An analogous derivation as in Eq. (2.254) yields: From  $\vec{v}^{\text{mol}} = 0$  it follows  $\vec{v}^{\text{vol}} = 0$ .

**Dilute binary systems** In dilute binary systems all reference velocities are approximately identical, as can be seen from Eq. (2.127) with  $K = 2$ ,  $a_1 \ll 1$ , and  $a_2 \simeq 1$

$$\vec{v}^a = a_1 \vec{v}_1 + a_2 \vec{v}_2 \simeq \vec{v}_2. \quad (2.256)$$

Using

$$\vec{J}_1^a = \rho_1(\vec{v}_1 - \vec{v}^a) \simeq 0 \quad (\rho_1 \ll 1) \quad (2.257)$$

$$\vec{J}_2^a = \rho_2(\vec{v}_2 - \vec{v}^a) \simeq 0 \quad (\vec{v}^a \simeq \vec{v}_2) \quad (2.258)$$

in Eq. (2.243) yields

$$\Sigma^a \simeq 0 \quad (\vec{v}^a \simeq \vec{v}_2, \rho_1 \ll 1). \quad (2.259)$$

Hence for steady temperature all reference velocities in dilute binary systems are negligible if compared to  $\vec{v}_1$ . For time-dependent temperature one obtains from Eq. (2.242)

$$\vec{\nabla} \cdot \vec{v}^a \simeq \alpha \frac{\partial T}{\partial t} \quad (\vec{v}^a \simeq \vec{v}_2, \rho_1 \ll 1). \quad (2.260)$$

### 2.2.4.4 Summary of Sections 2.2.4.1–2.2.4.3

1. Generally the reference velocities do not vanish. With the small  $\varepsilon$  from Eq. (2.224) one typically has  $\vec{v} \sim \varepsilon$ ,  $\vec{v}^{\text{mol}} \sim \varepsilon$ , and  $\vec{v}^{\text{vol}} \sim \varepsilon^2$  or  $\vec{v}^{\text{vol}} \sim \varepsilon$  depending on whether the temperature gradients are stationary ( $\sim \varepsilon^2$ ) or not ( $\sim \varepsilon$ ). Nevertheless, even for non-zero reference velocities simple diffusion equations can be derived, **if the temperature and concentration gradients are assumed to be small**. They read (cf. Eq. (2.226), Eq. (2.228), Eq. (2.231))

$$\begin{aligned} \frac{\partial c_k}{\partial t} &\approx -\vec{\nabla} \cdot \left( \frac{\vec{J}_k}{\rho} \right) \approx c_{k,0} c_{K,0} \mathcal{D}_{k,T} \Delta T + \sum_{i=1}^{K-1} \mathcal{D}_{ki} \Delta c_i \quad k = 1 \dots K-1 \\ \frac{\partial x_k}{\partial t} &\approx -\vec{\nabla} \cdot \left( \frac{\vec{J}_k^{\text{mol}}}{n M_k} \right) \approx x_{k,0} x_{K,0} D_{k,T}^* \Delta T + \sum_{i=1}^{K-1} D_{ki}^* \Delta x_i \quad k = 1 \dots K-1. \\ \frac{\partial \rho_k}{\partial t} &\approx -\vec{\nabla} \cdot \vec{J}_k^{\text{vol}} - \rho_k \alpha \frac{\partial T}{\partial t} \approx \rho_{k,0} \phi_{K,0} D_{k,T} \Delta T + \sum_{i=1}^{K-1} D_{ki} \Delta \rho_i - \rho_{k,0} \alpha \frac{\partial T}{\partial t} \\ & \quad k = 1 \dots K-1. \end{aligned}$$

and are all simultaneously valid. For a binary mixture ( $K = 2$ ) one has according to Eqs. (2.194)–(2.197)  $\mathcal{D}_{11} = D_{11}^* = D_{11} = D$  and  $\mathcal{D}_{1,T} = D_{1,T}^* = D_{1,T} - \alpha D / \phi_2 = D_T$ . For multicomponent mixtures with  $K > 2$  the relations between the diffusion coefficients are given by Eqs. (2.189)–(2.192).

2. **If the mean volume velocity is zero** (e.g. in isothermal systems without volume changes of mixing), the mass density solves according to Eq. (2.216)

$$\frac{\partial \rho_k}{\partial t} = -\vec{\nabla} \cdot \vec{J}_k^{\text{vol}} = \vec{\nabla} \cdot \left[ \rho_k \phi_K D_{k,T} \vec{\nabla} T + \sum_{i=1}^{K-1} D_{ki} \vec{\nabla} \rho_i \right] \quad k = 1 \dots K-1.$$

In general one may not conclude from  $\vec{v}^{\text{vol}} \equiv 0$  that also  $\vec{v} \equiv 0$ . The evolution equation for the weight fractions in case of vanishing mean volume velocity is given by Eq. (2.211) with  $\vec{v}^a = \vec{v}^{\text{vol}} = 0$  and  $\vec{J}_k^a = \vec{J}_k^{\text{vol}}$  from Eq. (2.188)

$$\frac{\partial c_k}{\partial t} = \frac{1}{\rho} \vec{\nabla} \cdot \left[ \rho_k \phi_K D_{k,T} \vec{\nabla} T + \sum_{i=1}^{K-1} D_{ki} \vec{\nabla} \rho_i \right] + \frac{c_k}{\rho} \vec{\nabla} \cdot (\rho \vec{v}). \quad (2.261)$$

3. **If the center of mass velocity is zero** (e.g. in isomer mixtures or isotopic mixtures with not too different molecular masses and stationary temperature distribution), it follows that also the mean volume velocity is zero and the corresponding fluxes agree  $\vec{J}_k^{\text{vol}} = \vec{J}_k$ .

Then the two diffusion equations Eq. (2.218) and Eq. (2.216)

$$\begin{aligned}\frac{\partial c_k}{\partial t} &= -\frac{1}{\rho} \vec{\nabla} \cdot \vec{J}_k = \frac{1}{\rho} \vec{\nabla} \cdot \left[ \rho c_k c_K \mathcal{D}_{k,T} \vec{\nabla} T + \rho \sum_{i=1}^{K-1} \mathcal{D}_{ki} \vec{\nabla} c_i \right] \quad k = 1 \dots K-1 \\ \frac{\partial \rho_k}{\partial t} &= -\vec{\nabla} \cdot \vec{J}_k = \vec{\nabla} \cdot \left[ \rho_k \phi_K \mathcal{D}_{k,T} \vec{\nabla} T - \sum_{i=1}^{K-1} \mathcal{D}_{ki} \vec{\nabla} \rho_i \right] \quad k = 1 \dots K-1.\end{aligned}$$

are simultaneously valid. Since all partial specific volumes are identical for vanishing center of mass velocity, it results  $(\partial \rho_j / \partial c_k) = (\partial c_j / \partial \rho_k)^{-1} = \rho \delta_{jk}$  and  $c_K = \phi_K$ . Therefore the relations (2.191, 2.192) simplify to

$$D_{ki} = \mathcal{D}_{ki} \quad (2.262)$$

$$D_{k,T} = \mathcal{D}_{k,T} + \frac{\alpha}{\rho_k \phi_K} \sum_{i=1}^{K-1} \mathcal{D}_{ki} \rho_i. \quad (2.263)$$

### 2.2.4.5 Heat Equation

The evolution equation for the temperature is found by differentiating the specific entropy  $s(T, c_k, p)$  with respect to time:

$$\frac{\partial s}{\partial t} = \frac{c_p}{T} \frac{\partial T}{\partial t} + \sum_{k=1}^K s_k \frac{\partial c_k}{\partial t} - \frac{\alpha}{\rho} \frac{\partial p}{\partial t}. \quad (2.264)$$

Here the specific heat at constant pressure  $c_p$  has been introduced and the Maxwell relation  $(\partial s / \partial p)_{T, \{c_i\}} = -\alpha / \rho$  has been used. With the help of Eqs. (2.64, 2.65, 2.70, 2.76, 2.77) one finds

$$\rho \frac{\partial c_k}{\partial t} = -\vec{\nabla} \cdot \vec{J}_k - \rho \vec{v} \cdot \vec{\nabla} c_k + \sum_{j=1}^r \nu_{kj} J_j \quad (2.265)$$

$$\rho \frac{\partial s}{\partial t} = -\frac{1}{T} \vec{\nabla} \cdot \vec{J}_Q + \sigma + \frac{1}{T^2} \vec{J}_Q \cdot \vec{\nabla} T - \sum_{k=1}^K \left( s_k \vec{\nabla} \cdot \vec{J}_k + s_k \rho \vec{v} \cdot \vec{\nabla} c_k + \rho_k \vec{v}_k \cdot \vec{\nabla} s_k \right), \quad (2.266)$$

where  $s = \sum s_k c_k$  has been used. If Eqs. (2.265, 2.266) are inserted into Eq. (2.264) the general heat equation

$$\rho c_p \frac{\partial T}{\partial t} = -\vec{\nabla} \cdot \vec{J}_Q + \alpha T \frac{\partial p}{\partial t} + \sigma T + \underbrace{\frac{1}{T} \vec{J}_Q \cdot \vec{\nabla} T - T \sum_{k=1}^K \left[ \rho_k \vec{v}_k \cdot \vec{\nabla} s_k + s_k \sum_{j=1}^r \nu_{kj} J_j \right]}_{\text{second order terms}} \quad (2.267)$$



is obtained.<sup>12</sup> The temperature increases not only if heat flows into the system, but also if irreversible processes occur within the system. The heat flux term  $\vec{\nabla} \cdot \vec{J}_Q$  is, however, usually much more important than the second order terms of Eq. (2.267), which are related to irreversible processes. For constant pressure

$$\rho c_p \frac{\partial T}{\partial t} = -\vec{\nabla} \cdot \vec{J}_Q \quad (2.268)$$

holds to very good approximation. The heat flow  $\vec{J}_Q$  in a binary mixture is given by Eq. (2.97). In liquids the Dufour effect is in general negligible and one has

$$\vec{J}_Q = -\kappa_0 \vec{\nabla} T = -\kappa_\infty \vec{\nabla} T = -\kappa \vec{\nabla} T, \quad (2.269)$$

where  $\kappa$  is the heat conductivity. Combining Eq. (2.268) and (2.269) yields the well known heat equation

$$\rho c_p \frac{\partial T}{\partial t} = \vec{\nabla} \cdot (\kappa \vec{\nabla} T). \quad (2.270)$$

In the presence of external heat sources, a source term has to be included in the heat equation yielding

$$\rho c_p \frac{\partial T}{\partial t} = \vec{\nabla} \cdot (\kappa \vec{\nabla} T) + \dot{Q}. \quad (2.271)$$

For small deviations from equilibrium,  $\kappa$  may be assumed to be approximately constant and with the definition of the thermal diffusivity

$$D_{th} = \frac{\kappa}{\rho c_p} \quad (2.272)$$

one obtains

$$\frac{\partial T}{\partial t} = D_{th} \Delta T + \frac{\dot{Q}}{\rho c_p} \quad (2.273)$$

We would like to emphasize that two approximations were necessary for the derivation of the heat equation: Both, the temperature increase due to irreversible processes and the Dufour effect, have been neglected.

### 2.2.5 Thermodynamic Driving Forces

The derivation of thermodynamic driving forces is closely related to the issue of different reference velocities. To deduce the actual hydrodynamic friction force on a diffusing particle, both, the relative flux and the flux in the laboratory reference frame have to be considered. In particular, relations between these fluxes are needed. In isothermal diffusion experiments one typically has  $\vec{v}^{\text{vol}} = 0$  and the flux relative to the mean volume velocity is identical to the flux in the laboratory reference frame (see Sec. 2.2.4.3). Hence the conversion formulae

<sup>12</sup>Eq. (2.267) is equivalent to Eq. (4-6.20) in Ref. [40] as can be seen with the help of Eq. (2.70) and Eq. (2.79) and by noting  $(c_p/T) \vec{\nabla} T - (\alpha/\rho) \vec{\nabla} p = \sum c_k \vec{\nabla} s_k$  and  $(\vec{\nabla} \mu_k)_T = \vec{\nabla} h_k - T \vec{\nabla} s_k$ .

from Sec. 2.2.1–2.2.2 can be used.

### 2.2.5.1 Diffusion Coefficient

First we will derive relations for the diffusion coefficient by considering the generalized forces appearing in the dissipation function. Then we will consider external forces, which allow a clearer definition of friction coefficients. An expression of the diffusion coefficient in terms of these friction coefficient will be obtained. Finally, the thermodynamic driving force, which is actually exerted on a particle during diffusion, will be calculated. For simplicity we will consider only binary mixtures. The binary diffusion coefficient  $D$  as introduced by Eq. (2.98) depends on concentration and temperature, but not on concentration gradients or temperature gradients. Hence the same  $D$  is measured, irrespective whether temperature gradients are present or not. Therefore we may derive an expression for  $D$  by considering an isothermal experiment.

**Definition of generalized friction coefficients** A generalized friction coefficient may be introduced with the help of Eq. (2.167)

$$\vec{X}_1^a = -\frac{\rho_1 T}{L_{11}^a} (\vec{v}_1 - \vec{v}^a) =: -f_1^a (\vec{v}_1 - \vec{v}^a), \quad (2.274)$$

where  $X_1^a$  is the generalized force from Eq. (2.172). The diffusion coefficient can be related to the generalized friction coefficient with the help of Eqs. (2.100, 2.172, 2.274)

$$D = \frac{\phi_2}{a_2^2} \frac{1}{f_1^a} \rho_1 \left( \frac{\partial \mu_1}{\partial \rho_1} \right)_{p,T} = \frac{x_2}{a_2^2} \frac{1}{f_1^a} x_1 \left( \frac{\partial \mu_1}{\partial x_1} \right)_{p,T}. \quad (2.275)$$

Here

$$\left( \frac{\partial \mu_1}{\partial c_1} \right)_{p,T} = \rho \frac{\phi_2}{c_2} \left( \frac{\partial \mu_1}{\partial \rho_1} \right)_{p,T} = \frac{x_1 x_2}{c_1 c_2} \left( \frac{\partial \mu_1}{\partial x_1} \right)_{p,T} \quad (2.276)$$

has been used, which follows from  $(\partial \rho_1 / \partial c_1) = \rho^2 v_2 = \rho \phi_2 / c_2$  and  $(\partial x_1 / \partial c_1) = x_1 x_2 / (c_1 c_2)$ . Special cases of Eq. (2.275) are

$$D = \frac{1}{\phi_2 f_1^{\text{vol}}} \rho_1 \left( \frac{\partial \mu_1}{\partial \rho_1} \right)_{p,T} \quad (\vec{v}^a = \vec{v}^{\text{vol}}, a_2 = \phi_2) \quad (2.277)$$

$$D = \frac{\phi_2}{f_1^{\text{rel}}} \rho_1 \left( \frac{\partial \mu_1}{\partial \rho_1} \right)_{p,T} \quad (\vec{v}^a = \vec{v}_2, a_2 = 1) \quad (2.278)$$

$$D = \frac{v_2}{f_{12}} \rho_1 \left( \frac{\partial \mu_1}{\partial \rho_1} \right)_{p,T} \quad (f_{12} = f_1^{\text{rel}} / \rho_2). \quad (2.279)$$

$f_{12}$  has been introduced in the context of the frictional formalism (cf. page 37) and can be related to  $L_{11}^{\text{rel}}$  with the help of Eq. (2.177). Eqs. (2.277), (2.278) and (2.279) are the

results of Schmitz [88], Berne and Pecora [7], and Vink [103], respectively.<sup>13</sup> Of course all these descriptions are equally valid. However, the physical significance of the different friction coefficients is not clear. Only in the dilute limit all reference velocities and all friction coefficients are identical (cf. Eq. (2.256)). By using

$$\lim_{x_1 \rightarrow 0} \left[ x_1 \left( \frac{\partial \mu_1}{\partial x_1} \right)_{p,T} \right] = \lim_{\rho_1 \rightarrow 0} \left[ \rho_1 \left( \frac{\partial \mu_1}{\partial \rho_1} \right)_{p,T} \right] = \frac{kT}{M_1} \quad (2.280)$$

Eq. (2.275) simplifies to

$$D = \frac{kT}{M_1 f_1^a} \quad (x_2, a_2 \rightarrow 1). \quad (2.281)$$

Eq. (2.281) is a well known result, which has already been found by Einstein [31, 32]. For a brief summary of Einstein's argument see Ref. [99]. Accordingly, in the dilute limit  $f_1^a M_1$  can be identified with the Stokes friction coefficient

$$f_1^a M_1 = 6\pi\eta R_{h,1} \quad (x_2, a_2 \rightarrow 1), \quad (2.282)$$

where  $\eta$  is the viscosity of the mixture and  $R_{h,1}$  the hydrodynamic radius of species 1.

At finite  $x_1$ , and in particular for  $x_1 \rightarrow 1$ , the interpretation of the friction coefficients becomes difficult. Moreover, a friction coefficient  $f_2^a$  for species 2 cannot be introduced by means of Eq. (2.274), as there exists only one independent generalized force in a binary mixture.

**Friction coefficients from consideration of external forces** We will now propose an alternative way to introduce friction coefficients. We will consider a homogenous mixture in the absence of temperature gradients ( $c_1, c_2, T$  constant), where the external forces  $\vec{F}_1$  and  $\vec{F}_2$  are exerted on particles of species 1 and 2. The resulting flux can be evaluated according to Eqs. (2.164, 2.167)

$$\begin{aligned} \vec{J}_1^{\text{rel}} &= -\frac{L_{11}^{\text{rel}}}{T} \vec{X}_1^{\text{rel}} = -\frac{L_{11}^{\text{rel}}}{T} \left[ \left( \frac{\partial \mu_1}{\partial p} \right)_{c_1, T} \vec{\nabla} p - \vec{F}_1 \right] = -\frac{L_{11}^{\text{rel}}}{T} \left[ v_1 (\rho_1 \vec{F}_1 + \rho_2 \vec{F}_2) - \vec{F}_1 \right] \\ &= \frac{L_{11}^{\text{rel}}}{T} [\phi_2 \vec{F}_1 - v_1 \rho_2 \vec{F}_2] = \frac{L_{11}^{\text{rel}}}{\rho_1 T} [\rho_1 \phi_2 \vec{F}_1 - \rho_2 \phi_1 \vec{F}_2] \end{aligned} \quad (2.283)$$

Here the mechanical equilibrium condition (2.89) and  $(\partial \mu_1 / \partial p)_{c_1, T} = v_1$  have been used.

Generally the frictional force on a particle  $p$  is given by

$$\vec{F}_p^{\text{frict}} = -\vec{F}_p^{\text{ext}} = -f_p \vec{v}_p, \quad (2.284)$$

<sup>13</sup>Note that these authors use molar rather than specific quantities:  $\mu'_1 = M_1 \mu_1$ ,  $v'_2 = v_2 M_2$ ,  $f_{\text{Schmitz}} = M_1 f_1^{\text{vol}}$ ,  $f_{\text{Berne}} = M_1 f_1^{\text{rel}} / N_A$ ,  $f_{\text{Vink}} = f_{12} M_1 M_2$ .

if an external force  $\vec{F}_p^{\text{ext}}$  is exerted on  $p$  and if  $p$  moves with constant velocity  $\vec{v}_p$ .  $f_p$  is the friction coefficient, which is defined by this equation. With the help of Eq. (2.284) we will now introduce friction coefficients  $f'_1$  and  $f'_2$  for the two species of the binary mixture. First we assume  $\vec{F}_2 = 0$ . Since  $\vec{F}_1$  is a force per unit mass, the force on one particle of species 1 is  $M_1\vec{F}_1$ . In the laboratory reference frame, this force is reduced due to a flow of particles 2 in the opposite direction, which is caused by the walls of the system. Hence we have to set up Eq. (2.284) in a reference system, that moves with  $\vec{v}_2$ :

$$M_1\vec{F}_1 = f'_1(\vec{v}_1 - \vec{v}_2) = \frac{f'_1}{\rho_1}\vec{J}_1^{\text{rel}} \quad (2.285)$$

Comparison of Eqs. (2.283, 2.285) yields

$$f'_1 = M_1 \frac{\rho_1 T}{L_{11}^{\text{rel}} \phi_2}. \quad (2.286)$$

In the same way the friction coefficient  $f'_2$  for species 2 can be introduced. Assuming  $\vec{F}_1 = 0$  and choosing a reference frame that moves with  $\vec{v}_1$ , one obtains

$$M_2\vec{F}_2 = f'_2(\vec{v}_2 - \vec{v}_1) = -\frac{f'_2}{\rho_1}\vec{J}_1^{\text{rel}} \quad (2.287)$$

and

$$f'_2 = M_2 \frac{\rho_1^2 T}{L_{11}^{\text{rel}} \rho_2 \phi_1}. \quad (2.288)$$

$f'_1$  and  $f'_2$  are related to each other by

$$f'_2 = \frac{M_2 \phi_2 \rho_1}{M_1 \phi_1 \rho_2} f'_1 = \frac{\phi_2 x_1}{\phi_1 x_2} f'_1 = \frac{M_2 v_2}{M_1 v_1} f'_1. \quad (2.289)$$

Eqs. (2.100, 2.172) yield

$$D = \frac{\rho_1 M_1}{f'_1} \left( \frac{\partial \mu_1}{\partial \rho_1} \right)_{p,T} = \frac{\rho_1}{f'_1} \left( \frac{\partial \mu'_1}{\partial \rho_1} \right)_{p,T} \quad (2.290)$$

with  $\mu'_1 = M_1 \mu_1$ . From Eqs. (2.276, 2.73) there results

$$\rho_1 \left( \frac{\partial \mu'_1}{\partial \rho_1} \right)_{p,T} = \frac{x_2}{\phi_2} x_1 \left( \frac{\partial \mu'_1}{\partial x_1} \right)_{p,T} = \frac{x_2}{\phi_2} x_2 \left( \frac{\partial \mu'_2}{\partial x_2} \right)_{p,T} = \frac{\phi_1 x_2}{\phi_2 x_1} \rho_2 \left( \frac{\partial \mu'_2}{\partial \rho_2} \right)_{p,T}. \quad (2.291)$$

Because of Eqs. (2.289, 2.291) the obtained expression for  $D$  is symmetric with

$$D = \frac{\rho_1}{f'_1} \left( \frac{\partial \mu'_1}{\partial \rho_1} \right)_{p,T} = \frac{\rho_2}{f'_2} \left( \frac{\partial \mu'_2}{\partial \rho_2} \right)_{p,T} \quad (2.292)$$

For ideally dilute solutions ( $\rho_1 \rightarrow 0$  or  $\rho_2 \rightarrow 0$ ) one obtains with the help of (2.280)

$$D = \frac{kT}{f'_i} \quad (\rho_i \rightarrow 0, i = 1, 2), \quad (2.293)$$

where  $f'_i$  can be identified with a Stokes friction coefficient

$$f'_i = 6\pi\eta R_{h,i} \quad (\rho_i \rightarrow 0, i = 1, 2). \quad (2.294)$$

**Actual hydrodynamic friction force on a diffusing particle** In the absence of external forces, pressure and temperature gradients, Eqs. (2.133, 2.164, 2.167, 2.286, 2.131, 2.142, 2.132, 2.289, 2.73) yield

$$f'_1(\vec{v}_1 - \vec{v}_2) = \frac{f'_1}{\rho_1} \vec{J}_1^{\text{rel}} = -\frac{f'_1}{\rho_1} \frac{L_{11}^{\text{rel}}}{T} (\vec{\nabla} \mu_1)_{p,T} = -\frac{(\vec{\nabla} \mu'_1)_{p,T}}{\phi_2} = -M_1 \vec{X}_1^{\text{vol}} \quad (2.295)$$

$$f'_1(\vec{v}_1 - \vec{v}^{\text{vol}}) = \frac{f'_1}{\rho_1} \vec{J}_1^{\text{vol}} = \frac{f'_1 \phi_2}{\rho_1} \vec{J}_1^{\text{rel}} = -(\vec{\nabla} \mu'_1)_{p,T} = -M_1 \vec{X}_1^{\text{rel}} \quad (2.296)$$

$$f'_2(\vec{v}_2 - \vec{v}^{\text{vol}}) = \frac{f'_2}{\rho_2} \vec{J}_2^{\text{vol}} = -\frac{f'_2 v_1}{\rho_2 v_2} \vec{J}_1^{\text{vol}} = \frac{x_1}{x_2} (\vec{\nabla} \mu'_1)_{p,T} = -(\vec{\nabla} \mu'_2)_{p,T}. \quad (2.297)$$

Obviously, the generalized forces are not the correct driving forces for the corresponding fluxes: Whereas  $\vec{X}_1^{\text{vol}}$  is the driving force for the relative flux  $\vec{J}_1^{\text{rel}}$ ,  $\vec{X}_1^{\text{rel}}$  is the driving force for the flux  $\vec{J}_1^{\text{vol}}$ . The result is, however, sensible: The actual hydrodynamic friction forces on particle 1 and 2 are given by  $f'_1 \vec{v}_1$  and  $f'_2 \vec{v}_2$ . If the mean volume velocity vanishes, these forces are equal to  $-(\vec{\nabla} \mu'_1)_{p,T}$  (cf. Eq. (2.296)) and  $-(\vec{\nabla} \mu'_2)_{p,T}$  (cf. Eq. (2.297)). A uniform body force  $-(\vec{\nabla} \mu_2)_{p,T}/v_2$  per unit volume acting on particles of component 1 and 2 alike does not produce relative motion of particles of species 1 and 2. In agreement with Eq. (2.295) the relative flux can be obtained by assuming that each particle of species 1 is acted on by a modified force

$$M_1 v_1 \left[ -\frac{(\vec{\nabla} \mu_1)_{p,T}}{v_1} + \frac{(\vec{\nabla} \mu_2)_{p,T}}{v_2} \right] \stackrel{(2.73)}{=} -\frac{(\vec{\nabla} \mu'_1)_{p,T}}{\phi_2} \quad (2.298)$$

and that particles of species 2 are force free. A similar reasoning can be found in Ref. [6]. Other authors have come to other conclusions [88, 90].

**Relation between chemical potential and osmotic pressure** In all formulae derived for the diffusion coefficient Eqs. (2.277, 2.278, 2.279, 2.290) there appears  $\rho_1(\partial\mu_1/\partial\rho_1)$ . This expression can be related to the osmotic pressure, which is defined according to

$$\pi(\mu_2, T, \rho_1) = p(\mu_2, T, \rho_1) - p_0(\mu_2, T). \quad (2.299)$$

$p_0$  is the pressure of the pure substance 2. Alternatively  $\pi$  can be written as a function of  $p$ ,  $T$  and  $\rho_1$ :

$$\pi(p, T, \rho_1) = p - p_0(\mu_2(p, T, \rho_1), T) \quad (2.300)$$

In the literature, both expressions  $(\partial\pi/\partial\rho_1)_{\mu_2, T}$  [90, 55, 115, 73] and  $(\partial\pi/\partial\rho_1)_{p, T}$  [88, 82, 13, 96] are found. Sometimes wrong formulae are used [88, 96] and many of the used relations only hold for incompressible fluids [82, 13, 115, 73]. Therefore we will now give a review of relations between the derivations of the chemical potential and the osmotic pressure with respect to  $\rho_1$ . We will explicitly point out, if incompressibility has been assumed.

From Eqs. (2.299, 2.300) and by taking into account the Gibbs Duhem relation (2.73) the derivations of the osmotic pressure  $\pi$  with respect to  $\rho_1$  are obtained

$$\left(\frac{\partial\pi}{\partial\rho_1}\right)_{\mu_2, T} = \left(\frac{\partial p}{\partial\rho_1}\right)_{\mu_2, T} \quad (2.301)$$

$$\left(\frac{\partial\pi}{\partial\rho_1}\right)_{p, T} = -\left(\frac{\partial p_0}{\partial\rho_1}\right)_{p, T} = -\left(\frac{\partial p_0}{\partial\mu_2}\right)_T \left(\frac{\partial\mu_2}{\partial\rho_1}\right)_{p, T} = \frac{\rho_1}{\rho_2 v_2^0} \left(\frac{\partial\mu_1}{\partial\rho_1}\right)_{p, T}, \quad (2.302)$$

where  $v_2^0$  is the specific volume of pure component 2. Expressions (2.301) and (2.302) may be related to each other by

$$\left(\frac{\partial\pi}{\partial\rho_1}\right)_{p, T} = \left(\frac{\partial\pi}{\partial\rho_1}\right)_{\mu_2, T} - \left(\frac{\partial\pi}{\partial\mu_2}\right)_{\rho_1, T} \left(\frac{\partial p}{\partial\rho_1}\right)_{\mu_2, T} \left(\frac{\partial\mu_2}{\partial p}\right)_{\rho_1, T} = \frac{\left(\frac{\partial\mu_2}{\partial p}\right)_{\rho_1, T}}{v_2^0} \left(\frac{\partial\pi}{\partial\rho_1}\right)_{\mu_2, T} \quad (2.303)$$

Here

$$\left(\frac{\partial\pi}{\partial\mu_2}\right)_{\rho_1, T} = \left(\frac{\partial p}{\partial\mu_2}\right)_{\rho_1, T} - \frac{1}{v_2^0} \quad (2.304)$$

has been used, which follows from Eq. (2.299). For incompressible fluids one has

$$\left(\frac{\partial\mu_2}{\partial p}\right)_{\rho_1, T} \approx \left(\frac{\partial\mu_2}{\partial p}\right)_{c_1, T} = v_2 \quad (\text{incompressible}) \quad (2.305)$$

and Eq. (2.303) simplifies to

$$\left(\frac{\partial\pi}{\partial\rho_1}\right)_{p, T} = \frac{v_2}{v_2^0} \left(\frac{\partial\pi}{\partial\rho_1}\right)_{\mu_2, T} \quad (\text{incompressible}). \quad (2.306)$$

If there are no volume changes upon mixing ( $v_2^0 \approx v_2$ ) one obtains

$$\left(\frac{\partial\pi}{\partial\rho_1}\right)_{p, T} = \left(\frac{\partial\pi}{\partial\rho_1}\right)_{\mu_2, T} \quad (\text{incompressible, } v_2^0 \approx v_2). \quad (2.307)$$

In a similar way the derivations of the chemical potentials  $(\partial\mu_1/\partial\rho_1)_{\mu_2, T}$  and  $(\partial\mu_1/\partial\rho_1)_{p, T}$

can be related to each other

$$\begin{aligned} \left(\frac{\partial\mu_1}{\partial\rho_1}\right)_{\mu_2,T} &= \left(\frac{\partial\mu_1}{\partial\rho_1}\right)_{p,T} - \left(\frac{\partial\mu_1}{\partial p}\right)_{\rho_1,T} \left(\frac{\partial p}{\partial\mu_2}\right)_{\rho_1,T} \left(\frac{\partial\mu_2}{\partial\rho_1}\right)_{p,T} \\ &= \left(\frac{\partial\mu_1}{\partial\rho_1}\right)_{p,T} \left[1 + \frac{\rho_1}{\rho_2} \frac{\left(\frac{\partial\mu_1}{\partial p}\right)_{\rho_1,T}}{\left(\frac{\partial\mu_2}{\partial p}\right)_{\rho_1,T}}\right]. \end{aligned} \quad (2.308)$$

The second equality sign follows with the help of the Gibbs Duhem relation (2.73). For incompressible fluids Eq. (2.308) reduces with the help of

$$\phi_i = \rho_i v_i = \rho_i \left(\frac{\partial\mu_i}{\partial p}\right)_{c_1,T} \approx \rho_i \left(\frac{\partial\mu_i}{\partial p}\right)_{\rho_1,T} \quad (\text{incompressible}) \quad (2.309)$$

to

$$\left(\frac{\partial\mu_1}{\partial\rho_1}\right)_{\mu_2,T} = \frac{1}{\phi_2} \left(\frac{\partial\mu_1}{\partial\rho_1}\right)_{p,T} \quad (\text{incompressible}), \quad (2.310)$$

which is used in Refs. [115, 73].

Finally, we will derive a general relation between chemical potential and osmotic pressure, which also holds for compressible fluids. With the help of the Gibbs Duhem relation (2.73) and Eq. (2.309) one finds

$$\left(\frac{\partial\mu_1}{\partial c_1}\right)_{p,T} = -\frac{c_2}{c_1} \left(\frac{\partial\mu_2}{\partial c_1}\right)_{p,T} = \frac{c_2}{c_1} \left(\frac{\partial\mu_2}{\partial p}\right)_{c_1,T} \left(\frac{\partial p}{\partial c_1}\right)_{\mu_2,T} = \frac{\phi_2}{\rho_1} \left(\frac{\partial p}{\partial c_1}\right)_{\mu_2,T}. \quad (2.311)$$

Now the weight fractions  $c_1$  can be replaced by the mass density  $\rho_1$  according to

$$\left(\frac{\partial\mu_1}{\partial\rho_1}\right)_{p,T} = \left(\frac{\partial\mu_1}{\partial c_1}\right)_{p,T} \left(\frac{\partial c_1}{\partial\rho_1}\right)_{p,T} \quad (2.312)$$

$$\left(\frac{\partial p}{\partial c_1}\right)_{\mu_2,T} = \left(\frac{\partial p}{\partial\rho_1}\right)_{\mu_2,T} \left(\frac{\partial\rho_1}{\partial c_1}\right)_{\mu_2,T} \quad (2.313)$$

$$\left(\frac{\partial\rho_1}{\partial c_1}\right)_{p,T} \left(\frac{\partial c_1}{\partial\rho_1}\right)_{\mu_2,T} = 1 - \left(\frac{\partial\rho_1}{\partial p}\right)_{c_1,T} \left(\frac{\partial p}{\partial\rho_1}\right)_{\mu_2,T} = 1 - \frac{\kappa}{\kappa_{\text{osm}}}, \quad (2.314)$$

where  $\kappa$  and  $\kappa_{\text{osm}}$

$$\kappa = \frac{1}{\rho_1} \left(\frac{\partial\rho_1}{\partial p}\right)_{c_1,T} = \frac{1}{\rho} \left(\frac{\partial\rho}{\partial p}\right)_{c_1,T} \quad (2.315)$$

$$\kappa_{\text{osm}} = \frac{1}{\rho_1} \left(\frac{\partial\rho_1}{\partial p}\right)_{\mu_2,T} = \frac{1}{\rho_1} \left(\frac{\partial\rho_1}{\partial\pi}\right)_{\mu_2,T} \quad (2.316)$$

are the isothermal and osmotic compressibility. Inserting Eqs. (2.312)–(2.314) into Eq. (2.311) yields

$$\rho_1 \left(\frac{\partial\mu_1}{\partial\rho_1}\right)_{p,T} = \frac{\phi_2}{\left(1 - \frac{\kappa}{\kappa_{\text{osm}}}\right)} \left(\frac{\partial p}{\partial\rho_1}\right)_{\mu_2,T} = \frac{\phi_2}{\left(1 - \frac{\kappa}{\kappa_{\text{osm}}}\right)} \left(\frac{\partial\pi}{\partial\rho_1}\right)_{\mu_2,T}. \quad (2.317)$$

In Ref. [55] Eq. (2.317) has been derived in a slightly different way.

### 2.2.5.2 Thermal Diffusion Coefficient

We will show, that the force acting on a thermodiffusing particle cannot be derived by considering the effects of external forces. This is only possible for isothermally diffusing particles (see Sec. 2.2.5.1).

Eq. (2.86) for a binary mixture reads

$$\vec{J}_1 = -\frac{L_{1q}}{T^2}\vec{\nabla}T - \frac{L_{11}}{T}[(\vec{\nabla}\mu_1)_T - (\vec{\nabla}\mu_2)_T - \vec{F}_1 + \vec{F}_2]. \quad (2.318)$$

In Sec. 2.2.5.1 we have seen that  $M_i(\vec{\nabla}\mu_i)_{p,T}$  can be interpreted as the thermodynamic force which acts on one particle of species  $i$  during isothermal diffusion. Hence the question arises, whether such a force can also be found for a thermodiffusing particle. With the help of Eq. (2.318) one may calculate the force, which brings a thermodiffusing particle to a standstill. If we assume a homogenous mixture ( $c_1$  constant), where a force  $\vec{F}_1$  is exerted on the particles of component 1 and  $\vec{F}_2 = 0$ , we obtain

$$\begin{aligned} \vec{J}_1 &= -\frac{L_{1q}}{T^2}\vec{\nabla}T - \frac{L_{11}}{T}\left[\left(\frac{\partial\mu_1}{\partial p}\right)_{c_1,T}\vec{\nabla}p - \left(\frac{\partial\mu_2}{\partial p}\right)_{c_1,T}\vec{\nabla}p - \vec{F}_1\right] \\ &= -\frac{L_{1q}}{T^2}\vec{\nabla}T + \frac{L_{11}}{T}\frac{\phi_2}{c_2}\vec{F}_1 \stackrel{!}{=} 0 \quad \Rightarrow \quad \vec{F}_1^{\text{stop}} = \frac{L_{1q}}{L_{11}}\frac{c_2}{\phi_2T}\vec{\nabla}T \end{aligned} \quad (2.319)$$

where Eqs. (2.89, 2.309) have been used. This “standstill–force”  $\vec{F}_1^{\text{stop}}$ , however, is not the force which acts on a moving thermodiffusing particle. As a flow field induced by external forces is influenced by backflow effects, the Onsager coefficient  $L_{11}^{\text{rel}}$  depends according to Eqs. (2.285, 2.286) on hydrodynamic interaction. Then, because of Eq. (2.172), also  $L_{11}$  does. On the other hand  $L_{1q}$ ,  $D_T$ , and the thermophoretic velocity are insensitive to backflow effects, as was shown theoretically [11] and experimentally [85]. Consequently, also the force acting on a moving thermodiffusing particle has to be independent of hydrodynamic interaction, i.e. independent of  $L_{11}$ .

We think that the flow field around a thermodiffusing particle (particle  $p$  of component 1) is conceptually different, depending on whether  $p$  is moving or not. According to arguments of Anderson [4], Semenov [91], and Würger [114], no macroscopic flow field (i.e.  $|\vec{v}| \sim r^{-3}$ ) arises in case of moving thermodiffusing particles. This is plausible since the net force on each volume element is equal to zero. Note that the same situation is encountered in electrophoresis. If  $p$  is stopped by an external force, it still generates the same flow of species 2 over its surface as if it was moving. This leads to a macroscopic flow field (i.e.  $|\vec{v}| \sim r^{-1}$ ) and therefore the “standstill–force”  $\vec{F}_1^{\text{stop}}$  depends on hydrodynamic interaction.

It should be mentioned that isothermal diffusion phenomena are different. Fickian diffusion is analogous to sedimentation, where a net force is exerted onto a volume element thus leading to a macroscopic flow field (i.e.  $|\vec{v}| \sim r^{-1}$ ).



### 2.2.6 Equations for the Analysis of Transient Grating Experiments

In the presence of temperature gradients the reference velocities generally do not vanish (cf. Sec. 2.2.4.3). The applied gradients in transient grating experiments are, however, very small ( $\vec{\nabla}T \approx 1 \text{ mK}/10 \mu\text{m}$ ). Therefore Eq. (2.226) may be used for the description of our thermal diffusion experiments (cf. Sec. 2.2.4.2). In the following only experiments on binary mixtures will be considered so that Eq. (2.226) simplifies to

$$\frac{\partial c}{\partial t} = \vec{\nabla} \cdot [D\vec{\nabla}c + c(1-c)D_T\vec{\nabla}T]$$

with  $c = c_1$  and  $1-c = c_2$ . Here the general binary diffusion coefficients  $\mathcal{D}_{1,T} = D_T$  and  $\mathcal{D}_{11} = D$  have been used (cf. Eqs. (2.194, 2.195) and corresponding explanations). Since second order terms may be neglected just as well in the evolution equation for the temperature, heat transport in transient grating experiments is described by the heat equation Eq. (2.271)

$$\rho c_p \frac{\partial T}{\partial t} = \vec{\nabla} \cdot (\kappa \vec{\nabla}T) + \dot{Q}.$$

Thus Eqs. (1.2, 1.3) from Chap. 1 have been derived.

## Chapter 3

# Boundary Effects in Holographic Grating Experiments

In this chapter we develop a reasonably simple two-dimensional model to account for heat conducting walls in transient grating experiments for the measurement of both heat and mass transport. Specifically, we show that the signal generated by the temperature grating depends on only three dimensionless parameters, which results in a significant reduction of the dimension of the parameter space when compared to the very detailed model of Wang and Fiebig [105] and Wang, Fiebig and Wu [106]. In the framework of our practically applicable model, the measured apparent thermal diffusivity can be related to its true value by simply finding the zero of an analytic function, instead of the much more time consuming task of solving a set of coupled partial differential equations (PDEs). In binary liquids the complex two-dimensional temperature profile also requires a two-dimensional treatment of the concentration distribution. The normalized heterodyne diffraction efficiency of the concentration grating, however, remains unaffected as long as signal contributions from the temperature grating within the wall are negligible. We have performed experiments to test our model over a wide range of both grating periods  $d$  and sample thicknesses  $l_s$  and found an excellent agreement between theoretical predictions and experimental data. Furthermore, our model yields the same results for the pure temperature signal as the complex, three-dimensional model of Wang et al., which proves that it contains, despite its simplicity, all relevant aspects of the problem.

### 3.1 Heat and Mass Diffusion Analysis

Our model for the description of coupled heat and mass transport in multicomponent liquids is based on the heat equation (Eq. 1.2)

$$\rho c_p \partial_t T = \vec{\nabla} \cdot [\kappa \vec{\nabla} T] + \dot{Q}$$

and the extended diffusion equation (Eq. (1.3)) for the concentration  $c$  (weight fractions)

$$\partial_t c = \vec{\nabla} \cdot \left[ D \vec{\nabla} c + c(1 - c) D_T \vec{\nabla} T \right].$$

In case of transient holographic grating experiments, the source term is given by the absorbed laser power density,  $\dot{Q} = \alpha I$ , with  $I$  being the light intensity within the holographic grating and  $\alpha$  the optical absorption coefficient. Before we treat the two dimensional problem of heat flow into the walls, we briefly review the one-dimensional model.

### 3.1.1 One-dimensional Model

A simple experiment is the following [111]: A holographic grating is written into the sample until the steady state is reached. At the time  $t = 0$  the writing beams are switched off.

$$I(x, t) = I_0(1 + \cos qx) \theta(-t) = \begin{cases} I_0(1 + \cos qx) & : t < 0 \\ 0 & : t > 0 \end{cases} \quad (3.1)$$

The sample absorbs energy from the light field and the temperature  $T$  evolves according to

$$\rho_s c_{p,s} \partial_t T = \kappa_s \partial_x^2 T + \alpha I \quad (3.2)$$

where  $\rho_s$  is the density of the sample,  $c_{p,s}$  the specific heat at constant pressure,  $\kappa_s$  the thermal conductivity, which is assumed to be constant, and  $\alpha$  the absorption coefficient. The resulting temperature change can be written as

$$T(x, t) = T_0(t) + T_q(t) \cos qx. \quad (3.3)$$

$T_0(t)$  describes the overall sample heating.  $T_q$  is the amplitude of the temperature grating and can be detected by the read-out laser beam. For  $t \geq 0$  it is given by

$$T_q = \frac{\alpha I_0}{\kappa_s q^2} \exp(-D_{th,s} q^2 t). \quad (3.4)$$

$D_{th,s} = \kappa_s (\rho_s c_{p,s})^{-1}$  is the thermal diffusivity of the sample.

For a binary liquid the spatial and temporal evolution of the concentration distribution  $c(\vec{r}, t)$  is obtained by solving the diffusion equation (Eq. (1.3)) in one dimension. Since temperature and concentration changes in our transient grating experiments are generally only very small, the diffusion coefficients  $D$  and  $D_T$  can be taken as constant and  $c(1-c)$  can be approximated by  $c_0(1-c_0)$ , where  $c_0$  is the average concentration:

$$\partial_t c = D \partial_x^2 c + D_T c_0 (1 - c_0) \partial_x^2 T \quad (3.5)$$

In analogy to Eq. (3.3) we split the concentration into two parts.

$$c(x, t) = c_0 + c_q(t) \cos qx \quad (3.6)$$

$c_q$  is the amplitude of the concentration grating and is the experimentally relevant variable. For a switching-off experiment as it is given by Eq. (3.1), the concentration grating amplitude decays exponentially.

$$c_q = -S_T c_0 (1 - c_0) \frac{\alpha I_0}{\kappa_s q^2} (D_{th,s} - D)^{-1} \left( D_{th,s} \exp(-D q^2 t) - D \exp(-D_{th,s} q^2 t) \right) \quad (3.7)$$

Here we introduced the Soret coefficient  $S_T = D_T/D$ .

Both the temperature grating and the concentration grating give rise to a refractive index grating which acts as an optical phase grating on a probing laser beam.

$$n(x, t) - n_0 = n_q(t) \cos qx = \left[ \left( \frac{\partial n}{\partial T} \right)_{c,p} T_q(t) + \left( \frac{\partial n}{\partial c} \right)_{T,p} c_q(t) \right] \cos qx \quad (3.8)$$

$n$  is the refractive index at the readout wavelength. The respective contrast factors are the temperature derivative of  $n$  at constant composition and pressure,  $(\partial n/\partial T)_{c,p}$ , and the concentration derivative of  $n$  at constant temperature and pressure,  $(\partial n/\partial c)_{T,p}$ .

For experiments conducted within the weak modulation depth limit the heterodyne diffraction efficiency  $\zeta_{het}$  is simply proportional to the refractive index modulation depth  $n_q$  and the sample thickness  $l_s$  [52].

$$\zeta_{het} \propto n_q l_s \quad (3.9)$$

$\zeta_{het}$  is the experimentally measured quantity. For the switching-off experiment (3.1) it decays according to

$$\zeta_{het} \propto \frac{\alpha I_0 l_s}{\kappa_s q^2} \left[ \left( \frac{\partial n}{\partial T} \right)_{c,p} \exp(-D_{th,s} q^2 t) - \left( \frac{\partial n}{\partial c} \right)_{T,p} S_T c_0 (1 - c_0) (D_{th,s} - D)^{-1} \left( D_{th,s} \exp(-D q^2 t) - D \exp(-D_{th,s} q^2 t) \right) \right], \quad (3.10)$$

as follows from Eqs. (3.4, 3.7, 3.8, 3.9).

### 3.1.2 Two-dimensional Model

Under realistic experimental conditions, systematic deviations from the one-dimensional model occur due to heat loss into the windows. To take this into account we propose the following model:

Fig. 3.1 shows the coordinate system for analysis. The region  $|z| < l_s/2$  is of sample material, which has thermal conductivity  $\kappa_s$ , density  $\rho_s$ , heat capacity  $c_{p,s}$  and thermal diffusivity  $D_{th,s} = \kappa_s(\rho_s c_{p,s})^{-1}$ . For simplicity we suppose the sample to be infinitely extended in  $x$ -direction. This is a good approximation, if the  $x$ -dimension  $L_x$  of the cuvette is much larger than the grating period  $d = 2\pi/q$ . In our experiments we have  $L_x = 3.5$  mm and  $d = 5 - 50$   $\mu\text{m}$ .

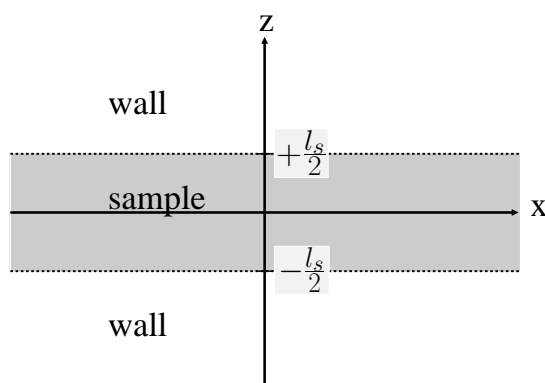


**Figure 3.1:** The coordinate system

The regions  $|z| > l_s/2$  are of wall material  $\kappa_w, \rho_w, c_{p,w}, D_{th,w} = \kappa_w(\rho_w c_{p,w})^{-1}$ . The approximation of infinite wall thickness is valid, if the penetration depth of the temperature grating into the wall is very small compared to the thickness of the cell wall. In our case the penetration depth is of order  $q^{-1} = 1 - 8 \mu\text{m}$  and the thickness of the cell wall is  $l_w = 1.25 \text{ mm}$ . There is no  $y$ -dependence.

In our model we postulate that the infinite area of sample is heated by two laser beams of uniform intensity, i.e. we consider the following switch-off experiment

$$I(x, z, t) = I_0(1 + \cos qx) \theta(-t) = \begin{cases} I_0(1 + \cos qx) & : t \leq 0 \\ 0 & : t > 0 \end{cases}. \quad (3.11)$$

In practice however, the heated area corresponds to the diameter of the heating laser beam  $w$  of a few millimeters. Moreover, the intensity distribution of the laser is not uniform but is a rotationally symmetric Gaussian (TEM<sub>00</sub> mode). Above all, the admixed dye absorbs the energy from the light field according to Beer's law, leading to an exponential decay  $\exp(-\alpha z)$  of the intensity, where  $\alpha$  is the absorption coefficient.

$$I^{\text{real}}(x, y, z, t) = I_0 \exp(-2(x^2 + y^2)/w^2) \exp(-\alpha z)(1 + \cos qx) \theta(-t) \quad (3.12)$$

Further difficulties might arise, if the overlap length  $z_0$  of the two beams in  $z$ -direction is of same order of magnitude as the sample thickness  $l_s$  [92, 10, 29]. Nevertheless Eq. (3.11) is a good approximation for our experiments. The diameter of the laser  $w \approx 3 \text{ mm}$  is very large compared to the grating period  $d = 2\pi/q \approx 5 - 50 \mu\text{m}$ . Typically, the absorption coefficients are small  $\alpha \approx 2/\text{cm}$ . For the thickest used cuvette with sample thickness  $l_s = 200 \mu\text{m}$  this leads to  $\exp(-\alpha l_s) = 0.96$ . Finally we use thin cuvettes with  $l_s \leq 200 \mu\text{m}$  and the two beams intersect at small angles  $\sin \theta < 0.0515$ , so that  $z_0/l_s \ll 1$  holds.

As the sample is infinitely extended in  $x$ -direction, the intensity distribution (3.11) leads to

temperature and concentration fields of the form

$$T(x, z, t) = T_0(z, t) + T_q(z, t) \cos qx \quad (3.13)$$

$$c(x, z, t) = c_0(z, t) + c_q(z, t) \cos qx. \quad (3.14)$$

The evolution equations for the amplitude  $T_q$  of the temperature gratings within the sample and the wall and for the amplitude  $c_q$  of the concentration grating are given by the heat equations

$$\rho_s c_{p,s} \partial_t T_q = \kappa_s (-q^2 + \partial_z^2) T_q + \alpha I_0 \theta(-t) \quad |z| < l_s/2 \quad (3.15)$$

$$\rho_w c_{p,w} \partial_t T_q = \kappa_w (-q^2 + \partial_z^2) T_q \quad |z| > l_s/2 \quad (3.16)$$

and the extended diffusion equation

$$\partial_t c_q = D(-q^2 + \partial_z^2) c_q + D_T c_0 (1 - c_0) (-q^2 + \partial_z^2) T_q \quad |z| < l_s/2. \quad (3.17)$$

The boundary conditions

$$T_q(|z| \rightarrow \infty) \rightarrow 0 \quad (3.18)$$

$$D(\partial_z c_q)|_{|z|=l_s/2^-} = -D_T c_0 (1 - c_0) (\partial_z T_q)|_{|z|=l_s/2^-} \quad (3.19)$$

and the matching conditions

$$T_q(|z|=l_s/2^-) = T_q(|z|=l_s/2^+) \quad (3.20)$$

$$\kappa_s (\partial_z T_q)|_{|z|=l_s/2^-} = \kappa_w (\partial_z T_q)|_{|z|=l_s/2^+}. \quad (3.21)$$

follow from continuity of temperature and heat flux and from vanishing mass flux into the wall. For solid-liquid interfaces the contact resistance is in general negligible [65].

The two-dimensional generalization of Eq. (3.9) is

$$\begin{aligned} \zeta_{het}(t) &= \zeta_{het,T,s}(t) + \zeta_{het,c}(t) + \zeta_{het,T,w}(t) \\ &\propto \left( \frac{\partial n_s}{\partial T} \right)_{c,p} \int_{-l_s/2}^{l_s/2} T_q(z, t) dz + \left( \frac{\partial n_s}{\partial c} \right)_{T,p} \int_{-l_s/2}^{l_s/2} c_q(z, t) dz \\ &\quad + \left( \frac{\partial n_w}{\partial T} \right)_{c,p} \left[ \int_{-\infty}^{-l_s/2} T_q(z, t) dz + \int_{l_s/2}^{\infty} T_q(z, t) dz \right]. \end{aligned} \quad (3.22)$$

Not only the temperature and concentration gratings in the sample with respective contrast factors  $(\partial n_s / \partial T)_{c,p}$  and  $(\partial n_s / \partial c)_{T,p}$  but also the temperature grating in the wall with contrast factor  $(\partial n_w / \partial T)_{c,p}$  contribute to the heterodyne diffraction efficiency. However, the contribution of the wall  $\zeta_{het,T,w}(t)$  is usually negligible as will be discussed later.

Before we proceed with the analysis, we would like to recapitulate the models of Nagasaka

et al. [68] and Wang et al. [105, 106] to make the differences to our model clear. Nagasaka et al. solve the three-dimensional heat equation in an infinite composite solid, where the region  $z > 0$  is of sample material and the region  $z < 0$  is of wall material. Since they use the method of Green's functions, they need the initial temperature distribution in the sample and the wall. They assume the initial temperature to be zero in the wall and periodic with wave vector  $q$  and space-independent amplitude  $\Delta T_0$  in the entire sample region  $z > 0$ . Wang et al. solve the three-dimensional heat equation in a rectangular parallelepiped of sample material. They consider the Gaussian intensity profile of the heating laser, but not the exponential decay  $\exp(-\alpha z)$  of the intensity due to absorption. The effect of the walls is accounted for in time dependent boundary conditions, which relate the temperature at the boundary to the heat flux into the wall. They do not motivate these boundary conditions, but to our knowledge they hold for infinite composite solids with heat generated only in the plane of separation at a constant rate per unit time (see Eq. 2.15 (9) in Ref. [12]).

### 3.1.3 Stationary Solutions

The stationary solutions are found by solving Eqs. (3.15)–(3.17) setting  $\partial_t T_q \equiv \partial_t c_q \equiv 0$  and  $\theta(-t) \equiv 1$  and taking into account the boundary and matching conditions (3.18)–(3.21). This corresponds to the situation where the grating has been switched on at  $t = -\infty$  and the observation is made at  $t = 0$  immediately before the laser is switched off.

$$T_q(z, t = 0) = \frac{\alpha I_0}{\kappa_s q^2} \left( 1 - \cosh(qz) \left[ \frac{\kappa_s}{\kappa_w} \sinh \frac{ql_s}{2} + \cosh \frac{ql_s}{2} \right]^{-1} \right), \quad |z| < l_s/2 \quad (3.23)$$

$$T_q(z, t = 0) = \frac{\alpha I_0}{\kappa_w q^2} \sinh \frac{ql_s}{2} \left[ \frac{\kappa_s}{\kappa_w} \sinh \frac{ql_s}{2} + \cosh \frac{ql_s}{2} \right]^{-1} \exp(-q(|z| - l_s/2)), \quad |z| > l_s/2 \quad (3.24)$$

$$c_q(z, t = 0) = -S_T c_0 (1 - c_0) T_q(z, t = 0), \quad |z| < l_s/2 \quad (3.25)$$

Eqs. (3.23, 3.24) are plotted in Fig. 3.2 for the binary mixture of tetralin–dodecane with a concentration of 50 wt % of each component at  $25^\circ\text{C}$  ( $\kappa_s = 0.13 \text{ W/mK}$ ), quartz glass as wall material ( $\kappa_w = 1.38 \text{ W/mK}$ ) and different sample thicknesses ( $l_s = 200 \mu\text{m}$ ,  $100 \mu\text{m}$ , and  $10 \mu\text{m}$ ) and grating periods ( $d = 25 \mu\text{m}$  and  $50 \mu\text{m}$ ).  $\alpha I_0 / \kappa_w = 5 \mu\text{K}/\mu\text{m}^2$  has been chosen according to typical experimental conditions. Both for increasing grating period  $d$  and for increasing sample thickness  $l_s$  the amplitude of the temperature grating  $T_q$  increases. The penetration depth of the temperature grating into the wall is independent of sample thickness  $l_s$  and increases with increasing grating period  $d$ . For thick samples ( $l_s = 200 \mu\text{m}$  and  $100 \mu\text{m}$ )  $T_q$  is nearly constant throughout the sample and its plateau value does not depend on the sample thickness. The temperature grating in the wall is negligible. The value  $T_q(z = 0)$  for  $d = 50 \mu\text{m}$  is approximately four times larger than  $T_q(z = 0)$  for  $d = 25 \mu\text{m}$ . This is in accordance with Eq. (3.4) of the one-dimensional model, which predicts  $T_q \propto q^{-2}$ . For  $l_s = 10 \mu\text{m}$ , however, dramatic deviations occur. The amplitudes are smaller than expected

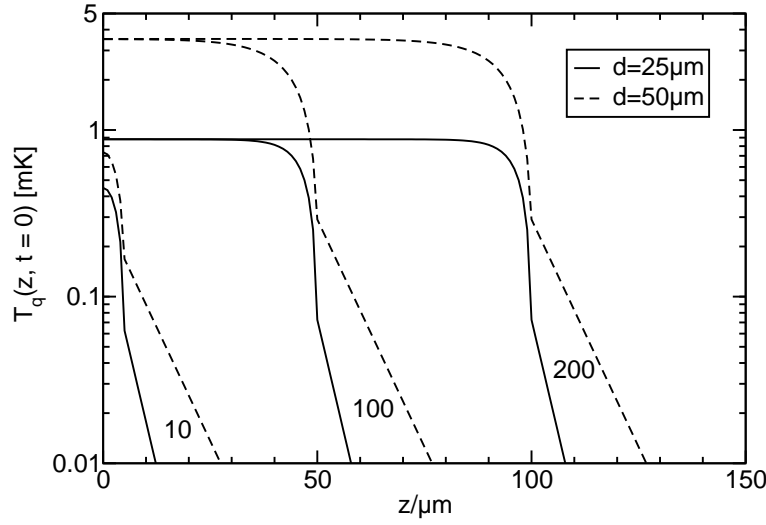


**Figure 3.2:** Stationary amplitude  $T_q(z, t = 0)$  of the temperature grating for  $\kappa_s/\kappa_w = 0.09$  and  $\alpha I_0/\kappa_w = 5 \mu\text{K}/\mu\text{m}^2$  as given by Eqs. (3.23, 3.24). The different line styles stand for the different grating periods  $d = 25 \mu\text{m}$  and  $50 \mu\text{m}$ . The curves are labeled with the sample thickness  $l_s$  in micrometers.

from  $T_q \propto q^{-2}$  because of heat loss into the wall. Furthermore the temperature within the sample no longer reaches a plateau and the temperature grating within the wall cannot be neglected.

The temperature distribution in the sample is given by Eq. (3.13). In the stationary case its periodic part  $T_q \cos(qx)$  can be evaluated from Eqs. (3.23, 3.24) as shown in Fig. 3.3. To facilitate comparison with Fig. 3.2 the parameters  $\kappa_s/\kappa_w = 0.09$  and  $\alpha I_0/\kappa_w = 5 \mu\text{K}/\mu\text{m}^2$  are the same in both figures. The contour lines in Fig. 3.3 reveal the penetration of the temperature grating into the cell wall. The thick solid grid lines for  $d = 25 \mu\text{m}$  and  $d = 50 \mu\text{m}$  correspond to the curves for the  $10 \mu\text{m}$  cuvette in Fig. 3.2.

For the stationary heterodyne diffraction efficiencies  $\zeta_{het,T,s}$ ,  $\zeta_{het,c}$ ,  $\zeta_{het,T,w}$  as defined in Eq. (3.22) follows for  $t = 0$

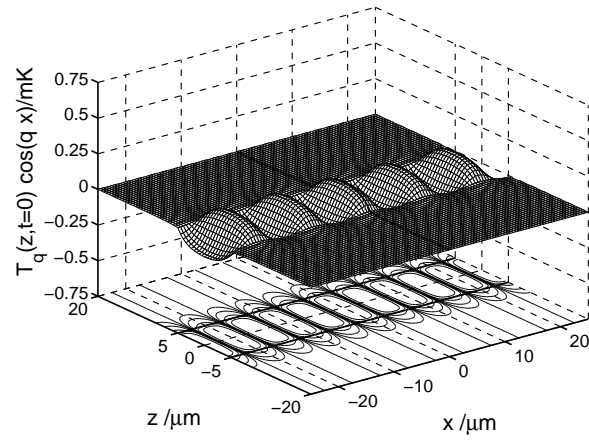
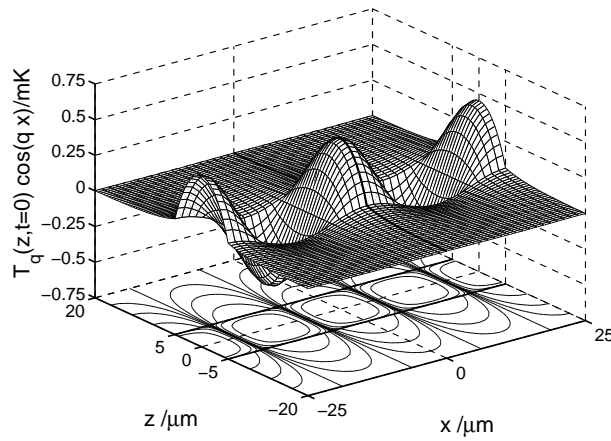
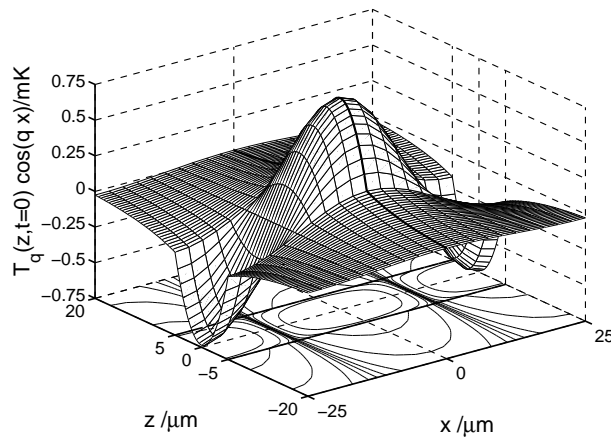
$$\zeta_{het,T,s}(t = 0) \propto \left( \frac{\partial n_s}{\partial T} \right)_{c,p} \frac{2 \alpha I_0}{\kappa_s q^3} \left( \frac{ql_s}{2} - \sinh \frac{ql_s}{2} \left[ \frac{\kappa_s}{\kappa_w} \sinh \frac{ql_s}{2} + \cosh \frac{ql_s}{2} \right]^{-1} \right) \quad (3.26)$$

$$\zeta_{het,c}(t = 0) = - \left( \frac{\partial n_s}{\partial c} \right)_{T,p} \left( \frac{\partial n}{\partial T} \right)_{c,p,s}^{-1} S_T c_0 (1 - c_0) \zeta_{het,T,s}(t = 0) \quad (3.27)$$

$$\zeta_{het,T,w}(t = 0) \propto \left( \frac{\partial n_w}{\partial T} \right)_{c,p} \frac{2 \alpha I_0}{\kappa_w q^3} \sinh \frac{ql_s}{2} \left[ \frac{\kappa_s}{\kappa_w} \sinh \frac{ql_s}{2} + \cosh \frac{ql_s}{2} \right]^{-1}. \quad (3.28)$$

Eqs. (3.26, 3.28) allow us to estimate the contribution of the temperature grating of the wall  $\zeta_{het,T,w}$  to the heterodyne diffraction efficiency. In Fig. 3.4 this has been done, again for the sample tetralin–dodecane, (50 wt %,  $T = 25^\circ\text{C}$ ) and quartz glass as wall material. In



(a)  $d = 10 \mu\text{m}$ (b)  $d = 25 \mu\text{m}$  (A wrong figure is displayed in Ref. [42].)(c)  $d = 50 \mu\text{m}$ 

**Figure 3.3:** Periodic part of the stationary temperature distribution for  $l_s = 10 \mu\text{m}$ ,  $\kappa_s/\kappa_w = 0.09$ ,  $\alpha I_0/\kappa_w = 5 \mu\text{K}/\mu\text{m}^2$ , and  $d = 10 \mu\text{m}, 25 \mu\text{m}$ , and  $50 \mu\text{m}$ . The sample extends from  $z = -5 \mu\text{m}$  to  $z = 5 \mu\text{m}$ . The contour lines belong to the temperatures  $T = \pm e^{-1}T_{\text{max}}, \pm e^{-2}T_{\text{max}}, \pm e^{-3}T_{\text{max}}, \pm e^{-4}T_{\text{max}}, \pm e^{-5}T_{\text{max}}$ , where  $T_{\text{max}} = T(x = 0, z = 0)$ .

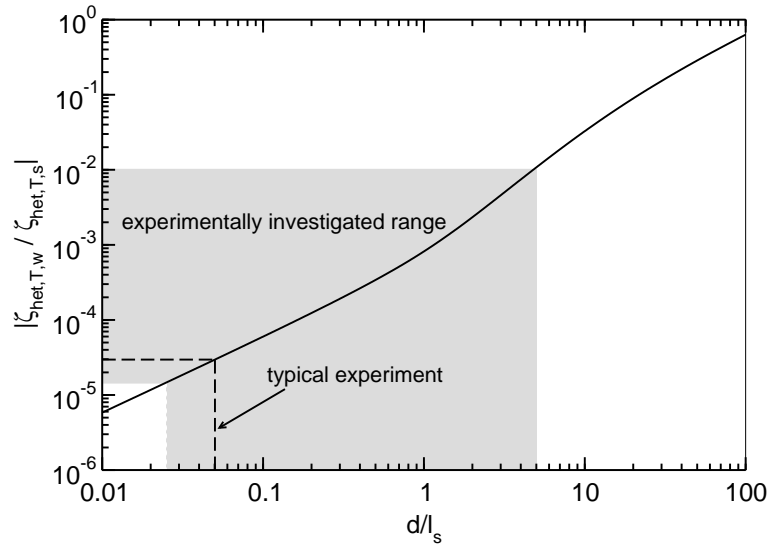


**Figure 3.4:** Ratio of the stationary heterodyne diffraction efficiencies of the wall  $\zeta_{het,T,w}$  and the sample  $\zeta_{het,T,s}$  as given by Eqs. (3.26, 3.28) against the ratio of grating period to sample thickness  $d/l_s$  for  $\kappa_s/\kappa_w = 0.09$ ,  $(\partial n_w/\partial T)_{c,p} = 9.72 \times 10^{-6}/\text{K}$ ,  $(\partial n_s/\partial T)_{c,p} = -4.39 \times 10^{-4}/\text{K}$ .

the experimentally investigated range  $d/l_s \approx 0.025 - 5$  the contribution of the wall  $\zeta_{het,T,w}$  does not exceed 1% of the contribution of the sample  $\zeta_{het,T,s}$ . Typical experiments are performed at  $d/l_s \approx 0.05$ , corresponding to  $\zeta_{het,T,w}/\zeta_{het,T,s} < 10^{-4}$ , and any signal stemming from the wall can safely be neglected. Fig. 3.5 shows the dependence of the stationary

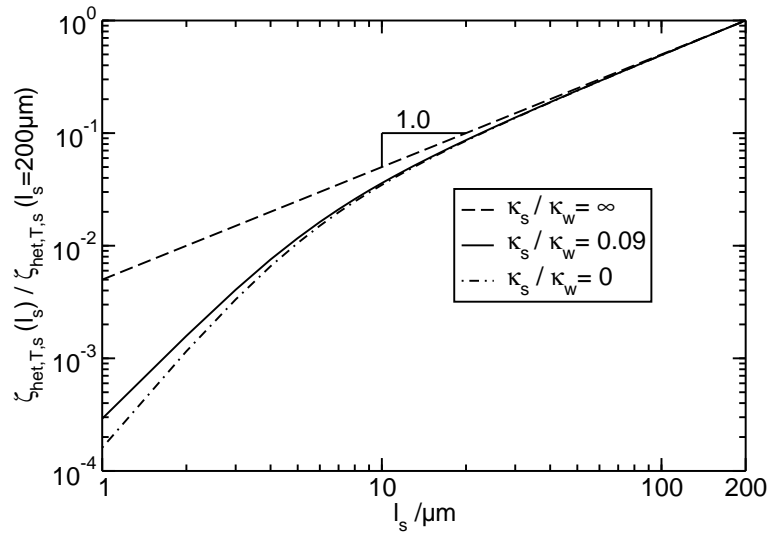


**Figure 3.5:** Normalized stationary heterodyne diffraction efficiency  $\zeta_{het,T,s}(l_s)/\zeta_{het,T,s}(l_s = 200 \mu\text{m})$  (3.26) as a function of sample thickness  $l_s$  for grating period  $d = 10 \mu\text{m}$ . ( $\kappa_s/\kappa_w = \infty$ : perfectly insulating walls,  $\kappa_s/\kappa_w = 0.09$ : sample tetralin–dodecane, 50 wt %,  $T = 25^\circ\text{C}$  and wall quartz glass,  $\kappa_s/\kappa_w = 0$ : good approximation for sample tetralin–dodecane, 50 wt %,  $T = 25^\circ\text{C}$  and wall sapphire with  $\kappa_s/\kappa_w = 0.004$ )

heterodyne diffraction efficiency  $\zeta_{het,T,s}(t=0)$  (3.26) on the sample thickness  $l_s$  for grating period  $d = 10 \mu\text{m}$ .  $\zeta_{het,T,s}$  has been normalized on its value at  $l_s = 200 \mu\text{m}$ . In a one dimensional model one would expect a linear decrease of the heterodyne diffraction efficiency with decreasing sample thickness  $l_s$  according to Eq. (3.9). In case of perfectly insulating walls  $\kappa_s/\kappa_w = \infty$  this is still true for the two-dimensional model. Otherwise, heat flows into the cell walls. The thinner the sample the more important becomes this effect and the heterodyne diffraction efficiency decreases faster than linear with decreasing  $l_s$ .

### 3.1.4 Time Dependent Solutions

#### 3.1.4.1 Decay of the Temperature Grating

The objective is to solve the evolution equations (3.15, 3.16) for the amplitude  $T_q(z, t)$  of the temperature grating for arbitrary times  $t > 0$ . The initial condition is given by the steady state solution (3.23, 3.24), the boundary and matching conditions by Eq. (3.18) and Eqs. (3.20, 3.21). From  $T_q(z, t)$  the experimentally relevant quantities  $\zeta_{het,T,s}(t)$  and  $\zeta_{het,T,w}(t)$  can be evaluated according to Eq. (3.22).

**Analytical solutions** For  $d/l_s \rightarrow 0$  and  $d/l_s \rightarrow \infty$  analytical expressions for the heterodyne diffraction efficiencies  $\zeta_{het,T,s}(t)$  and  $\zeta_{het,T,w}(t)$  as defined in (3.22) have been found by using the Laplace transformation method. If  $d/l_s \rightarrow 0$  (thick samples) they are given by

$$\begin{aligned} \frac{\zeta_{het,T,s}(t)}{\zeta_{het,T,s}(t=0)} &\rightarrow \exp(-D_{th,s} q^2 t) + O(d/l_s) \quad (3.29) \\ \frac{\zeta_{het,T,w}(t)}{\zeta_{het,T,w}(t=0)} &\rightarrow 1 - \frac{\kappa_s}{\kappa_s - \kappa_w} \left( \operatorname{erf} \sqrt{D_{th,w} q^2 t} - \frac{\kappa_w}{\kappa_s} \operatorname{erf} \sqrt{D_{th,s} q^2 t} \right) + \frac{\kappa_s}{\kappa_s - \kappa_w} \times \\ &\frac{\exp(-b D_{th,w} q^2 t)}{\sqrt{a}} \left( \operatorname{erf} \sqrt{a D_{th,w} q^2 t} - \operatorname{erf} \sqrt{a \frac{\kappa_w^2}{\kappa_s^2} D_{th,s} q^2 t} \right) + O(\exp(-ql_s)), \quad (3.30) \end{aligned}$$

where  $a = (D_{th,w} - D_{th,s}) \kappa_s^2 (\kappa_s^2 D_{th,w} - \kappa_w^2 D_{th,s})^{-1}$  and  $b = (\kappa_s^2 - \kappa_w^2) D_{th,s} (\kappa_s^2 D_{th,w} - \kappa_w^2 D_{th,s})^{-1}$ . Note that  $\operatorname{erf} \sqrt{a} t / \sqrt{a}$  is real also for negative  $a$ . Eq. (3.29) corresponds to the result of the one-dimensional model (see Eqs. (3.4, 3.8, 3.9)). The time evolution of the heterodyne diffraction efficiency of the wall is complicated, but of no importance as

$$\frac{\zeta_{het,T,s}(t=0)}{\zeta_{het,T,w}(t=0)} \rightarrow \frac{(\partial n_s / \partial T)_{c,p}}{(\partial n_w / \partial T)_{c,p}} \left[ \left( 1 + \frac{\kappa_w}{\kappa_s} \right) \frac{ql_s}{2} - \frac{\kappa_w}{\kappa_s} \right] \rightarrow \infty \text{ for } \frac{ql_s}{2} = \frac{\pi l_s}{d} \rightarrow \infty. \quad (3.31)$$

Hence, in the limit  $d/l_s \rightarrow 0$  all diffracted intensity comes from the sample and not from the wall (see also Fig. 3.4).

The case  $d/l_s \rightarrow \infty$  (infinitely thin samples) leads to

$$\frac{\zeta_{het,T,s}(t)}{\zeta_{het,T,s}(t=0)} \rightarrow \operatorname{erfc}\sqrt{D_{th,w} q^2 t} + O(l_s/d) \quad (3.32)$$

$$\frac{\zeta_{het,T,w}(t)}{\zeta_{het,T,w}(t=0)} \rightarrow \exp(-D_{th,w} q^2 t) + O(l_s/d) \quad (3.33)$$

and

$$\frac{\zeta_{het,T,s}(t=0)}{\zeta_{het,T,w}(t=0)} \rightarrow \frac{(\partial n_s/\partial T)_{c,p} q l_s}{(\partial n_w/\partial T)_{c,p} 2} \rightarrow 0 \text{ for } \frac{q l_s}{2} = \frac{\pi l_s}{d} \rightarrow 0, \quad (3.34)$$

i.e. the contribution of the sample to the heterodyne diffraction efficiency is negligible for  $d/l_s \rightarrow \infty$  and all signal is generated by the wall.

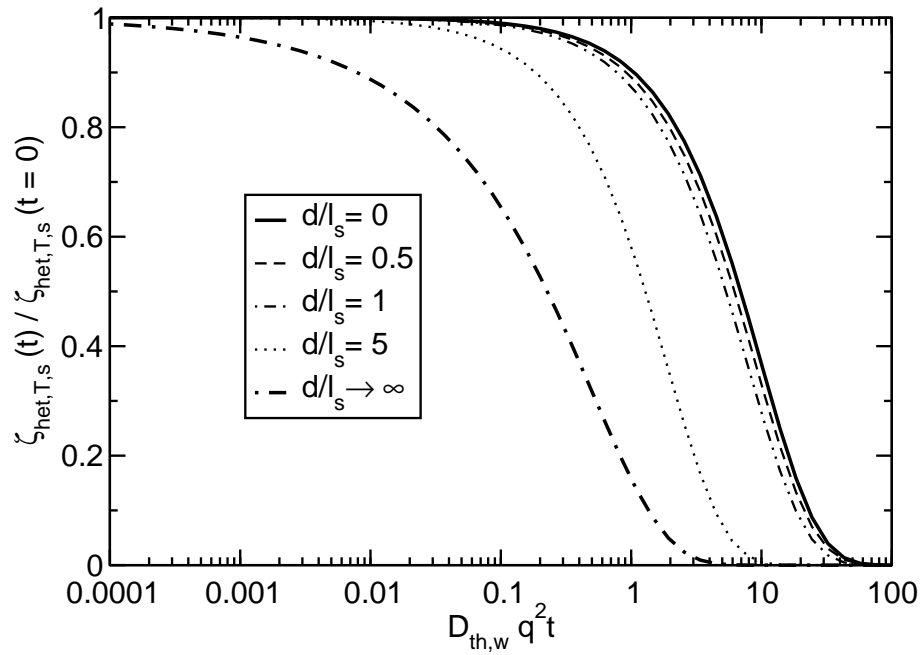
**Numerical solutions** For other values of  $d/l_s$  we solved the PDE (3.15, 3.16) with initial condition (3.23, 3.24), boundary condition (3.18) and matching conditions (3.20, 3.21) numerically. It is preferable to perform the simulations on scaled equations. Therefore we get results for the dimensionless temperature  $\tilde{T}_q = \kappa_w q^2 (\alpha I_0)^{-1} T_q$  that depends on the scaled time  $\tilde{t} = D_{th,w} q^2 t$ , the scaled space coordinates  $\tilde{x} = qx$ ,  $\tilde{z} = qz$  and the dimensionless parameters  $\kappa_s/\kappa_w$ ,  $D_{th,s}/D_{th,w}$  and  $d/l_s$ . The experimentally relevant quantities  $\zeta_{het,T,s}(t)$  and  $\zeta_{het,T,w}(t)$  as defined in Eq. (3.22) can be calculated from the scaled temperature  $\tilde{T}_q$  as follows

$$\frac{\zeta_{het,T,s}(t)}{\zeta_{het,T,s}(t=0)} = \frac{\int_0^{q l_s/2} \tilde{T}_q(\tilde{z}, D_{th,w} q^2 t) d\tilde{z}}{\int_0^{q l_s/2} \tilde{T}_q(\tilde{z}, t=0) d\tilde{z}} = \frac{\frac{\kappa_s}{\kappa_w} \int_0^{q l_s/2} \tilde{T}_q(\tilde{z}, D_{th,w} q^2 t) d\tilde{z}}{\frac{q l_s}{2} - \sinh \frac{q l_s}{2} \left[ \frac{\kappa_s}{\kappa_w} \sinh \frac{q l_s}{2} + \cosh \frac{q l_s}{2} \right]^{-1}} \quad (3.35)$$

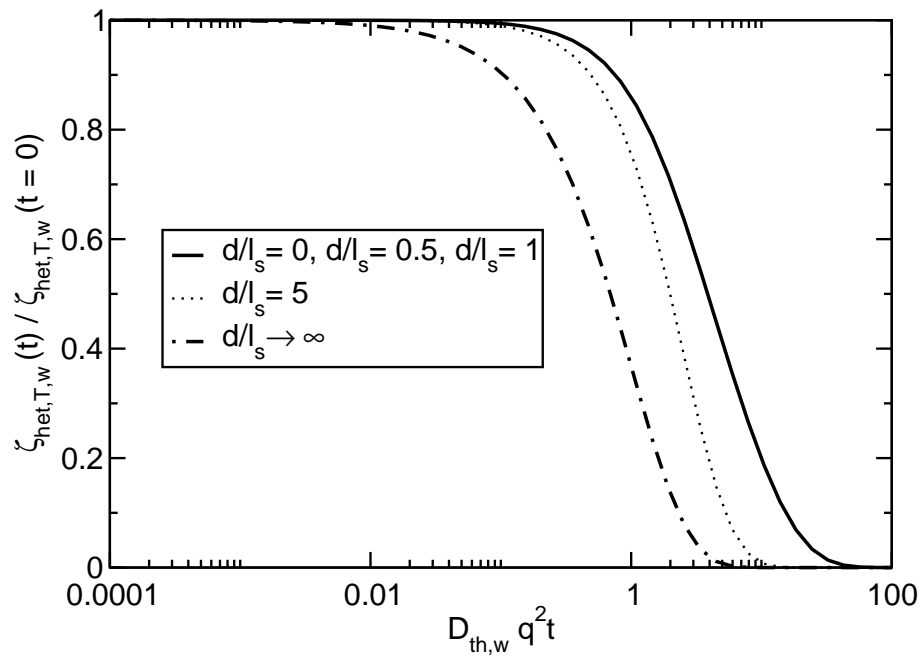
$$\frac{\zeta_{het,T,w}(t)}{\zeta_{het,T,w}(t=0)} = \frac{\int_{q l_s/2}^{\infty} \tilde{T}_q(\tilde{z}, D_{th,w} q^2 t) d\tilde{z}}{\int_{q l_s/2}^{\infty} \tilde{T}_q(\tilde{z}, t=0) d\tilde{z}} = \frac{\int_{q l_s/2}^{\infty} \tilde{T}_q(\tilde{z}, D_{th,w} q^2 t) d\tilde{z}}{\sinh \frac{q l_s}{2} \left[ \frac{\kappa_s}{\kappa_w} \sinh \frac{q l_s}{2} + \cosh \frac{q l_s}{2} \right]^{-1}}, \quad (3.36)$$

where the steady state solutions  $\zeta_{het,T,s}(t=0)$ ,  $\zeta_{het,T,w}(t=0)$  and  $\tilde{T}_q(\tilde{z}, t=0)$  are given by Eqs. (3.26, 3.28) and Eqs. (3.23, 3.24). Remember that the ratio of the two normalization factors,  $\zeta_{het,T,w}(t=0)/\zeta_{het,T,s}(t=0)$ , is plotted in Fig. 3.4 for the system tetralin–dodecane and quartz glass as wall material.

Figs. 3.6 and 3.7 show the simulated normalized heterodyne diffraction efficiencies (3.35) and (3.36). Also plotted are the analytical solutions (3.29, 3.30) and (3.32, 3.33). In Fig. 3.6 the results of the simulations are shown for typical experimental parameters  $\kappa_s/\kappa_w = 0.1$  and  $D_{th,s}/D_{th,w} = 0.1$ . Fig. 3.6(a) shows the results for the heterodyne diffraction efficiency of the sample's temperature grating. For  $d/l_s = 0$  it decays exponentially with time constant  $\tau_{th} = (D_{th,s} q^2)^{-1}$  according to Eq. (3.29). For increasing  $d/l_s$  it decreases faster. The temperature grating in the sample does not only decay because of heat diffusion in  $x$ -direction, but also because of heat flux into the wall. Remarkably, the heterodyne diffraction efficiencies

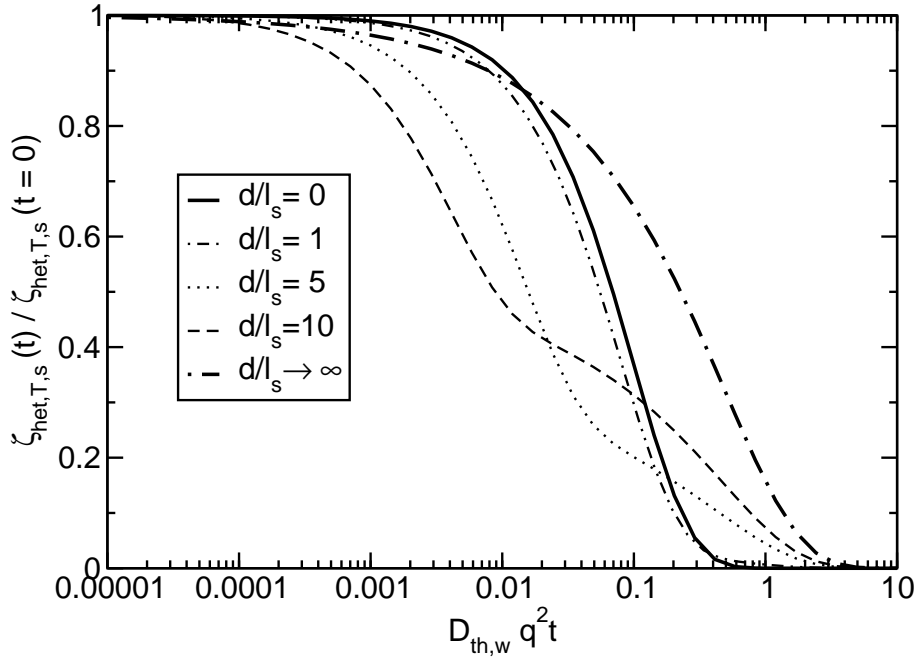


(a) Decay of the sample's temperature grating: normalized heterodyne diffraction efficiency  $\zeta_{het,T,s}(t)/\zeta_{het,T,s}(t=0)$

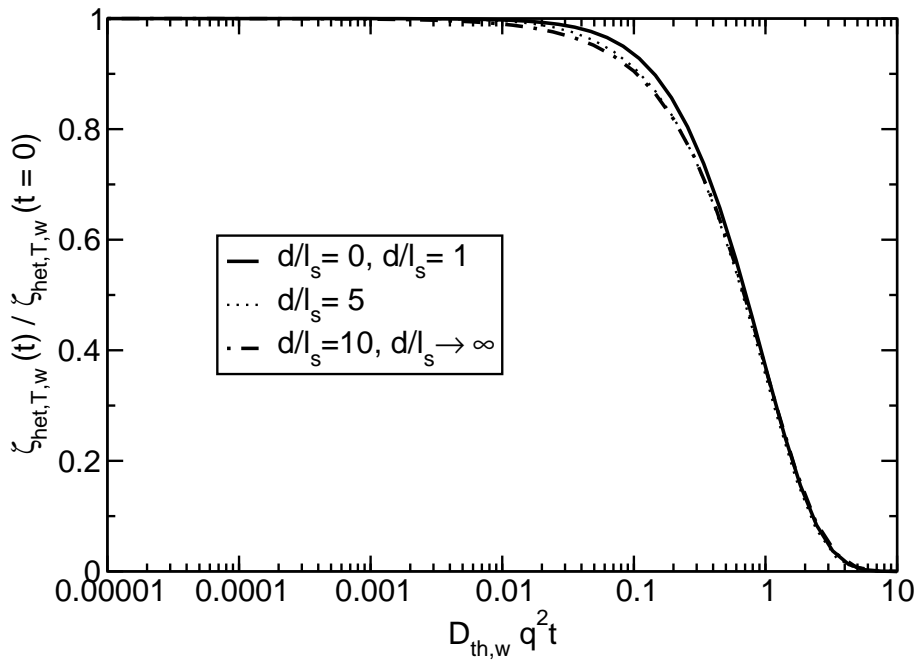


(b) Decay of the wall's temperature grating: normalized heterodyne diffraction efficiency  $\zeta_{het,T,w}(t)/\zeta_{het,T,w}(t=0)$

**Figure 3.6:** Decay of the temperature grating for  $\kappa_s/\kappa_w = 0.1$ ,  $D_{th,s}/D_{th,w} = 0.1$  and  $d/l_s = 0, 0.5, 1, 5$ , and  $d/l_s \rightarrow \infty$ .



(a) Decay of the sample's temperature grating: normalized heterodyne diffraction efficiency  $\zeta_{\text{het},T,s}(t)/\zeta_{\text{het},T,s}(t=0)$



(b) Decay of the wall's temperature grating: normalized heterodyne diffraction efficiency  $\zeta_{\text{het},T,w}(t)/\zeta_{\text{het},T,w}(t=0)$

**Figure 3.7:** Decay of the temperature grating for  $\kappa_s/\kappa_w = 0.1$ ,  $D_{\text{th},s}/D_{\text{th},w} = 10$  and  $d/l_s = 0, 1, 5, 10$ , and  $d/l_s \rightarrow \infty$ .

of the sample's temperature grating for not too large  $d/l_s > 0$  can still be described very well by exponential functions  $\exp(-t/\tau_{th})$  with time constants  $\tau_{th} < (D_{th,s}q^2)^{-1}$ . For example, exponential fits of the function  $\zeta_{het,T,s}(t)/\zeta_{het,T,s}(t=0)$  yield for  $d/l_s = 0.5$

$$\tau_{th} = \frac{9.06}{D_{th,w}q^2} = \frac{1}{1.104 D_{th,s}q^2} \quad \text{and} \quad \left| \frac{\zeta_{het,T,s}(t)}{\zeta_{het,T,s}(t=0)} - \exp(-t/\tau_{th}) \right| \leq 0.0053 \quad (3.37)$$

and for  $d/l_s = 5$

$$\tau_{th} = \frac{1.88}{D_{th,w}q^2} = \frac{1}{5.32 D_{th,s}q^2} \quad \text{and} \quad \left| \frac{\zeta_{het,T,s}(t)}{\zeta_{het,T,s}(t=0)} - \exp(-t/\tau_{th}) \right| \leq 0.0077. \quad (3.38)$$

Note that the same exponential fit will later be employed for the evaluation of the measured heterodyne diffraction efficiency. As the experimental data contain additive noise, the absolute rather than the relative error is the relevant quantity in Eqs. (3.37) and (3.38). It is obvious that for very large values of  $d/l_s$ , in particular for  $d/l_s \rightarrow \infty$ , an exponential fit of  $\zeta_{het,T,s}(t)/\zeta_{het,T,s}(t=0)$  does not make any sense. However, large values of  $d/l_s$  are experimentally irrelevant. We confirmed that in the experimentally investigated range  $d/l_s \approx 0.025 - 5$  an exponential description of the simulated heterodyne diffraction efficiencies of the sample's temperature grating works very well with deviations below 0.01, which is smaller than the typical noise amplitude (cf. Eqs. (3.37, 3.38)).

The decay of the temperature grating in the wall is presented in Fig. 3.6(b). The simulated results for  $d/l_s = 0.5$  and  $d/l_s = 1$  are very well approximated by the analytical solution (3.30) for  $d/l_s = 0$ . Differences between the three curves cannot be resolved in the plot. For our experiments the heterodyne diffraction efficiency of the wall's temperature grating is negligible, as has been shown in Fig. 3.4.

Under certain conditions, e.g. if the thermal diffusivity of the sample is much higher than the one of the wall, the heterodyne diffraction efficiencies might evolve in a quite complicated manner. Fig. 3.7 pictures the case  $\kappa_s/\kappa_w = 0.1$  and  $D_{th,s}/D_{th,w} = 10$ . For  $d/l_s = 5$  and  $d/l_s = 10$  the heterodyne diffraction efficiencies of the sample's temperature grating display a bimodal behavior (see Fig. 3.7(a)). The temperature grating in the sample decays because of heat diffusion in  $x$ -direction and because heat is transported into the wall. In the case  $D_{th,s}/D_{th,w} = 10$  heat cannot diffuse very effectively inside the wall. There comes a time when the temperature in the wall is higher than the temperature in the sample and heat will flow back from the wall into the sample. This leads to the second slow mode in the heterodyne diffraction efficiency of the sample's temperature grating.

**Calculation of the apparent thermal diffusivity  $D_{th,app}$**  As we have seen in Fig. 3.6(a), the heterodyne diffraction efficiencies of the sample's temperature grating for not too large values of  $d/l_s$  can be approximated by exponential functions. To analyze our experimental data, it would be sufficient to know the time constants  $\tau_{th} = (D_{th,app}q^2)^{-1}$  of these exponen-

tial functions. Knowledge of the exact temperature distribution  $T_q(z, t)$  is not necessary. Also the heterodyne diffraction efficiency of the wall's temperature grating is of no importance for our experiments.

A least square fit of  $\exp(-D_{th,app}q^2t)$  to the function  $\zeta_{het,T,s}(t)/\zeta_{het,T,s}(t=0)$  with  $D_{th,app}$  as adjustable parameter requires

$$f(D_{th,app}) = \int_0^\infty \left( \frac{\zeta_{het,T,s}(t)}{\zeta_{het,T,s}(t=0)} - \exp(-D_{th,app}q^2t) \right)^2 dt = \text{minimum.} \quad (3.39)$$

This is equivalent to finding  $D_{th,app}$  such that

$$-\frac{2 \int_0^\infty \zeta_{het,T,s}(t) \exp(-D_{th,app}q^2t) dt}{\zeta_{het,T,s}(t=0)} + \frac{1}{2 D_{th,app} q^2} = \text{minimum.} \quad (3.40)$$

Even though we do not know  $\zeta_{het,T,s}(t)$ , we can evaluate

$$\begin{aligned} \frac{\int_0^\infty \zeta_{het,T,s}(t) \exp(-D_{th,app}q^2t) dt}{\zeta_{het,T,s}(t=0)} &\stackrel{(3.22)}{=} \frac{\int_0^{l_s/2} \int_0^\infty T_q(z, t) \exp(-D_{th,app}q^2t) dt dz}{\int_0^{l_s/2} T_q(z, 0) dz} \\ &= \frac{\int_0^{l_s/2} \bar{T}_q(z, D_{th,app} q^2) dz}{\int_0^{l_s/2} T_q(z, t=0) dz}. \end{aligned} \quad (3.41)$$

$\bar{T}_q(z, p)$  denotes the Laplace transformation of  $T_q(z, t)$ . A Laplace transformation reduces a PDE to an ordinary differential equation (ODE). Therefore the Laplace transformation of the PDE (3.15, 3.16) can be easily solved. For  $z \leq l_s/2$  the solution is

$$\begin{aligned} \bar{T}_q(z, p) = & \frac{\alpha I_0}{\kappa_s p q^2} \left( \left[ 1 - \cosh(qz) \left[ \frac{\kappa_s}{\kappa_w} \sinh \frac{ql_s}{2} + \cosh \frac{ql_s}{2} \right]^{-1} \right] - \frac{1}{1 + \frac{p}{D_{th,s} q^2}} \left[ 1 - \right. \right. \\ & \left. \left. \frac{\sqrt{1 + \frac{p}{D_{th,w} q^2}} \cosh \left( \sqrt{1 + \frac{p}{D_{th,s}} qz} \right)}{\frac{\kappa_s}{\kappa_w} \sqrt{1 + \frac{p}{D_{th,s} q^2}} \sinh \left( \sqrt{1 + \frac{p}{D_{th,s} q^2}} \frac{ql_s}{2} \right) + \sqrt{1 + \frac{p}{D_{th,w} q^2}} \cosh \left( \sqrt{1 + \frac{p}{D_{th,s} q^2}} \frac{ql_s}{2} \right)} \right] \right). \end{aligned} \quad (3.42)$$

From Eqs. (3.40), (3.41), (3.23) and (3.42) follows that  $D_{th,app}$  has to fulfill the condition

$$g(D_{th,app}) = \text{minimum} \quad (3.43)$$



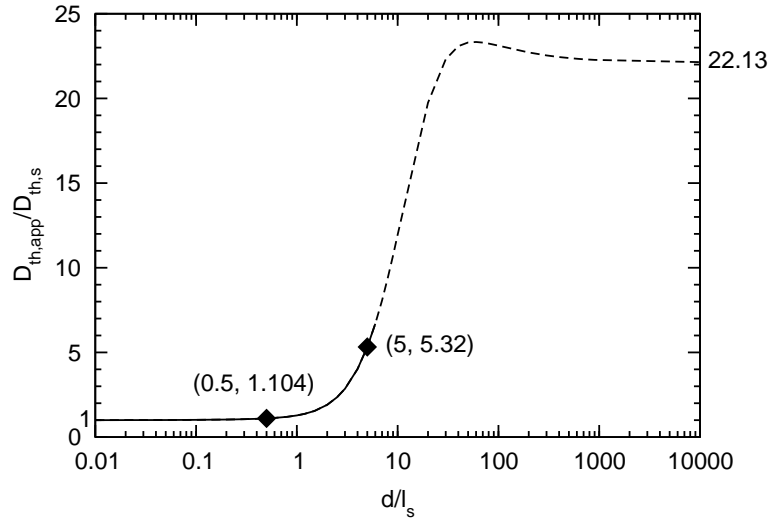


**Figure 3.8:** Solutions of Eq. (3.45) for  $D_{th,s}/D_{th,w} = 0.1$  and  $\kappa_s/\kappa_w = 0.1$ . Also plotted are the results for  $D_{th,app} = (\tau_{th} q^2)^{-1}$  according to Eqs. (3.37) and (3.38). The  $x$ - and  $y$ -coordinates are given in parenthesis.

with

$$g(x) = \frac{1}{x} \left( -3 \left[ \frac{ql_s}{2} - \frac{\sinh \frac{ql_s}{2}}{\frac{\kappa_s}{\kappa_w} \sinh \frac{ql_s}{2} + \cosh \frac{ql_s}{2}} \right] + \frac{4}{1 + \frac{x}{D_{th,s}}} \left[ \frac{ql_s}{2} - \frac{1}{\sqrt{1 + \frac{x}{D_{th,s}}}} \times \right. \right. \\ \left. \left. \frac{\sqrt{1 + \frac{x}{D_{th,w}}} \sinh \left( \sqrt{1 + \frac{x}{D_{th,s}}} \frac{ql_s}{2} \right)}{\frac{\kappa_s}{\kappa_w} \sqrt{1 + \frac{x}{D_{th,s}}} \sinh \left( \sqrt{1 + \frac{x}{D_{th,s}}} \frac{ql_s}{2} \right) + \sqrt{1 + \frac{x}{D_{th,w}}} \cosh \left( \sqrt{1 + \frac{x}{D_{th,s}}} \frac{ql_s}{2} \right)} \right] \right). \quad (3.44)$$

Eq. (3.43) leads to the conditional equation

$$\frac{\partial g}{\partial x} \Big|_{x=D_{th,app}} = 0, \quad (3.45)$$

which relates  $D_{th,app}$  to the parameters  $q$ ,  $l_s$ ,  $D_{th,s}$ ,  $D_{th,w}$ ,  $\kappa_s$ , and  $\kappa_w$ . Note that the ratio  $D_{th,app}/D_{th,s}$  respectively  $D_{th,app}/D_{th,w}$  only depends on the dimensionless parameters  $D_{th,s}/D_{th,w}$ ,  $\kappa_s/\kappa_w$  and  $ql_s$ . In a typical experiment  $D_{th,app}$  is measured and then the unknown parameter, e.g.  $D_{th,s}$ , is determined such that Eq. (3.45) is fulfilled.

Fig. 3.8 shows the solutions of Eq. (3.45) for  $D_{th,s}/D_{th,w} = 0.1$  and  $\kappa_s/\kappa_w = 0.1$ , i.e. for the same parameters as in Fig. 3.6(a). For  $d/l_s \rightarrow 0$  the apparent thermal diffusivity tends to the true thermal diffusivity of the sample,  $D_{th,app}/D_{th,s} \rightarrow 1$ . The earlier results (3.37) and (3.38) for  $D_{th,app} = (\tau_{th} q^2)^{-1}$  at  $d/l_s = 0.5$  and  $d/l_s = 5$  are indicated by filled diamonds. The dashed line shall remind us, that for too large values  $d/l_s$  an exponential fit of the

heterodyne diffraction efficiency  $\zeta_{het,T,s}(t)/\zeta_{het,T,s}(t=0)$  is no longer a good approximation. Nevertheless, the behavior of  $D_{th,app}/D_{th,s}$  for  $d/l_s \rightarrow \infty$  is in accordance with Eq. (3.32). An exponential fit  $\exp(-a_0x)$  of the function  $\text{erfc}\sqrt{x}$  leads to  $a_0 = 2.213$ , corresponding to  $D_{th,app}/D_{th,s} = 22.13$  in Fig. 3.8.

The conditional equation for  $D_{th,app}$  (3.45) is an important result, since solving Eq. (3.45) numerically is a much simpler task than simulating the PDEs (3.15, 3.16) with initial condition (3.23, 3.24), boundary condition (3.18) and matching conditions (3.20, 3.21). Eq. (3.45) can be used to analyze experimental data under the conditions, that the measured temperature signal decays approximately exponentially, the contributions of the wall to the heterodyne diffraction efficiency is negligible (can be checked by comparison of Eq. (3.26) and Eq. (3.28)), and the approximations of our model are valid (infinite extension in  $x$ -direction, infinite wall thickness, no  $y$ -dependence, laser intensity given by Eq. (3.11), no contact resistance between sample and wall). Under these premises the measured temperature signal is equal to  $\zeta_{het,T,s}(t)$ , it decays with time constant  $\tau_{th} = (D_{th,app}q^2)^{-1}$  and  $D_{th,app}$  can be determined according to Eq. (3.45).

### 3.1.4.2 Decay of the Concentration Grating

The concentration distribution  $c_q(z, t)$  evolves according to the extended diffusion equation (3.17) with initial condition (3.25) and boundary condition (3.19). To solve this problem the complete knowledge of  $T_q(z, t)$  is necessary. However, we are actually not so much interested in the concentration distribution  $c_q(z, t)$ . The relevant quantity is the measured heterodyne diffraction efficiency of the concentration grating  $\zeta_{het,c}(t)$  as defined in Eq. (3.22).

To obtain an evolution equation for  $\zeta_{het,c}(t)$  we integrate the extended diffusion equation (3.17) over the sample thickness ( $|z| < l_s/2$ ). Taking into account the boundary condition (3.19) and the definitions of the heterodyne diffraction efficiencies (3.22) we arrive at

$$\partial_t \zeta_{het,c} = -D q^2 \zeta_{het,c} - \left(\frac{\partial n_s}{\partial c}\right)_{T,p} \left(\frac{\partial n_s}{\partial T}\right)_{c,p}^{-1} D_T q^2 c_0 (1 - c_0) \zeta_{het,T,s}. \quad (3.46)$$

Eq. (3.46) is solved by

$$\zeta_{het,c}(t) = \zeta_{het,c}(t=0) \exp(-D q^2 t) - \left(\frac{\partial n_s}{\partial c}\right)_{T,p} \left(\frac{\partial n_s}{\partial T}\right)_{c,p}^{-1} D_T q^2 c_0 (1 - c_0) \int_0^t \zeta_{het,T,s}(t') \exp(-D q^2 (t - t')) dt', \quad (3.47)$$

where  $\zeta_{het,c}(t=0)$  is given by Eq. (3.27).

Further simplification of Eq. (3.47) is not possible without knowledge of  $\zeta_{het,T,s}(t)$ . In general we do not have an analytical expression for  $\zeta_{het,T,s}(t)$ , so that we do not have an analytical expression for  $\zeta_{het,c}(t)$  either. Making certain assumptions about  $\zeta_{het,T,s}(t)$ , however, allows us to obtain analytical approximations to Eq. (3.47).

If the heterodyne diffraction efficiency of the sample's temperature grating  $\zeta_{het,T,s}$  can be approximated exponentially

$$\zeta_{het,T,s}(t) = \zeta_{het,T,s}(t=0) \exp(-D_{th,app} q^2 t), \quad (3.48)$$

Eq. (3.47) simplifies to

$$\zeta_{het,c}(t) = \zeta_{het,c}(t=0) (D_{th,app} - D)^{-1} \left( D_{th,app} \exp(-D q^2 t) - D \exp(-D_{th,app} q^2 t) \right). \quad (3.49)$$

But we can get an approximate solution for  $\zeta_{het,c}(t)$  even without knowing precisely the time evolution of  $\zeta_{het,T,s}(t)$ . Whenever the temperature signal evolves fast on the timescale of the concentration signal ( $D_{th} \gg D$ ), the second term in Eq. (3.47) can be neglected and we get to

$$\zeta_{het,c}(t) = \zeta_{het,c}(t=0) \exp(-D q^2 t). \quad (3.50)$$

In the case  $D_{th} \gg D$  the concentration signal (3.50) decays exponentially always with the same time constant  $\tau = (Dq^2)^{-1}$ , independent from the ratio grating constant to sample thickness  $d/l_s$ .

### 3.1.4.3 Decay of the Total Heterodyne Diffraction Efficiency

The heterodyne diffraction efficiency is defined in Eq. (3.22). For realistic experimental parameters the heterodyne diffraction efficiency of the wall is negligible (see Fig. 3.4) and Eq. (3.22) reduces to

$$\zeta_{het}(t) = \zeta_{het,T,s}(t) + \zeta_{het,c}(t). \quad (3.51)$$

In the experimentally investigated range  $d/l_s \approx 0.025 - 5$  the heterodyne diffraction efficiencies of the sample's temperature grating can be approximated exponentially. Then the heterodyne diffraction efficiencies  $\zeta_{het,T,s}$  and  $\zeta_{het,c}$  are given by Eqs. (3.48, 3.49). Inserting Eqs. (3.48, 3.49) into Eq. (3.51) leads to

$$\begin{aligned} \zeta_{het}(t) &= \zeta_{het,T,s}(t=0) \exp(-D_{th,app} q^2 t) + \\ &\quad \zeta_{het,c}(t=0) (D_{th,app} - D)^{-1} \left( D_{th,app} \exp(-D q^2 t) - D \exp(-D_{th,app} q^2 t) \right) \\ &= \zeta_{het,T,s}(t=0) \left[ \exp(-D_{th,app} q^2 t) - \left( \frac{\partial n_s}{\partial c} \right)_{T,p} \left( \frac{\partial n_s}{\partial T} \right)_{c,p}^{-1} S_T c_0 (1 - c_0) \times \right. \\ &\quad \left. (D_{th,app} - D)^{-1} \left( D_{th,app} \exp(-D q^2 t) - D \exp(-D_{th,app} q^2 t) \right) \right]. \quad (3.52) \end{aligned}$$

Eq. (3.52) is identical to the equation of the one-dimensional model (3.10), except that the thermal diffusivity of the sample  $D_{th,s}$  has been replaced by the apparent thermal diffusivity  $D_{th,app}$ . This leads to the important result that neglected heat loss into the wall results

in a wrong thermal diffusivity  $D_{th,app}$ , whereas the correct values are still obtained for the collective diffusion coefficient  $D$ , the thermal diffusion coefficient  $D_T$ , and the Soret coefficient  $S_T$ . For a one-component system with  $c \equiv c_0 = 1$  Eq. (3.52) simplifies to

$$\zeta_{het}(t) = \zeta_{het,T,s}(t) = \zeta_{het,T,s}(t=0) \exp(-D_{th,app} q^2 t). \quad (3.53)$$

Eqs. (3.52) and (3.53) will be used as working equations to analyze the experimental data.

## 3.2 Experimental Technique and Sample Preparation

**Experimental technique** The holographic grating setup has been described in detail elsewhere [109, 53]. An argon ion laser (488 nm or 515.5 nm) was used for writing and a HeNe laser (632 nm) for readout of the refractive index gratings in a heterodyne detection scheme. The coherent superposition of the diffracted and the reference wave was detected with a single-mode optical fiber connected to a photomultiplier tube. The temperature was controlled by a circulating water thermostat and set to 25°C for all experiments. The contrast factor  $(\partial n / \partial c)_{T,p}$  was determined with an Abbe refractometer.  $(\partial n / \partial T)_{c,p}$  was determined interferometrically as described in Ref. [111].

**Sample preparation** The pure substances toluene, tetralin and dodecane have been purchased from Merck, Acros and Aldrich, respectively. The purities of the chemicals are in excess of 98%. Sample preparation is done in a similar way as for light scattering experiments. An inert dye (quinizarin) is added to the pure substances for optical absorption at the writing wavelength, but ideally not at the readout wavelength. While absorption at  $\lambda_r$  is not a principal problem, it results in avoidable sample heating. The absorption coefficient at the writing wavelength was  $\alpha \approx 2 \text{ cm}^{-1}$ . For the experiments with binary mixtures, these solutions were mixed with equal weights. The liquids were filled into thoroughly cleaned and dried cuvettes, discarding the first filling. After the second filling the cuvettes were closed with Teflon plugs and sealed with Parafilm. Before and after each measurement the cuvette was weighed. No weight loss was observed in any experiment. Cuvettes with layer thicknesses of  $l_s \approx 200, 100, 50, \text{ or } 10 \mu\text{m}$  (Hellma) and self made sapphire cells with  $l_s = 112 \text{ or } 119 \mu\text{m}$  were used. For the  $(\partial n / \partial T)_{c,p}$  measurement cuvettes with a path length of 10 mm (Hellma) were employed.

### 3.3 Results and Discussion

#### 3.3.1 Measurements on Pure Toluene

One-component systems with  $c = 1$  are suitable to study the decay of the temperature grating. As they cannot exhibit concentration modulations, the time evolution of the heterodyne diffraction efficiency can be related directly to the time evolution of the temperature grating.

In a first step we investigated toluene at  $T = 25^\circ\text{C}$  in cuvettes of two different wall materials, quartz glass and sapphire. Quartz glass is frequently used for optical experiments. At  $T = 25^\circ\text{C}$  and under normal pressure it has a thermal conductivity  $\kappa_w = 1.38\text{ W/mK}$  and a thermal diffusivity  $D_{th,w} = 84.8 \times 10^{-4}\text{ cm}^2/\text{s}$  [71]. However, if a good heat coupling between the sample and the thermal bath is desired, sapphire, having a very high thermal conductivity, is a much better choice. Under the same conditions as above,  $T = 25^\circ\text{C}$  and normal pressure, its thermal conductivity and thermal diffusivity are  $\kappa_w = 40\text{ W/mK}$  and  $D_{th,w} = 1300 \times 10^{-4}\text{ cm}^2/\text{s}$  [56].

To study the influence of the cell wall, we varied the sample thickness  $l_s$  as well as the grating period  $d$ . We used quartz glass cuvettes of thicknesses  $l_s = 12, 55, 100,$  and  $200\ \mu\text{m}$  and sapphire cuvettes of thicknesses  $l_s = 112$  and  $119\ \mu\text{m}$ . The thickness was measured interferometrically by counting the interference fringes in a spectrometer. The accuracy was generally better than 1%. The grating period was varied from  $d \approx 5\ \mu\text{m}$  up to  $d \approx 50\ \mu\text{m}$ .

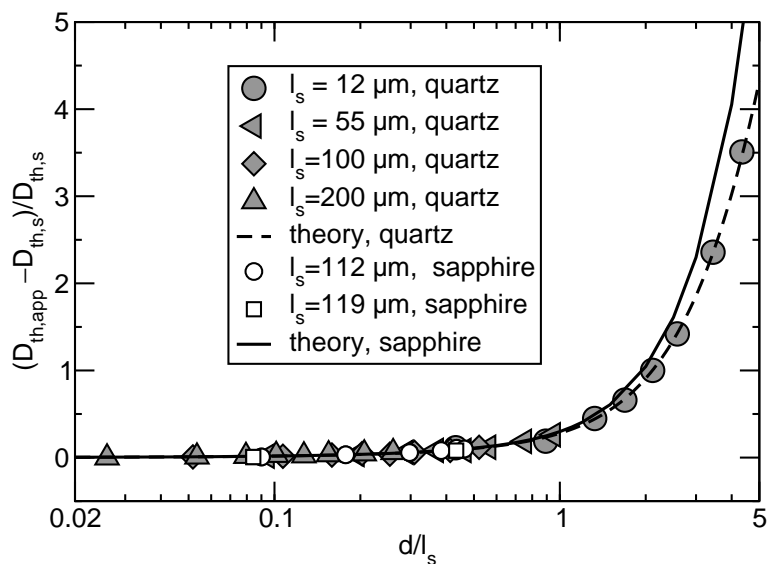


**Figure 3.9:** Results for toluene at  $T = 25^\circ\text{C}$ : plotted are the relative deviations  $(D_{th,app} - D_{th,s}) / D_{th,s}$  of the measured thermal diffusivity value  $D_{th,app}$  from the reference value  $D_{th,s} = 8.8 \times 10^{-4}\text{ cm}^2/\text{s}$  against the ratio of sample thickness to grating period  $d/l_s$ . Different symbols refer to different sample thicknesses  $l_s$ . Filled symbols are for quartz and open symbols for sapphire cells.

The experimentally measured decay of the heterodyne diffraction efficiency after switching

of the laser has been fitted to the working equation (3.53). The results for  $D_{th,app}$  are shown in Fig. 3.9. The  $x$  and  $y$  axes represent, respectively, the ratio of grating period to sample thickness  $d/l_s$  and the relative deviation of the experimental value  $D_{th,app}$  from the reference value  $D_{th,s} = 8.8 \times 10^{-4} \text{ cm}^2/\text{s}$ , which was obtained from the extrapolation for  $d/l_s \rightarrow 0$ . The theoretical curves have been calculated from (3.45) using  $D_{th,s}/D_{th,w} = 0.10$ ,  $\kappa_s/\kappa_w = 0.10$  for quartz glass and  $D_{th,s}/D_{th,w} = 0.007$ ,  $\kappa_s/\kappa_w = 0.004$  for sapphire. The experimentally measured values, both for quartz glass and sapphire, are described very well by the theoretical curves. As the theory predicts,  $D_{th,app}$  only depends on the ratio  $d/l_s$ . In the range  $d/l_s < 1$  the measured thermal diffusivity  $D_{th,app}$  is almost independent from the wall material and the results for sapphire cannot be distinguished from the results for quartz glass. For larger values of  $d/l_s$ , however, the temperature grating decays significantly faster in a sapphire cuvette, because of the more efficient heat transport into the wall. Regrettably no sapphire cells have been available for this parameter range.

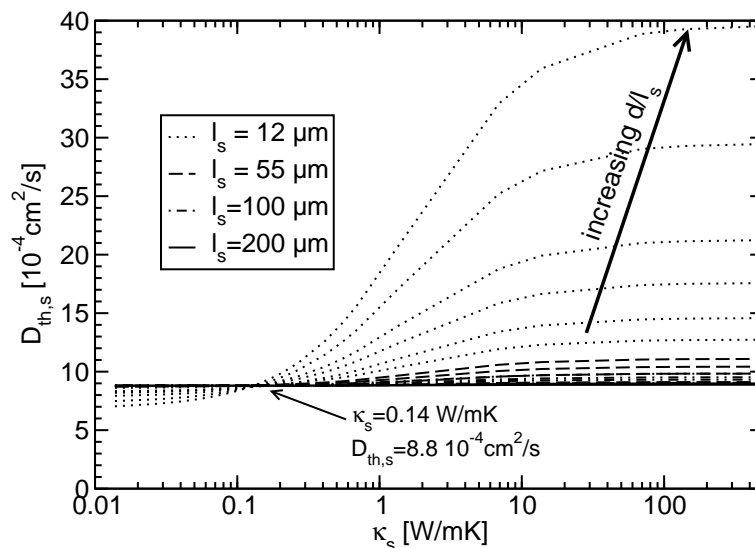


**Figure 3.10:** Determination of the thermal conductivity  $\kappa_s$  and the thermal diffusivity  $D_{th,s}$  of toluene using the results for toluene in quartz glass cuvettes (grey symbols in Fig. 3.9). Each single experiment yields a curve  $D_{th,s}(\kappa_s)$ . All curves of all different experiments intersect in the same point, which gives us the searched properties  $\kappa_s$  and  $D_{th,s}$  of toluene.

In Fig. 3.9 the theoretical curves have been evaluated from the ratios  $D_{th,s}/D_{th,w}$  and  $\kappa_s/\kappa_w$ , which requires knowledge of the thermal conductivity  $\kappa_s$  and the thermal diffusivity  $D_{th,s}$  of the sample. The usual situation, however, is different: The properties of the sample are unknown and shall be determined by analyzing the experimental data. This has been done in Fig. 3.10 for the measurements of toluene in quartz glass cuvettes (grey symbols in Fig. 3.9). One single experiment gives us a value for  $D_{th,app}$  at a certain  $d/l_s$ . From that we can calculate a curve  $D_{th,s}(\kappa_s)$  using Eq. (3.45), provided that we know the parameters  $\kappa_w$  and  $D_{th,w}$  of the wall. Then the true thermal conductivity  $\kappa_s$  and thermal diffusivity  $D_{th,s}$  of

the sample correspond to one point of the curve  $D_{th,s}(\kappa_s)$ . To determine  $\kappa_s$  and  $D_{th,s}$ , we have to calculate at least two curves  $D_{th,s}(\kappa_s)$  from two experiments at different  $d/l_s$  and find their point of intersection. This works especially well, if we use one experiment with small  $d/l_s \approx 0.1$  and one experiment with large  $d/l_s \approx 5$ . For toluene we found in this way  $D_{th,s} = 8.8 \times 10^{-4} \text{ cm}^2/\text{s}$  and  $\kappa_s = 0.14 \text{ W/mK}$ .

We would like to point out an important difference between the generally applied one-dimensional and our two-dimensional model. Assuming a one-dimensional model, one single experiment is sufficient to determine the thermal diffusivity of the sample  $D_{th,s}$ . The thermal conductivity  $\kappa_s$ , however, cannot be extracted from the experimental data. With our two-dimensional model, in contrast, at least two experiments at different  $d/l_s$  are required, but they yield both  $D_{th,s}$  and  $\kappa_s$ . From the intersecting curves in Fig. 3.10 it can be seen that  $D_{th,s}$  can always be determined with a high accuracy, whereas a precise measurement of  $\kappa_s$  requires at least one measurement with a large value of  $d/l_s$ . For small  $d/l_s$ , as employed for typical experiments, any reasonable assumption about  $\kappa_s$  leads to a good approximation to the true  $D_{th,s}$ .

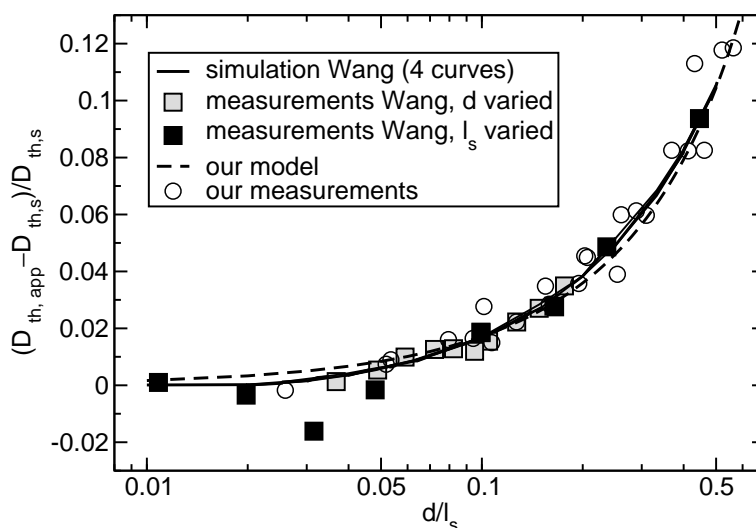


**Figure 3.11:** Comparison of our results for toluene in quartz glass cuvettes to the experimental and theoretical data obtained by Wang et al. [105, 106]. The axes are as in Fig. 3.9.

Fig. 3.11 compares our results for toluene in quartz glass cuvettes to the results obtained by Wang et al. [105, 106]. The meaning of the axes is the same as in Fig. 3.9. The experimental technique of Wang et al. differs only slightly from ours, but their theoretical model is much more complicated. They performed a three-dimensional numerical simulation on a PDE. The simulation parameters are the grating period  $d$ , the sample thickness  $l_s$ , the absorption coefficient  $\alpha$ , the thermal diffusivities of the sample  $D_{th,s}$  and of the wall  $D_{th,w}$ , the thermal conductivities of the sample  $\kappa_s$  and the wall  $\kappa_w$ , the pulse duration time  $t_h$  of the pulsed laser, and some more. So many parameters, however, do not seem to be necessary, as can be seen

in Fig. 3.11. If plotted against the ratio  $d/l_s$ , the results of all their simulations for toluene (Fig. 8 in [106]:  $d = 50 \mu\text{m}$ ,  $l_s$  varied,  $\alpha = 0.2 \text{ mm}^{-1}$ ,  $t_h = 800 \mu\text{s}$ ; Fig. 9 in [106]:  $d$  varied,  $l_s = 0.5 \text{ mm}$ ,  $\alpha = 0.2 \text{ mm}^{-1}$ ,  $t_h = 800 \mu\text{s}$ ; Fig. 3 in [105]:  $d = 50 \mu\text{m}$ ,  $l_s$  varied,  $\alpha = 0.8 \text{ mm}^{-1}$ ,  $t_h = 1200 \mu\text{s}$ ; Fig. 6 in [105]:  $d$  varied,  $l_s = 0.5 \text{ mm}$ ,  $\alpha = 0.8 \text{ mm}^{-1}$ ,  $t_h = 1200 \mu\text{s}$ ) coincide, at least within the resolution of the plot, on one single curve. Furthermore they are in very good agreement with results from our model, which depend only on the dimensionless parameters  $d/l_s$ ,  $D_{th,s}/D_{th,w}$  and  $\kappa_s/\kappa_s$  and have been obtained in a much simpler way, namely by finding the zero of Eq. (3.45). Moreover, Wang's experimental data (Fig. 4 in [105]:  $d = 50 \mu\text{m}$ ,  $l_s$  varied,  $\alpha = 0.8 \text{ mm}^{-1}$ ,  $t_h = 1200 \mu\text{s}$ ; Fig. 7 in [105]:  $d$  varied,  $l_s = 0.5 \text{ mm}$ ,  $\alpha = 0.8 \text{ mm}^{-1}$ ,  $t_h = 1200 \mu\text{s}$ ) is described very well by our theory. Unfortunately Wang et al. performed experiments and simulations only up to  $d/l_s = 0.5$ , so that it is not possible to compare the results over a wider range of  $d/l_s$ , where deviations from the one-dimensional model become more pronounced (Fig. 3.9).

### 3.3.2 Measurements on Binary Systems

Binary systems feature both a temperature and a concentration grating. We studied the binary mixtures of tetralin–dodecane and of tetralin–toluene at  $c = 0.5$  and  $T = 25^\circ\text{C}$ . The same quartz glass cuvettes of thicknesses  $l_s = 12, 55, 100, \text{ and } 200 \mu\text{m}$  as for toluene were used and the grating period was varied from  $d \approx 10 \mu\text{m}$  to  $d \approx 50 \mu\text{m}$ .

Fig. 3.12 shows four experimental curves measured for the system tetralin–dodecane at different sample thicknesses  $l_s$  and grating periods  $d$ . They correspond to zero power of the writing laser and have been obtained by extrapolation of five experimental curves at different laser powers between  $P = 50 \text{ mW}$  and  $P = 800 \text{ mW}$  to  $P = 0$ . This extrapolation is important for comparison of cuvettes with different sample thicknesses to exclude effects of sample heating. The normalized heterodyne diffraction efficiency  $\zeta_{het}(t)/\zeta_{het}(t=0)$  has been plotted against the reduced time  $Dq^2t$ , where the collective diffusion coefficient  $D = 6.5 \times 10^{-6} \text{ cm}^2/\text{s}$  of the system tetralin–dodecane has been obtained by fitting Eq. (3.52) to the experimental data (see Fig. 3.14). The fast and slow process correspond, respectively, to the decay of temperature and concentration grating. Whereas the temperature grating decays faster with increasing  $d/l_s$ , the concentration grating decays according to Eq. (3.50) always with the same time constant  $\tau = (Dq^2)^{-1}$ . Other than heat, mass cannot be transported into the cell walls. Therefore the integrated property  $\zeta_{het,c}$  as defined in Eq. (3.22) cannot decay faster than with  $\tau = (Dq^2)^{-1}$ , even if the dependence of the concentration distribution  $c_q(z, t)$  on  $z$  is very complicated and mass fluxes in  $z$ -direction are present. The ratio of the amplitudes of concentration and temperature signal  $\zeta_{het,c}(t=0)/\zeta_{het,T,s}(t=0)$  is, according to Eq. (3.27), independent of grating period  $d$  and sample thickness  $l_s$ .

Fitting all the other experimental curves extrapolated to zero laser power to the working equation (3.52) yields the apparent thermal diffusivity  $D_{th,app}$  (Fig. 3.13), the collective



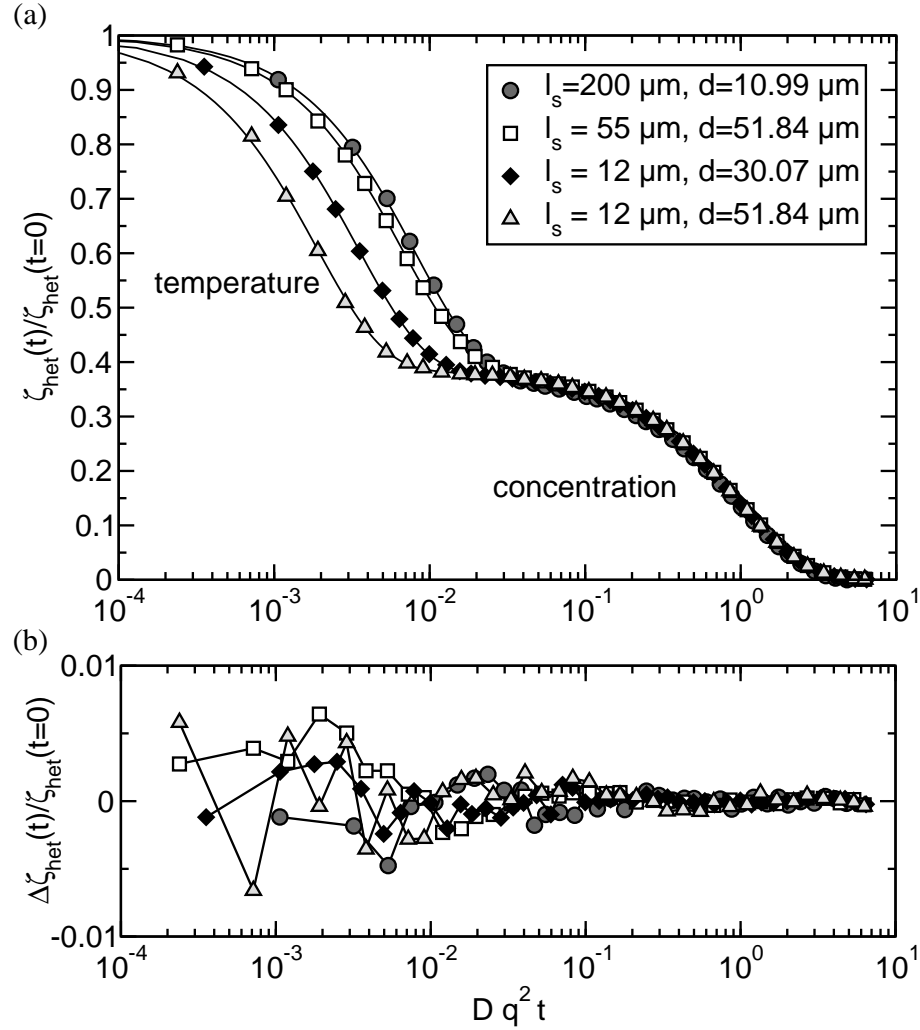


**Figure 3.12:** (a) Measured decay of the heterodyne diffraction efficiency  $\zeta_{het}(t)/\zeta_{het}(t=0)$  against the reduced time  $Dq^2t$  for the system tetralin–dodecane at different sample thicknesses  $l_s$  and grating periods  $d = 2\pi/q$ . The collective diffusion coefficient  $D = 6.5 \times 10^{-6} \text{ cm}^2/\text{s}$  is the same for all curves. Also plotted are the least–squares fits of Eq. (3.52) to the experimental data (solid lines). (b) Residuals

	$(\partial n_s/\partial T)_{c,p}$	$(\partial n_s/\partial c)_{T,p}$
tetralin–dodecane	$-4.39 \times 10^{-4}/\text{K}$	0.117
tetralin–toluene	$-5.15 \times 10^{-4}/\text{K}$	0.045

**Table 3.1:** Contrast factors for the binary systems tetralin–dodecane and tetralin–toluene, 50 wt %,  $T = 25^\circ\text{C}$ . The values for tetralin–dodecane are from Ref. [111].

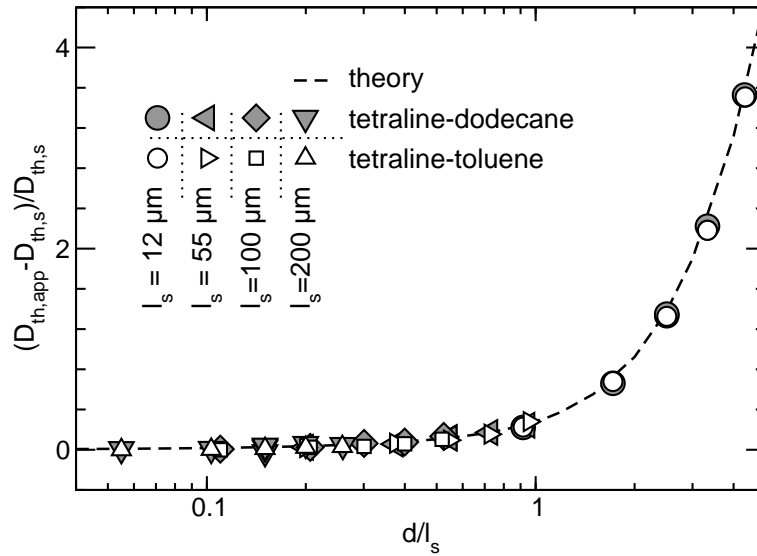


**Figure 3.13:** Results for the binary systems tetralin–dodecane (grey symbols) and tetralin–toluene (white symbols), 50 wt %,  $T = 25^\circ\text{C}$ : The relative deviations  $(D_{th,app} - D_{th,s})/D_{th,s}$  of the experimental value  $D_{th,app}$  from the reference value  $D_{th,s} = 8.0 \times 10^{-4} \text{ cm}^2/\text{s}$  for tetralin–dodecane and  $D_{th,s} = 8.4 \times 10^{-4} \text{ cm}^2/\text{s}$  for tetralin–toluene are plotted against the ratio of grating period to sample thickness  $d/l_s$ . Different symbols refer to different sample thicknesses  $l_s$ .

diffusion coefficient  $D$  (Fig. 3.14) and the Soret coefficient  $S_T$  (Fig. 3.15). To calculate the latter, the contrast factors  $(\partial n_s/\partial T)_{c,p}$  and  $(\partial n_s/\partial c)_{T,p}$  had to be measured (Tab. 3.1).

In Fig. 3.13 the relative deviation of the experimental value  $D_{th,app}$  from the reference value  $D_{th,s}$  ( $D_{th,s} = 8.0 \times 10^{-4} \text{ cm}^2/\text{s}$  for tetralin–dodecane and  $D_{th,s} = 8.4 \times 10^{-4} \text{ cm}^2/\text{s}$  for tetralin–toluene) is plotted against the ratio of grating period to sample thickness  $d/l_s$ . The theoretical curves have been evaluated from Eq. (3.45) with  $\kappa_s/\kappa_w = 0.09$ ,  $D_{th,s}/D_{th,w} = 0.09$  for tetralin–dodecane and  $\kappa_s/\kappa_w = 0.09$ ,  $D_{th,s}/D_{th,w} = 0.1$  for tetralin–toluene. In the range  $d/l_s \leq 5$  they differ less than 0.8% and cannot be distinguished within the resolution of the plot. The agreement between theory and experiment is excellent for both systems.

Figs. 3.14 and 3.15 show the measured collective diffusion coefficients  $D$  and Soret coefficients  $S_T$  against  $d/l_s$ . As already seen in Fig. 3.12 the concentration signal  $\zeta_{het,c}$  does not depend on  $d/l_s$  and therefore all experiments yield the same collective diffusion coefficients  $D$  and Soret coefficients  $S_T$ . Small deviations are only observable for the system tetralin–toluene at  $d = 51.84 \mu\text{m}$ , corresponding to a very small scattering angle of  $0.36^\circ$ , and  $l_s = 55$  and  $12 \mu\text{m}$ . However, it should be pointed out that, compared to the dramatic increase of the apparent thermal diffusivity  $D_{th,app}$ , these deviations are only minute. The system tetralin–dodecane, in contrast, does not show any dependence of  $D$  and  $S_T$  on  $d/l_s$  and behaves in perfect agreement with the predictions of our model.

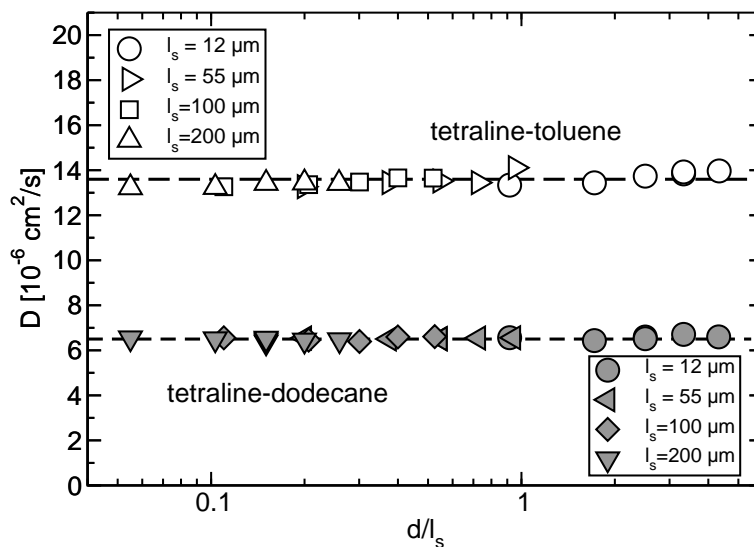


**Figure 3.14:** Results for the binary systems tetralin–dodecane (grey symbols) and tetralin–toluene (white symbols), 50 wt %,  $T = 25^\circ\text{C}$ : Measured collective diffusion coefficients  $D$  against the ratio of grating period to sample thickness  $d/l_s$ . Different symbols refer to different sample thicknesses  $l_s$ .

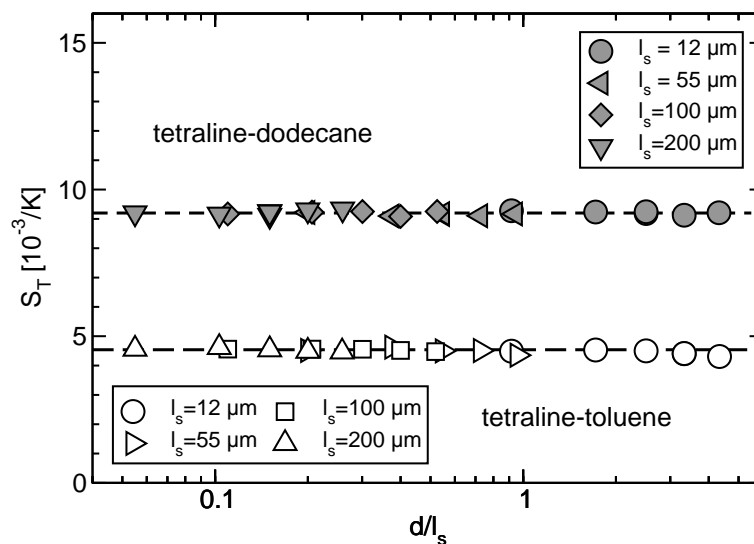


**Figure 3.15:** Results for the binary systems tetralin–dodecane (grey symbols) and tetralin–toluene (white symbols), 50 wt %,  $T = 25^\circ\text{C}$ : Measured Soret coefficients  $S_T$  against the ratio of grating period to sample thickness  $d/l_s$ . Different symbols refer to different sample thicknesses  $l_s$ .

### 3.4 Conclusion

For thin samples or large grating periods heat conducting walls become important in transient grating experiments. The heat loss into the cell walls leads to a nearly exponential decay of the temperature grating with a time constant  $\tau_{th} = (D_{th,app} q^2)^{-1} < (D_{th,s} q^2)^{-1}$ .  $D_{th,app}$  and  $D_{th,s}$  are the apparent and the true thermal diffusivities of the sample. The experimental results can be reproduced theoretically by solving the two-dimensional heat equations for the sample and the wall on condition that the temperature and the heat flux is continuous over the interface. Even though it was not possible to solve these PDEs analytically, a conditional equation (Eq. (3.45)) could be found, which relates the ratio  $D_{th,app}/D_{th,w}$  to the three dimensionless parameters  $d/l_s$ ,  $\kappa_s/\kappa_w$  and  $D_{th,s}/D_{th,w}$ .  $d$  is the grating period,  $l_s$  is the sample thickness,  $\kappa_s/\kappa_w$  is the thermal conductivity of the sample and the wall, respectively, and  $D_{th,w}$  is the thermal diffusivity of the wall. Whereas simulation of the PDEs requires substantial computational effort, the conditional equation (3.45) allows for easy determination of the parameters of the sample from the measured  $D_{th,app}$ . For this purpose the thermal diffusivity  $D_{th,w}$  and the thermal conductivity  $\kappa_w$  of the wall should be known. If the thermal conductivity  $\kappa_s$  of the sample is also known, the true thermal diffusivity  $D_{th,s}$  can be directly evaluated from the apparent thermal diffusivity  $D_{th,app}$ . For small ratios of grating period to sample thickness  $d/l_s < 0.5$ , as employed for typical experiments, the dependence of  $D_{th,app}$  on  $\kappa_s$  is weak. Any reasonable assumption about  $\kappa_s$  will lead to a good approximation for the true  $D_{th,s}$ . In case of unknown  $\kappa_s$ , one single experiment is not sufficient to evaluate the thermal diffusivity of the sample  $D_{th,s}$ . From two experiments at different grating periods  $d$  or sample thicknesses  $l_s$ , however,  $D_{th,s}$  as well as  $\kappa_s$  can be determined. For a precise determination of  $\kappa_s$  at least one measurement should be performed at a large  $d/l_s$ , where  $D_{th,app}$  depends stronger on  $\kappa_s$ .

Other than the temperature signal, the concentration signal is not affected by deviations from one-dimensional heat conduction. The complicated temperature distribution in the sample  $T_q(z, t) \cos(qx)$  leads to a complicated concentration distribution  $c_q(z, t) \cos(qx)$ , where mass fluxes in  $z$ -direction are present. Experimentally observable, however, is only the integrated property  $\int_{-l_s/2}^{l_s/2} c_q(z, t) dz$ . As mass cannot flow into the cell wall, this quantity can only decay by diffusion in  $x$ -direction. Therefore, independent from sample thickness and grating period, the concentration signal decays with  $\tau = (Dq^2)^{-1}$ , where  $D$  is the collective diffusion coefficient of the sample. The ratio of the stationary amplitudes of concentration and temperature signal can be evaluated analytically (Eq. (3.27)). It is proportional to the Soret coefficient  $S_T$  and independent from sample thickness and grating period. Thus, neither the time constant of the concentration signal nor its normalized amplitude depend on grating period or sample thickness. In transient grating experiments the walls significantly influence heat transport, but they have no effect on the measurement of mass transport.

## Chapter 4

# Optical Diffusion Cell with Periodic Resistive Heating

We have developed a new instrument for the measurement of heat, mass and thermal diffusion in liquids [43]. In the following the design of the sample cell with two interdigitating arrays for heterodyne readout will be described and the mechanism for signal generation will be analyzed in detail. From the time dependent diffraction efficiency the thermal diffusivity, the thermal and the Fickian diffusion coefficient and the Soret coefficient can be obtained. Similar to holographic grating experiments with very thin sample cells (cf. Chap. 3), heat penetration into the wall plays a major role and requires a detailed treatment. The suitability of the approach is demonstrated with measurements on reference systems. Stability issues of this prototype instrument will also be discussed.

### 4.1 Experimental Setup and Principles of Measurement

#### 4.1.1 Setup

The basic idea of the new method is explained in Fig. 4.1. We have built cuvettes that have a grating of conducting, transparent strips of indium tin oxide (ITO) on the inner side of one of their windows. The distance between two strips is  $d' = 20 \mu\text{m}$  but only every other strip is current-carrying. By flipping the switch the other set of strips is connected to the voltage source (1...10 V). The distance between two current-carrying strips as well as the grating period of the resulting temperature grating is  $d = 2d' = 2\pi/q = 40 \mu\text{m}$ . In this way the diffraction of the ITO-grating of period  $d'$  can be easily separated from the diffraction of the temperature grating. Having different grating periods the two gratings diffract at different angles (see Fig. 4.5). Of course another possibility to separate the diffraction of the two gratings would be to switch on and off only every other strip and do not care about the other set of strips. However, if the electric current flows alternately through the two sets of strips, only the periodic part of the temperature field is switched, whereas the overall heating stays nearly constant. This is a major advantage as will become clear later (Sec. 4.3.2). Furthermore, this technique allows to double the signal amplitude.

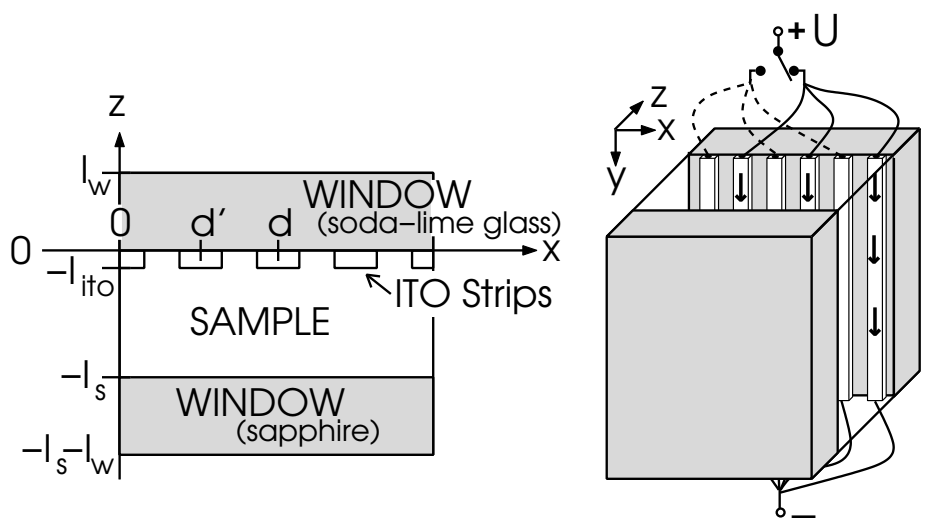


**Figure 4.1:** Sketch of the cell: A grating of transparent conducting strips (ITO) is on the inner side of one of the windows. When heated by an electric current  $I$  a temperature grating will build up in the sample. Only every other strip is current-carrying. This allows to separate the diffraction of the ITO-grating from the diffraction of the temperature grating.

Fig. 4.2 shows the design in detail. All structures have been made by photolithographic processes (see Sec. 4.1.2). First an ITO-pattern resembling interdigital electrodes has been sputtered onto the window. Each of the 150 ITO-strips is 3 mm long,  $10\ \mu\text{m}$  wide,  $l_{ito} = 175\ \text{nm}$  high and has an electrical resistance of about  $15\ \text{k}\Omega$ . Two sets of strips exist: set 1 and set 2. Set 1 is in electrical contact with the electrode 1, set 2 with the electrode 2 (see Fig. 4.2(a)). In a second step two layers of polyimide, an insulating and very resistant polymer, have been applied on the substrate. These layers are 5 to  $10\ \mu\text{m}$  thick and have holes of  $10\ \mu\text{m} \times 50\ \mu\text{m}$ . Fig. 4.2(b) shows their shape and position relative to the ITO-structure. Finally two 200 nm thick layers of chromium have been vapor deposited onto the insulating layers, as can be seen in Fig. 4.2(c). As illustrated in Fig. 4.3 the holes in the insulating layers and the chromium electrodes on top of them serve to contact independently all strips of set 1 and all strips of set 2. In that way the strips of one of the sets can be current-carrying, whereas no electric current passes through the other set of strips. The lateral dimensions of the ITO-electrodes are given in Fig. 4.2(a).

To switch between strips of set 1 and strips of set 2 a fast electronic switch ( $\tau_{\text{switch}} \approx 1\ \mu\text{s}$ ) was built, which can be controlled by a PC. The window with the strips is of soda lime glass, the opposite window is of sapphire (high thermal conductivity  $40\ \text{W}/(\text{mK})$ ) to keep the overall sample heating small. The thickness of the windows is  $l_w = 1\ \text{mm}$ . The soda lime glass window has lateral dimensions  $2\ \text{mm} \times 2\ \text{mm}$ , the sapphire window  $16\ \text{mm} \times 10\ \text{mm}$ . The two windows with a spacer of  $l_s \approx 100\ \mu\text{m}$  in between have been sealed with a solvent-resistant glue (Torr Seal, Varian) to form a cuvette. Two boreholes in the sapphire window allow filling of the cuvette and can be closed by Teflon plugs. Four wires with banana plugs

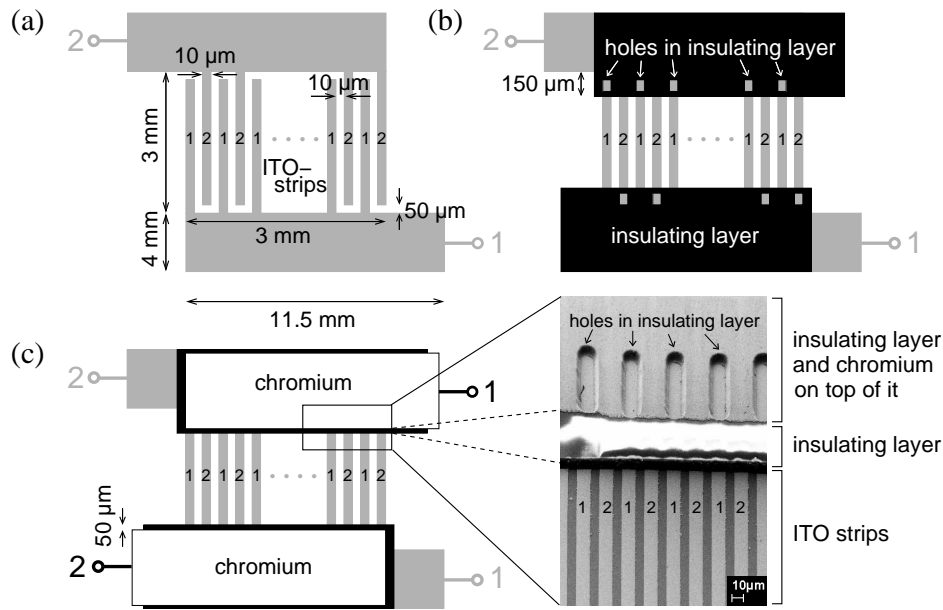


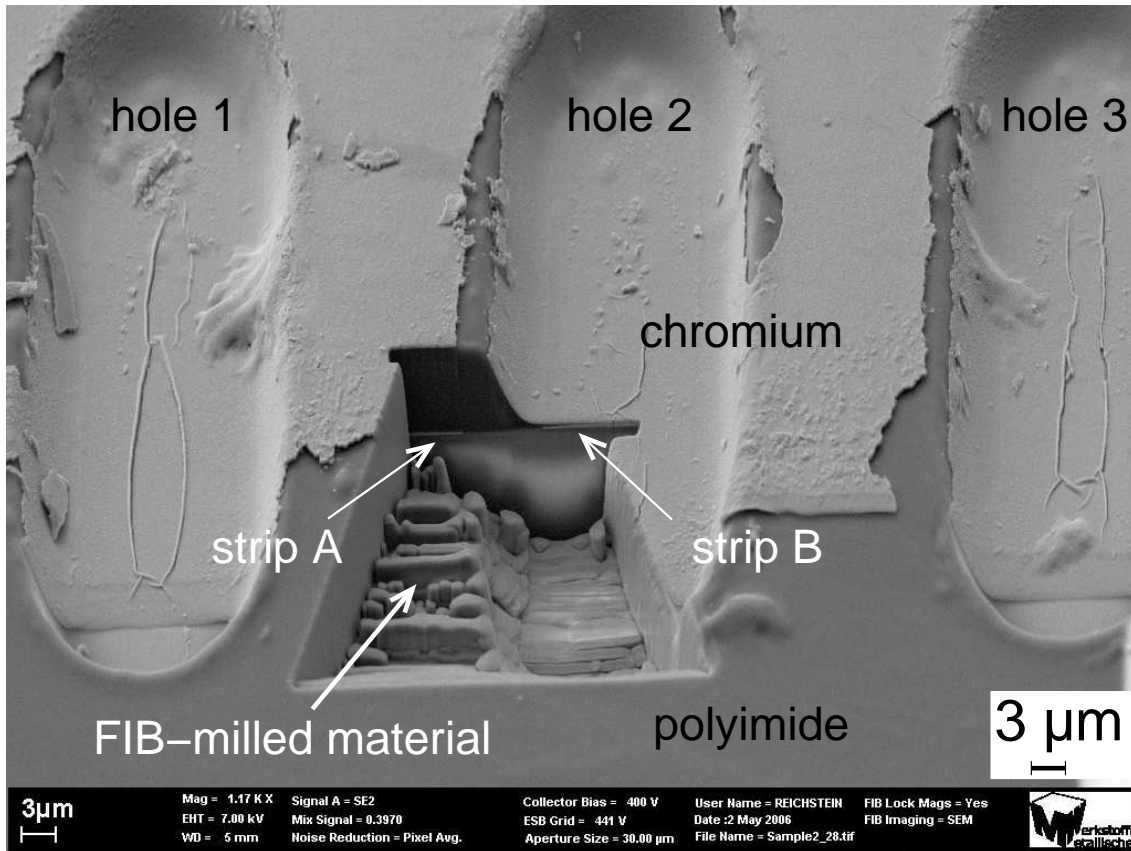
**Figure 4.2:** Multilayer-structure of ITO-strips, insulating layers and chromium layers on the cuvette window. Two sets of strips exist that can be alternately connected to the voltage source. The picture to the right below is a scanning electron microscope micrograph (SEM).

have been attached to the four electrodes by conductive lacquer (see Fig. 4.4).

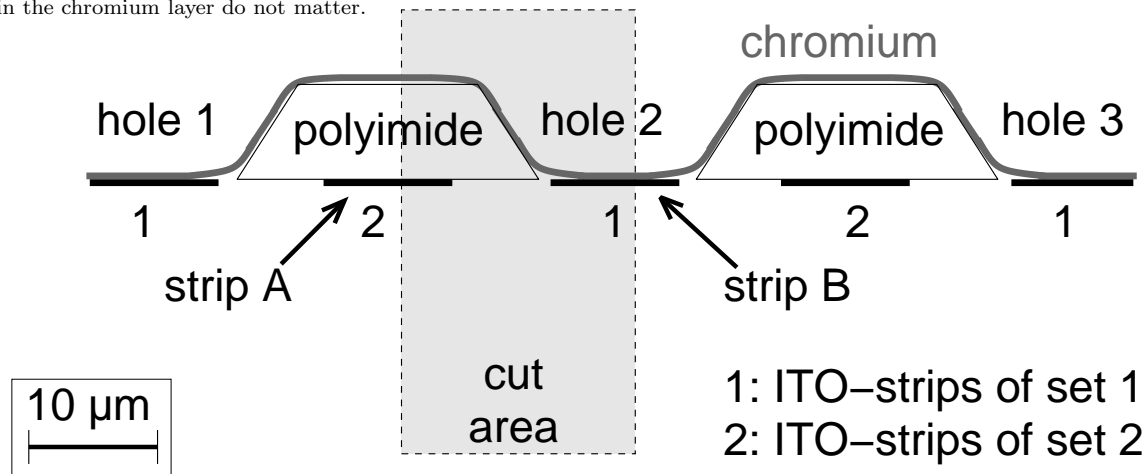
The experimental setup is shown in Fig. 4.5. Readout of the refractive index gratings is done similar to laser-induced transient grating experiments. A HeNe laser (633 nm) is used as reading laser and a heterodyne detection scheme (see Sec. 4.1.3) is employed. The coherent superposition of the diffracted and the reference wave is detected with a single-mode optical fiber connected to a photomultiplier tube. The phase between diffracted and reference wave is adjusted and stabilized by an active phase tracking mechanism as described in Ref. [52]. Typically, experiments have been averaged over 1000–2000 cycles. The contrast factors  $(\partial n/\partial c)_{T,p}$  and  $(\partial n/\partial T)_{c,p}$  can be determined with an Abbe refractometer and interferometrically as described in Ref. [111].

#### 4.1.2 Fabrication of Multilayer Structures

The ITO and the chromium structures have been patterned by lift of processes using an image reversal resist (TI 35ES MicroChemicals). Cleaning of the substrates, spin coating, soft baking, reversal baking, developing and stripping was performed according to the data sheet of the TI 35ES. A custom-built photo mask with anti reflective chrome on soda lime glass has been purchased from Photronics. The coated substrates have been exposed in a EVG 620 (EV Group) mask aligner. AZ 400 K (MicroChemicals) was used for developing. The ITO (ITO-target, Balzers, no reactive sputtering) was RF-sputtered using a Balzers BAS 450, operating at a sputtering power of 400 W and a sputtering rate of 7 nm/min in an



(a) Scanning electron microscope (SEM) micrograph visualizing the layer composition: A trapezium has been cut into the multilayer structure with a focused ion beam (FIB, ZEISS 1540 XB). For explanation compare to Fig. 4.3(b). It should be noted that the quality of the vapor deposited chromium layers was not always as bad as here (see Fig. 4.2 right below and Figs. 4.8(a,b)). Anyway, as long as the chromium layer makes contact with the ITO electrode, holes in the chromium layer do not matter.



(b) Schematic sketch of the multilayer structure explaining the SEM picture above (Fig. 4.3(a)).

**Figure 4.3:** Sectional view of the multilayer structure illustrating the function of the holes in the insulating layer



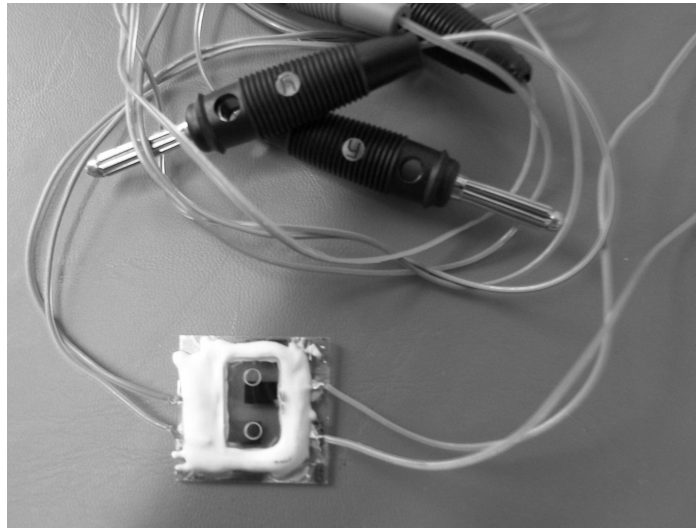


**Figure 4.4:** Photograph of the cuvette: the two windows with a spacer in between have been sealed to form a cuvette. The ITO strips are on the upper side of the lower window. The window above has two boreholes to allow filling of the cuvette. Four wires with banana plugs are attached to the four electrodes by conductive lacquer.

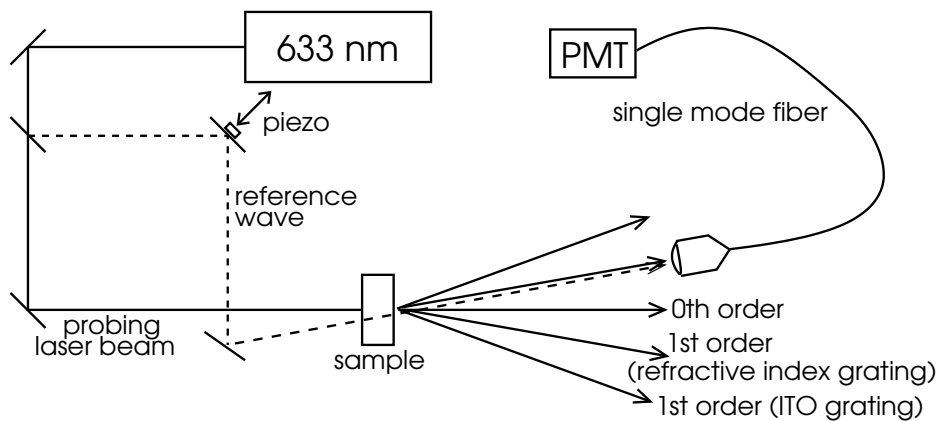


**Figure 4.5:** Sketch of experimental setup. A HeNe laser (633nm) is used for readout of the refractive index grating in a heterodyne detection scheme

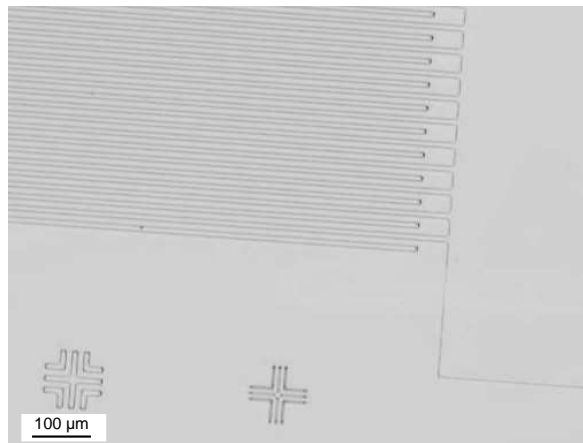


**Figure 4.6:** Light microscope picture of structured photo resist TI 35ES just before ITO-sputtering: Each strip is  $10\ \mu\text{m}$  wide. Two alignment marks can be seen.

argon atmosphere of pressure  $2 \cdot 10^{-3}$  mbar. A Balzers Ba 510 coating unit with a residual pressure of  $10^{-5}$  mbar was used for electron beam physical vapor deposition of chromium (Cr granulate,  $> 99.9\%$ , umicore) at a rate of  $3\ \text{\AA}/\text{s}$ . Finally the resist was stripped with technical acetone. Fig. 4.6 shows the structured TI 35ES resist after exposure and development ready for ITO-sputtering.

The insulating layers have also been structured by a photolithographic process. The photosensitive polyimide (HD 4000, HD MicroSystems) was processed according to the data sheet. Again the EVG 620 mask aligner was used for exposure. A negative exposure mask was prepared from a positive mask (Photronics, see above) in the same manner as the chromium layers except for using TI 35ES this time not as a negative, but as a positive resist. The initial idea was to use  $\text{SiO}_2$  or  $\text{Al}_2\text{O}_3$  for the insulating layers. In this case a positive exposure mask would have been needed and was therefore bought. However, these materials resulted in very holey layers when sputtered and did not serve as insulators. The exposed polyimide was developed with cyclopentanone (Fluka,  $> 99\%$ ) and rinsed with a symmetric mixture of cyclohexanone and  $\gamma$ -butyrolactone (both Fluka,  $> 99\%$  and  $> 98\%$ ). It was never possible to develop the polyimide completely, but the residues were always thinner than  $\approx 150\ \text{nm}$  and could be removed by  $\text{O}_2$  plasma edging in an Anatech SP 100 plasma system (Anatech Ltd.). The applied plasma power was 80 W, the pressure was approximately 0.5 Torr and the exposure time 15 min.

Many problems occurred during the fabrication of the multilayer structures. Initially the mask aligner was not correctly set up and wedge error compensation did not work. Therefore the substrate on the chuck of the mask aligner was tilted in relation to the mask (see Fig. 4.7(a)). This leads to a very non-uniform UV-intensity distribution on the substrate. The left side of the substrate and the mask are in contact as desired. The gap between substrate and mask to the right leads there to a smaller exposure dose due to reflection

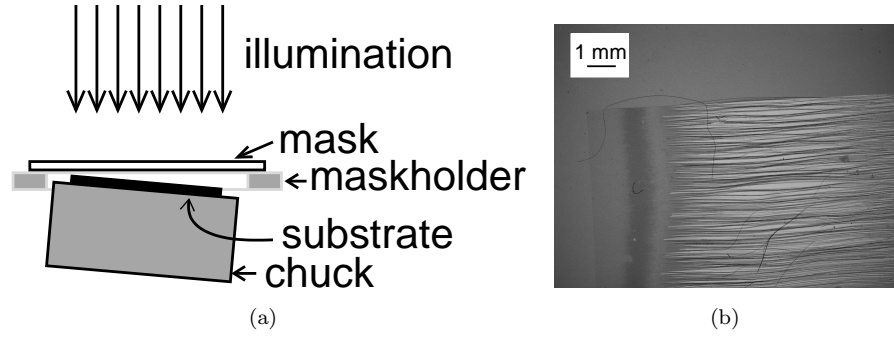


**Figure 4.7:** Mask aligner with wedge error: (a): Sketch of mask aligner: The substrate on the chuck is tilted in relation to the mask, (b): Resist after exposure and development: The exposure dose on the right side was too small and developing leads to peeling of resist structures. Each strip is  $10\ \mu\text{m}$  wide. Moreover interference fringes can be seen.

losses. Therefore an adequate developing time could not be found. Whereas the resist in Fig. 4.7(b) is not completely developed on the left hand side, it is overdeveloped on the right hand side. Moreover interference phenomena at a thin air wedge lead to a modulated intensity distribution known as Newton rings. This modulates the thickness of the developed resist irrespective of the microstructures. The resulting interference fringes can also be seen in Fig. 4.7(b). The structures in Fig. 4.7(b) is a  $2\ \text{cm} \times 2\ \text{cm}$  array of  $10\ \mu\text{m}$  wide strips with  $20\ \mu\text{m}$  distance, which has been initially used to find the correct process parameters. Later always the pattern explained in Fig. 4.2 and shown in Fig. 4.6 was used for the ITO-strips. Further problems with fabrication of the multilayer structures are listed in Fig. 4.8.

### 4.1.3 Heterodyne Detection

A distinction between homodyne and heterodyne detection must be made in optical scattering and diffraction experiments. Without careful treatment of the background, there is always the risk of mixed or unknown coherence conditions and the determined diffusion coefficients may be off by a factor of two. According to Ref. [52] heterodyne detection is superior to homodyne detection in situations as considered here.

The intensity  $I$  as seen by the detector contains both homodyne and heterodyne contributions

$$\begin{aligned}
 I &= |E_s + E_{\text{ref}} e^{i\phi} + E_c e^{i\theta}|^2 + E_{\text{inc}}^2 \\
 &= E_s^2 + E_{\text{ref}}^2 + E_c^2 + E_{\text{inc}}^2 \\
 &\quad + 2E_s E_{\text{ref}} \cos \phi + 2E_s E_c \cos \theta + 2E_{\text{ref}} E_c \cos(\theta - \phi).
 \end{aligned} \tag{4.1}$$

$E_s$  is the electric field amplitude of the diffracted beam, also called signal.  $E_c > 0$  is the coherent electric field amplitude of the background intensity. It originates from unavoidable scratches or dust particles on the cuvette windows.  $E_{\text{ref}} > 0$  is the electric field amplitude

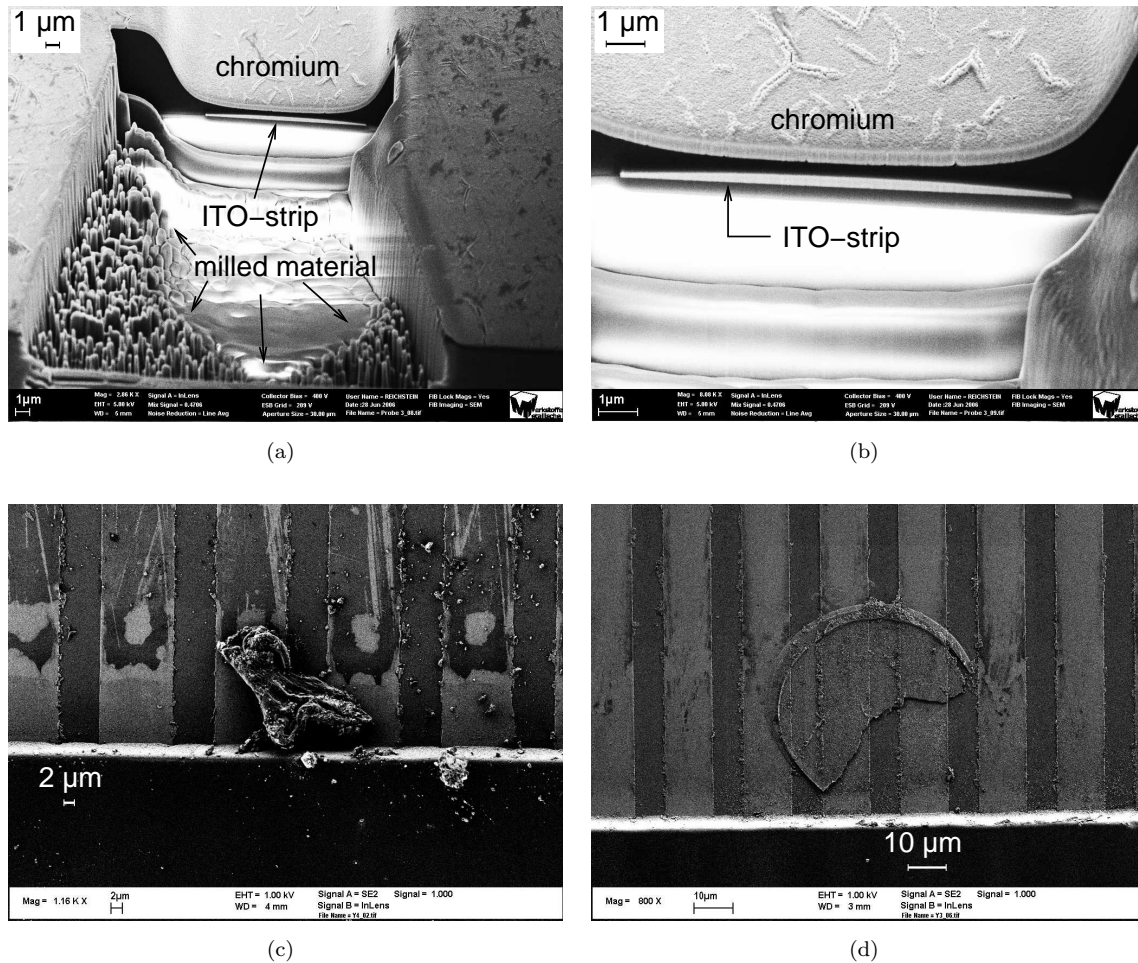


**Figure 4.8:** Some problems encountered during fabrication of multilayer structures:

(a): Since the polyimide is not completely developed, the chromium electrode is not in contact with the ITO-strip. This multilayer structure could not be used for experiments. As in Fig. 4.3 a trapezium has been cut into the multilayer structure with a focused ion beam.

(b): Zoom of (a)

(c): Because of the problem described in (a,b) the remaining polyimide was removed by plasma edging. Here plasma edging was over done and the ITO strips were burnt. This multilayer structure could not be used for experiments, as the resistance of the burnt ITO-strips is too high.

(d): Sometimes stripping of the ITO-sputtered substrates was difficult.  $\mu\text{m}$ -sized particles of ITO, which are not part of the desired structure, stuck to the substrate and electrically contacted ITO-strips of set 1 and set 2. In principle, the multilayer structure can still be used for experiments, as merely the amplitude  $T_q$  of the resulting temperature grating is reduced. By reducing  $T_q$  at constant total heating, however, unwanted transient heating effects become visible in the detected heterodyne diffraction efficiency at the expense of the real signal (see Sec. 4.3.2). Therefore these defects should be avoided.

All pictures are SEMs.

of the reference beam.  $E_{\text{inc}}$  is the incoherent electric field amplitude of the total background intensity.  $\phi$  is the phase shift between the signal  $E_s$  and the reference  $E_{\text{ref}}$ ,  $\theta$  is the phase shift between the signal  $E_s$  and the coherent background  $E_c$ . The phase of  $E_s$  is arbitrarily chosen to zero. The phase of the reference  $\phi$  may be adjusted by means of a piezo mounted mirror. Other than  $\phi$  the phase  $\theta$  cannot be properly controlled, as it depends on a randomly selected local oscillator on the cuvette window. Even though it may be changed by readjusting some mirrors, it cannot be set to an arbitrary value. For convenience the proportionality factor between  $E^2$  and  $I$  is set to unity.  $S_{\text{hom}} = E_s^2$  is the homodyne and  $S_{\text{het}} = 2E_s E_{\text{ref}} + 2E_s E_c \cos \theta$  is the heterodyne signal. The total background  $I_b^\phi = E_{\text{ref}}^2 + E_c^2 + E_{\text{inc}}^2 + 2E_{\text{ref}} E_c \cos(\theta - \phi)$  depends on  $\phi$ .

Part of the heterodyne signal  $S'_{\text{het}} = 2E_s E_{\text{ref}}$  can be separated if two measurements with  $\phi = 0$  and  $\phi = \pi$ ,

$$I_{\phi=0} = E_c^2 \sin^2 \theta + E_{\text{inc}}^2 + (E_s + E_c \cos \theta + E_{\text{ref}})^2 \quad (4.2)$$

$$I_{\phi=\pi} = E_c^2 \sin^2 \theta + E_{\text{inc}}^2 + (E_s + E_c \cos \theta - E_{\text{ref}})^2, \quad (4.3)$$

are combined according to

$$(I_{\phi=0} - I_{\phi=\pi})/2 = 2E_s E_{\text{ref}} + I'_{b,\phi=0} = S'_{\text{het}} + I'_{b,\phi=0}, \quad (4.4)$$

where  $I'_b = 2E_{\text{ref}} E_c \cos(\theta - \phi)$ . The heterodyne signal  $S'_{\text{het}}$  as determined from Eq. (4.4) is robust against non ideal phase jumps  $\pi + \delta$  or against a non ideal adjustment of the phase shift  $\phi = \phi_0 \neq 0$ , since

$$(I_{\phi=\phi_0} - I_{\phi=\phi_0+\pi+\delta})/2 = S'_{\text{het}}(\cos \phi_0 + \cos(\phi_0 + \delta))/2 + (I'_{b,\phi=\phi_0} + I'_{b,\phi=\phi_0+\delta})/2. \quad (4.5)$$

Merely the amplitude of  $S'_{\text{het}}$  is reduced and the background value changes, but the expression  $I_{\phi=\phi_0} - I_{\phi=\phi_0+\pi+\delta}$  remains free of homodyne contributions.

In Sec. 4.2 we will solve the differential equations always for switching on processes: No current has been flowing for  $t < 0$ , at  $t = 0$  the voltage is switched on and for  $t > 0$  the strips of set 1 are current-carrying. The corresponding electric field amplitude of the diffracted beam is given by

$$E_s^{\text{off} \rightarrow \text{on}}(t) = E_s^{0, \text{set } 1} \alpha(t), \quad (4.6)$$

where  $E_s^{0, \text{set } 1}$  is the signal produced by strips of set 1 in the stationary state and

$$\alpha(t) = \left( \int_0^t g(t') dt' \right) \left( \int_0^\infty g(t') dt' \right)^{-1}, \quad (4.7)$$

with  $g(t)$  being the linear response function. The experiments, however, have been actually conducted in a slightly different way. The voltage was not switched on and off, but was

switched between strips of set 1 and strips of set 2.  $E_s$  evolves according to

$$E_s^{i \rightarrow j}(t) = E_s^{0, \text{set } i}(1 - \alpha(t)) + E_s^{0, \text{set } j}\alpha(t), \quad (4.8)$$

if the voltage is switched over from strips of set  $i$  to strips of set  $j$  at  $t = 0$ . There is always a slight asymmetry and strips of set 1 do not produce the same signal as strips of set 2. Only for a perfectly symmetric cuvette both sets of strips would generate the same signal with  $E_s^{0, \text{set } 1} = -E_s^{0, \text{set } 2}$ . To be able to compare the experimental data (switching set 1  $\leftrightarrow$  set 2) to the theoretical results of Sec. 4.2 (switching off  $\rightarrow$  on), the function  $\alpha(t)$  has been extracted from the measured intensities  $I_{\phi=0}^{1 \rightarrow 2}$ ,  $I_{\phi=\pi}^{1 \rightarrow 2}$ ,  $I_{\phi=0}^{2 \rightarrow 1}$  and  $I_{\phi=\pi}^{2 \rightarrow 1}$  via

$$\alpha(t) = [y(t)/y(t \rightarrow \infty) + 1]/2, \quad (4.9)$$

where the purely heterodyne  $y(t)$  has to be evaluated according to

$$y(t) = (I_{\phi=0}^{1 \rightarrow 2} - I_{\phi=\pi}^{1 \rightarrow 2} - I_{\phi=0}^{2 \rightarrow 1} + I_{\phi=\pi}^{2 \rightarrow 1})/2 = S_{\text{het}}^{1 \rightarrow 2} - S_{\text{het}}^{2 \rightarrow 1}. \quad (4.10)$$

Remember that the motivation for this apparently complicated procedure is to keep the average heat insertion into the sample time invariant in order to avoid transient heating effects.

Of course all the above considerations implied  $E_{\text{ref}}$ ,  $E_c$  and  $E_{\text{inc}}$  to be constant. If they drift slowly in time,  $y(t)$  contains contributions of unknown time dependence and cannot be used to calculate  $\alpha(t)$ . Unfortunately, we were not able to reduce all (thermal) drift effects to zero. A slight drift of  $E_{\text{ref}}$  could be directly observed by blocking the probing beam and otherwise performing the experiment as usual (see Sec. 4.3.2). Nevertheless, for lack of alternatives, all data were analyzed according to Eqs. (4.9, 4.10) knowingly accepting some artefacts.

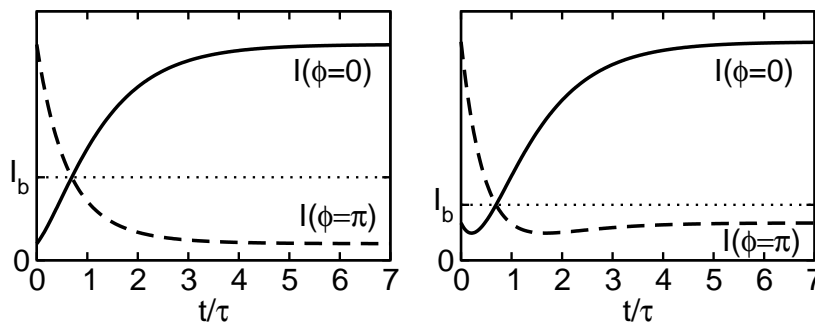


**Figure 4.9:** Possible signals  $I_{\phi=0}$  and  $I_{\phi=\pi}$  in a heterodyne detection scheme, where the reference is provided by a local oscillator on the cuvette window (laser-induced grating experiments): left:  $E_c > E_s^0$ , right  $E_c < E_s^0$

Despite of all similarities with laser-induced grating experiments we apply slightly different heterodyne detection schemes depending on whether the temperature grating is generated

optically or electrically. In laser induced grating experiments the reference wave may be provided by scratches on the cuvette window and the phase jump of  $\pi$  can be realized by shifting the phase of the diffracted beam. No extra reference beam is needed [52]. The result (1) in Ref. [52] is recovered from Eq. (4.1), if  $E_c$  in Eq. (4.1), is set to zero and  $E_{\text{ref}}$  is identified with the electric field amplitude generated by the local oscillator on the window ( $E_{\text{ref}} \rightarrow E_c$ ). Then, if we assume the following time dependence for  $E_s$

$$E_s = E_s^0(1 - 2e^{-t/\tau}), \quad (4.11)$$

two scenarios  $E_c > E_s^0$  and  $E_c < E_s^0$  are possible. The corresponding intensities  $I_{\phi=0}$  and  $I_{\phi=\pi}$  are shown in Fig. 4.9.

With the new technique the phase  $\theta$  between the diffracted beam and the local oscillator on the cuvette window cannot be controlled. A reference wave has to be provided by splitting off part of the readout beam, which is then aligned parallel to the diffracted signal beam (see Fig. 4.5). The phase  $\phi$  of this reference is controlled by means of a piezo mounted mirror. For this detection scheme and with  $E_s$  from Eq. (4.11) many possibilities for the signals  $I_{\phi=0}$  and  $I_{\phi=\pi}$  can be observed, depending on the values of  $E_s^0$ ,  $E_c$ ,  $E_{\text{ref}}$  and  $\theta$  (Fig. 4.10). Situations as  $E_c^+ < -E_s^0$  or  $E_c^- > E_s^0$  lead according to Eq. (4.4) to a small  $S_{\text{het}}$  and should be avoided by adequate adjustment.

#### 4.1.4 Sample Preparation

The pure substances toluene, dodecane, tetralin and isobutylbenzene have been obtained from Merck, Aldrich, Acros and Aldrich. The purities of the chemicals are in excess of 98%. Sample preparation is done in the same way as for light scattering. Other than for laser induced grating experiments no dye has to be added to the sample. For the experiments with binary mixtures, the solvents were mixed with equal weights. The liquids were filled into the thoroughly cleaned and dried cuvette. The cuvette was sealed with Teflon plugs.

## 4.2 Heat and Mass Diffusion Analysis

We use a similar model for the description of the experiment as in Sec. 3.1. However, the source term  $\dot{Q}$  in the heat equation (Eq. (1.2))

$$\rho c_p \partial_t T = \vec{\nabla} \cdot [\kappa \vec{\nabla} T] + \dot{Q},$$

is now given by the electrical power density. In case of a binary liquid also the extended diffusion equation (Eq. (1.3)) is needed, which describes the spatial and temporal evolution

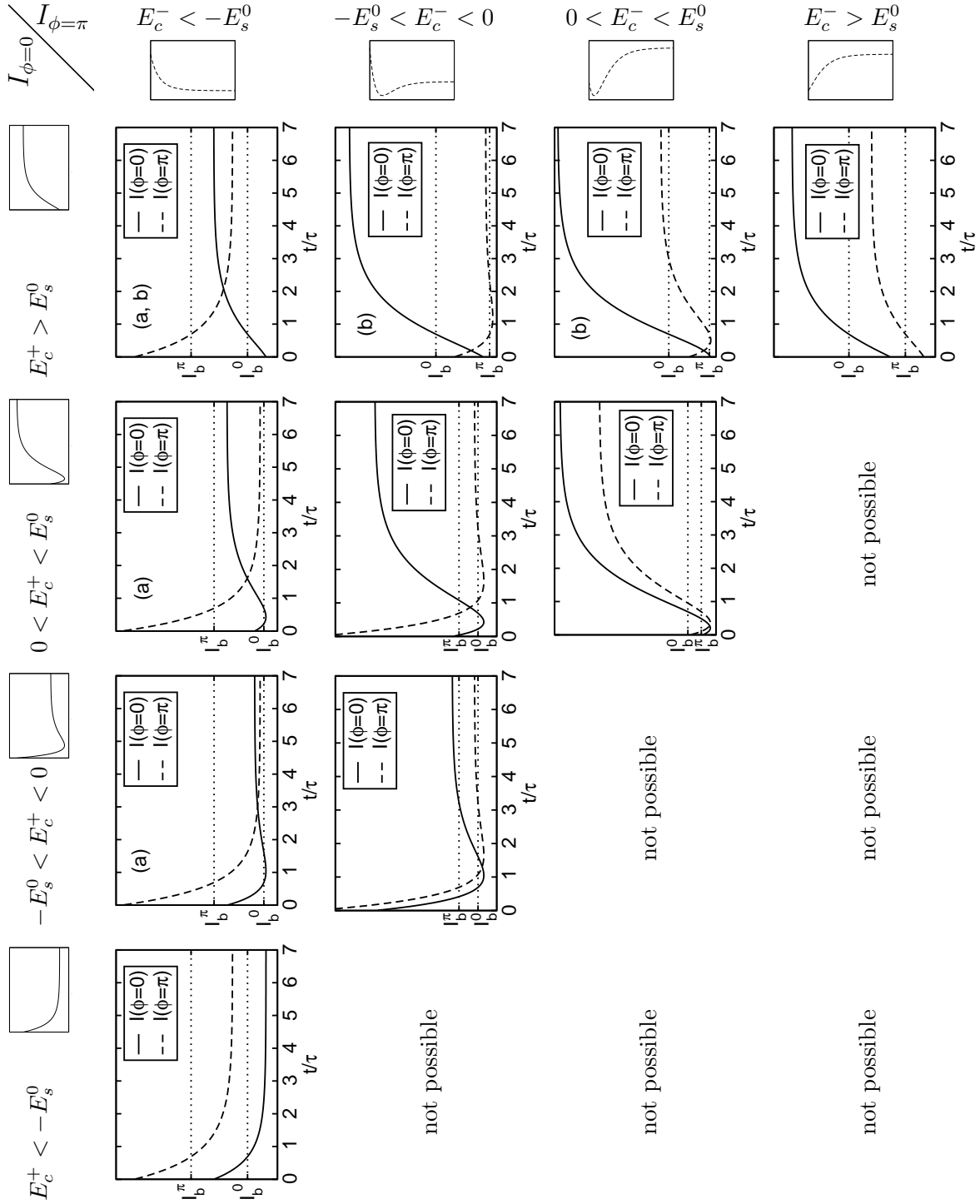


**Figure 4.10:** Possible signals  $I_{\phi=0}$  and  $I_{\phi=\pi}$  in a heterodyne detection scheme, where an extra reference beam is used (new technique).  $E_c^+$  and  $E_c^-$  are defined according to  $E_c^+ = E_c \cos \theta + E_{\text{ref}}$  and  $E_c^- = E_c \cos \theta - E_{\text{ref}}$ . The first column (first row) shows the four possible curve shapes for  $I_{\phi=0}$  ( $I_{\phi=\pi}$ ) and the corresponding conditions for  $E_c^+$  and  $E_s^0$  ( $E_c^-$  and  $E_s^0$ ). They can be combined in ten different ways resulting in ten different scenarios.

(a) also possible:  $I_{\phi=0} < I_{\phi=\pi}$  for all  $t$ , (b) also possible:  $I_{\phi=0} > I_{\phi=\pi}$  for all  $t$



of the concentration  $c$  of component 1 (weight fractions)

$$\partial_t c = \vec{\nabla} \cdot [D \vec{\nabla} c + c(1-c) D_T \vec{\nabla} T].$$

In the following we will take the thermal conductivity  $\kappa$ , the mass diffusion coefficient  $D$ , the thermal coefficient  $D_T$ , and  $c(1-c) \approx c_0(1-c_0)$  as constant, which is reasonable for small concentration and temperature changes.

### 4.2.1 Evolution Equations

Fig. 4.1 shows the coordinate system for analysis. The region  $-l_s < z < 0$  is of sample material, which has thermal conductivity  $\kappa_s$ , density  $\rho_s$ , heat capacity  $c_{p,s}$  and thermal diffusivity  $D_{th,s} = \kappa_s(\rho_s c_{p,s})^{-1}$ . The region  $0 < z < l_w$  is of soda lime glass ( $\kappa_w, \rho_w, c_{p,w}, D_{th,w} = \kappa_w(\rho_w c_{p,w})^{-1}$ ). For simplicity, we suppose the sample to be infinitely extended in  $x$ -direction and to be heated by an infinite number of infinitely thin ( $l_{ito} \rightarrow 0$ ) ITO-strips. This is a good approximation, if the grating period  $d$  is much smaller than the  $x$ -dimension of the heated area  $L_x$  but much larger than the thickness of the ITO-strips  $l_{ito}$  and if, additionally,  $l_{ito}$  is much smaller than the sample thickness  $l_s$  and the window thickness  $l_w$ , respectively. In our case, we have  $L_x = 3$  mm,  $d = 40$   $\mu$ m,  $l_{ito} = 175$  nm,  $l_s = 100$   $\mu$ m, and  $l_w = 1$  mm. As the thermal conductivity of sapphire is very high (40 W/(mK)), the temperature at  $z = -l_s$  is, by good approximation, given by the temperature of the thermal bath. There is no  $y$  dependence.

We expand the electrical power density per unit area  $S(x) = \dot{Q}(x) l_{ito}$  and the temperature and concentration fields in a Fourier series with  $q = 2\pi/d$ .

$$S(x) = \begin{cases} 4S_0 : & kd - \frac{d}{8} \leq x \leq kd + \frac{d}{8}, & k = 0, 1, 2, \dots \\ 0 & : \text{ else} \end{cases} \quad (4.12)$$

$$= S_0 \left[ 1 + 2 \sum_{k=1}^{\infty} \frac{\sin(\pi k/4)}{\pi k/4} \cos kqx \right] \quad (4.13)$$

$$= S_0 + S_q \cos qx + S_{2q} \cos 2qx + \dots \quad (4.14)$$

$$T(x, z, t) = T_0(z, t) + T_q(z, t) \cos qx + T_{2q}(z, t) \cos 2qx + \dots \quad (4.15)$$

$$c(x, z, t) = c_0(z, t) + c_q(z, t) \cos qx + c_{2q}(z, t) \cos 2qx + \dots \quad (4.16)$$

In our experiment we detect first order diffraction (see Fig. 4.5) and therefore only the first Fourier coefficients  $T_q$  and  $c_q$  are experimentally relevant.

Considering all approximations mentioned above,  $T_q$  and  $c_q$  initially being zero

$$T_q(z, t = 0) = c_q(z, t = 0) = 0 \quad (4.17)$$

evolve according to

$$\partial_t T_q = D_{th,s} (-q^2 + \partial_z^2) T_q \quad -l_s \leq z \leq 0 \quad (4.18)$$

$$\partial_t T_q = D_{th,w} (-q^2 + \partial_z^2) T_q \quad 0 \leq z \leq l_w \quad (4.19)$$

and

$$\partial_t c_q = D(-q^2 + \partial_z^2) c_q + D_T c_0 (1 - c_0) (-q^2 + \partial_z^2) T_q \quad -l_s \leq z \leq 0. \quad (4.20)$$

The boundary conditions

$$T_q(z = l_w) = T_q(z = -l_s) = 0 \quad (4.21)$$

$$D\partial_z c_q|_{z=z_{sb}} = -D_T c_0 (1 - c_0) \partial_z T_q|_{z=z_{sb}} \quad \text{where } z_{sb} = 0^-, -l_s \quad (4.22)$$

and the matching conditions

$$T_q(z = 0^+) = T_q(z = 0^-) \quad (4.23)$$

$$\kappa_w \partial_z T_q|_{z=0^+} + S_q = \kappa_s \partial_z T_q|_{z=0^-} \quad (4.24)$$

with  $S_q = \frac{4\sqrt{2}}{\pi} S_0$  follow from continuity of temperature and heat flux and from vanishing mass flux into the windows.

### 4.2.2 Refractive Index Grating and Heterodyne Diffraction Efficiency

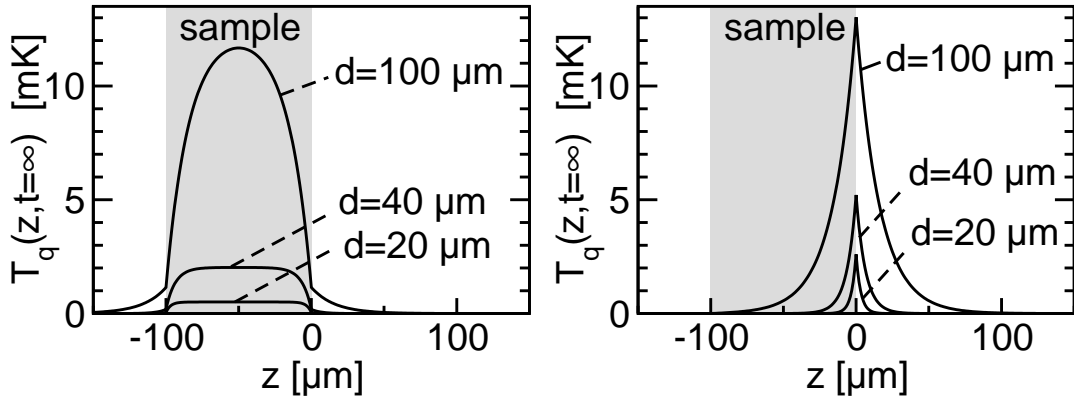
Both the temperature grating and the concentration grating give rise to a refractive index grating

$$n(x, z, t) = n_0(z, t) + n_q(z, t) \cos qx + n_{2q}(z, t) \cos 2qx + \dots, \quad (4.25)$$

which acts as an optical phase grating on a probing laser beam.  $n(x, z, t)$  is the refractive index at the readout wavelength. For experiments conducted within the weak modulation depth limit the first order heterodyne diffraction efficiency  $\zeta_{het}$  is simply proportional to the refractive index modulation depth  $n_q$  [29] or, in case of  $z$ -dependent  $n_q$ , to the integral over  $n_q$  along the  $z$ -direction:

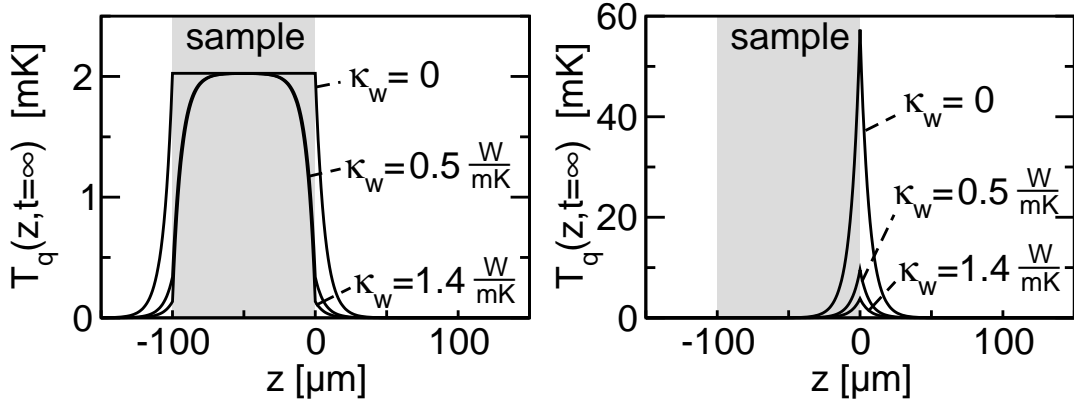
$$\begin{aligned} \zeta_{het}(t) &= \zeta_{het,T,s}(t) + \zeta_{het,c}(t) + \zeta_{het,T,w}(t) \\ &\propto \int_{-l_s}^0 \left( \frac{\partial n_s}{\partial T} \right)_{c,p} T_q(z, t) dz + \int_{-l_s}^0 \left( \frac{\partial n_s}{\partial c} \right)_{T,p} c_q(z, t) dz + \int_0^{l_w} \left( \frac{\partial n_w}{\partial T} \right)_p T_q(z, t) dz \end{aligned} \quad (4.26)$$

Not only the temperature and concentration gratings within the sample with respective contrast factors  $(\partial n_s / \partial T)_{c,p}$  and  $(\partial n_s / \partial c)_{T,p}$ , but also the temperature grating in the window with contrast factor  $(\partial n_w / \partial T)_p$  contribute to the refractive index grating and, thus, to the



(a) optical heating:  
influence of grating period  $d$   
for  $\kappa_s/\kappa_w = 0.1$  and  $\alpha I_0/\kappa_w = 5 \mu\text{K}/\mu\text{m}^2$

(b) electrical heating:  
influence of grating period  $d$   
for  $\kappa_s/\kappa_w = 0.1$  and  $S_0/\kappa_w = 500 \mu\text{K}/\mu\text{m}$



(c) optical heating:  
influence of heat conductivity of window  $\kappa_w$   
for  $\kappa_s = 0.1 \frac{\text{W}}{\text{mK}}$ ,  $d = 40 \mu\text{m}$  and  $\alpha I_0 = 5 \cdot 10^6 \frac{\text{W}}{\text{m}^2}$

(d) electrical heating:  
influence of heat conductivity of window  $\kappa_w$   
for  $\kappa_s = 0.1 \frac{\text{W}}{\text{mK}}$ ,  $d = 40 \mu\text{m}$  and  $S_0 = 500 \frac{\text{W}}{\text{m}^2}$

**Figure 4.11:** Stationary amplitude of the temperature grating for  $l_s = 100 \mu\text{m}$  in the case of optical and electrical heating, if the same power is absorbed in both experiments ( $S_0 = \frac{\pi}{4\sqrt{2}} S_q = \alpha I_0 l_s$ ).

heterodyne diffraction efficiency.

### 4.2.3 Stationary Solutions

The stationary solutions ( $t \rightarrow \infty$ ) can be found by solving Eqs. (4.18– 4.20) setting  $\partial_t T_q = \partial_t c_q \equiv 0$  and taking into account the boundary and matching conditions Eqs. (4.21–4.24). The solutions are especially simple for  $l_s, l_w \rightarrow \infty$ .

$$T_q(z, t \rightarrow \infty) = \frac{S_q}{q} \frac{1}{\kappa_w + \kappa_s} e^{-q|z|} \quad (4.27)$$

$$c_q(z, t \rightarrow \infty) = -S_T c_0 (1 - c_0) T_q(z, t \rightarrow \infty) \quad (z < 0) \quad (4.28)$$

Here we introduced the Soret coefficient  $S_T = D_T/D$ . The approximation of infinite window and sample thickness is valid, if the penetration depth of the temperature grating is small compared to the thicknesses of sample and window. In our experiment the penetration depth is of order  $q^{-1} = 40 \mu\text{m}/(2\pi) = 6 \mu\text{m}$  and the sample and window thicknesses are  $l_s = 100 \mu\text{m}$  and  $l_w = 1 \text{mm}$ . In Fig. 4.11 the stationary amplitude of the temperature grating  $T_q(z, t \rightarrow \infty)$  given by Eq. (4.27) is compared to the amplitude resulting from optical heating in a laser induced grating experiment. The latter is given by Eqs. (3.23, 3.24), if  $t = 0$  and  $z$  are replaced by  $t \rightarrow \infty$  and  $z - l_s/2$ . (In Sec. 3.1 the stationary state corresponds to  $t = 0$ , since switching off experiments have been considered there. Moreover different coordinate systems (Figs. 3.1 and 4.1) are used in Sec. 3.1 and in this section.) In our new experiment the sample is heated electrically at its boundary  $z = 0$ , whereas in a laser induced grating experiment the sample is heated optically in the volume  $-l_s \leq z \leq 0$  with power density  $\dot{Q}(x) = \alpha I_0(1 + \cos(qx))$ .  $\alpha$  is the absorption coefficient of the sample and  $I_0$  the intensity of the laser that generates the holographic grating. For  $S_0 = \alpha I_0 l_s$  the same power is absorbed in both experiments and a sensible comparison between optical and electrical heating is possible.  $\frac{\alpha I_0}{\kappa_w} = 5 \mu\text{K}/\mu\text{m}^2$ ,  $l_s = 100 \mu\text{m}$ ,  $\kappa_s/\kappa_w = 0.1$  and  $d = 40 \mu\text{m}$  correspond to typical experimental conditions. In Figs. 4.11(a) and 4.11(b) the influence of the grating period  $d$  is studied for  $\kappa_s/\kappa_w = 0.1$ . In the optical experiment  $T_q(z, t \rightarrow \infty)$  depends in a complicated way on  $d$  (cf. Sec. 3.1.3). For small  $d$  the maximum value  $T_q(z = -l_s/2, t \rightarrow \infty)$  is proportional to  $d^2$ , for very large  $d$  proportional to  $d$ . Moreover  $T_q(z, t \rightarrow \infty)$  changes its shape with increasing  $d$  markedly. While it is nearly constant throughout the sample for small  $d$ , it strongly varies within the sample for larger  $d$ . In the electrical experiment, in contrast, all  $T_q(z, t)$  can be scaled to lie on a common curve by  $\tilde{z} = qz$ ,  $\tilde{T}_q = qT_q$  for any  $d = 2\pi/q$ . To study the role of the heat conductivity of the window  $\kappa_w$  the values  $\kappa_w = 0$  (perfectly insulating walls),  $\kappa_w = 0.5$  (dense flint, an optical glass with very small  $\kappa_w$ ) and  $\kappa_w = 1.4$  (fused silica, an optical glass with very large  $\kappa_w$ ) have been considered in Figs. 4.11(c) and 4.11(d). In the optical experiment the shape of  $T_q(z, t \rightarrow \infty)$  changes with  $\kappa_w$ . Its maximum value  $T_q(z = -l_s/2, t \rightarrow \infty)$  is scarcely affected by  $\kappa_w$ . Again, in the electrical experiment all  $T_q(z, t)$  can be scaled to lie on a common curve by  $\tilde{T}_q = (\kappa_w + \kappa_s)T_q$ . The amplitude  $T_q(z, t \rightarrow \infty)$  grows with decreasing  $\kappa_w$  according to  $(\kappa_w + \kappa_s)^{-1}$ . One might have the idea to use an optical glass with small  $\kappa_w$ , e.g. dense flint, to maximize  $T_q$  and thus the heterodyne diffraction efficiency. It is, however, not clear, whether a small  $\kappa_w$  has any real advantage. With decreasing  $\kappa_w$  also unwanted transient heating effects increase. They lead to a thermal drift of the heterodyne signal and thus to erroneous values for diffusion and Soret coefficients (see Sec. 4.3.2). Hence we have chosen soda lime glass irrespective of its thermal conductivity  $\kappa_w$  because it is superior to dense flint and many other optical glasses concerning cost and chemical resistance.

According to Eq. (4.26) the heterodyne diffraction efficiencies are obtained from integration

of Eqs. (4.27, 4.28):

$$\zeta_{het,T,s}(t \rightarrow \infty) \propto \left( \frac{\partial n_s}{\partial T} \right)_{c,p} \frac{S_q}{q^2} \frac{1}{\kappa_w + \kappa_s} \quad (4.29)$$

$$\zeta_{het,T,w}(t \rightarrow \infty) \propto \left( \frac{\partial n_w}{\partial T} \right)_p \frac{S_q}{q^2} \frac{1}{\kappa_w + \kappa_s} \quad (4.30)$$

$$\zeta_{het,c}(t \rightarrow \infty) = - \left( \frac{\partial n_s}{\partial c} \right)_{T,p} \left( \frac{\partial n_s}{\partial T} \right)_{c,p}^{-1} S_T c_0 (1 - c_0) \zeta_{het,T,s}(t \rightarrow \infty) \quad (4.31)$$

It is instructive to compare the heterodyne diffraction efficiencies of the temperature grating achievable by electrical heating  $\zeta_{het,T,s}^{\text{el.}}$  (Eq. (4.29)) and by optical heating  $\zeta_{het,T,s}^{\text{opt.}}$  in a laser induced grating experiment (Eq. (3.26)). For  $\kappa_s/\kappa_w = 0.1$  and  $d/l_s = 0.4$  one finds  $\zeta_{het,T,s}^{\text{opt.}}/\zeta_{het,T,s}^{\text{el.}} = 5.4 \alpha I_0 l_s / S_0$ . This means that 5.4 times more power has to be absorbed in the new experiment to obtain the same heterodyne diffraction efficiency as in the laser induced grating experiment. In laser induced grating experiments the power density is usually  $\alpha I_0 \approx 5 \cdot 10^6 \text{ W/m}^3$ . For  $U = 1 \text{ V}$  the same power is absorbed in the new experiment with  $S_0 = \alpha I_0 l_s = 500 \frac{\text{W}}{\text{m}^2}$ , for  $U = 2.2 \text{ V}$  the same heterodyne diffraction efficiency is obtained with  $S_0 = 5.4 \alpha I_0 l_s = 2700 \frac{\text{W}}{\text{m}^2}$ . The applied voltage  $U$  can be related to the power density per unit area  $S_0$  by  $U = 3 \text{ mm} \sqrt{S_0 \cdot 200 \Omega}$ .

#### 4.2.3.1 Stationary Solutions for $l_{\text{ito}} \neq 0$

**Temperature grating in the stationary state for  $l_{\text{ito}} \neq 0$**  In case of not negligible thickness  $l_{\text{ito}}$  of the ITO strips the stationary temperature distribution  $T(x, z)$  solves

$$\partial_x[\kappa(x, z)\partial_x T(x, z)] + \partial_z[\kappa(x, z)\partial_z T(x, z)] + \dot{Q}(x, z) = 0, \quad (4.32)$$

where

$$\kappa(x, z) = \begin{cases} \kappa_s & : \text{ within sample} \\ \kappa_{\text{ito}} & : \text{ within ITO-strips} \\ \kappa_w & : \text{ within window} \end{cases} \quad (4.33)$$

$$= \begin{cases} \kappa_s & : z \leq -l_{\text{ito}} \\ \frac{\kappa_s + \kappa_{\text{ito}}}{2} + \frac{2(\kappa_{\text{ito}} - \kappa_s)}{\pi} \sum_{i=0}^{\infty} \frac{(-1)^i}{2i+1} \cos[(2i+1)2qx] & : -l_{\text{ito}} < z < 0 \\ \kappa_w & : z \geq 0 \end{cases} \quad (4.34)$$

$$\text{and } \dot{Q}(x, z) = \begin{cases} 4\dot{Q}_0 & : \text{ within heated ITO-strips} \\ 0 & : \text{ elsewhere} \end{cases} \quad (4.35)$$

$$= \begin{cases} 0 & : z \leq -l_{\text{ito}} \\ \dot{Q}_0 + 2\dot{Q}_0 \sum_{k=1}^{\infty} \frac{\sin(\pi k/4)}{\pi k/4} \cos kqx & : -l_{\text{ito}} < z < 0 \\ 0 & : z \geq 0 \end{cases} \quad (4.36)$$

If the approximations of infinite window and sample thickness  $l_w, l_s \rightarrow \infty$  and infinite extension in  $x$ -direction remain valid,  $T(x, z)$  has to satisfy the following boundary conditions

$$\partial_x T(x, z)|_{x=0} = \partial_x T(x, z)|_{x=d/2} = T(x, z \rightarrow \infty) = T(x, z \rightarrow -\infty) = 0. \quad (4.37)$$

For simplicity the ambient temperature has been set to zero. The temperature  $T(x, z)$  for  $x < 0$  and  $x > d/2$  can be obtained by symmetry considerations

$$T(d/2 + x, z) = T(d/2 - x, z), \quad T(x + d, z) = T(x, z). \quad (4.38)$$

We define

$$\Delta T(x, z) = T(x, z) - T_0(x, z), \quad (4.39)$$

where  $T_0(x, z)$  is the solution of

$$\partial_x[\kappa(x, z)\partial_x T_0(x, z)] + \partial_z[\kappa(x, z)\partial_z T_0(x, z)] + \dot{Q}_0 = 0. \quad (4.40)$$

Note that  $T_0(x, z)$  is a function of  $x$  with period  $d' = d/2 = \pi/q$ .  $\Delta T(x, z)$  solves

$$\partial_x[\kappa(x, z)\partial_x \Delta T(x, z)] + \partial_z[\kappa(x, z)\partial_z \Delta T(x, z)] + \dot{Q}(x, z) - \dot{Q}_0 = 0 \quad (4.41)$$

$\Delta T(x, z)$  is periodical with period  $d = 2\pi/q$  and can therefore be expanded in a Fourier series.

$$\Delta T(x, z) = T_{0q}(z) + T_q(z) \cos(qx) + T_{2q}(z) \cos(2qx) + \dots = \sum_{i=0}^{\infty} T_{iq}(z) \cos(iqx) \quad (4.42)$$

Inserting Eq. (4.42) in the heat equation (4.32) and considering the boundary conditions (4.37) one finds

$$z \geq 0: \quad T_{0q}(z) = 0, \quad T_{iq}(z) = A_i e^{-iqz} \quad (i \geq 1) \quad (4.43)$$

$$z \leq -l_{\text{ito}}: \quad T_{0q}(z) = 0, \quad T_{iq}(z) = B_i e^{iqz} \quad (i \geq 1) \quad (4.44)$$

where  $A_i$  and  $B_i$  are determined by the requirement of continuity of temperature and heat flux at  $z = 0$  and  $z = -l_{\text{ito}}$ . Unfortunately, calculation of  $A_i$  and  $B_i$  was not possible, since a solution for  $\Delta T(x, z)$  within  $-l_{\text{ito}} < z < 0$  could not be found because of problems with the convergence of the Fourier series. If  $\Delta T(x, z)$  is expanded in one single Fourier series within  $-l_{\text{ito}} < z < 0$ , the second derivative of this Fourier series with respect to  $x$  does not converge to  $\partial_x^2 \Delta T(x, z)$ . Three Fourier series within the heated ITO-strips ( $0 \leq x \leq d/8$ ), the sample ( $d/8 \leq x \leq 3d/8$ ) and the ‘‘cold’’ ITO-strips ( $3d/8 \leq x \leq d/2$ ) are also no solution to the problem, as they do not converge to the actual value of the temperature at  $x = d/8$  and  $x = 3d/8$ .

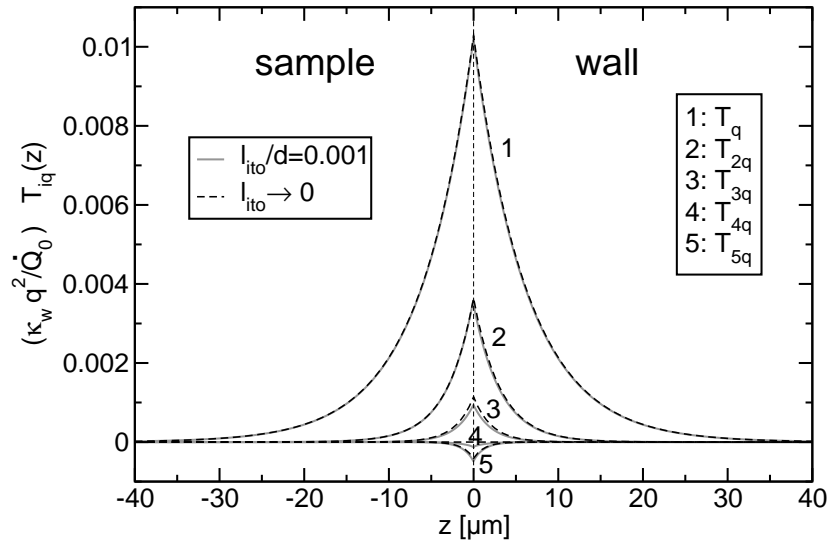


**Figure 4.12:** Lowest Fourier coefficients  $T_{iq}(z)$  as defined in Eq. (4.42). For  $l_{ito}/d = 0.001$  they have been calculated numerically. The analytical approximation (4.45) valid for small  $l_{ito}$  is also shown. ( $\kappa_s/\kappa_w = 0.1$ ,  $\kappa_{ito}/\kappa_w = 10$ ,  $d = 40 \mu\text{m}$ )

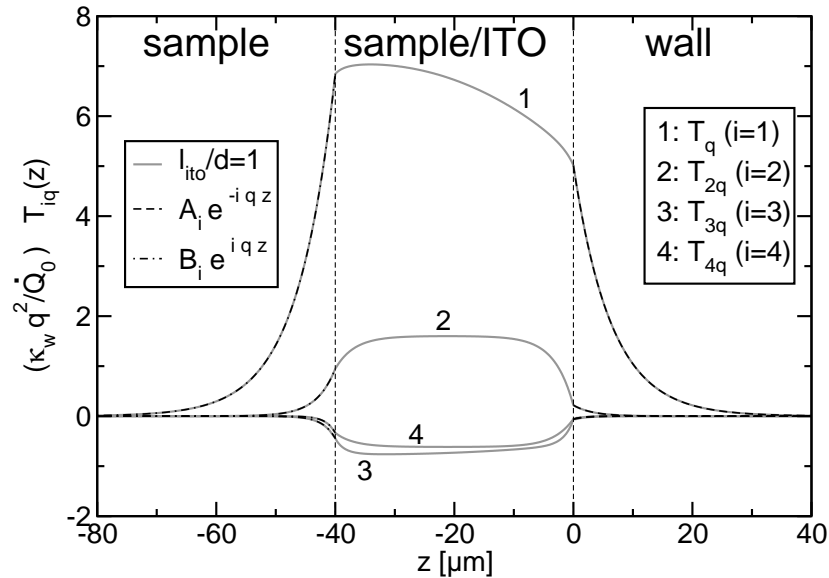


**Figure 4.13:** Lowest Fourier coefficients  $T_{iq}(z)$  as defined in Eq. (4.42) for  $l_{ito}/d = 1$ . Within sample and window  $T_{iq}(z)$  decays exponentially  $\propto \exp(\pm iqz)$ . The amplitudes  $A_i$  and  $B_i$  as well as the solution within  $-l_{ito} < z < 0$  have been determined numerically. ( $\kappa_s/\kappa_w = 0.1$ ,  $\kappa_{ito}/\kappa_w = 10$ ,  $d = 40 \mu\text{m}$ )

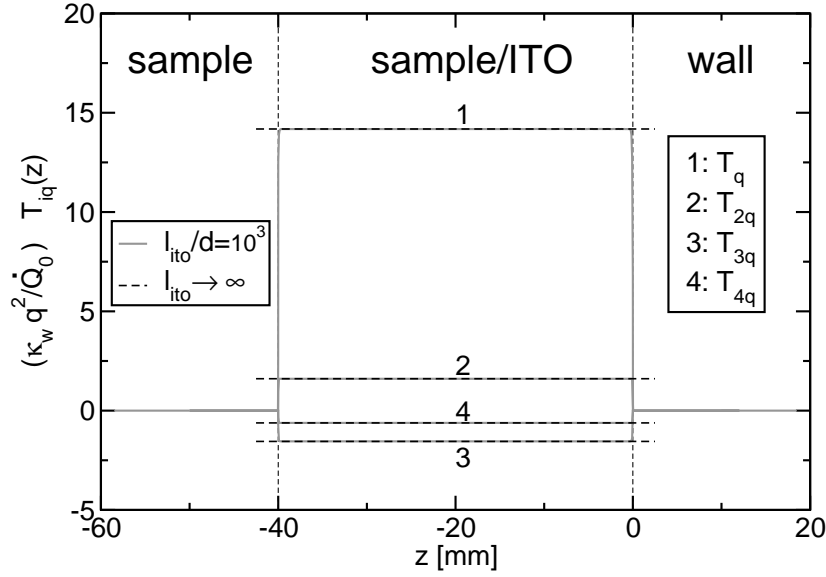


**Figure 4.14:** Lowest Fourier coefficients  $T_{iq}(z)$  as defined in Eq. (4.42). For  $l_{ito}/d = 1000$  they have been calculated numerically, for  $l_{ito} \rightarrow \infty$  an analytical solution (4.46) has been found. ( $\kappa_s/\kappa_w = 0.1$ ,  $\kappa_{ito}/\kappa_w = 10$ ,  $d = 40 \mu\text{m}$ )

Only for  $l_{ito} \rightarrow 0$  and for  $l_{ito} \rightarrow \infty$  analytical solutions could be found. For  $l_{ito} \rightarrow 0$  one obtains by combination of Eq. (4.27) and Eq. (4.36)

$$\Delta T(x, z) = \frac{2\dot{Q}_0 l_{ito}}{q} \frac{1}{\kappa_w + \kappa_s} \sum_{k=1}^{\infty} \frac{\sin(\pi k/4)}{(\pi k^2/4)} e^{-kq|z|} \cos(kqx). \quad (4.45)$$

In this case the  $k$ -th Fourier coefficient of  $\Delta T(x, z)$  originates from the  $k$ -th Fourier coefficient of  $\dot{Q}(x, z)$ . For  $l_{ito} \rightarrow \infty$  the  $z$ -dependence within  $-l_{ito} < z < 0$  can be neglected and one obtains

$$\begin{aligned} \Delta T(x) &= \dot{Q}_0 \begin{cases} -3x^2/(2\kappa_{ito}) + d^2(13/\kappa_s + 8/\kappa_{ito})/384 & : 0 \leq x \leq d/8 \\ (x - d/2)^2/(2\kappa_s) - d^2(14/\kappa_s + 1/\kappa_{ito})/384 & : d/8 \leq x \leq 3d/8 \\ (x - d/2)^2/(2\kappa_{ito}) - d^2(11/\kappa_s + 4/\kappa_{ito})/384 & : 3d/8 \leq x \leq d/2 \end{cases} \\ &= \frac{2\dot{Q}_0}{q^2 \kappa_{ito}} \sum_{k=1}^{\infty} \left\{ \left( \frac{\kappa_{ito}}{\kappa_s} - 1 \right) \left( 1 - \frac{\cos(\pi k/2)}{2} \right) \frac{\cos(\pi k/4)}{k^2} \right. \\ &\quad \left. + \frac{4}{\pi} \left[ 1 - \left( \frac{\kappa_{ito}}{\kappa_s} - 1 \right) \frac{\cos(\pi k/2)}{2} \right] \frac{\sin(\pi k/4)}{k^3} \right\} \cos(kqx). \end{aligned} \quad (4.46)$$

Other than for  $l_{ito} \rightarrow 0$  here there exists no direct relation between the first Fourier coefficient of  $\Delta T(x)$

$$T_q = \frac{4\sqrt{2}\dot{Q}_0}{\pi q^2} \left[ \frac{1}{\kappa_{ito}} + \frac{\pi}{4} \frac{\kappa_{ito} - \kappa_s}{\kappa_s \kappa_{ito}} \right] = \frac{\dot{Q}_q}{q^2} \left[ \frac{1}{\kappa_{ito}} + \frac{\pi}{4} \frac{\kappa_{ito} - \kappa_s}{\kappa_s \kappa_{ito}} \right] \quad (4.47)$$



and the first Fourier coefficient of the heating  $\dot{Q}_q \cos(qx)$ . The temperature distribution arising from  $\dot{Q}_q \cos(qx)$  is given by

$$\begin{aligned} \frac{\dot{Q}_q}{q^2} & \begin{cases} \cos(qx)/\kappa_{\text{ito}} + (1/\kappa_s - 1/\kappa_{\text{ito}})/\sqrt{2} & : 0 \leq x \leq d/8 \\ \cos(qx)/\kappa_s & : d/8 \leq x \leq 3d/8 \\ \cos(qx)/\kappa_{\text{ito}} - (1/\kappa_s - 1/\kappa_{\text{ito}})/\sqrt{2} & : 3d/8 \leq x \leq d/2 \end{cases} \\ & = \frac{\dot{Q}_q}{q^2} \frac{\kappa_{\text{ito}} + \kappa_s}{2\kappa_{\text{ito}}\kappa_s} \cos(qx) + \\ & \quad \frac{\dot{Q}_q}{q^2} \frac{\kappa_{\text{ito}} - \kappa_s}{\pi\kappa_{\text{ito}}\kappa_s} \sum_{j=0}^{\infty} \frac{(-1)^j}{2j+1} \left\{ \frac{\cos[(4j+1)qx]}{4j+1} - \frac{\cos[(4j+3)qx]}{4j+3} \right\}. \end{aligned} \quad (4.48)$$

Its first Fourier coefficient

$$\frac{\dot{Q}_q}{q^2} \left[ \frac{1}{\kappa_{\text{ito}}} + \frac{2 + \pi}{2\pi} \frac{\kappa_{\text{ito}} - \kappa_s}{\kappa_s \kappa_{\text{ito}}} \right] \quad (4.49)$$

is not equal to  $T_q$  as given by Eq. (4.47): This means, that  $T_q$  is not only generated by  $\dot{Q}_q$  but also by the  $\dot{Q}_{iq}$ 's with  $i > 1$ .

For arbitrary values of  $l_{\text{ito}}$  the temperature distribution  $\Delta T(x, z)$  can be evaluated numerically. Numerical solutions for  $\kappa_s/\kappa_w = 0.1$ ,  $\kappa_{\text{ito}}/\kappa_w = 10$  and  $d = 40 \mu\text{m}$  are shown in Fig. 4.12 ( $l_{\text{ito}}/d = 0.001$ ), Fig. 4.13 ( $l_{\text{ito}}/d = 1$ ) and Fig. 4.14 ( $l_{\text{ito}}/d = 1000$ ). In Fig. 4.12 and in Fig. 4.14 also the analytical solutions (4.45) and (4.46) for  $l_{\text{ito}} \rightarrow 0$  and  $l_{\text{ito}} \rightarrow \infty$  have been plotted. Obviously  $l_{\text{ito}} \rightarrow 0$  is a good approximation for  $l_{\text{ito}}/d = 0.001$ . For  $l_{\text{ito}}/d = 0.005$ , which corresponds to our experimental situation, the relative deviations between the numerical solution and the analytical approximation for negligible  $l_{\text{ito}}$  are smaller than 0.2% within the sample ( $z < 0$ ). Within the window ( $z > 0$ ) the relative deviations reach values up to 3.5%, which is however of no importance, since the heterodyne diffraction efficiency of the window is negligible in typical experiments (see Sec. 4.2.4.3).

**Refractive index grating for  $l_{\text{ito}} \neq 0$**  In case of negligible thickness of the ITO layer  $l_{\text{ito}} \rightarrow 0$  the amplitude of the refractive index grating  $n_q$  only depends on  $T_q$  and the higher Fourier harmonics do not need to be considered. For  $l_{\text{ito}} \neq 0$  this is no longer true. If no concentration modulations are present, the refractive index distribution within  $-l_{\text{ito}} \leq z \leq 0$  is given by

$$n(x, z) = \begin{cases} n_{\text{ito}} + (\partial n_{\text{ito}}/\partial T)_{c,p} T(x, z) & : \text{ within ITO-strips} \\ n_s + (\partial n_s/\partial T)_{c,p} T(x, z) & : \text{ within sample} \end{cases}. \quad (4.50)$$

$n_{\text{ito}}$  and  $n_s$  are the refractive indices of the ITO-strips and of the sample at the readout wavelength at ambient temperature. Remember that the ambient temperature has been set to zero. Therefore  $T(x, z)$  is the difference between the actual temperature at  $(x, z)$  and the ambient temperature.  $n(x, z)$  can be evaluated in a Fourier series. The first Fourier

coefficient of  $n(x, z)$  within  $-l_{ito} \leq z \leq 0$  is given by

$$n_q(z) = \frac{(\partial n_{ito}/\partial T)_{c,p} + (\partial n_s/\partial T)_{c,p}}{2} T_q(z) + \frac{(\partial n_{ito}/\partial T)_{c,p} - (\partial n_s/\partial T)_{c,p}}{\pi} \sum_{k=0}^{\infty} \frac{(-1)^k}{2k+1} \left( T_{(4k+1)q}(z) + T_{(4k+3)q}(z) \right), \quad (4.51)$$

where the  $T_{iq}(z)$  have been defined in Eq. (4.42). According to Eq. (4.51) higher Fourier harmonics of  $T(x, z)$  contribute to  $n_q(z)$  and thus to the heterodyne diffraction efficiency

$$\begin{aligned} \zeta_{het} - \zeta_{het,c} &\propto \int_{-\infty}^{-l_{ito}} (\partial n_s/\partial T)_{c,p} T_q(z) dz + \int_{-l_{ito}}^0 \left\{ \frac{(\partial n_{ito}/\partial T)_{c,p} + (\partial n_s/\partial T)_{c,p}}{2} T_q(z) \right. \\ &+ \left. \frac{(\partial n_{ito}/\partial T)_{c,p} - (\partial n_s/\partial T)_{c,p}}{\pi} \sum_{k=0}^{\infty} \frac{(-1)^k}{2k+1} \left( T_{(4k+1)q}(z) + T_{(4k+3)q}(z) \right) \right\} dz \\ &+ \int_0^{\infty} (\partial n_w/\partial T)_{c,p} T_q(z) dz \end{aligned} \quad (4.52)$$

For  $l_{ito} \rightarrow 0$  the second integral in Eq. (4.52) tends to zero, as the temperature is admittedly maximum but nevertheless finite within  $-l_{ito} \leq z \leq 0$ .

## 4.2.4 Time Dependent Solutions

### 4.2.4.1 Temperature Grating

For  $l_s, l_w \rightarrow \infty$  analytical albeit complicated solutions of Eqs. (4.17, 4.18, 4.19, 4.21, 4.23, 4.24) have been obtained in the following way. The solution  $\bar{T}_q(z, p)$  of the Laplace-transformed problem is easily found

$$\bar{T}_q(z, p) = \frac{S_q}{p} \frac{e^{\sqrt{q^2+p/D_{th,s}} z}}{\kappa_s \sqrt{q^2+p/D_{th,s}} + \kappa_w \sqrt{q^2+p/D_{th,w}}} \quad z \leq 0 \quad (4.53)$$

$$\bar{T}_q(z, p) = \frac{S_q}{p} \frac{e^{-\sqrt{q^2+p/D_{th,w}} z}}{\kappa_s \sqrt{q^2+p/D_{th,s}} + \kappa_w \sqrt{q^2+p/D_{th,w}}} \quad z \geq 0. \quad (4.54)$$

Now the inverse Laplace transforms of Eqs. (4.53, 4.54) have to be calculated. This will be first done for the case  $z = 0$ . The Laplace transform of the temperature at  $z = 0$  can be written as

$$\begin{aligned} \bar{T}_q(z=0, p) &= \frac{S_q}{q(\kappa_w^2 - \kappa_s^2)} \left\{ \frac{\kappa_w}{p \sqrt{1 + \frac{p}{D_{th,w} q^2}}} - \frac{\kappa_s}{p \sqrt{1 + \frac{p}{D_{th,s} q^2}}} \right. \\ &+ \left. \frac{\kappa_s \kappa_w}{\tilde{\kappa}^2} \frac{1}{p + \tilde{D}_{th} q^2} \left( \frac{\kappa_s}{\sqrt{1 + \frac{p}{D_{th,w} q^2}}} - \frac{\kappa_w}{\sqrt{1 + \frac{p}{D_{th,s} q^2}}} \right) \right\}, \end{aligned} \quad (4.55)$$

where

$$1/\tilde{\kappa} = \sqrt{\frac{D_{th,w} - D_{th,s}}{\kappa_w^2 D_{th,s} - \kappa_s^2 D_{th,w}}} \quad (4.56)$$

$$\tilde{D}_{th} = \frac{D_{th,s} D_{th,w} (\kappa_w^2 - \kappa_s^2)}{\kappa_w^2 D_{th,s} - \kappa_s^2 D_{th,w}}. \quad (4.57)$$

For typical parameters of window and sample  $\tilde{\kappa}$  and  $\tilde{D}_{th}$  are real and positive. However, all results presented here are also valid for imaginary  $\tilde{\kappa}$  and negative  $\tilde{D}_{th}$ . The temperature  $T_q(z, t)$  is real and positive in any case. Since

$$\begin{aligned} \bar{f}(p) &= \frac{1}{(p+a)\sqrt{1+p/b}} \\ \Rightarrow f(t) &= e^{-at} \frac{\sqrt{b}}{\sqrt{a-b}} \operatorname{erfi} \sqrt{(a-b)t} = e^{-at} \frac{\sqrt{b}}{\sqrt{b-a}} \operatorname{erf} \sqrt{(b-a)t}. \end{aligned} \quad (4.58)$$

holds for  $b > 0$  and real  $a$ , the inverse Laplace transform of Eq. (4.55) is given by

$$\begin{aligned} T_q(z=0, t) &= \frac{S_q}{q(\kappa_w^2 - \kappa_s^2)} \left\{ \kappa_w \operatorname{erf} \sqrt{D_{th,w} q^2 t} - \kappa_s \operatorname{erf} \sqrt{D_{th,s} q^2 t} \right. \\ &\quad \left. + \frac{\kappa_s \kappa_w}{\tilde{\kappa}} e^{-\tilde{D}_{th} q^2 t} \left[ \operatorname{erfi} \left( \frac{\kappa_s}{\tilde{\kappa}} \sqrt{D_{th,w} q^2 t} \right) - \operatorname{erfi} \left( \frac{\kappa_w}{\tilde{\kappa}} \sqrt{D_{th,s} q^2 t} \right) \right] \right\}. \end{aligned} \quad (4.59)$$

$\operatorname{erf} x$  is the error function and  $\operatorname{erfi} x = \operatorname{erf}(ix)/i$  is the imaginary error function.  $\operatorname{erfi} x$  is real for real  $x$ . For  $z > 0$  one has

$$\bar{T}_q(z, p) = \bar{T}_q(z=0, p) e^{-\sqrt{q^2 + p/D_{th,w}} z}. \quad (4.60)$$

and therewith, using the Faltung theorem

$$T_q(z, t) = \int_0^t T_q(z=0, \tau) \frac{z \exp\left[-\frac{z^2}{4D_{th,w}(t-\tau)}\right] e^{-D_{th,w} q^2 (t-\tau)}}{2\sqrt{\pi D_{th,w}} (t-\tau)^{3/2}} d\tau \quad z > 0. \quad (4.61)$$

The fraction in Eq. (4.61) is the inverse Laplace transform of  $e^{-\sqrt{q^2 + p/D_{th,w}} z}$ . In the same manner one finds for  $z < 0$

$$T_q(z, t) = \int_0^t T_q(z=0, \tau) \frac{-z \exp\left[-\frac{z^2}{4D_{th,s}(t-\tau)}\right] e^{-D_{th,s} q^2 (t-\tau)}}{2\sqrt{\pi D_{th,s}} (t-\tau)^{3/2}} d\tau \quad z < 0. \quad (4.62)$$

The integrals in Eqs. (4.61, 4.62) have to be solved numerically. In Figs. 4.15 and 4.16 this has been done for typical parameters  $\kappa_s/\kappa_w = 0.1$ ,  $D_{th,s}/D_{th,w} = 0.1$ ,  $d = 40 \mu\text{m}$ ,  $S_q = \frac{4\sqrt{2}}{\pi} S_0$ ,  $S_0/\kappa_w = 500 \mu\text{K}/\mu\text{m}$ . The temperature evolves fastest at  $z = 0$  and for increasing  $|z|$  more and more slowly. As  $D_{th,s}/D_{th,w} = 0.1$  the temperature in the sample  $T_q(-|z|, t)$  always

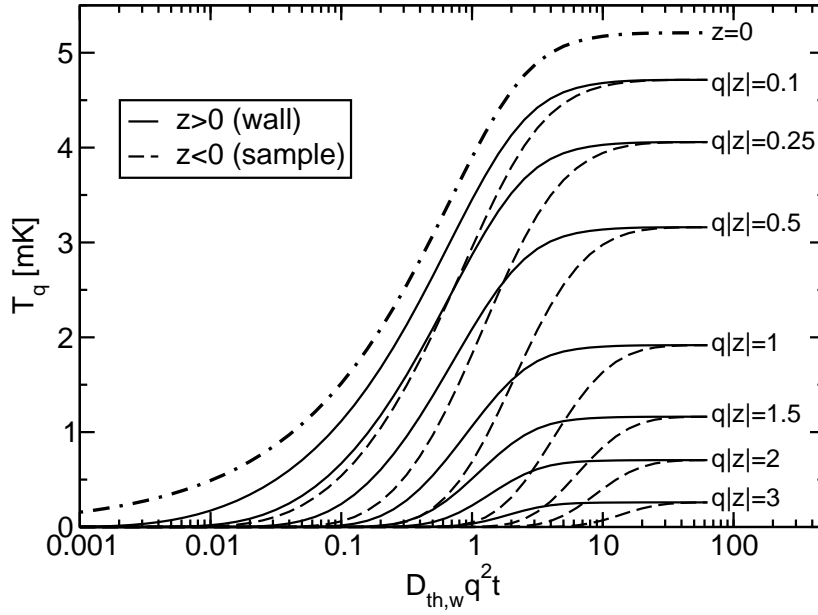


**Figure 4.15:** Time dependent amplitude of the temperature grating  $T_q(z, t)$  at various positions  $z$  for typical parameters  $\kappa_s/\kappa_w = 0.1$ ,  $D_{th,s}/D_{th,w} = 0.1$ ,  $d = 40 \mu\text{m}$ ,  $S_q = \frac{4\sqrt{2}}{\pi}S_0$ ,  $S_0/\kappa_w = 500 \mu\text{K}/\mu\text{m}$

evolves slower than the temperature in the window  $T_q(+|z|, t)$ . Only for very long times  $T_q(z, t \rightarrow \infty)$  becomes symmetrical with respect to  $z = 0$ .

Integration of Eqs. (4.61) and (4.62) over  $z$  leads to the heterodyne diffraction efficiencies  $\zeta_{het,T,s}$  and  $\zeta_{het,T,w}$  as defined in Eq. (4.26).

$$\zeta_{het,T,w}(t) \propto \left(\frac{\partial n_w}{\partial T}\right)_p \int_0^t T_q(z=0, \tau) \frac{\sqrt{D_{th,w}} e^{-D_{th,w} q^2 (t-\tau)}}{\sqrt{\pi (t-\tau)}} d\tau \quad (4.63)$$

$$\zeta_{het,T,s}(t) \propto \left(\frac{\partial n_s}{\partial T}\right)_{c,p} \int_0^t T_q(z=0, \tau) \frac{\sqrt{D_{th,s}} e^{-D_{th,s} q^2 (t-\tau)}}{\sqrt{\pi (t-\tau)}} d\tau. \quad (4.64)$$

Again the integrals in Eqs. (4.63, 4.64) have to be solved numerically to obtain  $\zeta_{het,T,s}(t)$  and  $\zeta_{het,T,w}(t)$ . This has been done for various samples (toluene: Figs. 4.17, 4.19; dodecane: Fig. 4.17; air: Fig. 4.18; binary mixture of isobutylbenzene and dodecane ( $c_0 = 0.5$ ): Fig. 4.22) and will be discussed in Sec. 4.3.

#### 4.2.4.2 Concentration Grating

With the temperature  $T_q(z, t)$  being known we could now solve the extended diffusion equation (4.20) for the concentration distribution  $c_q(z, t)$  with initial condition (4.17) and boundary condition (4.22). However, we are actually not so much interested in  $c_q(z, t)$ . The relevant quantity is the measured heterodyne diffraction efficiency  $\zeta_{het,c}$  as defined in Eq. (4.26).

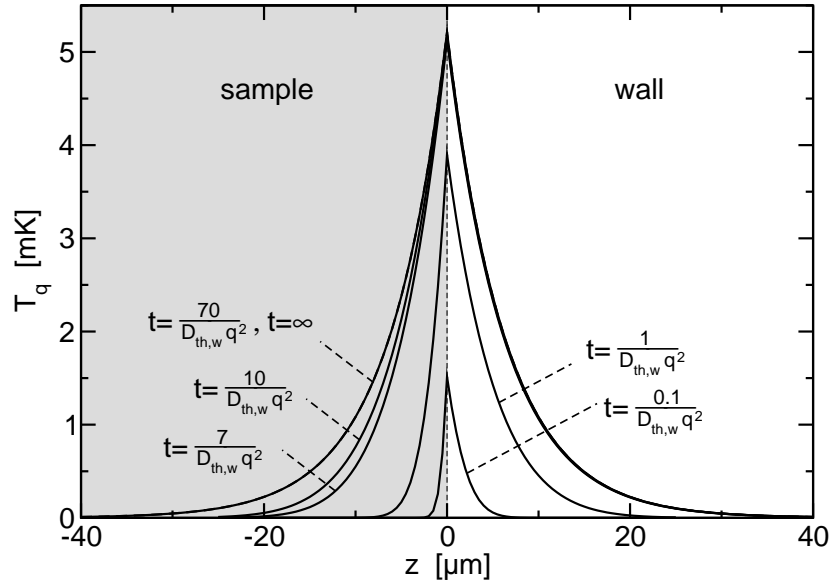


**Figure 4.16:**  $z$  dependent amplitude of the temperature grating  $T_q(z, t)$  at various times  $t$  for typical parameters  $\kappa_s/\kappa_w = 0.1$ ,  $D_{th,s}/D_{th,w} = 0.1$ ,  $d = 40 \mu\text{m}$ ,  $S_q = \frac{4\sqrt{2}}{\pi}S_0$ ,  $S_0/\kappa_w = 500 \mu\text{K}/\mu\text{m}$

To obtain an evolution equation for  $\zeta_{het,c}$ , we integrate Eq. (4.20) over the sample region ( $-l_s < z < 0$ ). Taking into account the boundary condition (4.22) we arrive at

$$\partial_t \zeta_{het,c} = -Dq^2 \zeta_{het,c} - \left( \frac{\partial n_s}{\partial c} \right)_{T,p} \left( \frac{\partial n_s}{\partial T} \right)_{c,p}^{-1} D_T q^2 c_0 (1 - c_0) \zeta_{het,T,s}. \quad (4.65)$$

Eq. (4.65) is solved by

$$\zeta_{het,c}(t) = - \left( \frac{\partial n_s}{\partial c} \right)_{T,p} \left( \frac{\partial n_s}{\partial T} \right)_{c,p}^{-1} D_T q^2 c_0 (1 - c_0) \int_{-\infty}^t \zeta_{het,T,s}(t') e^{-Dq^2(t-t')} dt', \quad (4.66)$$

which can be simplified to

$$\zeta_{het,c}(t) = \zeta_{het,c}(t \rightarrow \infty) [1 - e^{-Dq^2 t}], \quad (4.67)$$

if the temperature signal evolves fast on the timescale of the concentration signal ( $D_{th,s} \gg D$ ). For our experiments Eq. (4.67) is a good approximation and will be used throughout this chapter, since typically  $D_{th,s} \approx 10^{-3} \text{cm}^2/\text{s}$  and  $D \approx 10^{-5} \text{cm}^2/\text{s}$  for small molecules and less for polymeric or colloidal systems.

#### 4.2.4.3 Total Heterodyne Diffraction Efficiency

According to Eq. (4.26) the total heterodyne diffraction efficiency is given by

$$\zeta_{het}(t) = \zeta_{het,T,s}(t) + \zeta_{het,T,w}(t) + \zeta_{het,c}(t).$$

The heterodyne diffraction efficiencies of the window's and the sample's temperature grating,  $\zeta_{het,T,w}(t)$  and  $\zeta_{het,T,s}(t)$ , are given by Eqs. (4.63, 4.64) with (4.56, 4.57, 4.59). The heterodyne diffraction efficiency of the concentration grating  $\zeta_{het,c}(t)$  follows from Eq. (4.67) with (4.29, 4.31). In general the contribution of  $\zeta_{het,T,w}$  to the total heterodyne diffraction efficiency is negligible,

$$\zeta_{het}(t) = \zeta_{het,T,s}(t) + \zeta_{het,c}(t), \quad (4.68)$$

since the contrast factor of the window (soda lime glass)  $(\partial n_w/\partial T)_p = 2.8 \times 10^{-6}/\text{K}$  [89] is much smaller than the contrast factors of most samples. Organic solvents typically have  $(\partial n_s/\partial T)_{c,p} \approx -5 \times 10^{-4}/\text{K}$  [111]. There are only few exceptions to this rule, like water around 4 °C or the sample air with  $(\partial n_s/\partial T)_p = -0.87 \times 10^{-6}/\text{K}$ . In case of a one-component system with  $c \equiv 1$  one has  $\zeta_{het,c} \equiv 0$  and

$$\zeta_{het}(t) = \zeta_{het,T,s}(t) + \zeta_{het,T,w}(t). \quad (4.69)$$

For pure organic liquids the heterodyne diffraction efficiency of the window can be neglected and Eq. (4.69) further reduces to

$$\zeta_{het}(t) = \zeta_{het,T,s}(t). \quad (4.70)$$

The adequate equation for analysis of experiments on binary liquids is Eq. (4.68). It contains the known parameters  $q$ ,  $\kappa_w$ ,  $D_{th,w}$  and the unknown parameters of the sample  $\kappa_s$ ,  $D_{th,s}$ ,  $D$ ,  $S_T = D_T/D$ ,  $(\partial n_s/\partial T)_{c,p}$  and  $(\partial n_s/\partial c)_{T,p}$ . The parameter  $S_q$  enters linearly and is therefore of no importance as only normalized signals are studied. In principle, it would be possible to fit the experimental data by Eq. (4.68) to obtain  $\kappa_s$ ,  $D_{th,s}$ ,  $D$  and  $S_T = D_T/D$ , if the contrast factors  $(\partial n_s/\partial T)_{c,p}$  and  $(\partial n_s/\partial c)_{T,p}$  have been determined separately. This is, however, difficult due to the complicated expression (4.64) for  $\zeta_{het,T,s}(t)$ . Moreover, in many cases heat diffusion is not of interest and only mass and thermal diffusion phenomena shall be studied. We have found that a reasonable parameterization of the temperature signal is obtained by  $[1 - e^{-(t/\tau_{th})^\beta}]$ , which is much easier to handle than the full expression (4.64). Therefore the following working equation

$$\begin{aligned} \zeta_{het}(t) &= \zeta_{het,T,s}(t \rightarrow \infty)[1 - e^{-(t/\tau_{th})^\beta}] + \zeta_{het,c}(t \rightarrow \infty)[1 - e^{-Dq^2t}] \\ &= \zeta_{het,T,s}(t \rightarrow \infty) \left( 1 - e^{-(t/\tau_{th})^\beta} - A[1 - e^{-Dq^2t}] \right) \end{aligned} \quad (4.71)$$

with fit parameters  $\tau_{th}$ ,  $\beta$ ,  $D$  and  $A = (\partial n_s/\partial c)_{T,p} (\partial n_s/\partial T)_{c,p}^{-1} S_T c_0(1 - c_0)$  will be used for analysis of the thermal diffusion experiments.  $\tau_{th}$  and  $\beta$  are discarded, since they have no direct physical meaning. From the remaining fit parameters one obtains the diffusion coefficient  $D$ , the thermal diffusion coefficient  $D_T$ , and the Soret coefficient  $S_T = D_T/D$ , if  $(\partial n_s/\partial T)_{c,p}$  and  $(\partial n_s/\partial c)_{T,p}$  are known.

### 4.2.5 Sample Heating

The first term  $S_0$  in Eq. (4.14) causes overall heating of sample and windows. For one-dimensional heat transport along the  $z$ -axis the corresponding stationary temperature distribution  $T_0(z, t \rightarrow \infty)$  is linear within the sample and the windows. For simplicity the ambient temperature is set to zero. At  $z = -l_s - l_w$  and  $z = l_w$  one has radiation boundary conditions  $\mp \kappa_w \partial_z T_0 + HT_0 = 0$  with  $H$  being the convection heat transfer coefficient. At  $z = 0$  heat is produced and therefore  $\kappa_w \partial_z T_0|_{z=0^+} + S_0 = \kappa_s \partial_z T_0|_{z=0^-}$  holds. Within this model the following stationary temperature distribution is obtained:

$$T_0 = S_0 \frac{C_{\text{soda}}}{C} \left( C_{\text{sap}} + \frac{z + l_s}{\kappa_{w, \text{sap}}} \right) \quad -l_s - l_w \leq z \leq -l_s \quad (\text{window: sapphire}) \quad (4.72)$$

$$T_0 = S_0 \frac{C_{\text{soda}}}{C} \left( C_{\text{sap}} + \frac{z + l_s}{\kappa_s} \right) \quad -l_s \leq z \leq 0 \quad (\text{sample}) \quad (4.73)$$

$$T_0 = S_0 \frac{C_{\text{sap}} + \frac{l_s}{\kappa_w}}{C} \left( C_{\text{soda}} - \frac{z}{\kappa_{w, \text{soda}}} \right) \quad 0 \leq z \leq l_w \quad (\text{window: soda lime}), \quad (4.74)$$

where  $C_{\text{sap}} = H_{\text{sap}}^{-1} + l_w/\kappa_{w, \text{sap}}$ ,  $C_{\text{soda}} = H_{\text{soda}}^{-1} + l_w/\kappa_{w, \text{soda}}$  and  $C = C_{\text{sap}} + C_{\text{soda}} + l_s/\kappa_s$ .  $\kappa_{w, \text{soda}}$  and  $\kappa_{w, \text{sap}}$  are the thermal conductivities of soda-lime glass and sapphire. Elsewhere in this chapter  $\kappa_{w, \text{soda}}$  is called  $\kappa_w$  and  $\kappa_{w, \text{sap}}$  is approximated to be infinite.  $H_{\text{sap}}$  and  $H_{\text{soda}}$  are the convection heat transfer coefficients at  $z = -l_s - l_w$  and  $z = l_w$ . They depend on the surface geometry, on the nature of motion of the surrounding air (free or forced convection) and on the air's thermodynamic and transport properties. According to Ref. [47] typical values for free convection of gases are  $H = 2 \dots 25 \text{ W}/(\text{m}^2 \text{ K})$ . In our experiment we have  $l_s = 100 \mu\text{m}$ ,  $l_w = 1 \text{ mm}$ ,  $\kappa_s \approx 0.1 \text{ W}/(\text{mK})$ ,  $\kappa_{w, \text{soda}} = 1.12 \text{ W}/(\text{mK})$ ,  $\kappa_{w, \text{sap}} = 40 \text{ W}/(\text{mK})$  and therewith  $l_s/\kappa_s \approx l_w/\kappa_{w, \text{soda}} \approx 10^{-3} \text{ Km}^2/\text{W}$  and  $l_w/\kappa_{w, \text{sap}} = 2.5 \cdot 10^{-5} \text{ Km}^2/\text{W}$ . Thus one has  $H_{\text{sap}}^{-1}, H_{\text{soda}}^{-1} \gg l_s/\kappa_s, l_w/\kappa_{w, \text{sap}}, l_w/\kappa_{w, \text{soda}}$  and Eqs. (4.72, 4.73, 4.74) simplify to

$$T_0 \approx \frac{S_0}{H_{\text{sap}} + H_{\text{soda}}} \quad \text{for all } z. \quad (4.75)$$

With  $S_0 = 500 \text{ W}/\text{m}^2$  and  $H_{\text{sap}} = H_{\text{soda}} = 10 \text{ W}/\text{m}^2\text{K}$  one obtains from Eq. (4.75)  $T_0 = 25 \text{ K}$ . Obviously this overestimates the overall heating. The one-dimensional model does not describe correctly the situation. In the experiment only an area of  $A_{\text{heated}} = 3 \text{ mm} \times 3 \text{ mm}$  is heated, whereas the total surface of the cuvette is approximately  $5 \text{ cm}^2$ . Lateral heat transport within the cuvette and emission over the entire cuvette surface result in smaller warming of sample and windows than predicted by Eq. (4.75). A rough estimation for the actual  $T_0$  can be obtained as follows. Because of  $H_{\text{sap}}^{-1}, H_{\text{soda}}^{-1} \gg l_s/\kappa_s, l_w/\kappa_{w, \text{sap}}, l_w/\kappa_{w, \text{soda}}$  the temperature rise  $T_0$  can be approximated to be constant within sample and windows. Then,  $T_0$  can be related to  $S_0$  via

$$S_0 A_{\text{heated}} = \int \vec{j}_q d\vec{A} \approx H_{\text{sap}} T_0 A_{\text{sap}} + H_{\text{soda}} T_0 A_{\text{soda}}, \quad (4.76)$$

where  $\vec{j}_q$  is the heat current. The integral in Eq. (4.76) has been evaluated using the radiation boundary condition. Instead of the entire cuvette surface only its front  $A_{\text{sap}} = 1.6 \text{ cm} \times 1 \text{ cm}$  and its back side  $A_{\text{soda}} = 2 \text{ cm} \times 2 \text{ cm}$  need to be considered thanks to its small thickness of 2.1 mm. Using again  $S_0 = 500 \text{ W/m}^2$  and  $H_{\text{sap}} = H_{\text{soda}} = 10 \text{ W/m}^2\text{K}$  one finds a reasonable  $T_0 \approx 0.5 \text{ K}$ . Temperature rises of the same order of magnitude have been reported for laser induced grating experiments [52].

Huge convection heat transfer coefficients up to  $H = 20 \text{ kW}/(\text{m}^2\text{K})$  can be reached if a liquid e.g. water flows over the surface of the cuvette [47]. In such a case the thermal contact resistances  $H_{\text{sap}}^{-1}$  and  $H_{\text{soda}}^{-1}$  are negligible. If we additionally assume  $\kappa_{w,\text{sap}} \rightarrow \infty$  and  $\kappa_{w,\text{soda}} = \kappa_w$ , we obtain from the one-dimensional model (4.72, 4.73, 4.74)

$$T_0 = \frac{S_0}{\kappa_s} \frac{\frac{l_w}{\kappa_w}}{\frac{l_s}{\kappa_s} + \frac{l_w}{\kappa_w}} (l_s + z) \quad -l_s \leq z \leq 0 \text{ (sample)} \quad (4.77)$$

$$T_0 = \frac{S_0}{\kappa_w} \frac{\frac{l_s}{\kappa_s}}{\frac{l_s}{\kappa_s} + \frac{l_w}{\kappa_w}} (l_w - z) \quad 0 \leq z \leq l_w \text{ (window: soda lime)}. \quad (4.78)$$

Within these approximations the maximum temperature is given by

$$T_0(z=0) = \frac{S_0}{\frac{\kappa_w}{l_w} + \frac{\kappa_s}{l_s}} \approx 0.25 \text{ K} \quad (4.79)$$

and the heat flux through the window and through the sample are equal because of

$$\frac{\kappa_s \partial_z T_0|_{z<0}}{\kappa_w \partial_z T_0|_{z>0}} = \frac{\kappa_s}{\kappa_w} \frac{l_w}{l_s} \approx 1. \quad (4.80)$$

The parameters for evaluation of Eqs. (4.79) and (4.80)  $S_0 = 500 \text{ W/m}^2$ ,  $l_w = 1 \text{ mm}$ ,  $l_s = 100 \mu\text{m}$ ,  $\kappa_s \approx 0.1 \text{ W}/(\text{mK})$ ,  $\kappa_w = 1.12 \text{ W}/(\text{mK})$  have been chosen according to typical experimental conditions. Because of lateral heat transport the actual temperature rise in case of negligible thermal contact resistances  $H_{\text{sap}}^{-1}$  and  $H_{\text{soda}}^{-1}$  will be one to two orders of magnitude smaller than predicted by Eq. (4.79). However,  $H^{-1} \approx 0$  is hardly achievable as an optical experiment with water flowing permanently over the surfaces of the cuvette is not easy to design.

## 4.3 Validation of the Method

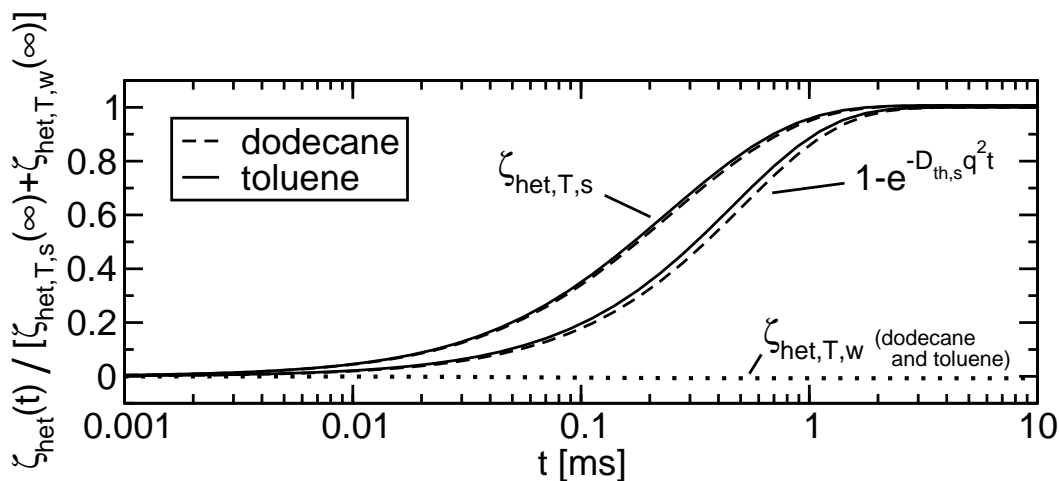
### 4.3.1 Measurement of Heat Diffusion

One-component systems, which cannot exhibit concentration modulations, are suitable to study the build-up of the temperature grating. To verify the theoretical predictions of Sec. 4.2.4.1 we studied in a first step pure toluene, pure dodecane and an empty cuvette.

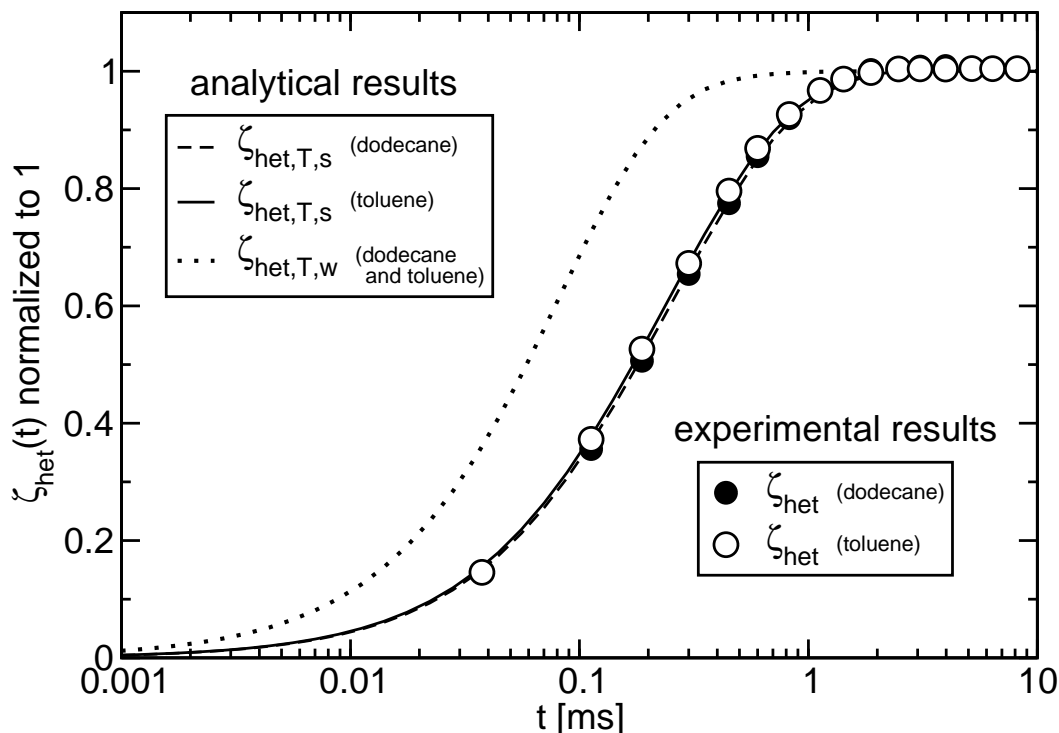


Fig. 4.17 shows the results for dodecane and toluene. The theoretical curves have been calculated from Eqs. (4.63, 4.64) using the following parameters: dodecane:  $D_{th,s} = 7.89 \cdot 10^{-4} \text{ cm}^2/\text{s}$ ,  $\kappa_s = 0.13 \text{ W/mK}$  [107, 111]; toluene:  $D_{th,s} = 8.8 \cdot 10^{-4} \text{ cm}^2/\text{s}$ ,  $\kappa_s = 0.14 \text{ W/mK}$  [42]; soda–lime glass (crown glass):  $\kappa_w = 1.12 \text{ W/mK}$ ,  $D_{th,w} = 57.7 \cdot 10^{-4} \text{ cm}^2/\text{s}$  [89]. As can be seen in Fig. 4.17(a), the heterodyne diffraction efficiency of the window  $\zeta_{het,T,w}(t)$  is negligible if compared to the heterodyne diffraction efficiency of the sample  $\zeta_{het,T,s}(t)$ .  $\zeta_{het,T,s}(t)$  rises much faster than an exponential curve with time constant  $\tau_{th} = (D_{th,s}q^2)^{-1}$ . To be able to compare the time evolution of  $\zeta_{het,T,s}(t)$  and  $\zeta_{het,T,w}(t)$  they have been normalized to unity in Fig. 4.17(b). As expected from the values of the thermal diffusivities, the heterodyne diffraction efficiency of the sample evolves slower than the heterodyne diffraction efficiency of the window. Since dodecane and toluene have similar thermal diffusivities and heat conductivities, also the corresponding heterodyne diffraction efficiencies are similar. In particular  $\zeta_{het,T,w}(t)$  of dodecane and toluene cannot be distinguished within the resolution of the plot. Also shown in Fig. 4.17(b) are the experimental data on toluene and dodecane. The experiments have been performed using voltages between 1 and 2 V. The measured heterodyne diffraction efficiencies  $\zeta_{het}(t)$  did not depend on the applied voltage and were very reproducible. Moreover they are perfectly explained by theory. As can be seen in Fig. 4.17(a) the signal from the window  $\zeta_{het,T,w}(t)$  is negligible and one expects  $\zeta_{het}(t) = \zeta_{het,T,s}(t)$  – in excellent agreement with the experiment.

In case of an empty cuvette, however, the heterodyne diffraction efficiency of the window is no longer negligible. The contrast factors of air  $(\partial n_s/\partial T)_p = -0.87 \times 10^{-6}/\text{K}$  and of soda–lime glass  $(\partial n_w/\partial T)_p = 2.8 \times 10^{-6}/\text{K}$  are of same order of magnitude. Again,  $\zeta_{het,T,s}(t)$  and  $\zeta_{het,T,w}(t)$  have been calculated from Eqs. (4.63, 4.64). The parameters for air  $D_{th,s} = 1530 \cdot 10^{-4} \text{ cm}^2/\text{s}$  and  $\kappa_s = 0.02 \text{ W/mK}$  have been taken from Ref. [41]. Note that  $\tilde{\kappa}$  as defined in Eq. (4.56) is purely imaginary for the sample air. Even so  $T_q(z, t)$  is real, since  $\tilde{\kappa}^{-1} \text{erfi}(x/\tilde{\kappa}) = -(\text{Im } \tilde{\kappa})^{-1} \text{erf}(x/\text{Im } \tilde{\kappa})$  for  $\tilde{\kappa} = i \text{Im } \tilde{\kappa}$ . The results for  $\zeta_{het,T,s}(t)$ ,  $\zeta_{het,T,w}(t)$  and  $\zeta_{het}(t) = \zeta_{het,T,s}(t) + \zeta_{het,T,w}(t)$  are shown in Fig. 4.18(a). Due to the huge thermal diffusivity of air  $D_{th,s} = 1530 \cdot 10^{-4} \text{ cm}^2/\text{s}$  the heterodyne diffraction efficiency of the sample  $\zeta_{het,T,s}(t)$  evolves faster than that of the window  $\zeta_{het,T,w}(t)$ . Although the stationary heterodyne diffraction efficiency of the wall is larger than the stationary heterodyne diffraction efficiency of the sample ( $\zeta_{het,T,w}(\infty) > |\zeta_{het,T,s}(\infty)|$ ), at very short times  $t < 0.007 \text{ ms}$  one has  $\zeta_{het,T,w}(t) < |\zeta_{het,T,s}(t)|$ . Accordingly  $\zeta_{het}(t) = \zeta_{het,T,s}(t) + \zeta_{het,T,w}(t)$  is negative at very short times and positive for longer times. In Fig. 4.18(b) the measured heterodyne diffraction efficiencies for the sample air are compared to the normalized analytical results from Fig. 4.18(a) above. Because of the small contrast factors, the experimental signals were extremely small. To be able to detect a signal a voltage of  $U = 10 \text{ V}$  had to be applied. For long times the measured heterodyne diffraction efficiencies did not reach plateau values, but drifted slowly and irreproducibly away. This drifting can be explained by transient heating of the whole cuvette (see Sec. 4.3.2), which is pronounced for  $U = 10 \text{ V}$ . But also on short times

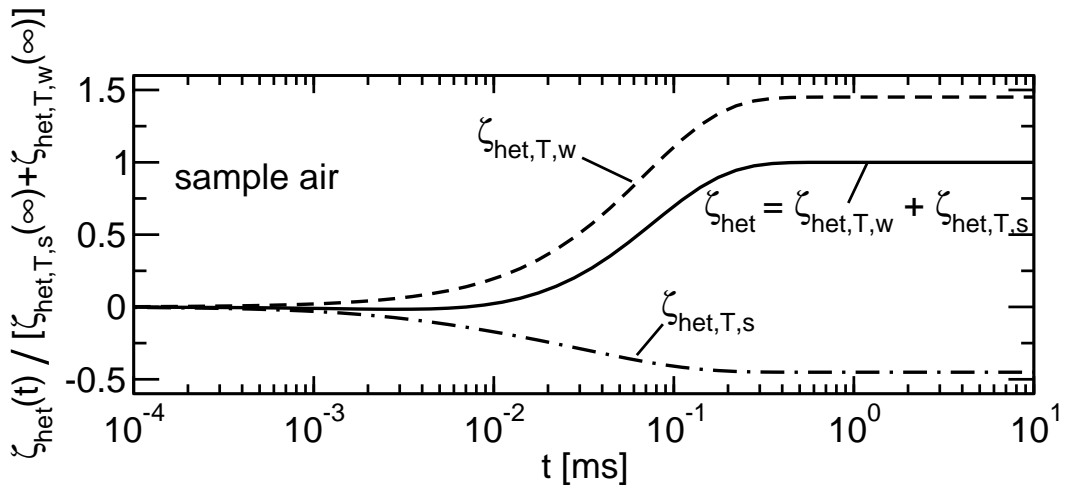


(a) Time dependent heterodyne diffraction efficiencies of sample ( $\zeta_{het,T,s}$ ) and window ( $\zeta_{het,T,w}$ ) for the samples dodecane and toluene as obtained from Eqs. (4.63,4.64). These signals are compared to an exponential rise with time constant  $\tau_{th} = (D_{th,s}q^2)^{-1}$ .

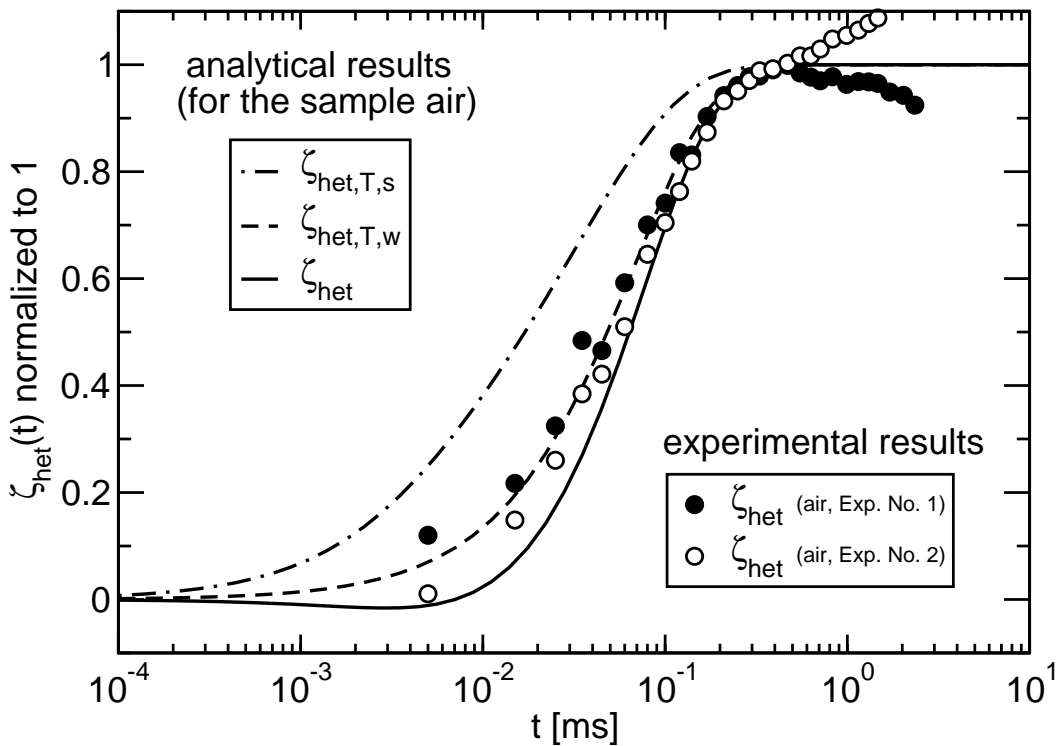


(b) Experimentally determined total heterodyne diffraction efficiency  $\zeta_{het}$  of pure dodecane and pure toluene. Also shown are the normalized theoretical diffraction efficiencies from Fig. 4.17(a) above.

**Figure 4.17:** Heterodyne diffraction efficiencies for the samples dodecane and toluene



(a) Time dependent, normalized heterodyne diffraction efficiencies of sample ( $\zeta_{het,T,s}$ ) and window ( $\zeta_{het,T,w}$ ) as well as the total heterodyne diffraction efficiency  $\zeta_{het} = \zeta_{het,T,s} + \zeta_{het,T,w}$  for the sample air as obtained from Eqs. (4.63,4.64).



(b) Experimentally determined total heterodyne diffraction efficiency  $\zeta_{het}$  using an empty cuvette. Also shown are the normalized theoretical diffraction efficiencies from Fig. 4.18(a) above.

**Figure 4.18:** Heterodyne diffraction efficiencies for the sample air

the agreement between measured and theoretically predicted  $\zeta_{het}$  is very poor. Strangely, the experimental total heterodyne diffraction efficiency  $\zeta_{het}$  seems to be better described by the theoretical heterodyne diffraction efficiency of the window  $\zeta_{het,T,w}$ . Possibly, convection inhibits build-up of the temperature grating within the empty cuvette, whereas the temperature grating within the window evolves in almost the same manner as in a convection-free situation described by Eqs. (4.63, 4.64). Then one has  $\zeta_{het,T,s}(t) \approx 0$  and  $\zeta_{het}(t) \approx \zeta_{het,T,w}(t)$ . To summarize, build-up of the temperature grating in organic liquids can be very well explained by our theory. For the sample air problems have been encountered. However, the main goal of our apparatus is to study processes in liquids and understanding of these processes is absolutely satisfactory.

### 4.3.2 Thermal Stability of the Heterodyne Signal

In Fig. 4.19 three types of experiments on pure toluene at a voltage of  $U = 2\text{ V}$  are compared: switching on and off strips of set 1, switching on and off strips of set 2 and switching between strips of set 1 and strips of set 2. The experimentally obtained heterodyne diffraction efficiencies are compared to the theoretical prediction of Sec. 4.3.1. For  $t < 10\text{ ms}$  the agreement between experiment and theory is very good in all cases. For longer times, however, an unwanted and irreproducible drift of the heterodyne signal appears in the experiments where only one set of strips is switched. Obviously, transient heating of sample and cuvette causes considerable phase drifting of the involved beams  $E_s$ ,  $E_c e^{i\theta}$  and  $E_{\text{ref}} e^{i\phi}$  and thus becomes visible in the measured intensity. The degree of perturbation by thermal drift effects depends on the uncontrollable phase  $\theta$  of the local oscillator, which explains the unreproducibility of the experimental curves. These drift effects vanish almost completely, if the voltage is switched between strips of set 1 and strips of set 2. Only by introducing this alternate switching concept, long time instabilities due to fluctuating thermal load of the entire sample are suppressed and measurement periods characteristic for mass diffusion become accessible.

The heterodyne diffraction efficiencies in Fig. 4.19 have been calculated from the measured intensities  $I_{\phi=0}$  and  $I_{\phi=\pi}$  according to Eqs. (4.9, 4.10). The averaged  $I_{\phi=0}$  and  $I_{\phi=\pi}$  are shown in Fig. 4.20. Switching occurs at  $t = 0$ ,  $t = 337.5\text{ ms}$  and  $t = 675\text{ ms}$ . As has been already seen in Fig. 4.19, signal drifts are almost completely suppressed for alternate switching. Furthermore the signal amplitude is twice as high as for switching on and off.

Diffusion processes in binary systems have similar time constants  $\tau \approx 50\text{ ms}$  as the time constant of the transient heating effects. This makes analysis of the corresponding heterodyne diffraction efficiencies complicated, as the two processes cannot be separated. Fig. 4.21 shows the measured intensities  $I_{\phi=0}$  and  $I_{\phi=\pi}$  for the symmetric mixture of tetralin and dodecane ( $c_0 = 0.5$ ) at  $U = 1.5\text{ V}$ , where the voltage has been alternately switched between strips of set 1 and strips of set 2. Other than for one-component systems, one cannot tell from this

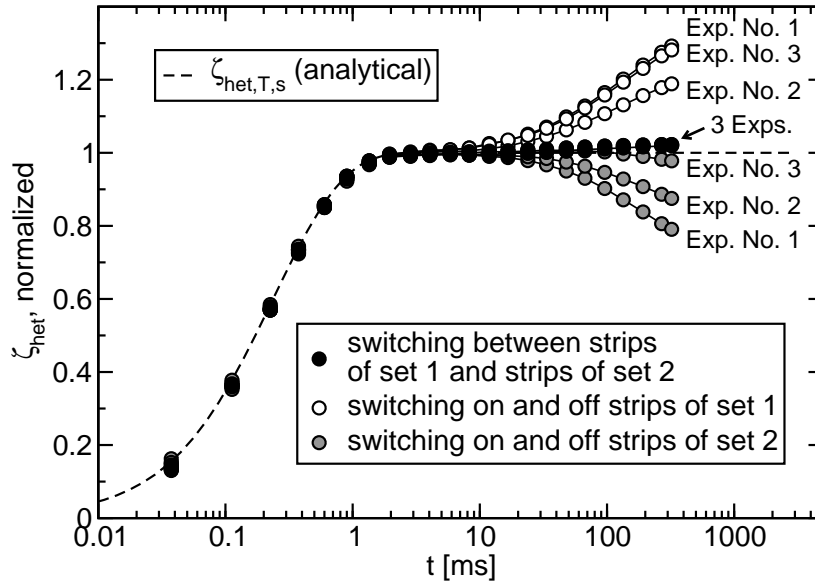


**Figure 4.19:** Normalized heterodyne diffraction efficiency of pure toluene at  $U = 2$  V. Three different types of experiments are compared: switching on and off strips of set 1, switching on and off strips of set 2 and switching between strips of set 1 and strips of set 2

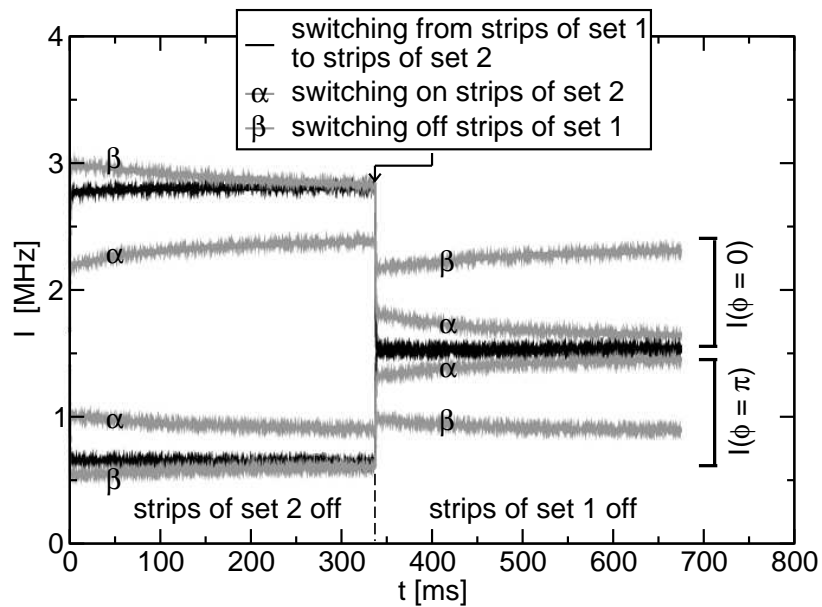


**Figure 4.20:** Measured intensities  $I_{\phi=0}$  and  $I_{\phi=\pi}$  for pure toluene at  $U = 2$  V. Three different types of experiments are compared: switching on and off strips of set 1, switching on and off strips of set 2 and switching between strips of set 1 and strips of set 2

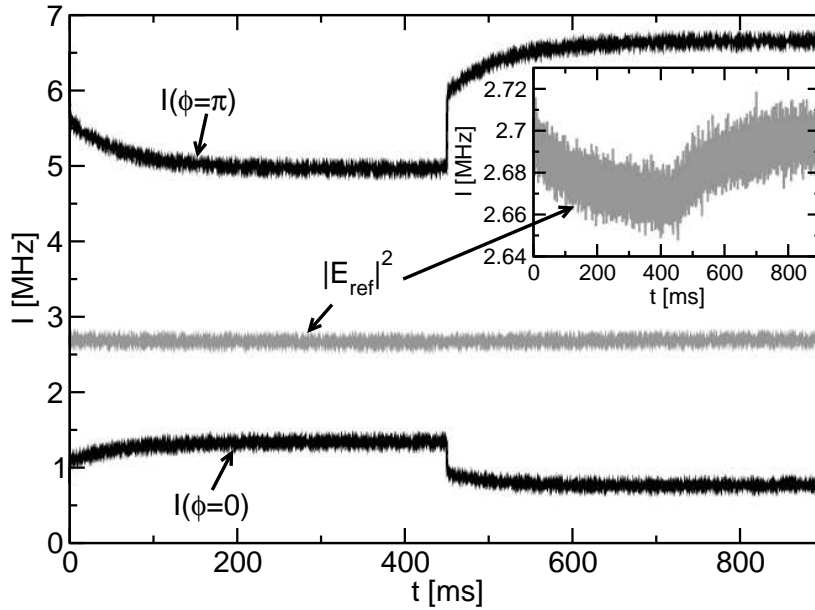


**Figure 4.21:** Measured intensities  $I_{\phi=0}$  and  $I_{\phi=\pi}$  for the symmetric mixture of tetralin and dodecane ( $c_0 = 0.5$ ) at  $U = 1.5$  V. The voltage has been switched alternately between strips of set 1 and strips of set 2. In a second step the probing beam has been blocked and only the reference beam has been recorded while otherwise performing the experiment as before.

data whether transient heating effects disturb the signal. However, by blocking the probing beam and otherwise performing the experiment as usual, thermal drift effects can be directly observed. As can be seen in the inset, the intensity of the reference beam shows a slight time dependence with a time constant of about 50 ms

$$|E_{\text{ref}}|^2 \approx |E_{\text{ref}}^0|^2 + \epsilon[1 - e^{-t/(50 \text{ ms})}] \quad (4.81)$$

even for alternate switching. For switching on and off only one set of strips the amplitude  $\epsilon$  increases by a factor of 5 to 10. The recorded intensity  $|E_{\text{ref}}|^2$  is a coherent superposition of the transmitted light and the scattered light from scratches or dust on the cuvette window. The phases of these local oscillators drift with respect to each other due to transient heating effects, which explains the time dependency in Eq. (4.81). Further examinations revealed that the amplitude  $\epsilon$  depends quadratically on the applied voltage  $\epsilon \propto U^2$ , i.e. linear on the heating power. Since the signals stemming from the temperature and concentration grating also increase quadratically with increasing  $U$ , the degree perturbation of the heterodyne signal by thermal drift effects does not depend on the applied voltage.

As has already been mentioned, it was not possible to completely eliminate all transient heating effects. Because the cuvette is slightly asymmetric, the thermal load is not exactly identical for both sets of strips and a slight long-time drift of the signal also remains for alternate switching. This can further be reduced by averaging over repeated minor readjustments

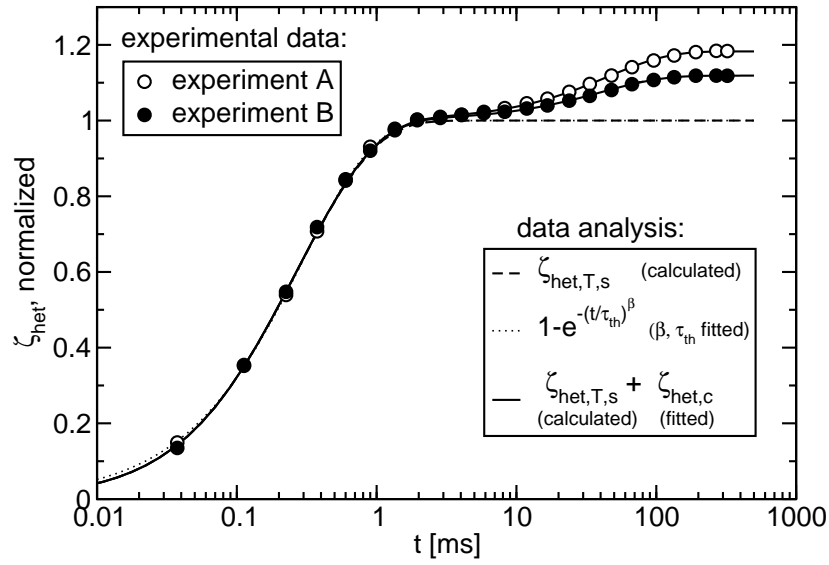


**Figure 4.22:** Normalized heterodyne diffraction efficiencies of the symmetric mixture IBB–dodecane ( $c_0 = 0.5$  g/g). For details on data analysis and fitting refer to text.

of some mirrors, which result in random variations of the phase angle  $\theta$ .

### 4.3.3 Measurement of Mass and Thermal Diffusion

Having discussed and understood heat diffusion processes in Sec. 4.3.1, we will now test the applicability of our new technique for measurements of diffusion and thermal diffusion. We have chosen the three binary mixtures of dodecane, isobutylbenzene (IBB) and tetralin at a concentration of  $c_0 = 0.5$  g/g, as their Soret, diffusion and thermal diffusion coefficients already have been determined in a benchmark test [75] and are well known. All measurements have been performed at room temperature  $T \approx 25$  °C.

Fig. 4.22 shows the normalized heterodyne diffraction efficiency of IBB–dodecane as obtained from two different experiments. The fast and the slow process correspond, respectively, to the build–up of the temperature and the concentration grating. In addition, irreproducible contributions from transient heating effects are contained in the slow mode (see Sec. 4.3.2). These drift effects cannot be treated quantitatively and are ignored in the analysis. The slow mode is identified with  $\zeta_{\text{het},c}$  and fitted by Eq. (4.67). The fast mode can be described theoretically by evaluating the heterodyne diffraction efficiency of the sample’s temperature grating  $\zeta_{\text{het},T,s}$  from Eq. (4.64) using  $D_{th,s} = 7.7 \times 10^{-4}$  cm<sup>2</sup>/s and  $\kappa_s = 0.14$  W/mK. However, in this section we are not interested in heat diffusion, but only in mass and thermal diffusion. Therefore, instead of complex calculations according to Eq. (4.64), the temperature signal can simply be fitted to  $[1 - e^{-(t/\tau_{th})^\beta}]$ , as has already been explained in Sec. 4.2.4.3. A very good agreement between the measured temperature signal, the calculated heterodyne

		$(\partial n/\partial T)_{c,p}$ [ $10^{-4} \text{ K}^{-1}$ ]	$(\partial n/\partial c)_{T,p}$
IBB-dodecane	$(c_0 = 0.5 \text{ g/g})$	-4.51	0.0628
tetralin-IBB	$(c_0 = 0.5 \text{ g/g})$	-4.74	0.0544
tetralin-dodecane	$(c_0 = 0.5 \text{ g/g})$	-4.39	0.1170

**Table 4.1:** Contrast factors from Ref. [111]

diffraction efficiency and this fit function is found in Fig. 4.22. Four fit parameters are involved:  $\tau_{th}$  and  $\beta$  are discarded. The two other fit parameters  $A$  and  $\tau_c = (Dq^2)^{-1}$  yield  $S_T$  and  $D$ , if the contrast factors  $(\partial n_s/\partial T)_{c,p}$  and  $(\partial n_s/\partial c)_{T,p}$  are known.

Fig. 4.23 shows the obtained fit parameters  $A$  and  $\tau_c = (Dq^2)^{-1}$  for the system IBB-dodecane. The scatter around the mean value is caused by thermal drift effects. The error bars represent standard deviations. The measurements have been performed using voltages of  $U = 1.5 \text{ V}$  and  $U = 2 \text{ V}$ . Again, no dependence on  $U$  was found. The amplitude  $A$  of the signal varies slowly from experiment to experiment, which can be explained by a slow drift of the uncontrollable phase  $\theta$  defined in Eq. (4.1). The arrows indicate that some mirrors have been readjusted to alter the phases of the involved beams before performing the next experiment. This leads to an abrupt change of  $A$ . The time constant of the slow mode  $\tau_c$  shows a slightly different behavior than  $A$ . It varies stronger and faster from experiment to experiment. Moreover, pronounced jumps after readjusting the mirrors cannot be observed for  $\tau_c$ . Our experimental results are compared to the values for  $A$  and  $\tau_c$ , which are expected from the benchmark [75]. Agreement is found within the errors.

For the two other mixtures, tetralin-IBB and tetralin-dodecane, mean values of  $A$  and  $\tau_c$  have been obtained in the same way by averaging over approximately 80 experiments, where each experiment has been averaged over approximately 2000 cycles. From these mean values the coefficients  $S_T$ ,  $D$ , and  $D_T = S_T D$  have been evaluated and are listed in Tab. 4.2 under “electrical heating”. Contrast factors have been taken from Tab. 4.1. For comparison also the benchmark results [75] and the results obtained from laser induced grating experiments (optical heating) [111] are given in Tab. 4.2. Within the errors all coefficients agree. However, the experimental errors in case of electrical heating are larger than for optical heating, where transient heating effects can be reduced to zero. Since transient heating effects make an additive, non multiplicative contribution to the signal, they become less important for larger signals. Therefore the smallest errors are found for the system tetralin-dodecane. Here the amplitude of the signal is rather large ( $A = -0.63$ ) and contributions of transient heating effects become almost negligible. The “most difficult” mixture is tetralin-IBB with  $A = -0.1$ . Even though thermal drift effects can lead to larger as well as smaller signal amplitudes, generally they seem to lead to an overestimation of  $S_T$  and an underestimation of  $D$ . These two effects cancel out in the thermal diffusion coefficient  $D_T = S_T D$ , which is in very good agreement with the benchmark values.



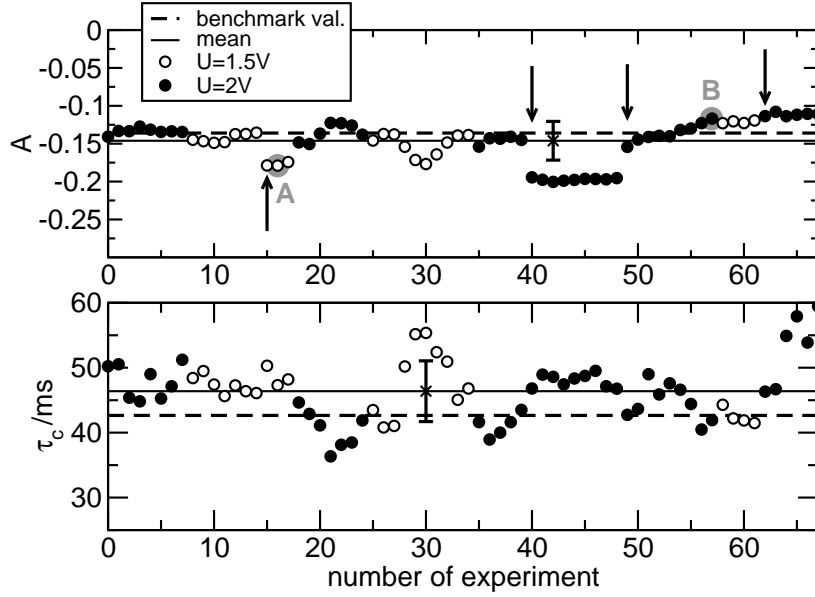


**Figure 4.23:** Obtained fit parameters  $A$  and  $\tau_c = (Dq^2)^{-1}$  for the system IBB–dodecane ( $c_0 = 0.5$  g/g).  $A$  and  $B$  refer to the respective experiments in Fig. 4.22. The arrows indicate readjustment of some mirrors. The values expected from the benchmark test [75] are also included.

		IBB-dodecane $c_0 = 0.5$ g/g	tetralin-IBB $c_0 = 0.5$ g/g	tetralin-dodecane $c_0 = 0.5$ g/g
$D$ [ $10^{-6}$ cm $^2$ s $^{-1}$ ]	opt. heating	$9.9 \pm 0.6$	$8.4 \pm 0.7$	$6.26 \pm 0.09$
	benchmark	$9.5 \pm 0.4$	$8.5 \pm 0.6$	$6.21 \pm 0.06$
	el. heating	$8.8 \pm 0.9$	$7.5 \pm 1.4$	$6.3 \pm 0.2$
$S_T$ [ $10^{-3}$ K $^{-1}$ ]	opt. heating	$3.95 \pm 0.08$	$3.46 \pm 0.07$	$9.45 \pm 0.09$
	benchmark	$3.9 \pm 0.1$	$3.3 \pm 0.3$	$9.5 \pm 0.5$
	el. heating	$4.2 \pm 0.7$	$3.6 \pm 0.9$	$9.5 \pm 0.4$
$D_T$ [ $10^{-8}$ cm $^2$ s $^{-1}$ K $^{-1}$ ]	opt. heating	$3.9 \pm 0.2$	$2.9 \pm 0.2$	$5.9 \pm 0.1$
	benchmark	$3.7 \pm 0.2$	$2.8 \pm 0.1$	$5.9 \pm 0.3$
	el. heating	$3.7 \pm 0.7$	$2.7 \pm 0.8$	$6.0 \pm 0.3$

**Table 4.2:** Comparison of results for the coefficients  $D$ ,  $S_T$  and  $D_T$  as determined from laser induced transient grating experiments [111] (optical heating), in the benchmark [75] and by the new technique (electrical heating)

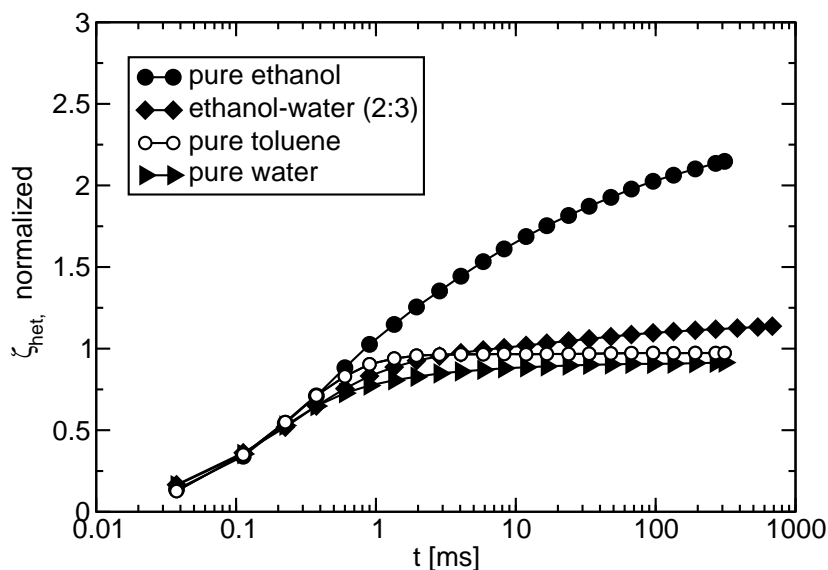


**Figure 4.24:** Normalized heterodyne diffraction efficiency for pure water, pure ethanol and a ethanol–water mixture. Unexplained effects occur and neither heat nor mass diffusion can be determined from these curves. Pure toluene, in contrast, still behaves as expected.

An important advantage of the new technique is that no dye needs to be added to the sample. This is particularly interesting for aqueous systems, where inert dyes are difficult to find. We therefore tried to measure pure water (milli pore, 18 M $\Omega$ ), pure ethanol (Merck, > 99.9%), and an ethanol–water mixture (ethanol:  $c_0 = 0.4$  g/g). As can be seen in Fig. 4.24, a strange, unexplainable albeit reproducible behavior was found. Build–up of a temperature grating and a concentration grating cannot be identified in these curves. In between, we made measurements on pure toluene to test the cuvette and correct temperature signals were obtained. Obviously, polar liquids cause additional unexpected problems, which might be explained by electrochemical reactions at the ITO electrodes. Potentially, this can be prevented by covering the ITO strips with a thin and inert protective layer.

## 4.4 Conclusion

We have developed a new instrument for the measurement of heat, mass, and thermal diffusion based on electrical heating of ITO strip arrays on a micrometer scale and optical readout by diffraction. The measurement process and signal generation have been analyzed in detail. An analytical solution of the time dependent, two dimensional heat equation was found, assuming sample and window to be semi–infinite. It describes correctly the build–up of the temperature grating as has been checked experimentally for the pure liquids dodecane and toluene and for the binary symmetric mixture of IBB and dodecane. Hence, the new technique is well suited for the determination of thermal diffusivities of liquids.

---

Mass and thermal diffusion have been measured in the three “benchmark mixtures” IBB–dodecane, tetralin–IBB, and tetralin–dodecane. The experimental data have been analyzed by fitting of a simple working equation (4.71), which has been derived by solving the two-dimensional extended diffusion equation. The obtained fit parameters yield the Soret coefficient  $S_T$ , the diffusion coefficient  $D$  and the thermal diffusion coefficient  $D_T = S_T D$ , if the contrast factors  $(\partial n / \partial c)_{T,p}$  and  $(\partial n / \partial T)_{c,p}$  are known.  $S_T$ ,  $D$ , and  $D_T$  could be determined correctly for all mixtures within the experimental errors. The errors are, however, larger than in laser-induced grating experiments. Responsible for this are transient heating effects of similar time constants as  $(Dq^2)^{-1}$ , which disturb the signal in an unreproducible manner depending on the particular, uncontrollable phase relation between the involved beams. The thermal drift of the heterodyne signal could not be completely eliminated, but still reduced by keeping the average thermal load on sample and cuvette approximately constant during the experiment. This has been achieved by switching the voltage alternately between two sets of strips instead of switching on and off only one set of strips. Asymmetries of the cuvette, which lead to unbalanced thermal loads of the two sets of strips, remain a problem. Construction of a more symmetric cuvette would further reduce transient heating effects and allow for a more precise determination of  $S_T$  and  $D$ . Up to now polar liquids cannot be measured in our cuvettes. The reason is still not clear, but possibly electrochemical effects occur at the ITO–electrodes, which could be inhibited by a thin protective layer over the ITO–strips. More work is needed to clarify and resolve this problem.

## Chapter 5

### Summary

In the first part of Chap. 2 we have given a brief review of the thermodynamic–phenomenological theory relevant for a correct description of the Soret effect. It comprises the formulation of the first law in open systems, the calculation of the entropy production, and the derivation of the phenomenological equations. This section is based on the books by de Groot and Mazur [16] and by Haase [40] and contains also some own results. We have explicitly derived a relation between reversible work and dissipation function, if heat and mass are exchanged reversibly and irreversibly between the two homogenous phases of a non–isothermal heterogenous system. Moreover we have discussed in detail, whether Onsager coefficients are invariant against shifts of enthalpy or entropy zero. Furthermore some comments on recent literature work have been made, since thermodynamic principles are not always correctly incorporated.

The aim of the second part of Chap. 2 was to obtain evolution equations for the composition variables (extended diffusion equation) and the temperature (heat equation), which allow for the interpretation of the time–resolved experiments of Chaps. 3 and 4. The derivation of the extended diffusion equation is closely related to the issue of different reference velocities. Therefore general diffusion fluxes relative to arbitrary reference velocities have been introduced, phenomenological equations have been derived for these fluxes with the help of Prigogine’s theorem, and general diffusion coefficients have been defined by generalizing the considerations of Ref. [16] to non–isothermal systems. With this preparatory work done, we could show that an extended diffusion equation holds, if a certain reference velocity is zero, or, if all gradients are small and second order terms may be neglected. Existing models have been extended and modified to obtain the conditions for vanishing of a reference velocity in a non–isothermal multicomponent system. Furthermore an evolution equation for the temperature, the heat equation, has been derived. Finally the problem of thermodynamic driving forces has shortly been treated. Even though it seems to have little relation to reference velocities and evolution equations, interesting results for the actual hydrodynamic friction force acting on a diffusing particle could be found by using the relations previously derived in this section.

In Chaps. 3 and 4 we have treated the measurement of heat, mass and thermal diffusion in transient grating experiments.

In Chap. 3 we have presented a two-dimensional model to account for the role of heat conducting walls in the measurement of heat transport and Soret effect driven mass transport in transient holographic grating experiments. Heat diffusion into the walls leads to non-exponential decay of the temperature grating. Under certain experimental conditions it can be approximated by an exponential function and assigned an apparent thermal diffusivity  $D_{th,app} < D_{th,s}$ , where  $D_{th,s}$  is the true thermal diffusivity of the sample. The ratio  $D_{th,app}/D_{th,s}$  depends on only three dimensionless parameters,  $d/l_s$ ,  $\kappa_s/\kappa_w$ , and  $D_{th,s}/D_{th,w}$ .  $d$  is the grating period,  $l_s$  the sample thickness,  $\kappa_s$  and  $\kappa_w$  the thermal conductivities of sample and wall, respectively, and  $D_{th,w}$  the thermal diffusivity of the wall. If at least two measurements are performed at different  $d/l_s$ , both  $D_{th,s}$  and  $\kappa_s$  can be determined. Instead of costly solving partial differential equations, the unknown parameters can be obtained by finding the zero of an analytic function. For thin samples and large grating periods, heat conduction into the walls plays a predominant role and consequently the concentration grating in binary mixtures is no longer one-dimensional. Nevertheless, the normalized heterodyne diffraction efficiency of the concentration grating remains unaffected and the true mass and thermal diffusion coefficient and the correct Soret coefficient are still obtained from a simple one-dimensional model. All theoretical predictions have been tested by experiments on pure and binary liquids over a wide range of grating periods and sample thicknesses. Excellent agreement has been found in all cases.

A new transient grating technique for the measurement of heat, mass and thermal diffusion in liquids has been introduced in Chap. 4. Similar to holographic grating experiments, a temperature grating is created in the sample. Thermal expansion transforms the temperature into a refractive-index grating, which is read by diffraction of a readout laser beam. In a multicomponent mixture an additional concentration grating is formed by thermal diffusion driven by the temperature gradients of the temperature grating. Differently to laser induced dynamic grating experiments we use Joule heating instead of optical heating. For that purpose we have built cuvettes which have a grating of transparent conducting strips on the inner side of one of their windows. If heated by an electric current a temperature grating will build up in the sample. Both, the heat equation and the extended diffusion equation, have been solved in two dimensions to allow for quantitative data analysis. Our apparatus and method of analysis have been validated by measurements of heat, mass and thermal diffusion in pure and binary liquids. Heat diffusion can be correctly determined as was shown for pure toluene, pure dodecane and the symmetric mixture of isobutylbenzene–dodecane. Mass and thermal diffusion was studied in the three symmetric mixtures of dodecane, isobutylbenzene and tetralin. The obtained diffusion and Soret coefficients agree with the literature values within the experimental errors. Uncompensated transient heating effects limit the resolution of the experimental technique.

## Deutsche Zusammenfassung

Der erste Teil des zweiten Kapitels gibt einen kurzen Überblick über die thermodynamisch-phenomenologische Theorie, und zwar vor allem im Hinblick auf Diffusion und Thermodiffusion. Er umfasst die Formulierung des ersten Hauptsatzes in offenen Systemen, die Berechnung der Entropieproduktion und die Herleitung der phänomenologischen Gleichungen. Obwohl dieses Unterkapitel auf den Büchern von de Groot und Mazur [16] und von Haase [40] basiert, enthält es doch auch einige eigene Ergebnisse. So wurde beispielsweise sowohl reversibler als auch irreversibler Wärme- und Massenaustausch zwischen den zwei homogenen Phasen eines nicht isothermen heterogenen Systems untersucht. Daraus konnte der Zusammenhang zwischen reversibler Arbeit und Dissipationsfunktion explizit hergeleitet werden. Weiterhin wurde ausführlich diskutiert, ob Onsager Koeffizienten invariant gegen Verschiebungen des Enthalpie- und Entropienullpunktes sind. Mit Hilfe dieser eigenen Resultate wurden Widersprüche zu thermodynamischen Gesetzen in kürzlich erschienenen Publikationen gefunden.

Das Ziel des zweiten Teils des zweiten Kapitels war es, Entwicklungsgleichungen für die Kompositionsvariablen (erweiterte Diffusionsgleichung) und für die Temperatur (Wärmediffusionsgleichung) zu erhalten, die eine Auswertung der zeitaufgelösten Experimente aus den Kapiteln 3 und 4 ermöglichen. Um die erweiterte Diffusionsgleichung herzuleiten, muss man als erstes die Problematik verschiedener Referenzgeschwindigkeiten verstanden haben. Deswegen wurden zunächst verallgemeinerte Diffusionsflüsse relativ zu beliebigen Referenzgeschwindigkeiten eingeführt, für die man dann zum einen phänomenologische Gleichungen mit Hilfe des Theorems von Prigogine herleiten und zum anderen verallgemeinerte Diffusionskoeffizienten definieren kann. Dazu wurden die Betrachtungen aus Ref. [16] auf nicht isotherme Systeme verallgemeinert. Mit dieser Vorarbeit konnte gezeigt werden, dass erweiterte Diffusionsgleichungen gelten, wenn eine bestimmte Referenzgeschwindigkeit null ist, oder wenn alle Gradienten klein sind und Terme zweiter Ordnung vernachlässigt werden können. Existierende Modelle wurden erweitert und modifiziert, um die Bedingungen für das Verschwinden einer Referenzgeschwindigkeit in einem nicht isothermen, multikomponentigen System zu erhalten. Außerdem wurde eine Entwicklungsgleichung für die Temperatur, die Wärmediffusionsgleichung, hergeleitet. Der letzte Abschnitt des Unterkapitels behandelt die sogenannten thermodynamischen Kräfte. Obwohl sie anscheinend wenig mit Referenzgeschwindigkeiten und Entwicklungsgleichungen zu tun haben, konnten interessante Ergebnisse für die tatsächliche hydrodynamische Reibungskraft auf ein diffundierendes Teilchen aus den zuvor hergeleiteten Beziehungen gewonnen werden.

Kapitel 3 und 4 befassen sich mit der Messung von Wärme-, Massen- und Thermodiffusion in transienten Gitterexperimenten.

In Kapitel 3 wurde ein zweidimensionales Modell vorgestellt, um den Einfluss von wärmeleitenden Küvettenwänden auf die Messung von Wärme- und Massentransport in transienten holographischen Gitterexperimenten zu berücksichtigen. Wärmediffusion in die Wände führt zu einem nicht exponentiellen Abfall des Temperaturgitters. Unter bestimmten experimentellen Bedingungen kann er aber durch eine exponentielle Funktion mit einer apparenten thermischen Diffusivität  $D_{th,app} < D_{th,s}$  angenähert werden.  $D_{th,s}$  ist die tatsächliche thermische Diffusivität der Probe. Das Verhältnis  $D_{th,app}/D_{th,s}$  hängt nur von drei dimensionslosen Parametern,  $d/l_s$ ,  $\kappa_s/\kappa_w$ , und  $D_{th,s}/D_{th,w}$  ab.  $d$  ist die Gitterperiode,  $l_s$  die Probendicke,  $\kappa_s$  und  $\kappa_w$  die Wärmeleitfähigkeiten von Probe und Wand und  $D_{th,w}$  die thermische Diffusivität der Wand. Wenn mindestens zwei Messungen bei verschiedenen  $d/l_s$  durchgeführt werden, können sowohl  $D_{th,s}$  als auch  $\kappa_s$  bestimmt werden. Dazu ist keine aufwändige Simulation von partiellen Differentialgleichungen nötig, da die unbekannt Parameter aus der Nullstelle einer analytischen Funktion berechnet werden können. Für dünne Proben und große Gitterperioden wird die Wärmediffusion in die Wände sehr wichtig und das Konzentrationsgitter in einer binären Mischung ist folglich nicht mehr eindimensional. Die normierte heterodyne Beugungseffizienz des Konzentrationsgitters bleibt davon jedoch unbeeinflusst und die wahren Soret- und Diffusionskoeffizienten können weiterhin aus einem einfachen eindimensionalen Model ermittelt werden. Alle theoretischen Vorhersagen wurden durch Experimente an einkomponentigen und binären Flüssigkeiten über einen großen Bereich von Gitterperioden und Probendicken getestet. In allen Fällen war die Übereinstimmung hervorragend.

Eine neue transiente Gittermethode für die Messung von Wärme-, Massen- und Thermodiffusion in Flüssigkeiten wurde in Kapitel 4 entwickelt. Ähnlich wie bei holographischen transienten Gitterexperimenten wird ein Temperaturgitter in der Probe erzeugt. Die thermische Expansion wandelt dieses Temperaturgitter in ein Brechungsindexgitter um, das durch Beugung eines Lasersstrahls ausgemessen werden kann. In einer mehrkomponentigen Mischung bildet sich wegen der Thermodiffusion, die durch die Gradienten des Temperaturgitters getrieben wird, ein zusätzliches Konzentrationsgitter aus. Anders als in holographischen transienten Gitterexperimenten wird die Probe bei der neuen Methode nicht optisch sondern elektrisch geheizt. Dazu wurden Küvetten konstruiert, die ein Gitter aus transparenten und leitfähigen Streifen auf der Innenseite eines Fensters haben. Wenn diese Streifen durch einen elektrischen Strom erwärmt werden, entsteht ein Temperaturgitter in der Probe. Sowohl die Wärmediffusionsgleichung als auch die erweiterte Diffusionsgleichung wurden in zwei Dimensionen gelöst, um die Messdaten quantitativ auswerten zu können. Durch Messungen von Wärme-, Massen- und Thermodiffusion in einkomponentigen und binären Flüssigkeiten konnte bestätigt werden, dass unser neues Messgerät in Verbindung mit der vorgeschlagenen Auswertemethode korrekt funktioniert. Wärmediffusion wurde in reinem Toluol, reinem Dodekan und in der symmetrischen Mischung aus Isobutybenzol und Dodekan richtig bestimmt.

Massen- und Thermodiffusion wurde in den drei symmetrischen Mischungen aus Dodekan, Isobutybenzol und Tetralin untersucht. Die gewonnenen Massen- und Thermodiffusionskoeffizienten stimmen innerhalb der Fehler mit den Literaturwerten überein. Nicht kompensierte transiente Aufheizungseffekte limitieren die Auflösung der Technik.



## Bibliography

- [1] J. N. Agar. The rate of attainment of Soret equilibrium. *Trans. Faraday Soc.*, 56:776–787, 1960.
- [2] S. Alves, A. Bourdon, and A. M. F. Neto. Generalization of the thermal lens model formalism to account for thermodiffusion in a single-beam Z-scan experiment: Determination of the Soret coefficient. *J. Opt. Soc. Am. B*, 20:713–718, 2003.
- [3] S. Alves, G. Demouchy, A. Bee, D. Talbot, A. Bourdon, and A. M. F. Neto. Investigation of the sign of the Soret coefficient in different ionic and surfacted magnetic colloids using forced Rayleigh scattering and single-beam Z-scan techniques. *Philos. Mag.*, 83:2059–2066, 2003.
- [4] J. L. Anderson. Colloid transport by interfacial forces. *Ann. Rev. Fluid Mech.*, 21:61–99, 1989.
- [5] P. Atkins. *Physical chemistry*. Freeman, New York, 6th edition, 1999.
- [6] G. K. Batchelor. Brownian diffusion of particles with hydrodynamic interaction. *J. Fluid Mech.*, 74:1–29, 1976.
- [7] B. J. Berne and R. Pecora. *Dynamic light scattering*. Wiley, New York, 1976.
- [8] F. Bloisi, L. Vicari, P. Cavaliere, S. Martellucci, J. Quartieri, P. Mormile, and G. Pierattini. Soret effect in forced Rayleigh scattering. *Appl. Phys. B*, 44:103, 1987.
- [9] M. M. Bou-Ali, O. Ecenarro, J. A. Madariaga, C. M. Santamaria, and J. J. Valencia. Thermogravitational measurement of the Soret coefficient of liquid mixtures. *J. Phys. Condens. Matter*, 10:3321–3331, 1998.
- [10] D. B. Brayton. Small particle signal characteristics of a dual-scatter laser velocimeter. *Applied Optics*, 13:2346–2351, 1974.
- [11] F. Brochard and P. G. de Gennes. Soret effect of flexible macromolecules. *C. R. Acad. Sc., Serie II*, 293:1025–1027, 1981.
- [12] H. S. Carslaw and J. C. Jaeger. *Conduction of heat in solids*. Oxford University Press, Oxford, London, 1973.
- [13] W. D. Comper, B. N. Preston, and P. Daivis. The approach of mutual diffusion coefficients to molecular weight independence in semidilute solutions of polydisperse dextran fractions. *J. Phys. Chem.*, 90:128–132, 1986.
- [14] P. Costeseque, M. El-Maataoui, and E. Riviere. Selective enrichments induced by thermogravitational diffusion in porous medium on hydrocarbon species of crude oil and specific case of paraffin isomers. *Entropie*, 30:94–100, 1994.

- 
- [15] B. J. de Gans, R. Kita, B. Müller, and S. Wiegand. Negative thermodiffusion of polymers and colloids in solvent mixtures. *J. Chem. Phys.*, 118:8073–8081, 2003.
- [16] S. R. de Groot and P. Mazur. *Non-equilibrium thermodynamics*. Dover Publications, Inc., New York, 1984.
- [17] C. Debuschewitz and W. Köhler. Molecular origin of thermal diffusion in benzene plus cyclohexane mixtures. *Phys. Rev. Lett.*, 87:055901, 2001.
- [18] P. Debye and A. M. Bueche. Thermal diffusion of polymer solutions. In H. A. Robinson, editor, *High polymer physics*, pages 497–527, Brooklyn, New York, 1948. Chemical Publishing Co.
- [19] J. K. G. Dhont. Thermodiffusion of interacting colloids. I. A statistical thermodynamics approach. *J. Chem. Phys.*, 120:1632–1641, 2004.
- [20] J. K. G. Dhont. Thermodiffusion of interacting colloids. II. A microscopic approach. *J. Chem. Phys.*, 120:1642–1653, 2004.
- [21] J. K. G. Dhont, S. Wiegand, S. Duhr, and D. Braun. Thermodiffusion of charged colloids: Single-particle diffusion. *Langmuir*, 23:1674–1683, 2007.
- [22] S. Duhr, S. Arduini, and D. Braun. Thermophoresis of DNA determined by microfluidic fluorescence. *Eur. Phys. J. E*, 15:277–286, 2004.
- [23] S. Duhr and D. Braun. Thermophoretic depletion follows Boltzmann distribution. *Phys. Rev. Lett.*, 96:168301, 2006.
- [24] S. Duhr and D. Braun. Why molecules move along a temperature gradient. *PNAS*, 103:19678–19682, 2006.
- [25] J. F. Dutrieux, J. K. Platten, G. Chavepeyer, and M. M. Bou-Ali. On the measurement of positive Soret coefficients. *J. Phys. Chem. B*, 106:6104–6114, 2002.
- [26] O. Ecenarro, J. A. Madariaga, J. Navarro, C. M. Santamaria, J. A. Carrión, and J. M. Savirón. Thermogravitational column as a technique for thermal-diffusion factor measurement in liquid-mixtures. *Separation Sci. Technol.*, 24:555–568, 1989.
- [27] O. Ecenarro, J. A. Madariaga, J. Navarro, C. M. Santamaria, J. A. Carrión, and J. M. Savirón. Fickian and thermal-diffusion coefficients from liquid thermogravitational columns. *J. Phys. Condens. Matter*, 2:2289–2296, 1990.
- [28] O. Ecenarro, J. A. Madariaga, J. Navarro, C. M. Santamaria, J. A. Carrión, and J. M. Savirón. Thermogravitational thermal-diffusion in liquid polymer-solutions. *Macromolecules*, 27:4968–4971, 1994.
- [29] H. J. Eichler, P. Günter, and D. W. Pohl. *Laser-induced dynamic gratings*. Springer, Berlin, Heidelberg, New York, Tokyo, 1986.
- [30] H. J. Eichler, G. Salje, and H. Stahl. Thermal-diffusion measurements using spatially periodic temperature distributions induced by laser light. *J. Appl. Phys.*, 44:5383–5388, 1973.

- [31] A. Einstein. Über die von der molekularkinetischen Theorie der Wärme geforderte Bewegung von in ruhenden Flüssigkeiten suspendierten Teilchen. *Ann. Phys.*, 17:549, 1905.
- [32] A. Einstein. Elementare Theorie der Brownschen Bewegung. *Z. Elektrochem.*, 14:235–239, 1908.
- [33] W. Enge and W. Köhler. Correlation between the Soret coefficient and the static structure factor in a polymer blend. *Eur. Phys. J. E*, 15:265, 2004.
- [34] W. Enge and W. Köhler. Thermal diffusion in a critical polymer blend. *Phys. Chem. Chem. Phys.*, 6:2373, 2004.
- [35] K. Ghorayeb and A. Firoozabadi. Molecular, pressure, and thermal diffusion in nonideal multicomponent mixtures. *AIChE J.*, 46:883–891, 2000.
- [36] M. Giglio and A. Vendramini. Thermal-diffusion measurements near a consolute critical-point. *Phys. Rev. Lett.*, 34:561–564, 1975.
- [37] M. Giglio and A. Vendramini. Soret-type motion of macromolecules in solution. *Phys. Rev. Lett.*, 38:26–30, 1977.
- [38] R. B. Gupta and J. M. Prausnitz. Vapor-liquid equilibria for solvent-polymer systems from a perturbed hard-sphere-chain equation of state. *Ind. Eng. Chem. Res.*, 35:1225–1230, 1996.
- [39] R. Haase. *Thermodynamik der Mischphasen*. Springer, Berlin, Göttingen, Heidelberg, 1956.
- [40] R. Haase. *Thermodynamics of irreversible processes*. Dover, New York, 1969.
- [41] A. Hammer, K. Hammer, and H. Hammer. *Taschenbuch der Physik*. J. Lindauer Verlag, München, Germany, 8th edition, 1997.
- [42] M. Hartung and W. Köhler. The role of heat-conducting walls in transient grating experiments. *Eur. Phys. J. E*, 17:165–179, 2005.
- [43] M. Hartung and W. Köhler. Optical cell with periodic resistive heating for the measurement of heat, mass and thermal diffusion in liquid mixtures. *Rev. Sci. Instr.*, 78:084901, 2007.
- [44] M. Hartung and W. Köhler. The concept of reversible work in thermal diffusion. 2008, submitted to *J. Chem. Phys.*
- [45] M. Hartung, J. Rauch, and W. Köhler. Thermal diffusion of dilute polymer solutions: The role of solvent viscosity. *J. Chem. Phys.*, 125:214904, 2006.
- [46] H. Hervet, W. Urbach, and F. Rondelez. Mass diffusion measurements in liquid-crystals by a novel optical method. *J. Chem. Phys.*, 68:2725–2729, 1978.
- [47] Frank P. Incropera and David P. DeWitt. *Introduction to heat transfer*. Wiley, New York, 4th edition, 2002.
- [48] L. J. T. M. Kempers. A thermodynamic theory of the Soret effect in a multicomponent liquid. *J. Chem. Phys.*, 90:6541–6548, 1989.

- [49] J. G. Kirkwood, R. L. Baldwin, P. J. Dunlop, L. J. Gosting, and G. Kegeles. Flow equations and frames of reference for isothermal diffusion in liquids. *J. Chem. Phys.*, 33:1505–1513, 1960.
- [50] R. Kita, G. Kircher, and S. Wiegand. Thermally induced sign change of Soret coefficient for dilute and semidilute solutions of poly(N-isopropylacrylamide) in ethanol. *J. Chem. Phys.*, 121:9140, 2004.
- [51] W. Köhler and B. Müller. Soret and mass diffusion coefficients of toluene/n-hexane mixtures. *J. Chem. Phys.*, 103:4367–4370, 1995.
- [52] W. Köhler and P. Rossmannith. Aspects of thermal diffusion forced Rayleigh scattering: Heterodyne detection, active phase tracking, and experimental constraints. *J. Phys. Chem.*, 99:5838, 1995.
- [53] W. Köhler and R. Schäfer. Polymer analysis by thermal-diffusion forced Rayleigh scattering. *Adv. Polym. Sci.*, 151:1–59, 2000.
- [54] P. Kolodner, H. Williams, and C. Moe. Optical measurement of the Soret coefficient of ethanol water solutions. *J. Chem. Phys.*, 88:6512–6524, 1988.
- [55] M. M. Kopsverkhoven, A. Vrij, and H. N. W. Lekkerkerker. On the relation between diffusion, sedimentation, and friction. *J. Chem. Phys.*, 78:2760–2763, 1983.
- [56] Korth Kristalle. Data sheet of Al<sub>2</sub>O<sub>3</sub>, 2003.
- [57] L. D. Landau and E. M. Lifschitz. *Lehrbuch der theoretischen Physik, Band 6, Hydrodynamik*. Akademie-Verlag, 1974.
- [58] G. H. Langhammer, H. Pfennig, and K. Quitzsch. Thermodiffusion (Ludwig-Soret-effekt) von Makromolekülen in Lösung. *Z. Elektrochem.*, 62:458–480, 1958.
- [59] V. Louli and D. Tassios. Vapor-liquid equilibrium in polymer-solvent systems with a cubic equation of state. *Fluid Phase Equilibria*, 168:165–182, 2000.
- [60] C. Ludwig. Diffusion zwischen ungleich erwärmten Orten gleich zusammengesetzter Lösungen. *Sitz. Ber. Akad. Wiss. Wien Math.-Naturw. Kl.*, 20:539, 1856.
- [61] J. Luettmer-Strathmann. Non-equilibrium thermodynamics of thermodiffusion in liquid mixtures with application to TDFRS experiments in ternary mixtures. unpublished, 2003.
- [62] J. Luettmer-Strathmann and J. V. Sengers. The transport properties of fluid mixtures near the vapor-liquid critical line. *J. Chem. Phys.*, 104:3026–3047, 1996.
- [63] N. Y. R. Ma and A. L. Beyerlein. Thermogravitational thermal-diffusion in binary-mixtures of chloroform with acetone, benzene, toluene, and mesitylene. *J. Phys. Chem.*, 87:245–250, 1983.
- [64] Y. Marcus. *The properties of solvents*. Wiley, Chichester, 1998.
- [65] S. Maruyama and T. Kimura. A study on thermal resistance over a solid-liquid interface by the molecular dynamics method. *Thermal Science & Engineering*, 7:63, 1999.

- [66] G. Meyerhoff and K. Nachtigall. Diffusion, thermodiffusion, and thermal diffusion of polystyrene in solution. *J. Polym. Sci.*, 57:227, 1962.
- [67] K. Nachtigall and G. Meyerhoff. Die Messung der Diffusionskoeffizienten von Hochpolymeren in Lösung mit einer konvektionsfreien Thermodiffusionszelle. *Makromol. Chemie*, 33:85–88, 1959.
- [68] Y. Nagasaka, T. Hatakeyama, M. Okuda, and A. Nagashima. Measurement of the thermal diffusivity of liquids by the forced Rayleigh scattering method: Theory and experiment. *Rev. Sci. Instr.*, 59:1156–1168, 1988.
- [69] H. Ning, J. Buitenhuis, J. K. G. Dhont, and S. Wiegand. Thermal diffusion behavior of hard-sphere suspensions. *J. Chem. Phys.*, 125:204911, 2006.
- [70] H. Ning and S. Wiegand. Experimental investigation of the Soret effect in acetone/water and dimethylsulfoxide/water mixtures. *J. Chem. Phys.*, 125:221102, 2006.
- [71] Oriel instruments. Data sheet of fused silica, 2003.
- [72] S. Pan, M. Z. Saghir, M. Kawaji, C. G. B. Jiang, and Y. Yan. Theoretical approach to evaluate thermodiffusion in aqueous alkanol solutions. *J. Chem. Phys.*, 126:014502, 2007.
- [73] G. D. J. Phillies. Comments on “Remarks on the mutual diffusion coefficient of Brownian particles”. *J. Chem. Phys.*, 84:5972–5973, 1986.
- [74] R. Piazza, S. Iacopini, and B. Triulzia. Thermophoresis as a probe of particle-solvent interactions: The case of protein solutions. *Phys. Chem. Chem. Phys.*, 6:1616–1622, 2004.
- [75] J. K. Platten, M. M. Bou-Ali, P. Costeseque, J. F. Dutrieux, W. Köhler, C. Leppla, S. Wiegand, and G. Wittko. Benchmark values for the Soret, thermal diffusion and diffusion coefficients of three binary organic liquid mixtures. *Philos. Mag.*, 83:1965–1971, 2003.
- [76] J. K. Platten, J. F. Dutrieux, and G. Chavepeyer. Soret effect and free convection: a way to measure Soret coefficients. In S. Wiegand and W. Köhler, editors, *Thermal Nonequilibrium Phenomena in Fluid Mixtures*, pages 313–333, Heidelberg, 2002. Springer.
- [77] D. W. Pohl. 1st stage of spinodal decomposition observed by forced Rayleigh scattering. *Phys. Lett. A*, 77:53, 1980.
- [78] D. W. Pohl, S. E. Schwarz, and V. Irniger. Forced Rayleigh scattering. *Phys. Rev. Lett.*, 31:32–35, 1973.
- [79] J. M. Prausnitz, R. N. Lichtenthaler, and E. G. de Azevedo. *Molecular thermodynamics of fluid phase equilibria*. Prentice Hall, New Jersey, 3rd edition, 1999.
- [80] I. Prigogine. *Etude thermodynamique des phénomènes irréversibles*. Desoer, Liège, 1947.
- [81] S. A. Putnam and D. G. Cahill. Micron-scale apparatus for measurements of thermodiffusion in liquids. *Rev. Sci. Instr.*, 75:2368, 2004.

- 
- [82] J. Rauch. *Diffusion und Thermodiffusion in Polymerlösungen*. PhD thesis, Universität Bayreuth, 2006.
- [83] J. Rauch, M. Hartung, A. F. Privalov, and W. Köhler. Correlation between thermal diffusion and solvent self-diffusion in semidilute and concentrated polymer solutions. *J. Chem. Phys.*, 126:214901, 2007.
- [84] J. Rauch and W. Köhler. Diffusion and thermal diffusion of semidilute to concentrated solutions of polystyrene in toluene in the vicinity of the glass transition. *Phys. Rev. Lett.*, 88:185901, 2002.
- [85] J. Rauch and W. Köhler. On the molar mass dependence of the thermal diffusion coefficient of polymer solutions. *Macromolecules*, 38:3571–3573, 2005.
- [86] R. Rusconi, L. Isa, and R. Piazza. Thermal-lensing measurement of particle thermophoresis in aqueous dispersions. *JOSA B*, 21:605–616, 2004.
- [87] M. E. Schimpf and J. C. Giddings. Characterization of thermal-diffusion in polymer-solutions by thermal field-flow fractionation - dependence on polymer and solvent parameters. *J. Polym. Sci., Part B: Polym. Phys.*, 27:1317–1332, 1989.
- [88] K. S. Schmitz. *An introduction to dynamic light scattering by macromolecules*. Acad. Press, Boston, 1990.
- [89] Schott. Optical glass catalog, 2006.
- [90] J. M. Schurr. The thermodynamic driving force in mutual diffusion of hard spheres. *Chem. Phys.*, 65:217–223, 1982.
- [91] S. N. Semenov. private communication, 2004.
- [92] A. E. Siegman. Bragg diffraction of a gaussian beam by a crossed-gaussian volume grating. *J. Opt. Soc. Am.*, 67:545–550, 1977.
- [93] Ch. Soret. Sur l'état d'équilibre que prend, du point de vue de sa concentration, une dissolution saline primitivement homogène, dont deux parties sont portées à des températures différentes. *Arch. Sci. Phys. Nat. Geneve*, 2:48–61, 1879.
- [94] R. Spill, W. Köhler, G. Lindenblatt, and W. Schaertl. Thermal diffusion and Soret feedback of gold-doped polyorganosiloxane nanospheres in toluene. *Phys. Rev. E*, 62:8361–8368, 2000.
- [95] D. Stadelmaier. Anisotrope Transportkoeffizienten in Flüssigkristallen. Master's thesis, Universität Bayreuth, 2006.
- [96] P. Stepanek, W. Brown, and S. Hvidt. Relaxation of concentration fluctuations in a shear field. *Macromolecules*, 29:8888–8893, 1996.
- [97] K. Thyagarajan and P. Lallemand. Determination of thermal-diffusion ratio in a binary mixture by forced Rayleigh scattering. *Opt. Commun.*, 26:54–57, 1978.
- [98] H. J. V. Tyrrell. *Diffusion and heat flow in liquids*. Butterworths, London, 1961.
- [99] C. Van den Broeck, F. Lostak, and H. N. W. Lekkerkerker. The effect of direct interactions on brownian diffusion. *J. Chem. Phys.*, 74:2006–2010, 1981.

- [100] S. Van Vaerenbergh and J. C. Legros. Modelisation de la diffusion multiconstituant: l'exemple des systemes ternaires. *Entropie*, 198/199:77, 1996.
- [101] S. Van Vaerenbergh and J. C. Legros. Soret coefficients of organic solutions measured in the microgravity SCM experiment and by the flow and Benard cells. *J. Phys. Chem. B*, 102:4426–4431, 1998.
- [102] D. C. Venerus, J. D. Schieber, H. Iddir, J. D. Guzman, and A. W. Broerman. Relaxation of anisotropic thermal diffusivity in a polymer melt following step shear strain. *Phys. Rev. Lett.*, 82:366, 1999.
- [103] H. Vink. Mutual diffusion and self-diffusion in the frictional formalism of non-equilibrium thermodynamics. *J. Chem. Soc., Faraday Trans. 1*, 81:1725–1730, 1985.
- [104] A. Voit. *Photothermische Strukturierung binärer Polymermischungen*. PhD thesis, Universiät Bayreuth, 2007.
- [105] J. Wang and M. Fiebig. Measurement of the thermal diffusivity of liquids with a laser-induced thermal-grating technique: An experimental investigation of systematic errors. *International Journal Of Thermophysics*, 17:1229–1239, 1996.
- [106] J. Wang, M. Fiebig, and G. Wu. Numerical simulation and error analysis for thermal diffusivity measurements using laser-induced thermal grating technique. *International Journal Of Thermophysics*, 17:329–345, 1996.
- [107] R. C. Weast and M. J. Astle. *CRC handbook of chemistry and physics*. CRC Press, Inc., Boca Raton, Florida, 63rd edition, 1982–83.
- [108] S. Wiegand. Thermal diffusion in liquid mixtures and polymer solutions. *J. Phys. Condens. Matter*, 16:R357–R379, 2004.
- [109] S. Wiegand and W. Köhler. Measurement of transport coefficients by an optical grating technique. In S. Wiegand and W. Köhler, editors, *Thermal Nonequilibrium Phenomena in Fluid Mixtures*, pages 189–210, Heidelberg, 2002. Springer.
- [110] G. Wittko. *Über den Einfluss molekularer Parameter auf die Transporteigenschaften organischer Lösungsmittel*. PhD thesis, Universiät Bayreuth, 2007.
- [111] G. Wittko and W. Köhler. Precise determination of the Soret, thermal diffusion and mass diffusion coefficients of binary mixtures of dodecane, isobutylbenzene and 1,2,3,4-tetrahydronaphtalene by a holographic grating technique. *Philos. Mag.*, 83:1973–1987, 2003.
- [112] G. Wittko and W. Köhler. Universal isotope effect in thermal diffusion of mixtures containing cyclohexane and cyclohexane-d(12). *J. Chem. Phys.*, 123:014506, 2005.
- [113] A. Würger. Heat capacity-driven inverse Soret effect of colloidal nanoparticles. *Europhys. Lett.*, 74:658–664, 2006.
- [114] A. Würger. Thermophoresis in colloidal suspensions driven by Marangoni forces. *Phys. Rev. Lett.*, 98:138301, 2007.
- [115] N. Yoshida. Remarks on the mutual diffusion coefficient of Brownian particles. *J. Chem. Phys.*, 83:1307–1310, 1985.

- [116] K. J. Zhang, M. E. Briggs, R. W. Gammon, and J. V. Sengers. Optical measurement of the Soret coefficient and the diffusion coefficient of liquid mixtures. *J. Chem. Phys.*, 104:6881–6892, 1996.
- [117] K. J. Zhang, M. E. Briggs, R. W. Gammon, J. V. Sengers, and J. F. Douglas. Thermal and mass diffusion in a semidilute good solvent-polymer solution. *J. Chem. Phys.*, 111:2270–2282, 1999.



## Danksagung

An erster Stelle möchte ich mich bei meinem ersten Chef Werner Köhler bedanken. In einer immer harmonischen Atmosphäre hat er mich optimal gefördert, so dass ich viel von ihm lernen konnte. Sowohl zu experimentellen Problemen als auch zu theoretischen Fragestellungen hatte er fast immer die richtigen Ideen und eine sehr zuverlässige physikalische Intuition. Gleichzeitig war er guten Argumenten stets zugänglich und offen für neue Sichtweisen. Einen besseren Doktorvater kann ich mir nicht vorstellen.

Mein zweiter Chef während meiner Promotion war Helmut Brand, der mir über die gesamte Zeit eine Landesstelle zur Verfügung stellte. Er achtete immer darauf, mich nicht mit zu vielen Lehrverpflichtungen zu belasten und mir so bestmögliche Arbeitsbedingungen zu ermöglichen. Dafür danke ich ihm sehr.

Bei Alois Seilmeier bedanke ich mich für die Übernahme des Zweitgutachtens und die damit verbundene Zeit und Mühe.

Besonderen Dank schulde ich Jan Dhont für viele interessante und lohnende Diskussionen in Jülich und Bayreuth, für seine außergewöhnliche Offenheit und für das Gutachten.

Katrin Stark danke ich für ihre Zuverlässigkeit und ihren Einsatz bei allen verwaltungstechnischen Problemen und Fragen zum Promotionsverfahren. Bei Helmut Brand, Werner Köhler, Alois Seilmeier und Ernst Rößler bedanke ich mich für eine angenehme Atmosphäre im Promotionskolloquium.

Insbesondere beim Lithographieprojekt halfen mir sehr viele Leute: Besonders wichtig war dabei Klaus Müller, der sämtliche Chrom-, ITO- und Siliziumdioxidschichten aufdampfte oder sputterte. Dafür und auch für seine Anteilnahme an allen Erfolgen und Misserfolgen möchte ich mich ganz herzlich bedanken. Für unzählige REM-Bilder meiner Proben danke ich Werner Reichstein, Clarissa Abetz und Steffen Hartmann. Werner Reichstein machte zusätzlich FIB-Schnitte. Durch seinen wirklich außergewöhnlichen Einsatz konnte er so den Grund für das anfängliche Nichtfunktionieren der Multilayerstrukturen finden. Vielen, vielen Dank! An dieser Stelle auch einen herzlichen Dank an Uwe Glatzel, der die Benutzung seiner FIB-Anlage gestattete. Bei Pramod Pullarkat bedanke ich mich für das Ausleihen der e-beam-Maske und für seine entscheidende Hilfe ganz zu Beginn des Projekts: Ihm gelang es mit einer einfachen Quecksilberdampflampe, Tesafilm, blauen Nitrilhandschuhen und einem Wecker die ersten funktionierenden Streifenstrukturen überhaupt herzustellen, was mit dem teuren Maskaligner wegen eines erst später behobenen "wedge errors" zunächst nicht möglich war.

Sehr hilfreiche Ratschläge zur Herstellung von Isolationsschichten verdanke ich Walter Riess, Simone Wiegand, Andreas Offenhäusser, Regina Stockmann und Michael Prömpers. Alfons Becker und Michael Heimler bauten schnell einen schnellen Schalter. Jürgen Gmeiner und Patricia Freitag halfen mir bei Problemen mit dem Plasmaätzter. Pit Strohriegel war der Experte für Fragen der Lackchemie. Die Benutzung des Maskaligners ermöglichten mir Ralf Pihan oder, wenn er nicht da war, Wolfgang Michel und Margot Lenich, die mir dann bei der Schlüsselsuche halfen. Bei Arbeiten im Chemielabor von EP IV bekam ich nette Gesellschaft und nützliche Tipps von Manuela Dezi, Carmen Perez León, Silke Oellerich, und Waltraud Joy. Vielen Dank Euch allen!

Eines der schönsten Dinge meiner Promotionszeit war das Zusammenarbeiten (und manchmal auch Nichtarbeiten) in unserer Arbeitsgruppe. Für Hilfe bei experimentellen Problemen und Computerfragen, Entgegennahme von Telefonanrufen, Tipps zu Laptopkauf, Fahrradreparatur und Herdinstallation, Trost bei gescheiterten Experimenten, Kochrezepte für japanische Suppen, die Wärmflasche im Doktorwagen, unzählige Tassen Tee, tiefgründige Gespräche auf Nikis Couch, Diskussionen über Vor- und Nachteile von transatlantischen Beziehungen, gemeinsame Verzweiflung über Immobilienpreise in München, Muster für Bewerbungsunterlagen und Lebenslauf, u.v.m. bedanke ich mich bei Albert Voit, Gerhard Wittko, Dominik Stadelmaier, Philipp Schleiffer, Wolfgang Enge, Robert Kellner, Steffen Hartmann, Florian Schwaiger, Stefan Frank, Andreas Königer und Börn Meier.

Außerdem danke ich Evelyn Hülsmann und Karin Baier  
Michael Heimler, Waltraud Joy und Werner Reichstein  
Lothar Kador, Jürgen Köhler und Werner Köhler  
André Leopold, Renate Müller, Markus Bauer, Carmen Perez León, Hanna Engelke, Erwin Lang, Patricia Freitag und Michael Häckel  
Hubert Audorff, Jürgen Baier, Paul Böhm, Christian Brock, Dominique Ernst, Richard Hildner, Christiane Hofmann, Christoph Jung, Peter Karich, Lisa Krapf, Ralf Kunz, Silke Oellerich, Tobias Pflock, Martin Richter, Philipp Schreier und Florian Spreitler  
für die hervorragende Atmosphäre am Lehrstuhl EP IV, gute Unterhaltung in der Kaffecke und gemeinsame Unternehmungen.

Bei Silke Oellerich möchte ich mich zusätzlich dafür bedanken, dass ich im letzten 3/4 Jahr meiner Promotion in ihrem gemütlichen Gästebett schlafen durfte.

Für Aufmunterung und Ablenkung danke ich Pablo und meiner Familie.